Hybrid SHCC-concrete beams

Shear capacity of innovative hybrid concrete structures with SHCC lamellas applied laterally

THE CIVIL ENGINEERING MASTER'S THESIS AT DELFT UNIVERSITY OF TECHNOLOGY (TU DELFT)

TU Delft

Bartosz Budnik

Master's Thesis Project

Shear capacity of innovative hybrid concrete structures with SHCC lamellas applied laterally

by

Bartosz Budnik

in partial fulfilment of the requirements for the degree of

Master of Science in Structural Engineering

at the Delft University of Technology,

to be defended publicly on Tuesday 17 January 2023 at 15:00.

Student number: 4689518

Thesis committee:

Dr. ir. M. Luković (*Chair*)	TU Delft
MSc S. He	TU Delft
Dr. J. S. Dragaš	University of Belgrade
Dr. ir. B. Šavija	TU Delft

An electronic version of this thesis is available at http://repository.tudelft.nl/.

TU Delft

Publication date:

20th January 2023

Preface

At the outset, I would like to express my gratitude to advisors and supervisors without whom this work would be extremely difficult, not to say, troublesome to complete.

I would like to thank my committee chair, Dr. ir. Mladena Luković, for her cast iron commitment to this project and her unwavering positive attitude. She was always ready to help. Also, I had the pleasure of attending her courses {CTB3335 Betonconstructies 2 (ENG: Concrete Structures 2) & CIE5130 Capita Selecta Concrete Structure} during my education at TU Delft. The knowledge, which I have obtained from those classes, will be an indispensable tool in my future career. I want to thank her for it once again.

I would like to express my personal gratitude to MSc Shan He, my daily supervisor, for his effort and the extra time that he has contributed during this long project. But also for the lessons where he taught me about properties related to Strain Hardening Cementitious Composite and showing me how to properly measure them. Besides, I had a great time working with him. Somehow he could make the work more enjoyable. Without his creativity, fast thinking and knowledge, the project most probably be lost.

I would like to thank Dr. Jelena S. Dragaš for her well-structured remarks during the long process and for her brilliant observations during the experiment. Without her expertise and extraordinary spotting skills of defects on the surface of a material, the description of experimental data would never be so rich in detail. Even though she lives so far away, I was lucky enough to meet her in person during her visit to TU Delft. It was a great pleasure to meet her and her team in real life.

I would like to acknowledge the effort of Dr. ir. Branko Šavija during the assessment process. His valuable feedback helped me to improve this work.

Beside people from my thesis committee, I would also like to thank the lab staff. They help me during preparing of specimens and during actual testing the. They help me by using various machines that I could not use myself. Especially MSc Jakub Pawłowicz, Albert Bosman, Ton Blom and Maiko van Leeuwen for making the atmosphere in the Stevinlab so enjoyable.

Special thanks to MSc Yitao Huang for his immense effort in this project. I greatly appreciate his involvement in this project! He was so heavily involved in this project that I had constant feeling that he is one of the members of my thesis committee.

I wanted to express my gratitude for the help that I received from MSc Zhenxu Qian in organizing the DIC set-ups. She is a real expert in this field.

My deepest gratitude to my family for supporting me in this life challenge. I hope that I did not bore you to death with my endless stories about concrete and SHCC.

Bartosz Budnik
Enschede, November 2022

Abstract

Strain Hardening Cementitious Composite (SHCC) is an innovative type of fibre-reinforced cement-based composite that has superior tensile properties. Because of this, it holds the potential to enhance the shear capacity of reinforced concrete (RC) beams, if applied properly.

Experimental research was thus carried out with the purpose of investigating the shear behaviour of reinforced concrete beams enhanced with thin SHCC laminates (10 mm in thickness) in their webs (henceforth referred to as hybrid SHCC-concrete beams). This research distinguishes itself from other studies by the fact that the hybrid beams were manufactured by casting conventional concrete inside pre-cast SHCC laminates, consequently, forming an interface between concrete and SHCC. Moreover, two different types of SHCC-concrete interface designs have been used in the hybrid beams, namely smooth and profiled ones. Furthermore, beams with and without transverse reinforcement (stirrups) were both prepared in order to investigate the effect of two specific methods of shear reinforcing (i.e., SHCC and stirrups) on each other. On top of that, one of the hybrid beams with stirrups has been supported only at its normal concrete core to uncover any irregularities in the shear behaviour compared to a beam supported at its full-width. Conventional RC beams (without SHCC laminates) were also prepared as references. All beams were tested in a three-point bonding set-up while monitored by two separate systems: Digital Image Correlation (DIC) and Linear Variable Data Transformers (LVDTs). The camera images were analysed by the software package, GOM Correlate 2019. During the casting of the beams, samples of all materials were taken and tested to establish their mechanical properties for quality control purposes.

Results show that the hybrid beams have obtained higher shear capacity than the control group. Only the hybrid beams with a minimum amount of shear reinforcement were capable to activate SHCC web laminates to their full extent. In the case of hybrid beams without transverse reinforcement (TR), only half of SHCC laminate potential was utilised approximately.

This study proves that, by applying advanced material (i.e., SHCC) properly, an efficient way of improving the shear capacity of an RC beam can be achieved, so long there is minimum TR provided. If a minimum transverse reinforcement is not present, the benefits of shear enhancement by SHCC become less effective due to the low Young's modulus of SHCC.

Contents

1

Introduction

"The imperial vastness of late Roman architecture was made possible by the invention of concrete."

Iain McGilchrist

1.1 Problem context

Concrete is the most widely used construction material in the world due to its low price, versatility, and easy applicability [1, 2]. Regardless of how well designed and constructed is a concrete structure, it has to be assessed and maintained on regular bases to achieve its anticipated service life. Occasionally durability of concrete is an issue and thus a lot of maintenance and/or repair will be needed which is costly [3]. Moreover, in the era of circular-economy and carbon neutrality, low price and versatility may not be sufficient to guarantee concrete its dominant presence [2]. Instead, sustainable development would most likely drive our economy in the future. Hence, the sustainability of construction materials will be increasingly prominent.

To resolve this dilemma, new construction materials should be adopted because they give us more opportunities. And indeed, one promising new innovative cement-based material, Strain-Hardening Cementitious Composite (SHCC), supports the values of our new era. The SHCC is a special type of fibre-reinforced cement-based composite that has a superior crack width control ability under tension [4]. Its fibres help to achieve higher ultimate tensile strain compared to normal concrete (NC). This with an improved crack width control ability is the main advantage of SHCC, and therefore, SHCC possesses enhanced improved durability [5] as compared to NC.

However, the structures made only from SHCC will be much more expensive than the typical concrete structures [6]. The presence of fibres in SHCC not only increases the cost but also leads to a higher burden on the environment [7]. Therefore, the solution to our problem might be in hybrid systems which combine SHCC and NC. In this way, the material is used optimally, hence lowering the burden on the environment while at the same time keeping material cost competitive. This hybrid system is therefore more durable, sustainable and economical. One of the possible ways to realize the hybrid system is by placing SHCC in the outer layers of a normal reinforced concrete (RC) beam. In this way, the superior mechanical properties of SHCC are utilised and reinforcement in an RC beam can be perhaps reduced. U-shape shells made out of SHCC will presumably be manufactured in a precast concrete element factory. This could mean that the prefabricated SHCC shells could be used as formwork for cast-in-situ NC which will reduce the costs even further.

Some research has already been performed on the influence of hybrid systems of outer SHCC layers. The experimental study of Luković et al. [5] has investigated the cracking behaviour of RC beams with reinforced SHCC layers in the tension zone. It has been proved that hybrid systems have better cracking behaviour compared to conventional RC beams. Huang came to the same conclusion in [8]. The micro-cracking, and thus, the cracking pattern can be influenced by choosing the interface property and the fibre type. Extensive research on this topic can be found in [9]. When it comes to the shear behaviour of a hybrid system, the studies are very limited. Fortunately, shear strengthening layers made out of SHCC are found to be very promising according to the numerical study conducted by [10].

1.2 Problem statement

In structural design, Serviceability Limit State (SLS) and Ultimate Limit State (ULS) must be satisfied according to good engineering practice and legal regulations. The ULS guarantees structural safety, while the SLS secures functionality and prevents discomfort among users under normal conditions. Within the ULS design, special attention is paid to the analysis of the brittle failures. Those types of failures should not be governing mechanisms during the

overloading of a structure due to their sudden and rapture nature. Engineers prefer failure mechanisms that warn before reaching their limits because it gives room for correction and thus prevents deaths and/or painful injuries.

This Master's Thesis Project will focus on investigating the contribution of SHCC web layers to the shear capacity of RC beams with and without shear reinforcement. A shear failure in concrete members or structures is classified as a brittle and sudden failure and therefore should not be the governing failure mechanism of structural members. It is expected that the SHCC laminates will enhance the shear capacity of a hybrid structure as compared to a conventional RC structure. This can be inferred from the previous mentioned studies, see section 1.1.

Moreover, the fracture behaviour under shear load is not yet fully understood in hybrid systems, as the fracture properties are influenced by a lot of factors such as concrete strength, curing age, volume fraction of fibres, aggregates, and SHCC-NC interface. The technique of installing SHCC laminates has some issues which may reduce its strengthening effectiveness such as: debonding of an SHCC laminate from an NC core and the surface pre-treatment during manufacturing.

1.3 Hypothesis

If an outer strain-hardening cementitious composite layer is added to a reinforced concrete beam, the shear capacity of this hybrid system would be significantly improved compared to an RC beam with an equivalent size.

1.4 Significance of study

If the hypothesis turns out to be true that SHCC web layers do significantly increase the shear capacity of an RC beam then it could mean a reduction or even redundancy of the minimum shear reinforcement. Hence, the sustainability of such concrete elements would increase. Moreover, SHCC web layers could be used in retrofitting existing concrete structures — this is much more sustainable than demolishing and building new structures.

The shear testing is essential for new materials or combinations of materials since the mechanical behaviour of composites can be significantly different from their individual components. Moreover, knowledge about shear behaviour is required to fulfil the ULS criteria. Hence, multiple experiments have to be performed to develop and calibrate shear capacity models of the hybrid SHCC-concrete system before it can be used in practice.

Furthermore, this study could improve and/or introduce ideas for manufacturing thin precast elements from SHCC. But it may also highlight unknown issues during prefabrication laminates. For example, the thinnest through-thickness of an SHCC laminate has to be verified because of operational and effective reasons. Unlike previous research on this topic, this study aims to add a shear keys pattern onto thin SHCC laminates to increase their interface bonding strength with a normal concrete core.

1.5 Research question and sub-questions

The principal aim of this thesis is to verify the hidden potential of the hybrid system. To investigate the problem statement explained above, the following research questions were formulated:

Main research question:

To what extent can the shear capacity be enhanced by having thin SHCC web layers attached to the reinforced concrete beam when compared to the control reinforced concrete beam?

Sub-questions:

1) Which parameters have a positive impact on the shear capacity of an interface connection between old SHCC and new normal concrete?
2) To what extent do different curing conditions affect the SHCC shrinkage? Which interface better prevents the negative effects of the differential drying shrinkage rate between SHCC and NC in the short term, be it smooth or profiled interface?
3) What is the response of SHCC web laminates in the beams with and without transverse reinforcement?
4) What is the consequence on the shear capacity of a hybrid beam supported at its full width (including SHCC laminates) versus a hybrid beam supported only at the width of a normal concrete part?
5) How to correctly predict the shear resistance of an RC beam with SHCC web layers?

1.6 Methodology

The main research question will be answered by subjecting the full-size specimen beams to the three-point bending test. In total six beams were tested for this research and were arranged in two series of three beams, see Table 1. In each series of the beams, the reference RC beam was tested as the control specimen. In the first series, two hybrid beams without transverse reinforcement (TR) were loaded. The difference between those beams is interfaces between SHCC laminates and normal cores: smooth versus profiled interface (adding a pattern of shear keys on laminate). However, the first series of the beams is not a realistic scenario since engineers are obligated by Eurocode 2 (EC2) to use the minimum amount of shear reinforcement even though shear failure is not governing failure. Therefore, the beams in the second series were provided with transverse reinforcement prescribed by EC2. In this series, two hybrid beams were tested with the same interfaces between SHCC laminates and normal cores, namely profile one. Those two hybrid beams in this series are the same, but they were supported differently: the first hybrid beam was supported at its full width (core + two SHCC laminates) like the rest of the beams; the second hybrid beam was supported only on its normal concrete core. The difference in boundary conditions of hybrid beams is related to the fourth sub-question which will be answered in Chapter 4. It is speculated that those different boundary conditions could have implications on the behaviour of a hybrid beam due to different load transfers near the supports.

The first sub-question will be answered by conducting a literature investigation (Chapter 2) into the strength of the old-new interface concrete connections between SHCC and normal concrete, but not only limited to this specific topic. When shear stress is large enough at the interface between normal concrete and SHCC, the poor interface may delaminate. Delamination could also occur when the relative shrinkage of SHCC and normal concrete reach the critical level. Based on new knowledge from the literature review, the most promising solutions for interface connections have been selected for implementation in the main experiment (three-point bending tests on hybrid beams).

The second sub-question will be answered by performing shrinkage tests under two different curing conditions, see Chapter 4. The first curing condition will be the standardized

procedure of keeping specimens for 28 days in the climate room since it is commonly used by scientists. As such, the results will be much easier to compare with other results. The second curing condition will be a reflection of the treatment condition of SHCC laminates during the manufacturing process of the hybrid beams. For this sub-question, 'short term' is defined as two / three days.

Table 1 Overview of all beam specimens in this experiment

		First series		Second series	
Control Group	*Type*	RC beam		RC beam	
	Number of specimens	1		1	
	Transverse reinforcement	**No**		**Yes, minimum**	
	Support width	**Full**		**Full**	
	Are SHCC web layers attached?	**No**		**No**	
Experimental Group	*Type*	Hybrid beam		Hybrid beam	
	Number of specimens	1	1	1	1
	Transverse reinforcement	**No**	**No**	**Yes, minimum**	**Yes, minimum**
	Support width	**Only width of NC core**	**Only width of NC core**	**Full beam width**	**Only width of NC core**
	Are SHCC web layers attached?	Yes, smooth laminates	Yes, profiled laminates	Yes, profiled laminates	Yes, profiled laminates

The third sub-question will be answered in Chapter 6. Since normal concrete and SHCC have different values for Young's modulus, it is not straightforward how a hybrid beam will respond when additional ductility is introduced in the form of stirrups. Of course, this will have an implication for the strategy for finding a practical way of predicting the shear capacity of a hybrid beam.

The fifth sub-question will be answered in Chapter 6. Currently, there are no standardised guidelines which would predict the shear resistance of a hybrid beam. However, it might be possible to adjust existing procedures for calculating the shear resistance of an RC beam in order to estimate the shear capacity of a hybrid beam.

In the final analysis, all obtained knowledge and results will lead to a clear answer to the main research question. The recommendation for follow-up research – and possible solutions or actions to address unresolved issues will be made as well.

1.7 Thesis outline

This master's thesis report consists of a total of seven chapters including the current Introduction chapter (Chapter 1). The second chapter gives a brief review of studies related to the topic of this research. The third chapter shows the design calculation of the RC beams used in this study as the control group. The fourth chapter reports the manufacturing processes of all specimens used in this project in detail. The fifth chapter provides the experimental results of

this research with a bit of analysis. In the sixth chapter, more deep analysis is presented alongside theoretical predictions of (hybrid) beams from this and other studies using analytical models from current literature and codes. The results are then critically examined and discussed their meaning at the end. To sum up, the conclusions are given in the seventh chapter with proper recommendations for future studies.

2

Literature Study

"Of all things, I liked books best."

Nikola Tesla

This chapter gives a review of theories, parameters, and limitations that need to be addressed in order to make the experiments objective, repeatable, and complete. Crack patterns and/or debonding of interfaces in a hybrid system are the main concerns when it comes to predicting the shear failure mechanism, and especially, the shear capacity of the hybrid system. The interaction between SHCC and normal concrete may lead to complex behaviours that could be observed during the experiments due to their heterogeneous nature. Ultimately, it could be that the SHCC-concrete interface strength may be the limiting factor for the shear capacity of a hybrid beam due to premature bond failure, therefore knowledge about the influence parament of bond strength is necessary.

2.1 Shear failure of reinforced concrete beams without transverse reinforcement

Although a shear failure in a concrete member is known for at least 100 years, Eurocode 2 still adopts a rather conservative model to predict the capacity for this failure mode. However, it is not done without good reason. This type of failure is characterised as brittle because it provides no warning and is sudden. Moreover, the shear capacity given by Eurocode 2 is based on experimental data, but with the absence of theoretical background. After many decades of research, scientists still debate the unique mechanical model that could cover all feasible design configurations. Of course, there are plenty of theoretical concepts with their equations but they have still their own merit and demerits. There are also debates about the definition of shear failure. The general definition of shear failure according to Yang [11] is as follows:

"A brittle failure occurring under a shear force, with diagonal cracks developing in the span."

This definition connects a shear force to the diagonal cracking of concrete. But there are a couple of ways in which concrete members could fail under shear loading. There are three shear failure mechanisms in RC beams that can be distinguished in the literature: Diagonal Tension Failure, Shear Compression Failure, and Splitting Shear Failure. Some literature adopts other names for those type of failures. For example, 'Splitting Shear Failure' is also called 'True Shear Failure' by [12] or 'Failure of Compression Strut' by [13].

In general, the shear capacity of beams is mainly influenced by three factors: the shear span parameter (η_a), steel ratio in the tensile zone (ρ), and compressive strength of concrete (f_c). η_a is the ratio between the shear span 'a' (the distance between support and force vector in a three-point bending setup) and the effective depth of a beam 'd' (the distance between the centroid of longitudinal reinforcement to the furthest fibre in the compression zone).

Next to those factors, researchers have indicated many other aspects that play a role in the shear capacity of beams. Ghaffar et al. [12] have listed a couple of them and those are aggregate interlocking, the density of concrete, the specimen size (size effect), fibre volume in a concrete mix, the tensile strength of concrete, the geometry of a specimen, boundary conditions of support and loading plates, spreading of tensile reinforcement and end anchorage of tension reinforcement.

Many scientific researchers investigating the shear capacity like to keep most of those factors constant and they vary usually one of the three main factors to observe the correlation with a failure mechanism. For this purpose, the shear span parameter (η_a) is often a variable parameter in such experiments. The following shear failure mechanisms are often distinguished by scientists and engineers:

2.1.1 Diagonal Tension Failure

This failure mode begins at the outer fibres in the tensile zone. Flexural (vertical) cracks start to appear in this zone due to exceeding the flexural tensile strength. Then, as load increases, the cracks continue to incline and will form so-called inclined flexural cracks. The inclination is caused by shear force. One of the cracks would try to reach the application point of load, see Figure 1. This crack encounters resistance as it tries to reach the compression zone and therefore it inclines further to the point that it becomes almost flat. After this stage, the crack starts to extend significantly at the plateau to the point that the mechanism is unable to sustain increasing loading. Researchers have called this load-transfer mechanism an 'arch mechanism'.

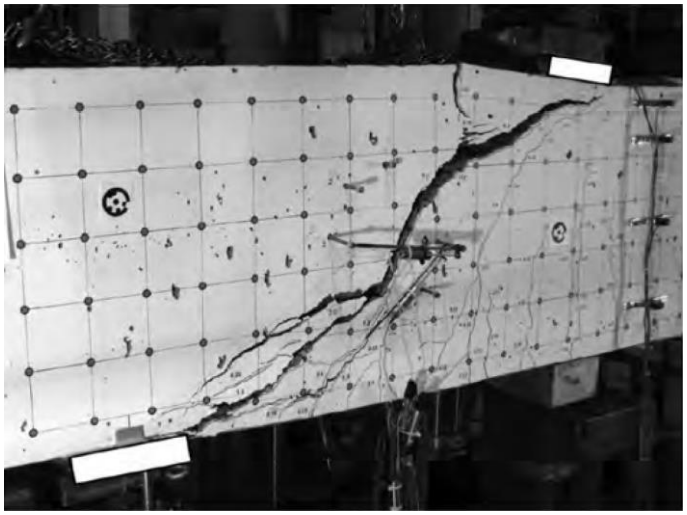

Figure 1 Example of Diagonal Tension Failure in a reinforced concrete beam [13]

Diagonal Tension Failure develops in beams with $\eta_a \approx 2{,}5 \sim 6$ accoridng to [11]. But, according to [12], Diagonal Tension Failure occurs *always* when $\eta_a > 2{,}0$. In the end, the other parameters e.g. f_c and ρ if this specific mechanism may actually develop or not at $\eta_a = 2{,}0 \sim 2{,}5$ because as mentioned earlier, they also do influence shear capacity.

2.1.2 Shear Compression Failure

Shear Compression Failure occurs when the concrete strut is crushed at the compressive zone around the application of load. After this concrete crush, the secondary effect would develop in the form of a diagonal crack. This failure can be seen in Figure 2. This type of shear failure is expected for beams with $\eta_a \approx 1 \sim 2{,}5$ according to [12].

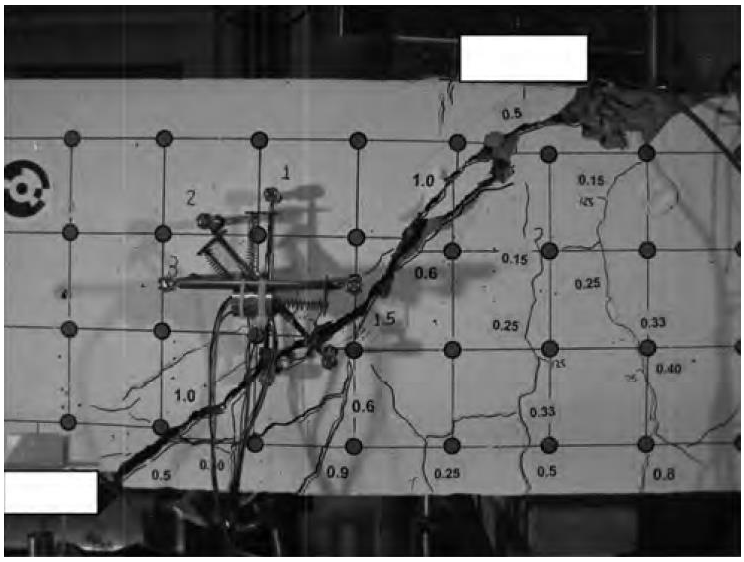

Figure 2 Example of Shear Compression Failure in a reinforced concrete beam [13]

The tension cracks are unable to fully develop due to the small span between applied force and support. Hence, the load will be transferred mainly by shear, so the failure will initiate at the neutral axis forming a diagonal (shear) crack before appearing of flexural cracks in the tension zone. A void does not transfer load, so shear stress starts to propagate into uncracked depth leading to propagation of the initial crack. The transfer mechanism of the load is comparable to a 'tied arch'. When the diagonal crack propagates to the compression zone, it

starts to reduce the compression height zone. This means that the compression force vector is smeared over a smaller area. And if this height will be reduced further, it will lead to the crushing of concrete in this zone.

2.1.3 Splitting Shear Failure / True Shear Failure / Failure of Compression Strut

The Splitting Shear Failure occurs in deep beams, as seen in Figure 3. Those beams have η_a less than 1,0 according to [12]. The span is too small to carry a significant part of the load by flexural mechanism. The inclination of the vector between support reaction and load is therefore also small. Hence, the inner splitting tensile component of this diagonal vector is smaller compared to other failure mechanisms. Obviously, the shear capacity is larger in such a case. There are two final failures that could occur. Sometimes, concrete is crushed in the region of the support but also it may happen that splitting shear failure develops.

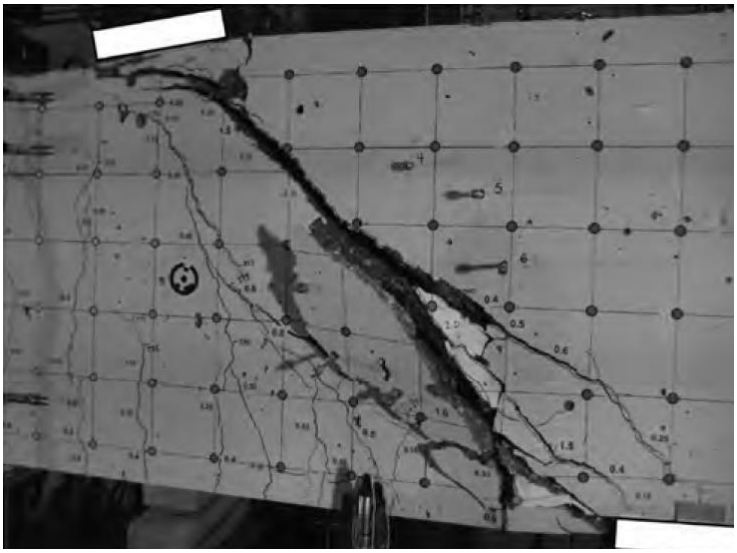

Figure 3 Example of Failure of Compression Strut in a reinforced concrete beam [13]

2.1.4 Shear transfer in the absence of transverse reinforcement

In general, flexural cracks appears before diagonal cracks because the compressive strength of concrete is significantly higher than the tensile strength. Both the compressive and tensile strength of concrete influence the shear failure process [11]. Although, researchers dispute shear resistance equations/models of Eurocode 2 however some shear transfer mechanisms are widely accepted by the scientific community, see Figure 4:

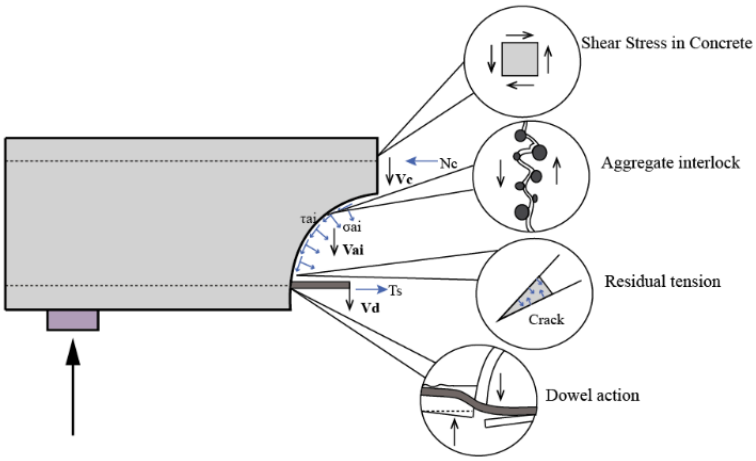

Figure 4 Overview of shear-resisting mechanisms on crack [14]

Shear stress in uncracked concrete

According to the theory of elasticity, the shear stress distribution of a cross-section should follow a parabolic distribution. Note that the cracked part of concrete does not contribute to the shear resistance of a cross-section, as seen in Figure 5. In theory, if the height of the crack is known the boundary conditions can be set up. In practice, it is impossible to set up those boundary conditions and often models have to be simplified.

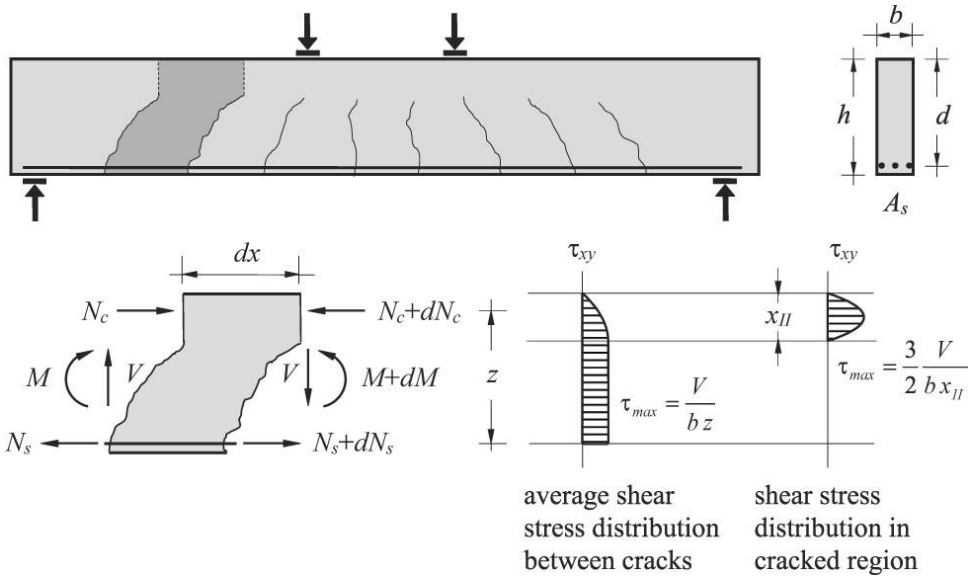

Figure 5 Shear stress distributions in cracked beam [15]

Aggregate interlocking

Aggregate interlocking is the friction resistance that a shear plane in concrete encounters when two cracked surfaces are tried to be moved. The friction resistance is generated between sticking aggregates in the crack, and not between the cement matrix and an aggregate. The cement matrix is weaker than the aggregate, so the cement paste matrix will crush upon contact with it. It is, therefore, preferable to have rougher crack surfaces because it creates more contacts between aggregates which leads to a higher shear capacity according to [14]. The increase in maximum aggregate size increases the roughness of the crack surface according to [15]. Hence, for example in high-strength concrete, the aggregate interlocking does not play a significant role because relatively small aggregates are used in such types of concrete.

The basic mechanism of aggregate interlock created by Walraven in 1981 and further improved by Millard and Johnson in 1985 distinguished three main contributors in their model: the maximum aggregate size, the concrete strength, and the crack surface displacements. The model assumes that aggregates are uncompressible to simply a problem a bit. In the era of the Finite Elements Method, more sophisticated models were built, but often they required those variables as well in addition to the additional parameters for their inputs like for example shapes of aggregates and Young's modulus of cement paste and aggregates.

Residual Tensile Strength

Concrete is not homogeneous material, therefore it is unlikely that the newly created crack at the surface has fully penetrated to a through-thickness of the concrete member. According to [14], NC is able to transmit tensile stresses even if it is cracked however the crack width cannot exceed approx. 0,1 mm. In literature, the relationship between tensile stress and crack width is

often referred to as 'tension softening'. According to [14], the residual tensile stress in crack plays important for shear transfer. However, researchers did not yet agree on the mathematical function of this relationship.

Dowel action

The dowel action is a shear strength mechanism generated as a result of cooperation between the longitudinal reinforcement and enclosing concrete around the rebars. This mechanism does not only increase the shear capacity of a beam but also improves the post-peak behaviour. After reaching peak load, beams behave more plastic than in the case of the pure concrete beam where rupture is more sudden.

2.2 Shear strengthening of RC beams with outer SHCC layers

In this section, the general properties of SHCC would be presented. Those properties are important for bonding strength between new-old concrete connections. Further, the environmental impact that SHCC could have on our planet will also be discussed. After giving these points, an overview of experiments of shear strengthening with SHCC will be provided.

2.2.1 General properties of Strain Hardening Cementitious Composite

Strain Hardening Cementitious Composite is cement-based material with fine aggregates and micro-fibres. According to Luković [4], those fibres enable "microcrack bridging property" and thus increase bond strength and abrasive resistance [16] but also decrease crack widths and frailty. It has therefore enhanced crack control ability as it exhibits multiple microcracks instead of one concentrated crack. Furthermore, this material shows strain hardening behaviour under tension as seen in Figure 6; so researchers decided to call it 'Strain hardening'. A high deformability may often be observed up to a tensile strain of approximately 5%. For sake of comparison, the approximate maximum tensile strain of normal concrete is roughly 0,01%.

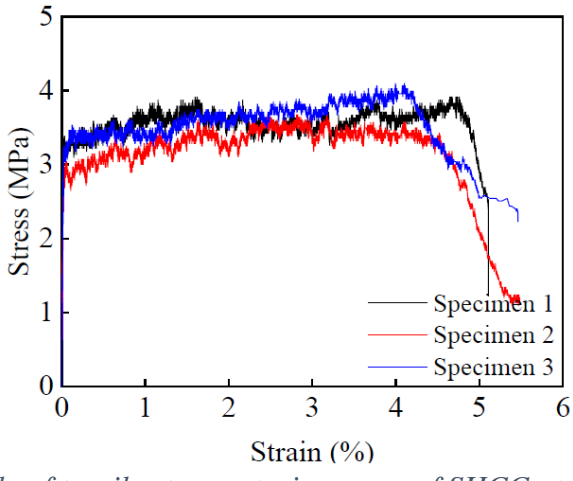

Figure 6 Example of tensile stress–strain curves of SHCC at age 28 days [17]

Characteristic behaviours of SHCC are small crack widths ranging from 60 μm to 100 μm [4] and significant (by two orders of magnitude) ductility after cracking compared to NC [18]. Small crack widths in SHCC give two major advantages. Firstly, it has good self-healing properties [19]. Secondly, water permeability by those cracks is smaller compared to uncracked concrete [20]. It is therefore expected that the service life of SHCC is greater than that of normal concrete. However, SHCC is not financially acceptable for the construction industry if SHCC

is to be used to completely replace traditional reinforced concrete due to the more expensive ingredients used in SHCC. Polyvinyl Alcohol (PVA), as well as other types of fibres, often increase the total cost of SHCC, therefore their use must be justified.

Fibres

There are many types of fibres used in SHCC. According to [18], the role of different fibres has an influence on strength of the interface between SHCC and concrete. The most common fibres from the literature review are Polyvinyl Alcohol (PVA) fibres, High Modulus Polyethylene (HMPE) fibres and steel fibres. However, the latter fibres are used in steel fibre–reinforced concrete (SFRC).

Figure 7 Photo on the left: Polyvinyl Alcohol (PVA) fibres [21]. Photo on the centre: High Modulus Polyethylene (HMPE) fibres [22]. Photo on the right: steel fibres [23].

Those fibres have an important job to do in the microstructure after a crack forms. They increase the post-cracking strength known as toughness. A frequent misconception about fibres is the belief that fibres stop cracks from forming. The fibres do not stop the crack. The crack will appear at the same load as in the case of normal concrete, but the fibres stabilise the crack. And as mentioned in the 2.2.1 section, the small crack width results in longer technical life of the structure because tight crack width can slow down the ingress of chloride ions and thus prevent reinforcement from corroding. The exact effect of fibres on concrete or SHCC behaviour depends on the type of fibres and volume fraction of those fibres.

The polyvinyl-alcohol (PVA) fibres have hydrophilic surfaces due to the presence of a hydroxyl group in their structures. According to [24], those fibres can survive at an elevated temperature of 150°C without a reduction of strength. They are excellent at forming a strong chemical bond with the matrix [18], so a significant amount of energy is needed to break this bond. This influence negatively the ductility of SHCC because the fibres may rupture early than the slippage of the bond occurs. They have also a good reputation for high resistance to alkali [24], UV, chemicals and abrasion according to manufacture [21] and are stable under heat and moisture exposure [25]. Furthermore, they do not have a risk of corrosion. The disadvantage of those fibres is their price compared to other alternatives. However, this may change in upcoming decades if the demand for those fibres increases in upcoming decades.

The high modulus polyethylene (HMPE) fibres are long chains of aliphatic hydrocarbon [26] making it a thermoplastic substance with a glass transition temperature of approximately -120°C. This kind of polymer chain is not susceptible to chemical attack [27]. This is because polyethylene does not possess any chemical groups that could attract acids, alkalis, or other chemicals at room temperature which could break this chain. This gives HMPE fibres very good chemical resistance. However, due to their hydrophobic nature, those fibres form weak adhesion bonds with cementitious matrix [18]. Furthermore, HMPE fibres possess high tensile strength and modulus of elasticity, but at the same time, keep density low. In perspective, those

fibres are approximately twice as strong as PVA fibres according to [18]. However, the ultimate strain, at which HMPE fibre breaks, is relatively low, but a still considerable amount of energy is needed to be broken [27]. Higher tensile strength in combination with a weak matrix-fibre interface leads to higher ductility of SHCC compared to SHCC with PVA fibres [28].

Steel fibres are the most common type of fibres used in practice due to their relatively cheap production costs. According to [29], the compressive strength is marginally improved by those fibres but the tensile strength can be enhanced by up to 40%. The post-peak ultimate strain and ductility are significantly improved as well. The bonding strength between the matrix and steel fibres can be much easier adjusted than other types of fibres. Next to friction and adhesion at the interface between fibres and matrix, steel fibres with (anchor) hooks are possible to be manufactured to create mechanical interlocking with matrix [30]. The disadvantages of steel fibres are high self-weight and poor workability without any supplementary cementitious material or any admixture [29]. According to [31], steel fibres embedded in concrete are prone to corrosion when expose to chemical or low-pH environments. However, when concrete is well-compacted and sufficient coverage is applied, it is no threat to member integrity and performance. The damage will be limited only to the exposed surfaces.

Shrinkage

According to Luković [4], fibres and fibre-matrix interface are responsible for the neglectable amount of moisture transport, therefore they do not contribute to the driving mechanism of e.g. drying shrinkage which is caused by the moisture migration to a lower relative humidity environment. Drying shrinkage is technically the volume reduction measured in an unloaded specimen at a constant temperature caused by exposing the material to a lower relative humidity environment than the initial one of its pores. However, there are fibres that do absorb a significant amount of moisture e.g. natural fibres. According to [32], natural fibres will swell or shrink depending on relative humidity. This change in strain has an influence on the bond between fibre and matrix.

The amount of drying shrinkage of SHCC is significantly higher when compared to that of the normal concrete [33]. The typical drying shrinkage of normal concrete lays between 0,052% and 0,078% [34]. The ultimate drying shrinkage strain of SHCC may lays between 0,120% and 0,180% [35, 36]. This means that the drying shrinkage of SHCC is at least twice as large as for normal concrete. The primary cause of such large drying shrinkage of SHCC is caused by relatively larger cement content in typical SHCC compared to typical concrete. Since the shrinkage of aggregates is significantly less (almost not noticeable) than that of the hydration product of cement, a material with higher cement content will shrink more. The secondary cause is the small aggregate size that is used in SHCC together with a combination of low water content. In general, SHCC makes use of fine particles, hence the pores in the microstructure will be smaller compared to normal concrete where the coarse and fine aggregates are in equilibrium under the condition that the same water-cement ratio has been used [37]. Those smaller radii of pores will result in higher menisci stresses, so the impact on strain due to shrinkage increases. In the case of restrained strain, the tensile stress starts to build up in the material. After exceeding the tensile strength of SHCC, cracks will appear in the material. No localized cracks in SHCC will appear. It will have rather many fine shrinkage cracks [4].

Both aggregates and fibres control the shrinkage behaviour of cementitious composite. Aggregates, especially coarse particles, are reducing the total shrinkage and are beneficial for stable crack growth. Contrastingly, fibres are more beneficial for controlling crack widths but

also more effective in the absence of large aggregate particles according to [4]. The latter displays higher strain hardening behaviour.

Environmental burden of Strain Hardening Cementitious Composite

On the edge of climate change, no corner of the globe would be free from the consequences of rising temperatures. The number of wildfires increases; sea levels are rising; contamination of drinking water is increasing; and the rate of decrease in biodiversity has never been faster due to human activity. Those events may seem overwhelming at first but there are things that our civilization can do to prevent them from happening. For instance, if a structure has a longer service life, in other words, is more durable, but at the same time more sustainable then this could be one of the main pillars of preventing global climate change from happening. In contrast to the past, the modern civil engineer is more aware of problems that the traditional linear building process may lead to.

Among all construction materials, concrete is currently the most used material on the planet. Unfortunately, concrete requires huge volumes of primary resources, which leads at the end to the depletion of natural resources. The production of cement is a highly energy-intensive process because the cement kiln has to operate at a high temperature of approximately 1450 to 1600°C. To sustain this heat energy, a large volume of fossil fuel is burned leading to the release of pollution into the air, water and soil. The largest problem is the emission of huge quantities of carbon dioxide (CO_2) into the atmosphere due to the burning of fossil fuels. The same quantity of CO_2 is released during the decomposition of calcium carbonate ($CaCO_3$) into calcium oxide (CaO) and CO_2. The environmental impact of the production of concrete may seem bad, but well designed concrete members can last for many decades even in a harsh environment. So, the environmental burden can be spread over many years to come and after all, concrete may be a sustainable alternative if it is applied wisely.

The environmental impact of SHCC is higher than normal concrete for two reasons. Firstly, SHCC makes use of fibres that have to produce and transport. This ingredient is not used in normal concrete. Secondly, the lack of coarse aggregates in SHCC leads to higher consumption of cement compared to normal concrete. To analysis the environmental burden of both materials in-depth, Li [7] has conducted a Life Cycle Analysis (LCA) of SHCC, see Figure 8. The functional unit in this paper was defined as '1000 kg material'. The above-mentioned reasons are clearly visible in the results of [7]. Even though a super-plasticizer is used in small quantities, it shows a significant environmental impact of SHCC compared to RC. Therefore, the use of a super-plasticizer should be classified as the third reason.

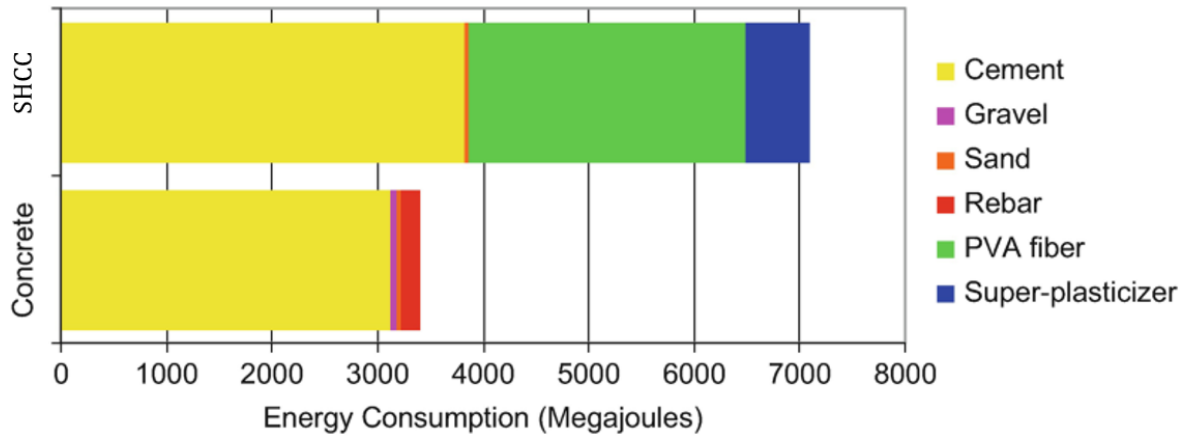

Figure 8 Energy consumption per 1000 kg of steel reinforced concrete and SHCC [7]

There are ways to improve the sustainability of SHCC. According to [27], HMPE fibre has lower carbon footprint material compared to steel fibre and any other synthetic fibre (e.g. PVA fibre) due to the higher strength/weight ratio of HMPE fibre compared to the rest. However, the introduction of recycled aggregates ('green sand') into SHCC does not outweigh a decrease in the performance of crack width control [7]. This study also refers to the higher specific heat of SHCC compared to fibre-less mortar which is beneficial for building heat management when used as an outer face in a building. This could potentially reduce energy consumption when used in façade applications.

All in all, SHCC should not be used at places where excellent durability aspects of SHCC cannot be utilized due to its relatively high environmental impact. Instead, SHCC should be used as a durability enhancement for RC concrete to maximize material performance.

2.2.2 Bonding properties of Strain Hardening Cementitious Composite to concrete

Before discovering Engineering Cementitious Composite[1] (ECC), people used NC or mortar to repair old concrete structures. This type of repair was plagued by debonding of the interface. To improve the service performance of concrete structures, people started to apply SHCC instead as a repair material. For this reason, scientists were more interested in the bonding properties of an interface between new SHCC to old normal concrete. As consequence, the properties of an interface between old NC and new SHCC attracted more attention from the scientific community. For this reason, the effect of an interface between new normal concrete and older SHCC is currently not widely investigated in the literature. So having no other choice, the knowledge gathered from the literature in this subsection would be mostly based on the first type of interface.

The bonding strength of an SHCC-to-concrete interface under shear loads depends on the compressive strength of SHCC and NC, the curing age of the specimen, the curing environment (temperature and relative humidity), the interface roughness, the fibres type and (if applied) additional binding agent strength. Those influencing factors were experimentally investigated by Tian et al. [38] and Gao et al. [39].

The research of [38] has found that the roughness of an interface is the most dominant factor in the failure mode while SHCC strength class and fibre types play a secondary role. The higher roughness of a surface provides a higher contact area as was already explained in 2.1.4 under the headline 'Aggregate interlocking'. To determine the roughness of a surface, the vertical heights of aggregates on the interface are measured and then the average height (the interface roughness value) is evaluated. According to [40], the limit value for the interface roughness value is about 4-5 mm. Higher than this limit result in a weaker interface. In those experiments, the bond strength between cast-in-situ UHTCC and old concrete specimens was tested in a pull-out setup. UHTCC, which is the abbreviation for Ultra-High Toughness Cementitious Composite, is similar to SHCC but with much higher strength. Furthermore, the research of [38] has found that higher SHCC compressive strength leads to higher interface shear strength and that the PVA fibres with higher ultimate tensile strength only marginally influence the shear strength according to [38].

Two types of specimens are widely used to investigate the shear bonding strength of an interface, see Figure 9. Three slant shear specimens consisting of ECC with 28-day compressive strength of 39,9 (±0,38) MPa and normal concrete C35/45 have been tested in the research of [39]. The mean shear strength value that has been found at room temperature equals 5,5 MPa. However, two of three specimens have been broken before loading, so there is no data about the standard deviation and the variation coefficient. Furthermore, the heat treatment up to 200 °C after standard curing for 28 days has a beneficial effect on the strength. The shear strength

[1] It is the other name for the Strain Hardening Cementitious Composite (SHCC).

value at 200 °C equals 6,87 (±0,87) MPa with the variation of coefficient at 12,7%. The shear strength values beyond 200 °C perform worse than at room temperature.

The research of [38] has used single-sided shear specimens to obtain shear strength value. In this research, one type of normal concrete C40/50 and four different types of ECC with different average 28-day compressive strengths (from 21,7 MPa up to 40.8 MPa) have been used for specimens. The interface shear strength was found in a range between 0,33 (±0,04) MPa for low-strength class ECC and 1,11 (±0,15) MPa for high-strength class ECC. The specimens with a thick epoxy resin layer with coarse aggregates applied on the interface result in the following shear strength range: 0,86 (±0,08) MPa for low-strength class ECC and 3,33 (±0,13) MPa for high-strength class ECC.

To enhance the bonding strength of an interface, additives could be added at the cement manufacturing stage. According to [40, 41], fly ash, slag, and silica fume are improving the bond properties of an interface. But there is also admixture that could improve this property, for example expansive agent and SBR latex [40]. According to the slant shear test conducted by [41], 52,8% higher bonding strength is obtained by SHCC with slag at age of 28 days compared to the monolithic concrete reference specimens. SHCC with fly ash reached only 36,4% improved the bonding strength compared to the reference specimens. The reference specimens were made of concrete with 28-day compressive strength of 31,9 (±1,1) MPa.

The results of [25, 41, 42] show that concrete with PVA fibres has significantly better bonding performance than normal concrete, so in general, an SHCC-to-concrete interface is stronger than a concrete-to-concrete interface.

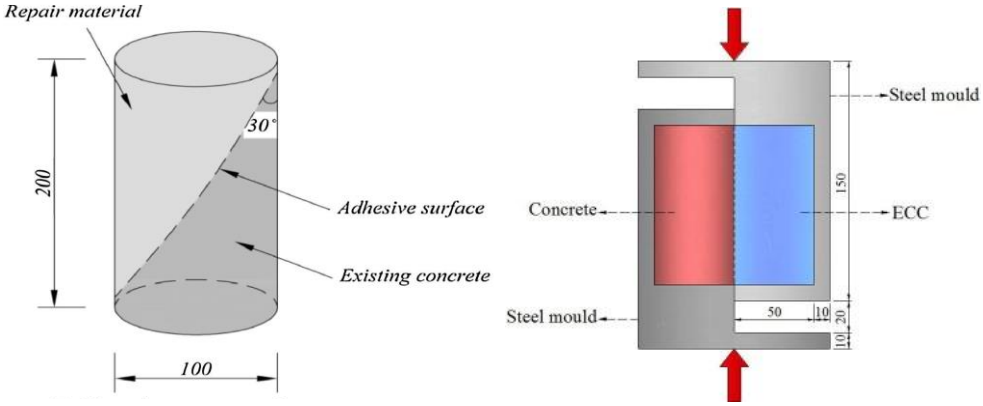

Figure 9 Left: The slant shear specimen according to American ASTM C882 standard [39]. Right: Single-sided shear test setup [38].

The main conclusion drawn from these experiments is that SHCC is able to achieve a strong bond with other concrete surfaces. Moreover, this should be possible without any beforehand preparation of a surface. This is a rather promising clue for not only the main experiment of this thesis but more for practical applications wherein practices such preparation is most likely very costly. Of course, a thick epoxy resin layer with coarse aggregates gives the highest interface shear strength but it is unlike to be used in practice due to high cost. Nevertheless, it can increase the strength by a factor of 3, as demonstrated in the research [38].

Shrinkage of interface

The differential (drying and/or thermal) shrinkage between SHCC laminate and NC can cause failure bonding at the interface. Thermal and drying shrinkage are the major contributors to this kind of failure because of moisture migration according to Luković [4]. Due to restrained shrinkage deformations, the stress is generated which cause delamination between SHCC and

normal concrete. Therefore, the properties of SHCC should be chosen not only strictly on strength performance but also the exposure environment of the system.

Next to material properties, an interlocking mechanism plays a significant role in counteracting the shrinkage of an interface between SHCC and regular concrete. Despite reviewing the database of scientific papers and books, no experiment has been found which conducted measurements of effectiveness on a profile interface between SHCC and normal concrete.

2.2.3 Experimental benchmarks on RC beams with shear strengthening using SHCC

Major advantages and disadvantages of SHCC have been described above. In theory, an optimal solution would be to apply SHCC and NC together in a so-called hybrid system. In this way, those materials should cover their shortcomings. Some hybrid SHCC-concrete beams have been already tested in the past under shear loads. This section will give an overview of the gathered knowledge from those experiments.

Before 2015, there was hardly any knowledge about the shear behaviour of hybrid SHCC-concrete beams. The first research on the shear behaviour of RC beams without transverse reinforcement strengthened by SHCC layers was conducted by Zhang et al. [43] in 2015. In 2019, Wang et al. [44] conducted a similar experiment but on slightly larger members and along with thicker SHCC layers. A year later, Wei et al. [45] published their work on the shear behaviour of hybrid RC beams with transverse reinforcement. The experiment was successful however their hybrid beams experienced minor delamination of SHCC laminates just before the peak load.

There are also some other types of hybrid beams strengthened by SHCC elements tested on shear capacity. In 2018, Wu et al. [46] tested RC beams strengthened by precast thin-walled (20 mm) U-shape UHTCC. Multiple M16 penetrating bolts have been added to improve the integration of the U-shape. The increase in shear strength reached 67,4% [46]. In 2020, Shang et al. [47] proved that U-shape SHCC with stirrups is an effective way of shear-strengthening damaged RC beams due to fire. The recent research (2022) by Li et al. [48] shows the great potential of thin-walled (15 mm and 25 mm) U-shapes in their experiments on the shear strengthening of RC beams with and without transverse reinforcement. The increase in shear strength ranged between 8,40% and 66,39% [48].

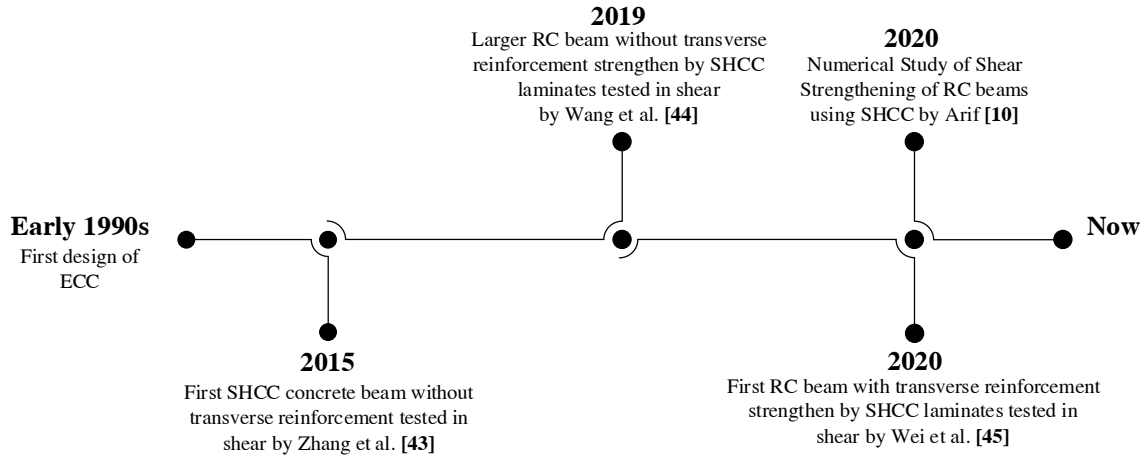

Figure 10 Timeline of studies of shear strengthening of RC beams using SHCC laminates.

The following pages will be devoted to two experimental studies by Zhang et al. [43] and Wei et al. [45]. Those studies were selected due to similarity in the research questions of those papers and this master thesis. Results from those studies have been compared to the results of this thesis, see chapter 4.

Experimental investigation by Zhang et al. (2015) on shear capacity of RC beams without transverse reinforcement strengthen by SHCC laminates

On 23 January 2015, the research paper [43] titled "*Failure behavior of strain hardening cementitious composites for shear*" has been published and was written by Zhang et al. This paper presents an experimental investigation of an RC beam without transverse reinforcement strengthened by SHCC laminates. This research focuses mainly on the amount of increased shear load carrying capacity of such a hybrid beam. Additionally, they documented the crack pattern of their hybrid beams.

Table 2 Mix proportions of SHCC [43]

Component	Dry Weight [kg/m^3]
Cement {not specified}	1267,9
Silica fume	230,8
Fine sand	153,9
Expansion agent	40,0
Water	338,5
Superplasticizer	15,4
PE fibres	14,6
Air reducing agent	0,06

In Table 2, the list of ingredients was provided for SHCC with 28-day compressive strength of 91 MPa used during the experiment [43]. As it can be deducted, the water-cement ratio equals 0,27 and water to binder (cement + silica fume) ratio equals 0,22. The results obtained from the uniaxial tensile test on the dog bone specimens are shown in Figure 11. Young's modulus of SHCC is estimated to equal 29 GPa.

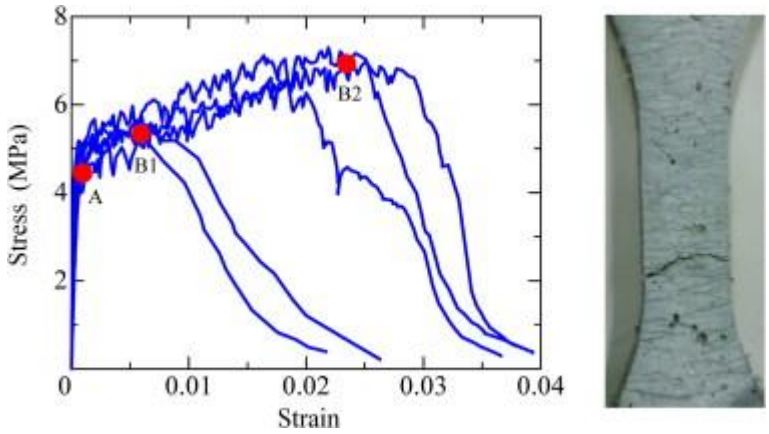

Figure 11 Uniaxial tensile test results of SHCC [43]

The list of ingredients of normal concrete was not provided in this paper. The only information known about this concrete is that it had the 28-day compressive strength of 27 MPa and Young's modulus of 23,5 GPa.

In Figure 12, the schematization of the hybrid beam is shown. The specimens were

reinforced with two steel longitudinal ribbed bars with a diameter of 10 mm. No shear reinforcement has been applied. The steel, which was used for this reinforcement, has a yield strength of 345 MPa and Young's modulus of 200 GPa [43]. The beam span has been chosen to be 1 m which results in 0,5 m of shear span and this corresponds to $\eta_a \approx 3{,}0$. The cross-section of 100 mm by 200 mm was strengthened by casting SHCC laminates with a thickness of 5 mm or 10 mm on two sides. But before SHCC was cast on the side surface, those sides 'were washed out using a retarder to obtain roughed surfaces' quoting from [43].

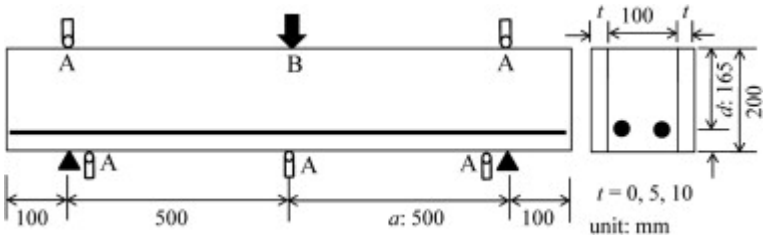

Figure 12 Geometry of RC beams strengthened by SHCC laminates [43]

Figure 13 shows the results of the experiment. The beam strengthened by 10 mm SHCC laminates has reached the highest shear load capacity of about 90 kN. That is almost twice the capacity of the reference beam. The beam strengthened by 5 mm SHCC laminates has reached about 70 kN. Even though Young's modulus of this SHCC is higher than the normal concrete, the beams followed the same linear elastic branch up to a certain point.

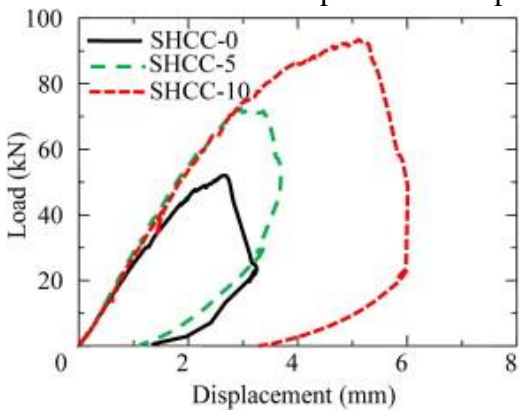

Figure 13 Load–displacement curve. SHCC-0 is the RC beam without SHCC laminates. SHCC-5 is the RC beam with 5 mm thick SHCC laminates. SHCC-10 is the RC beam with 10 mm thick SHCC laminates. [43]

It appears that angle of the diagonal crack is smaller for the beams strengthen by SHCC laminates than the RC beam without SHCC laminates, see Figure 14.

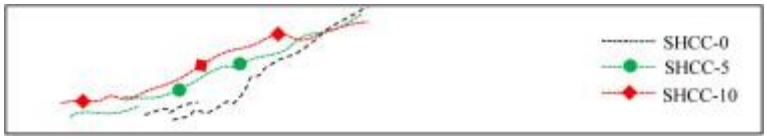

Figure 14 Positions of localized cracks. SHCC-0 is the RC beam without SHCC laminates. SHCC-5 is the RC beam with 5 mm thick SHCC laminates. SHCC-10 is the RC beam with 10 mm thick SHCC laminates. [43]

Those results show that the SHCC laminates enhance the shear capacity of RC beams without transverse reinforcement. Furthermore, the ductility of the strengthened beams improves as well.

Experimental investigation by Wei et al. (2020) on shear capacity of RC beams with transverse reinforcement strengthen by high strength SHCC laminates

In 2020, the research paper [45] titled "*Shear strengthening of reinforced concrete beams with high strength strain-hardening cementitious composites (HS-SHCC)*" was published. The experiment conducted in this paper has a more realistic scenario than the previous paper since transverse reinforcement had been applied as in the practice. This research tries to answer the following question: whether SHCC laminates are efficient in the shear strengthening of reinforced concrete structures?

Table 3 Mix proportions of HS-SHCC [45]

Component	Massa ratio
Cement {not specified}	0,8
Silica fume	0,2
Sand	0,3
Water	0,2

+ 2% PE fibres by volume of the mixture

Table 3 provides the ingredient list for the HS-SHCC mix used in this paper. According to tests on small cubes (40×40×40 mm^3) by Wei et al. [45], 28-day compressive strength of 120 MPa has been reached. Further, the tensile strength of 10 MPa on dog bone specimens has been reported, as seen in Figure 15. This material has Young's modulus of 35 GPa

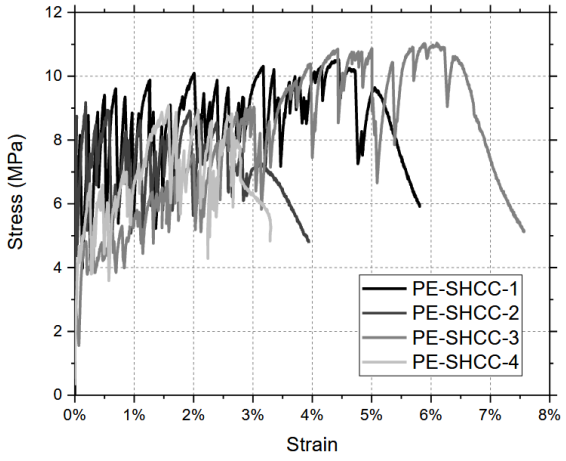

Figure 15 Tensile stress-strain curves of HS-SHCC after 28 days [45]

The properties of the normal concrete were as follows: 36 MPa for 28-day compressive strength, and 26 GPa for Young's modulus. The compressive strength was tested on cubes 100 mm × 100 mm × 100 mm.

This research paper [45] documents experimental beams with two different shear span parameters: 'Group A' with $\eta_a = 1{,}5$, and 'Group B' with $\eta_a = 2{,}5$. Since the shear span parameter of 'Group B' is close to the shear span parameter that will be used in this master's thesis, only 'Group B' will be extracted from the paper. In this group, four beams have been tested: two reference beams and two hybrid beams. The detailed geometries of the beams are shown in Figure 16. The hybrid beams were only strength on one side (in the red area). The reinforcement steel has a yield strength of 585 MPa and Young's modulus of 200 GPa according to [45]. The SHCC laminates had a thickness of 10 mm and were cured for 28 days.

Those laminates were cast directly on the surfaces of the beams. The loading speed for all beams was set to 0,01 mm/s.

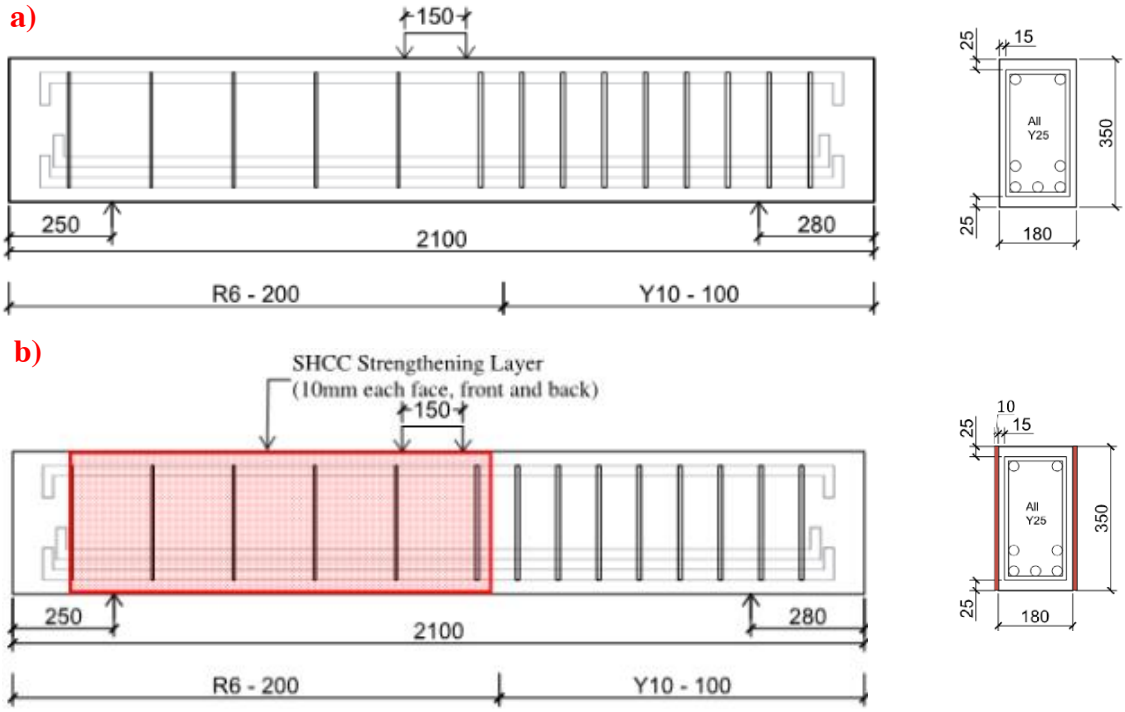

Figure 16 Group B: a) Geometry of reference RC beams. b) Geometry of hybrid beams strengthen by HS-SHCC laminates (red area). [45]

All beams have failed in shear and developed large diagonal cracks. Furthermore, the hybrid beams developed minor debonding of SHCC laminates but they did not completely delaminate from the beams. In Figure 17, the results of the experiment are shown. The shear capacity of the hybrid beam has increased by 18,82% compared to the reference beams [45]. The strength of the hybrid beams was governed by the strength of the interface between normal concrete and HS-SHCC. This could mean that the utilization of HS-SHCC laminates was not complete, thus the hybrid beams could reach a higher shear capacity than the results presented in Figure 17. The shear failures of the hybrid beams were still brittle like the shear failures of the reference beams.

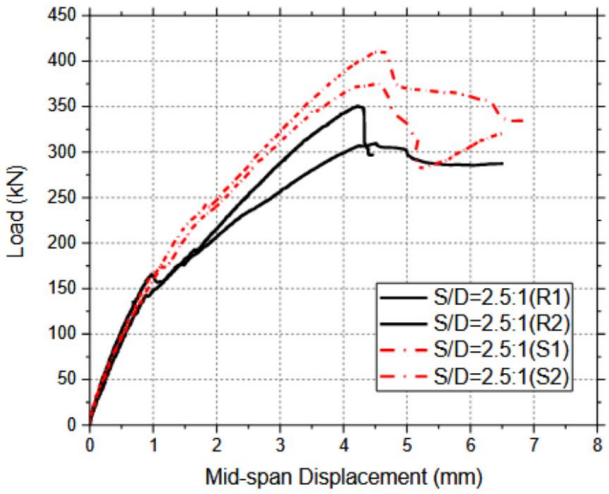

Figure 17 Load–displacement curve. R1 and R2 are the refence beams. S1 and S2 are hybrid beams. [45]

2.3 Conclusions of the Literature Study

Based on the above literature study, the following conclusions can be drawn:

- The shear capacity of a longitudinally reinforced concrete beam without transverse reinforcement is primarily governed by the shear span parameter (η_a), steel ratio in the tensile zone (ρ), and compressive strength of concrete (f_c).
    - Ghaffar et al. [12] have listed more factors which have a (minor) influence on the shear capacity. These are aggregate interlocking, the density of concrete, specimen size (size effect), fibre volume in concrete, the tensile strength of concrete, geometry of a specimen, boundary conditions of support and loading plates, and dowel action (spreading of tensile reinforcement and end anchorage of tension reinforcement).
- Strain Hardening Cementitious Composite has superior tensile properties to concrete. Those properties are highly dependent on the compositions of a mix, so there is no universal value for certain properties:
    - The main benefit of SHCC is its high ductility. The range of tensile strain at 90% strength is somewhere between 2% and 5% [17, 43].
    - A typical crack pattern of SHCC, as seen in Figure 11, has multiple parallel cracks. This is more advantageous than one concentrated crack like in normal concrete because the width of an individual SHCC crack is significantly smaller. The width of cracks in SHCC is ranging between 60 μm and 100 μm according to Luković [4]. The advantages of smaller crack width are:
        - Good self-healing properties,
        - Smaller water permeability: water with ions is one of the ingredients that lead to the corrosion of reinforcement. Furthermore, the effects of freeze-thaw cycles are smaller.
    - The common range of the tensile strength of an SHCC is between 2 to 8 MPa. Yet, it highly depends on many factors like compressive strength, fibre volume fraction and type of fibres. There have also been developed high strength strain-hardening cementitious composites (HS-SHCC) with over 10 MPa tensile strength [45].
- SHCC has great durability but does not belong to the least environmental burden materials according to Li [7]. SHCC can be more sustainable than normal concrete only if its superior properties are utilized. In other cases, there is more damage done to the natural environment than it is worth.
- Thus answering the first sub-question: there is still a lack of knowledge regarding the interface concrete connection between old SHCC and new normal concrete. Most of the current experiments [38, 39, 41] on this subject have been performed on the interface between new SHCC and old normal concrete. Based on experiments [38] conducted by Tian et al., the positive effect on the interfacial shear strength is mainly due to higher SHCC compressive strength and interfacial roughness. The secondary parameter, which is positively correlated with the interfacial shear strength, is the ultimate tensile strength of fibres according to data [38]. Based on experiments [39] conducted by Gao et al., the limited temperature treatment (< 200 °C) might be beneficial to the bonding performance of the interface, but at extreme values (> 200 °C) the interfacial shear strength is lower. Furthermore, Şahmaran et al. [41] have discovered that SHCC with

slag has higher bond shear strength than SHCC with fly ash. But the contribution of slag in SHCC should be denoted as the secondary parameter since primary parameters (SHCC compressive strength and interfacial roughness) had much greater effects on the interfacial shear strength.

The main unresolved aspects of those experiments are the unrealistic loading scenarios and actual environmental conditions that members are exposed to in practice. Specifically, there are no members with pure shear (moment = 0) alone: there is always an interaction between shear and moment. Further, the geometry of the interface will not always be plain. The structures are more complex and varied. They come in all shapes and forms.

Despite those aspects, it has been discovered that the most effective way to increase interfacial strength between SHCC and normal concrete is to add roughness to the surface and increase the strength of SHCC. This can be used as guidance during designing the hybrid interface.

- The biggest disadvantage of SHCC is its significant magnitude and rate of drying shrinkage compared to that of normal concrete. In most cases, the drying shrinkage of SHCC is at least twice as high as that of NC. This has a huge negative consequence for interfaces between old SHCC and new normal concrete because they are prone to delamination at an older age.
- In the recent past, scientists have conducted a few experimental investigations [43, 44, 45] of shear behaviour on RC beams with SHCC laminate. Using SHCC the laminates with a thickness of 10 mm improves shear capacity between 18% and 50% based on those papers. The shear failures of those hybrid beams were still brittle and sudden as the control groups. Some of the tested hybrid beams show debonding of SHCC laminates which resulted in premature failure.

3

Design of beams

"The best design is the simplest one that works."

Albert Einstein

The three-point bending test will be conducted on four hybrid SHCC-concrete beams (the experimental group) and two reference RC beams (the control group). This chapter shows only the design calculations of the control group according to Eurocode 2. It is crucial for the success of this experiment that all beams fail in shear. Therefore, a large margin of difference between shear and flexural capacity is left to assure the desired failure mechanism.

The first section shows the calculation of the shear and flexural capacities of the RC beam without shear reinforcement according to Eurocode 2 approach. In the second section, the calculation of the shear and flexural capacities of the RC beam with shear reinforcement according to the Eurocode 2 approach are shown. In the paragraph below, the main parameters are listed which have been used for the design of those beams.

Material properties and mechanical properties for all RC beams

The effective span of all beams is chosen to be 1 m. The beams have a rectangular cross-section with dimensions of 200 mm × 120 mm. Hence, every shear span parameter (η_a) remained equal to 3. The self-weight of beams is neglected. The beams are loaded by the concentrated load 'F' at mid-span. The beams are simply supported. The target capacities are based on theoretical mean values:

Geometric parameters:

$Span$	$L = 1$	$[m]$
$Cover$	$c = 25$	$[mm]$
$Height$	$h = 200$	$[mm]$
$Width$	$b = 120$	$[mm]$
$Second\ moment\ of\ area$	$I = \frac{1}{12} \cdot b \cdot h^3 = 8 \cdot 10^7$	$[mm^4]$

Reinforcement parameters:

$Average\ yield\ strength$	$f_{ym} = 560$	$[MPa]$
$Diameter\ of\ longitudinal\ reinforcement$	$\emptyset_{16}^{L} = 16$	$[mm]$
$Numbers\ of\ longitudinal\ rebars$	$n = 2$	$[-]$
$Area\ of\ longitudinal\ reinforcement$	$A_{sl} = n \cdot \frac{\pi \cdot \emptyset_{16}^{L\ 2}}{4} = 402{,}12$	$[mm^2]$
$Effective\ height$	$d = h - c - \frac{\emptyset_{16}^{L}}{2} = 167$	$[mm]$
$Longitudinal\ reinforcement\ ratio$	$\rho_{sl} = \frac{A_{sl}}{b \cdot d} \cdot 100\% = 2{,}01$	$[\%]$

Concrete parameters:

Properties of C20/25 according to NEN-EN 1992-1-1:2011 Table 3.1:

$Characterstic\ compressive\ strength$	$f_{ck} = 20$	$[MPa]$
$Mean\ compressive\ strength$	$f_{cm} = 28$	$[MPa]$
$Mean\ Young's\ modulus$	$E_{cm} = 30$	$[GPa]$

3.1 Target capacity of RC beam without transverse reinforcement (first series)

Shear capacity

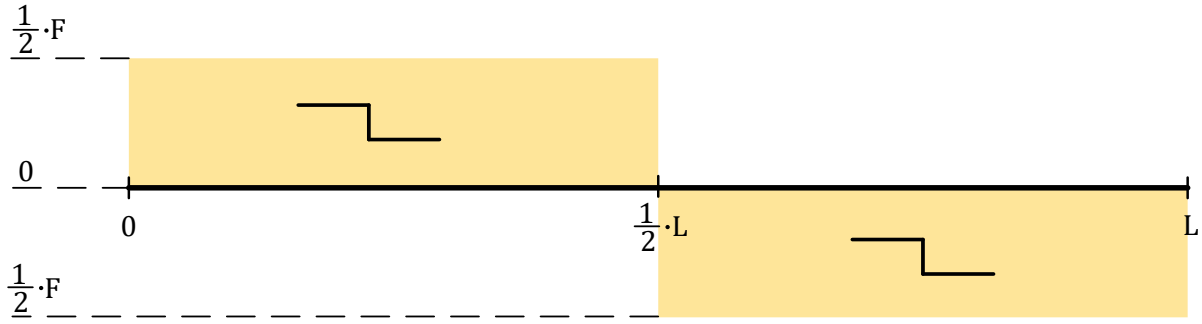

Figure 18 Shear diagram of a simply supported beam loaded by concentrated load at the midspan.

The percentage of longitudinal reinforcement (ρ_l) that contributes to the shear strength is defined as follows:

$$\rho_l = \min\{\rho_{sl}\,; 2{,}0\%\} = \min\{2{,}01\%; 2{,}0\%\} = 2{,}0\% \qquad \textit{(Eq. 3.0)}$$

According to NEN-EN 1992-1-1:2011 §6.2.2:

$$k = \min\left\{1 + \sqrt{\frac{200}{d}}; 2{,}0\right\} = \min\left\{1 + \sqrt{\frac{200}{167}}; 2{,}0\right\} = 2{,}0 \qquad \textit{(Eq. 3.1)}$$

$$v_{Rm,min} = 0{,}035 \cdot k^{\frac{3}{2}} \cdot \sqrt{f_{cm}} + k_1 \cdot \sigma_{cp} = 0{,}035 \cdot 2^{\frac{3}{2}} \cdot \sqrt{28} + 0{,}15 \cdot 0 = 0{,}524\,\frac{N}{\text{mm}^2} \qquad \textit{(Eq. 3.2)}$$

$$v_{Rm,c} = 0{,}18 \cdot k \cdot (\rho_{sl} \cdot f_{cm})^{\frac{1}{3}} = 0{,}18 \cdot 2 \cdot (2{,}0 \cdot 28)^{\frac{1}{3}} = 1{,}379\,\frac{N}{\text{mm}^2} \qquad \textit{(Eq. 3.3)}$$

$$V_{Rm,c} = max\{v_{Rd,min}; v_{Rm,c}\} \cdot \text{b} \cdot d = 1{,}379 \cdot 120 \cdot 167 = 27{,}63\ \text{kN} \qquad \textit{(Eq. 3.4)}$$

Thus, the shear capacity of the beam equals:

$$F_V = V_{Rm,c} \cdot 2 = 27{,}63 \cdot 2 = 55{,}3\ \text{kN} \qquad \textit{(Eq. 3.5)}$$

Flexural capacity

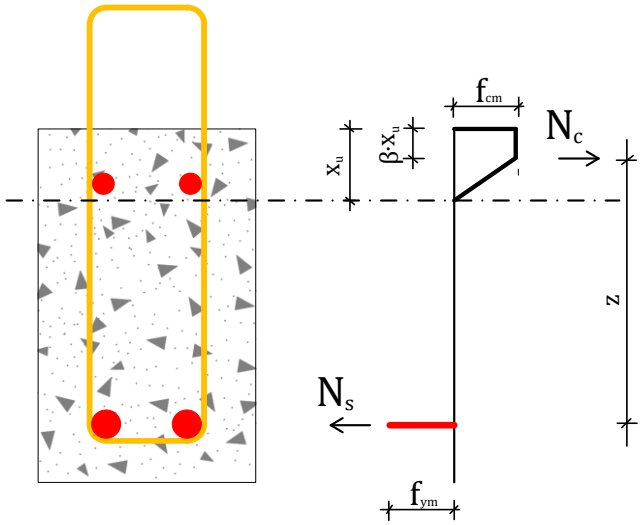

Figure 19 Internal forces in cross-section generated by ultimate moment.

$$N_s = A_{sl} \cdot f_{ym}; \quad N_c = \alpha \cdot x_u \cdot b \cdot f_{cm} \qquad \textit{(Eq. 3.6)}$$

$$\sum Forces = N_c - N_s = 0 \rightarrow x_u = \frac{A_{sl} \cdot f_{ym}}{\alpha \cdot b \cdot f_{cm}} = \frac{402{,}12 \cdot 560}{\frac{3}{4} \cdot 120 \cdot 28} = 89{,}36\ mm \qquad \textit{(Eq. 3.7)}$$

$$z = d - \beta \cdot x_u = 167 - \frac{7}{18} \cdot 89{,}36 = 132{,}25\ mm \qquad \textit{(Eq. 3.8)}$$

$$M_{Rm} = N_s \cdot z = 402{,}12 \cdot 560 \cdot 132{,}25 = 29{,}78\ kNm \qquad \textit{(Eq. 3.9)}$$

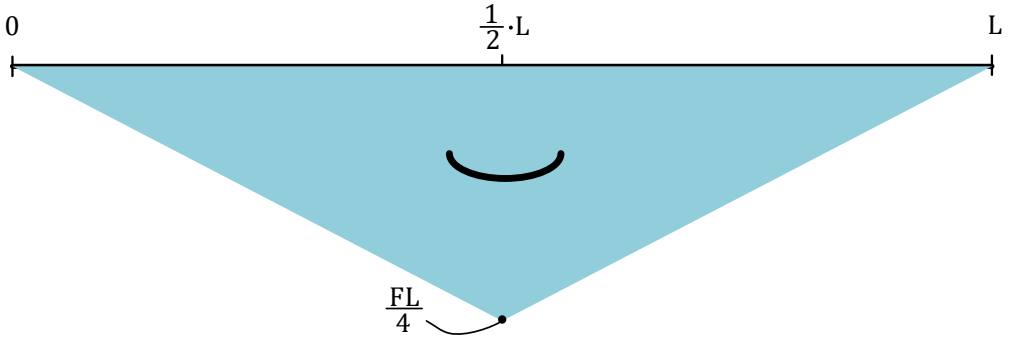

Figure 20 Moment diagram of a simply supported beam loaded by concentrated load at the midspan.

So, the moment capacity of the beam equals:

$$F_M = \frac{M_{Rm} \cdot 4}{L} = \frac{29{,}78 \cdot 4}{1} = 119{,}1\ \text{kN} \qquad \textit{(Eq. 3.10)}$$

As shown above, the shear capacity (55,3 kN) of this design is lower than its moment capacity (119,1 kN), therefore shear failure is expected.

3.2 Target capacity of reference beam with (minimum) transverse reinforcement (second series)

Shear capacity

The minimum shear reinforcement ratio in the Netherlands according to NEN-EN 1992-1-1+ C2:2011 §9.2.2(5) equals:

$$\rho_{w,min} = \frac{0{,}08 \cdot \sqrt{f_{cm}}}{f_{ym}} = \frac{0{,}08 \cdot \sqrt{28}}{560} = 7{,}56 \cdot 10^{-4} \qquad \textit{(Eq. 3.11)}$$

$$\rho_w = \frac{A_{sw}}{s \cdot b_w \cdot \sin(\alpha)} \qquad \textit{(Eq. 3.12)}$$

$$\rightarrow \frac{A_{sw,min}}{s} = \rho_{w,min} \cdot b_w \cdot \sin(\alpha) = 7{,}56 \cdot 10^{-4} \cdot 120 \cdot \sin(90°) = 90{,}71 \text{ mm}^2/m \qquad \textit{(Eq. 3.13)}$$

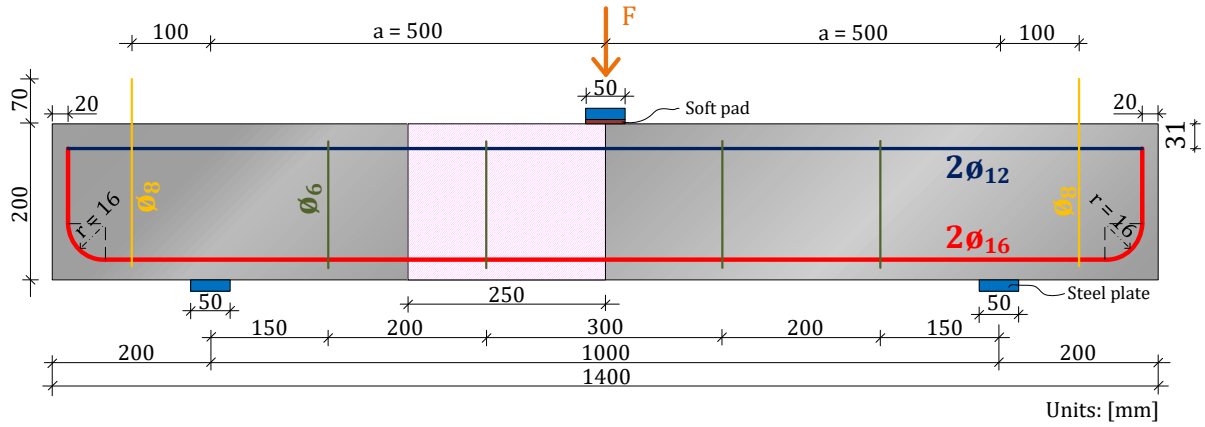

Figure 21 Side view for proposed reinforcement design. The highlighted area indicates the most loaded stirrup.

Thus minimum shear area within length s:

$$A_{sw,min} = \frac{A_{sw,min}}{s} \cdot s = 90{,}71 \cdot 0{,}25 = 22{,}68 \text{ mm}^2 \qquad \textit{(Eq. 3.14)}$$

The smallest practical diameter is 6 mm. The area of $\emptyset_{sw}6$ shear reinforcement with two legs:

$$A_{sw,6} = 2 \cdot \frac{\pi \cdot \emptyset_{sw}{}^2}{4} = 2 \cdot \frac{\pi \cdot 6^2}{4} = 56{,}55 \text{ mm}^2 \qquad \textit{(Eq. 3.15)}$$

The shear resistance according to NEN-EN 1992-1-1+ C2:2011 §6.2.3(3):

$$V_{Rm,s} = \frac{A_{sw,6}}{s} \cdot z \cdot f_{ym} \cdot \cot(\theta) = \frac{56{,}55}{250} \cdot 132{,}25 \cdot 560 \cdot \cot(21{,}8°) = 41{,}9\ kN \qquad \textit{(Eq. 3.16)}$$

$$V_{Rm,max} = \frac{\alpha_{cw} \cdot b \cdot z \cdot v_1 \cdot f_{cm}}{\cot(\theta) + \tan(\theta)} = \frac{1 \cdot 120 \cdot 132{,}25 \cdot 0{,}6 \cdot 28}{\cot(21{,}8°) + \tan(21{,}8°)} = 91{,}9\ kN \qquad \textit{(Eq. 3.17)}$$

$$V_{Rm} = min\{V_{Rm,s}; V_{Rm,max}\} = 41{,}9\ kN \qquad \textit{(Eq. 3.18)}$$

Thus, the shear capacity of the beam equals:

$$F_V = V_{Rm} \cdot 2 = 41{,}9 \cdot 2 = 83{,}8 \text{ kN} \qquad \textit{(Eq. 3.19)}$$

The shear capacity is lower than flexural capacity. This means that the beam will fail in shear.

Flexural capacity

The flexural capacity of RC beam with or without transverse reinforcement is the same, therefore the moment capacity of the beam has been already calculated in Eq. 3.10. Hence, the shear capacity of 83,8 kN is still lower than the flexural capacity of 119,1 kN. This beam should fail in shear as well.

4

Experimental program

"A scientist in his laboratory is not a mere technician:
he is also a child confronting natural phenomena
that impress him as though they were fairy tales."

Maria Skłodowska-Curie

The description of the manufacturing process of four hybrid SHCC-concrete beams, two reference beams, and their corresponding specimens is provided in this chapter. In the first series, two hybrid SHCC-concrete beams and one reference beam with longitudinal steel ribbed bars were tested. The main objective of the first series was to investigate the behaviour of shear failure of hybrid SHCC-concrete beams without transverse reinforcement with outer SHCC layers. The point of attention was the interface between SHCC and normal concrete. In the second series, two hybrid beams with longitudinal and vertical (shear) reinforcement were tested. The main objective of the second series was to investigate the behaviour of shear failure of hybrid SHCC-concrete beams with transverse reinforcement. The second goal was to investigate the influence of boundary conditions on the behaviour of a hybrid beam. This chapter also includes a list of the materials with their properties, as well as descriptions of specimen preparation, casting procedure and the testing set-up.

4.1 Experimental design

4.1.1 Cross-section designs of (hybrid) beams

The main test program consists of two series of hybrid SHCC-concrete beams with a height of 200 mm and a width of 120 mm. C20/25 has been selected for normal concrete class strength. The reinforcement design was based on the work of Haung et al. [49].

The beams from the first series are reinforced with two steel B500 longitudinal ribbed bars with a diameter of 16 mm. The distance between the main longitudinal bars equals 28 mm. No 'effective' transverse (shear) reinforcement has been placed, but only two stirrups (⌀8 B500) have been provided for more convenient lifting operations. Those lifting stirrups do not affect the shear capacity of a beam. Furthermore, two steel B500 longitudinal rebars with a diameter of 12 mm in the compression zone have been placed. Those bars are needed only for execution reasons and provided a neglectable shear capacity of a cross-section.

Two of the three beams from the first series have been strengthened by outer SHCC side layers. The emphasis is on the interface between normal concrete and SHCC, therefore two different hybrid beam designs were invented. The first beam is strengthened by two smooth SHCC laminates with a through-thickness of 10 mm and without any surface preparation, see Figure 22b). The second beam is strengthened by two SHCC laminates with shear keys height of 10 mm and a thinner through-thickness of 10 mm and without any surface preparation, see Figure 22c). Please note that the detailed design of SHCC laminates with shear keys is discussed in section 4.3. The last beam remains unstrengthen and will be referred to as the reference beam, see Figure 22a). The side covers equal 30 mm (including the through-thickness of SHCC laminate). The bottom cover equals 25 mm.

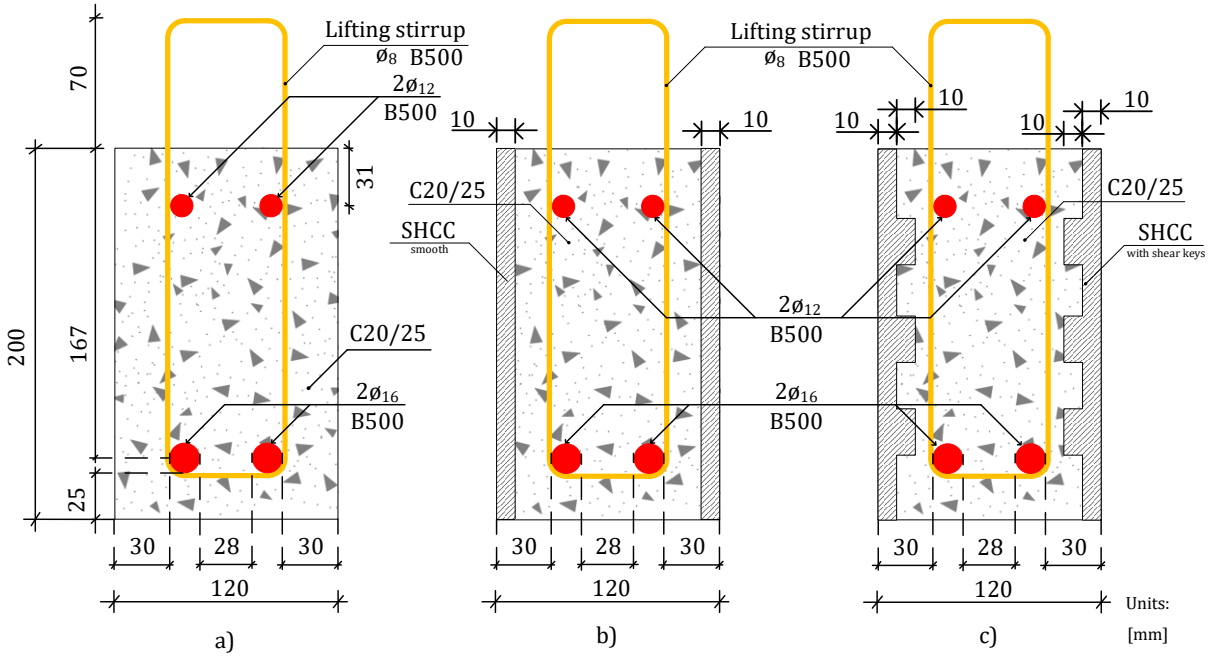

Figure 22 The cross-sections of the first series of the beams.
a) Reference RC cross-section. b) Hybrid cross-section with smooth SHCC laminates.
c) Hybrid cross-section with SHCC laminates with shear keys.

The cross-section designs of the second series consist of one conventional reinforcement concrete cross-section and two hybrid cross-sections, see Figure 23. Both hybrid cross-sections are strengthened by two SHCC laminates with shear keys (the dimensions

remained unchanged). The emphasis is on the different supporting boundary conditions, see section 4.4.1. In practice, engineers are obligated to apply a minimum amount of shear reinforcement in accordance with Eurocode 2, in order to make sure the design shear resistance is larger than the design load. This is done due to prevent brittle failure of concrete as it is explained in section 2.1. To reflect the realistic scenario in the experiment, four stirrups (⌀6 B500) have been provided with governing stirrup spacing of 250 mm, see Figure 25.

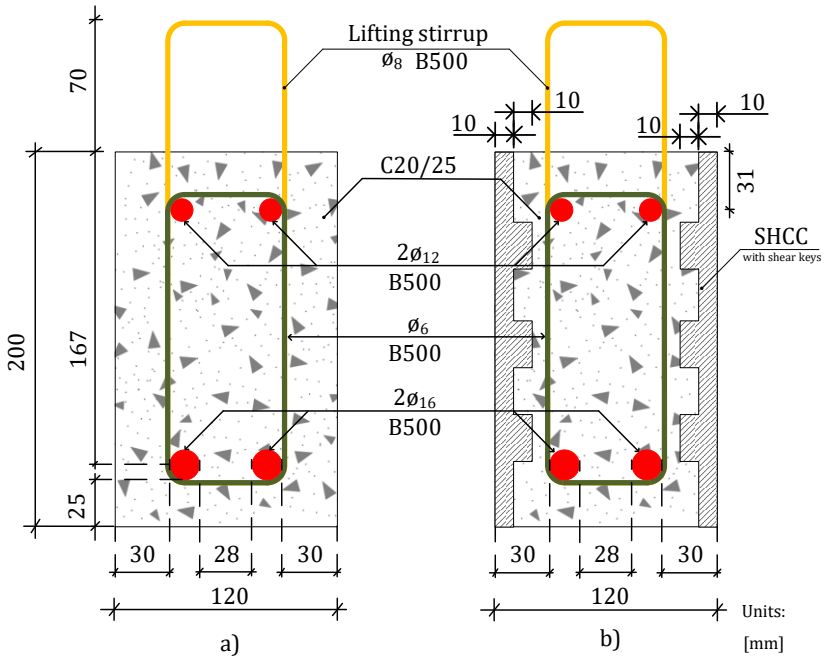

Figure 23 The cross-sections of the second series of the beams.
a) Reference RC cross-section with vertical (shear) reinforcement.
b) Hybrid cross-section with SHCC laminates with shear keys.

4.1.2 Designs of (hybrid) concrete beams in sideview

Since shear failure behaviour and the corresponding capacity of a beam are the objects of the investigation, a three-point bending test setup has been selected. This setup produces the flexural peak stresses at the midpoint but since a flexural crack at this location is not the subject of research, a four-point bending test setup is not necessary. The beam span has been chosen to be 1 m which results in 0,5 m of shear span and this corresponds to $\eta_a \approx 3{,}0$. This value of the shear span parameter is commonly encountered in practices. Additionally, the beams have been made extra longer by adding 0,2 m on each side. This extra length is needed to place the lifting stirrup and counter some concentration of stresses near the support. This means that the total length of beams equals 1,4 m. The detailed designs are shown below:

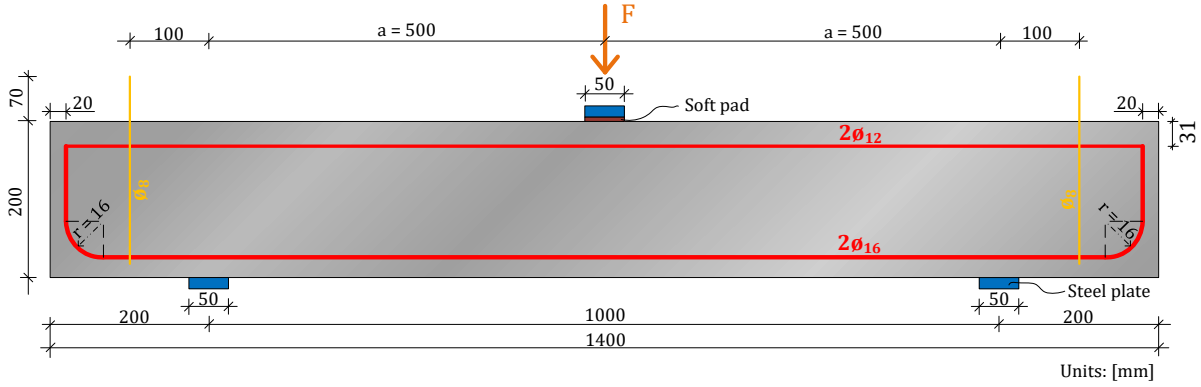

Figure 24 Design of (hybrid) concrete beams of the first series in side view.

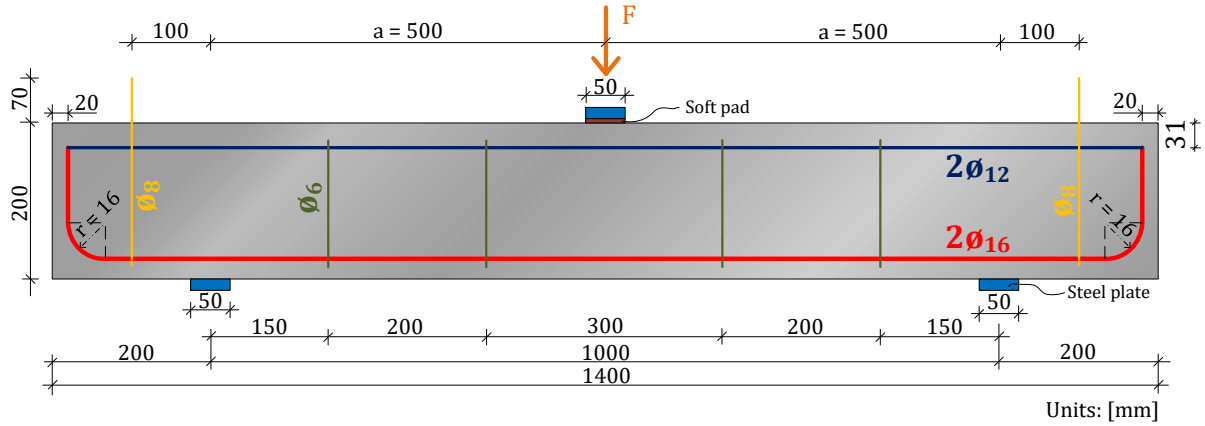

Figure 25 Design of (hybrid) concrete beams of the second series in side view.

4.2 Materials

The recipes for materials, which have been used during the casting of specimens, would be presented in this section. First, SHCC composition will be discussed and after that the composition of normal concrete.

4.2.1 Strain-Hardening Cementitious Composite mixture

The composition of SHCC consists of cement, limestone powder, PVA fibres, water and superplasticizer, see Figure 26. The more detailed composition of SHCC can be found in Table 4. This SHCC mix was developed by MSc Shan He and was published in [50]. The water-to-binder ratio equals 0,40 and a polycarboxylate-based superplasticizer (MasterGlenium 51 con. 35% NL) to binder ratio equals 0,23. The binder, CEM III/B 42.5 N, is delivered from ENCI (the Netherlands) and it consists of 66–80% blast furnace slag (BFS) and 20–34% clinker according to [50]. The fibre volume equals 2,02%. The properties of PVA fibre from Kuraray (Japan) are found in Table 5. The water-to-powder ratio equals 0,27 and the filler-to-binder ratio equals 0,50. The filler is finely grinded limestone powder. It is produced by Calcitec® from Carmeuse (Belgium). The procedure for standardized mixing of SHCC has been provided in Appendix A which has been followed during the preparation of SHCC batches.

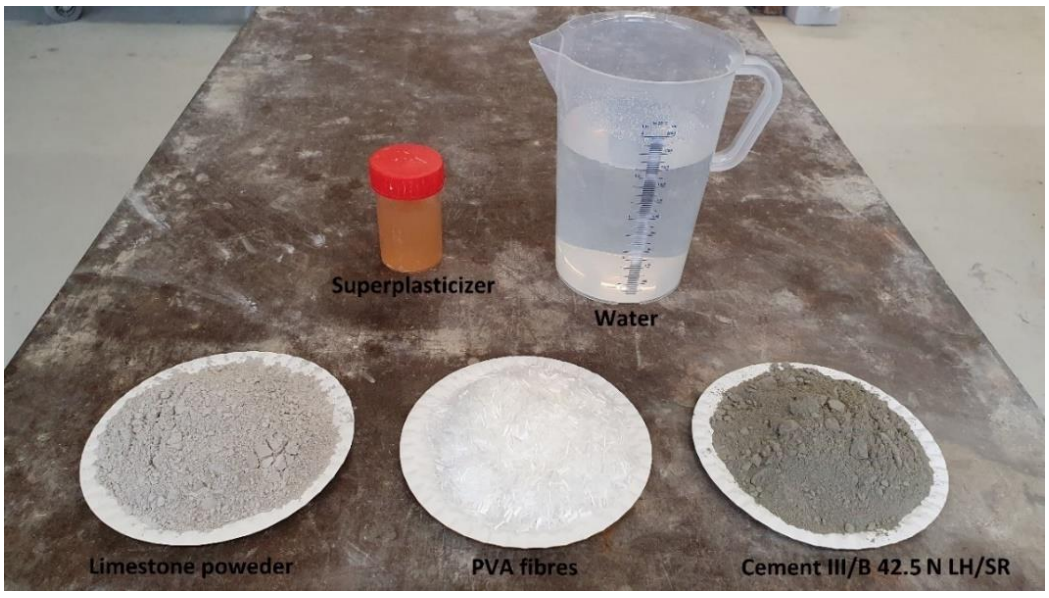

Figure 26 Ingredients for Strain-Hardening Cementitious Composite

Table 4 SHCC mix design developed by He [50]

Component	Dry Weight [kg/m^3]	Volume [L]
CEM III/B 42.5 N LH/SR	1050	354,730
Limestone Powder	525	194,44
Water	420	420,00
Superplasticizer	2,4	2,00
PVA fibres	26	20,00
Air content		9
Total Volume		**1000**

As described in subsection 2.2.1, the environmental impact of SHCC is considerable compared to normal concrete looking only at the functional unit of 1000 kg material. Therefore, quoting from [18], „the SHCC mix used in this study is developed at TU Delft in efforts to produce green SHCC by using locally available materials in the Netherlands." The same suppliers for ingredients for the experiments have been used as in the work of [18] and [50].

Table 5 Physical and mechanical properties of PVA fibre according to [18] and [50]

Property	PVA fibre
Tensile Strength (MPa)	1640
Young's Modulus (GPa)	41,100
Density (kg/m^3)	1300
Diameter (mm)	0,04
Length (mm)	8
Surface oiling coating (wt.%)	1,2

4.2.2 Normal concrete mixture

The role of normal concrete composition is not the topic of this study and to decrease the number of factors that could influence the aim of the research, therefore it has been decided to use only one type of NC mix for all specimens. To assure shear failure by given dimensions in section 4.1, C20/25 has been selected. This has relatively low-value strength properties, but it is still used in practice these days. In Table 6, the composition of the concrete mix used in the experiments is shown. The water-cement ratio equals 0,60 and superplasticizer (MasterGlenium 51 con. 35% NL) to binder ratio equals 0,10. This mix was developed by Blagojević [52]. Note that a maximum aggregate size (D_{max}) used in this mix equals 16 mm. To prevent blocking the aggregates between reinforcement, the ACI 211.1-91 specified that the minimum clear spacing between individual reinforcing bars is limited to:

$$\frac{3}{4} \cdot minimum\ distance\ between\ reinforcement = \frac{3}{4} \cdot 28 = 21\ mm \geq D_{max} = 16\ mm$$

Table 6 Concrete mix design developed by Blagojević [52]

Component	Dry Weight [kg/m^3]	Volume [L]
CEM I 42.5 N	260	82,28
Sand 0,125 – 0,250 mm	78,830	29,86
Sand 0,250 – 0,500 mm	256,199	97,05
Sand 0,500 – 1 mm	256,199	97,05
Sand 1 – 2 mm	157,661	59,72
Sand 2 – 4 mm	98,538	37,33
Gravel 4 – 8 mm	394,152	149,30
Gravel 8 – 16 mm	729,181	276,21
Water	156	156
Superplasticizer	0,26	0,22
Air content		15
Total Volume		**1000**

4.3 Specimen preparation – casting and curing

In this section, the fabrication and curing process of laminates for hybrid beams will be discussed. Thereafter, the manufacture and curing of hybrid and reference beams will be explained in detail. The fabrication of the quality control samples and curing will be described at the end of the section.

4.3.1 SHCC laminates, hybrid beams and reference beam

As described in section 4.1.1, there are two designs for laminates: a smooth one and one with shear keys. The detailed design of a laminate with shear keys is shown in Figure 27. This laminate board has a through-thickness of 10 mm just like a smooth laminate has. The shear keys have a cylindrical shape with a height of 10 mm and a diameter of 25 mm. The prior small-scale experiment showed that shear keys with a width of 10 mm cast vertically are not reliable because very few fibres make bridges between a shear key and laminate board (see Appendix B) due to too small notches in the mould. To ensure that the fresh normal concrete with D_{max} of 16 mm can flow freely between shear keys, the distance between shear keys' edges is not smaller than 25 mm.

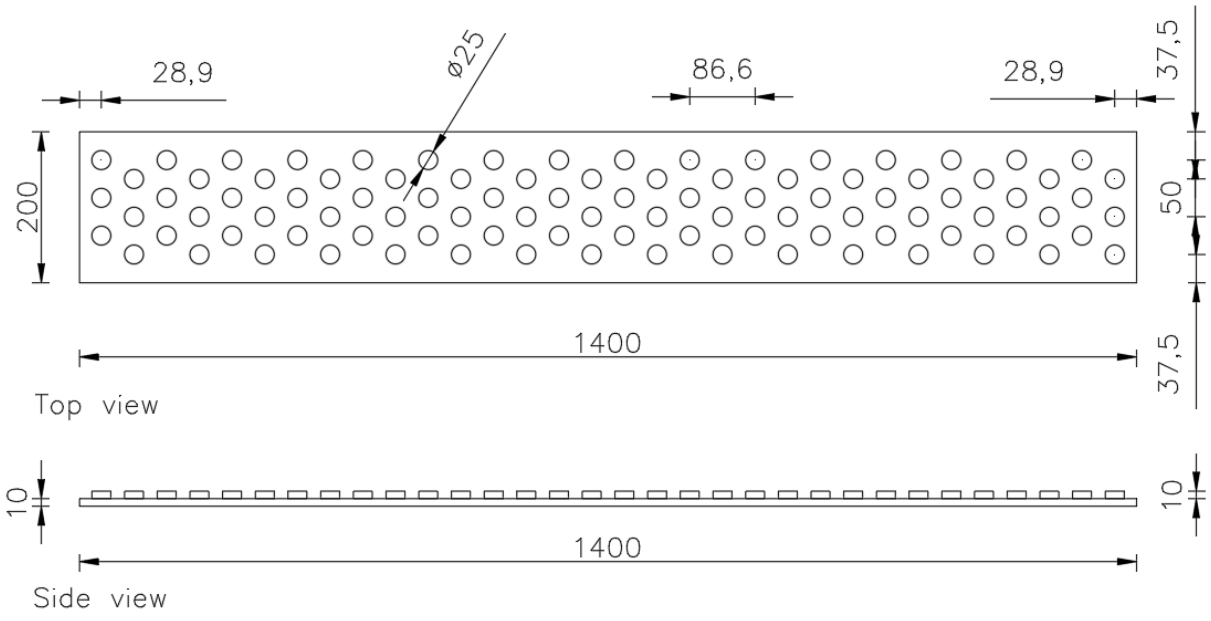

Figure 27 Design of laminate with shear keys. Length unit in [mm].

Figure 28 a) Wooden cylindrical studs with a diameter of 25 mm. b) Process of gluing wooden studs to board formwork with double-sided tape. c) Formwork board with studs.

Figure 29 a) Mould for rubber mesh. b) Single rubber mesh. c) Rubber meshes glued on formwork board.

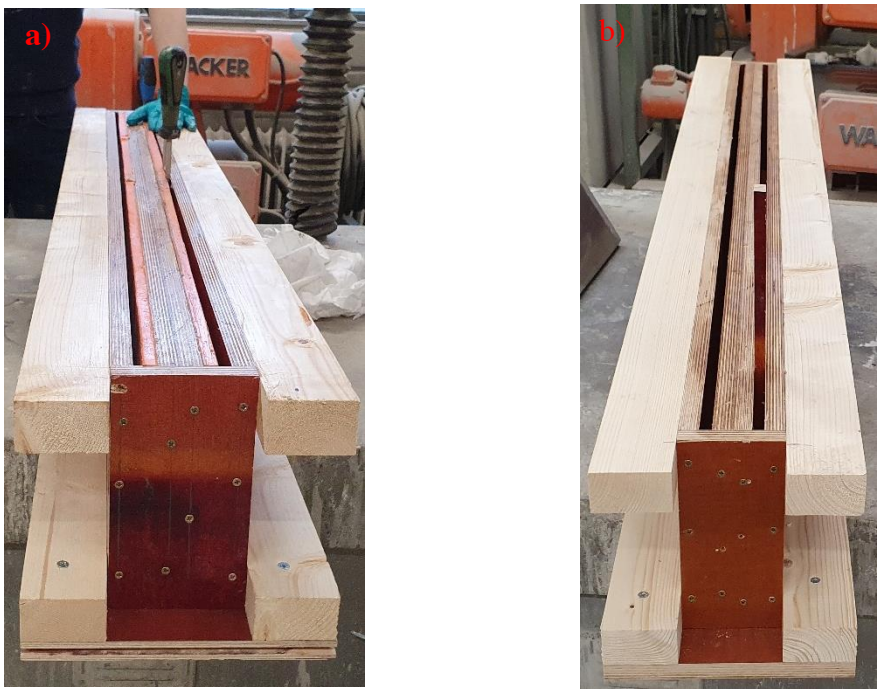

Figure 30 a) Mould for laminates with shear keys. b) Mould for smooth laminates.

The first step in the fabricating of a laminate with shear keys was to glue wooden cylindrical studs onto the formwork board according to the design shown in Figure 27. Such board with studs (see Figure 28) was placed inside the beforehand prepared mould. Straightaway, this mould was filled with fluid silicone rubber (Poly-Service 8510 set), see Figure 29a). After waiting at least 6 hours, the rubber mesh was ready to be demoulded, see Figure 29b). In total, two rubber meshes were fabricated. They are shown in Figure 29c) glued to the new formwork board. This new formwork board was placed in the mould shown in Figure 30a). Figure 30b) is the picture of the mould to fabricate smooth laminates. Both moulds were filled with SHCC and after waiting around 24 hours, the laminates were sufficiently hardened to be demoulded. Two smooth laminates and two laminates with shear keys were fabricated for the first series of the beams, shown in Figure 31 and 32. For the second series of the beams, four laminates with shear keys were fabricated, see Figure 36.

Fabrication of the first series of the beams

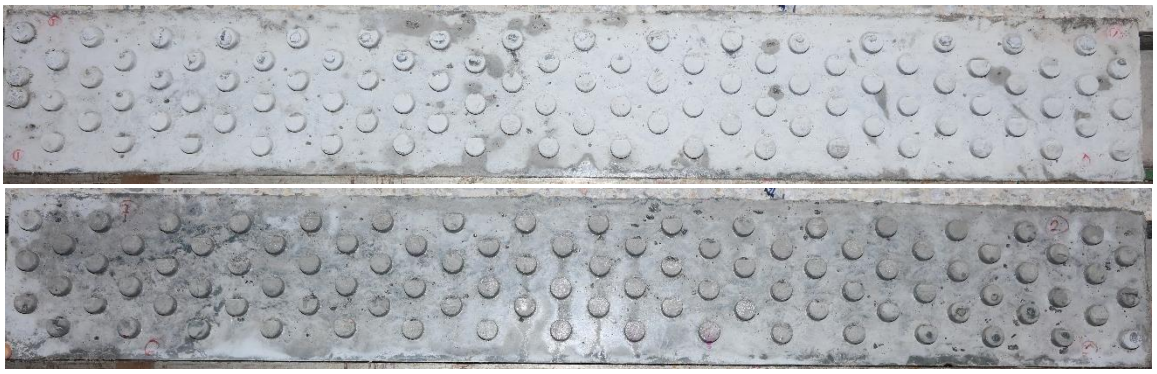

Figure 31 SHCC laminates with shear keys (the first series of the beams)

Figure 32 SHCC smooth laminates (the first series of the beams)

The laminates were cured under the standard curing condition (20 (± 2) °C and relative humidity >95%) for 14 days. After this period, they were removed from the curing room and dried to avoid additional moisture in the interface. This extra water could weaken the bearing capacity of the interface because this additional water would locally increase the water-cement ratio of normal concrete.

After drying, the laminates were ready to be positioned in the mould with the reinforcement cages, see Figure 33. Plastic spacers were placed to ensure a uniform cover but also to prevent shifting the reinforcement cages during the vibrating of the mould. Later, the mould was filled with normal concrete up to one-third of its height and then it was vibrated. This procedure was repeated two more times to fill the mould completely. The beams were sealed for 28 days using a plastic sheet (Figure 34) and have been kept under a constant temperature of 20 (± 2) °C.

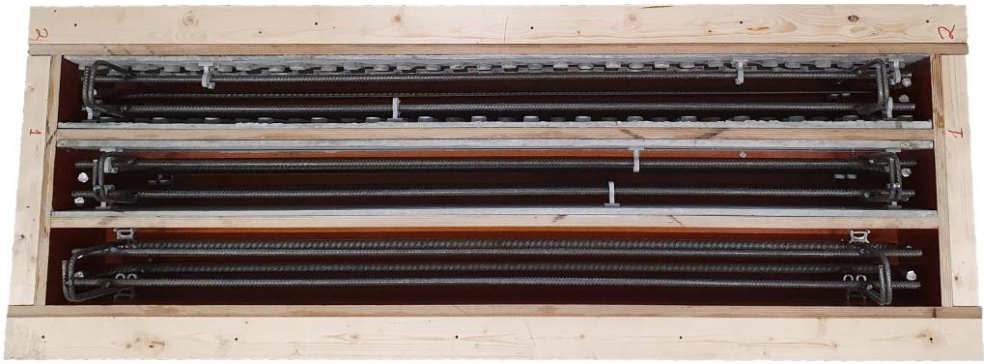

Figure 33 Mould for two hybrid beams and reference beam (the first series of the beams)

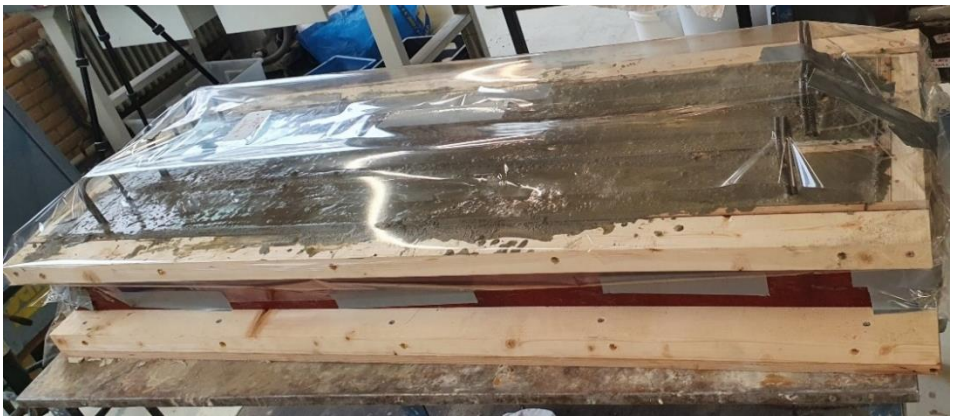

Figure 34 Two hybrid beams and one reference beam sealed (the first series of the beams)

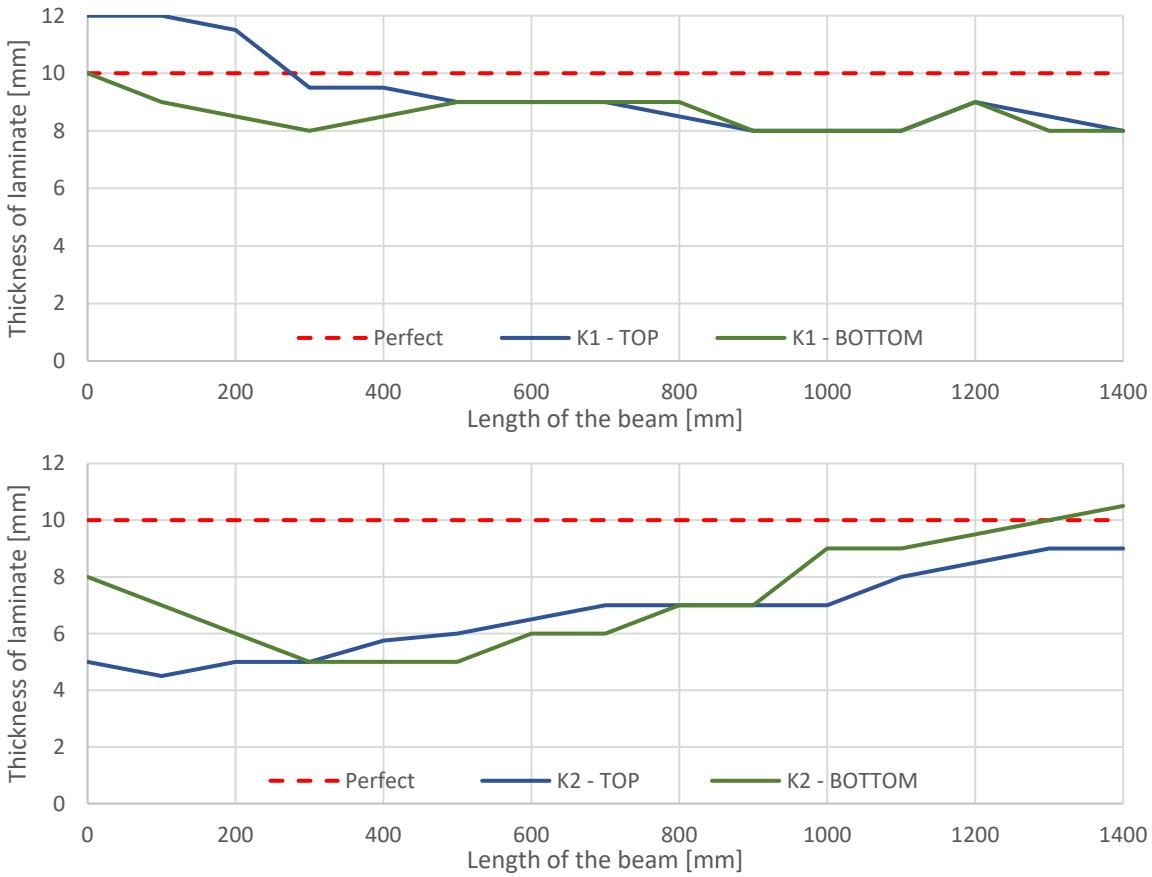

Figure 35 The deviation of through-thickness of shear keys laminates in respect to the perfect laminate. The top graph shows the through-thickness versus the length of K1 laminate. The bottom graph shows the through-thickness versus the length of K2 laminate.

The through-thickness of shear keys laminates K1 and K2 deviate from 10 mm at certain spots, see Figure 35. The reason for this deviation is due to the unequal thickness of rubber meshes, see Figure 29 b) and c). During the hardening of those rubber meshes, the mould displayed in Figure 29 a) has deformed significantly due to the outwards pressure of liquid rubber. Hence, the rubber meshes were in some places thicker. This should not be surprising because this mould was heavily exploited in the past.

The laminates have been placed in the mould (see Figure 33) in such a way that the thinner part of K2 laminate is compensated by the thicker part of K1 laminate. As a reminder, 200 mm and 1200 mm are the locations of the supports. At the location of 300 mm, which is close to one of the supports, the lowest total through-thickness has been measured. Approximately 30% of the ideal total through-thickness is missing.

Fabrication of the second series of the beams

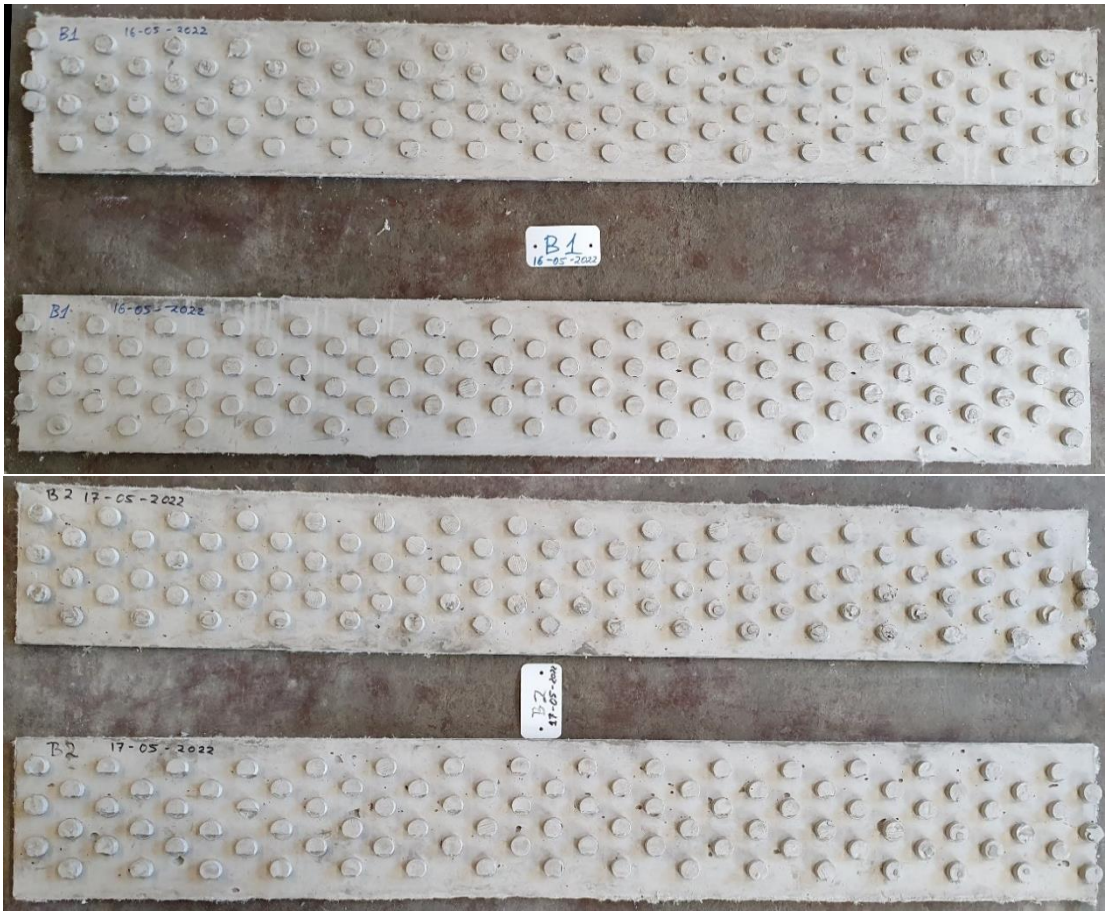

Figure 36 SHCC laminates with shear keys (the second series of the beams)

Laminates for the second series of the beams have been cured for 21 days in the standard curing condition (20 (± 2) °C and relative humidity >95%). That is one week longer than in the case of the first series. The reason behind this is that the delivered reinforcement was not in accordance with the drawings that have been sent to the factory. It had to be corrected manually in the laboratory Stevin II.

Figure 37 Mould for two hybrid beams and reference beam (the second series of the beams)

After drying, the laminates and reinforcement cages have been placed in the mould, see Figure 37. From an execution point of view, shear keys are slightly inconvenient. A few shear keys were in the way of some stirrups. Plastic spacers were placed at the bottom and the sides to ensure a uniform cover. The mould was ready to be filled with normal concrete. Here as well, the mould was filled up to one-third of its height first and then vibrated. This procedure was repeated two more times to fill the mould fully. The beams were sealed for 35 days by using a plastic sheet (Figure 38) at a constant temperature of 20 (± 2) °C. That is one week longer than in the case of the first series due to logistic problems in the laboratory.

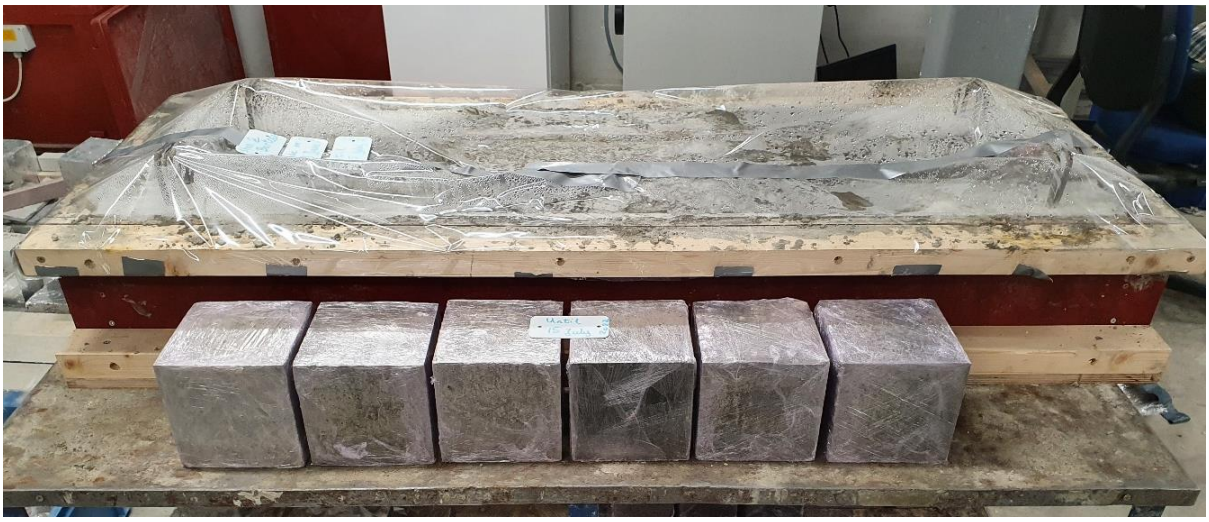

Figure 38 Two hybrid beams and one reference beam sealed (the second series of the beams)

4.3.2 SHCC cube specimens, SHCC dog bone specimens and SHCC prisms specimens

During manufacture process of the beams, five separate batches of SHCC have been casted. Three batches were needed to cast all laminates in the first series and two batches in the second series. Casting all laminates with all quality control groups in one batch was not possible due to limiting volume of the mixer. To ensure that the properties of SHCC are in a desirable range, the quality check for every batch has been performed.

In case of the first series of the beams: one batch was consumed by two smooth laminates, so there was need for only one quality group. However, one batch was consumed for every laminate with shear keys and therefore, two quality groups were prepared, and as consequence, one laminate is referred to as ‘K1’ and the other one is referred to as ‘K2’.

In case of the second series of the beams: one batch was consumed by two laminate with shear keys which results in one quality group referred to as ‘B1’. The quality group of the second batch is referred to as ‘B2’.

Figure 39 SHCC cube specimens 40 mm × 40 mm × 40 mm

To control compressive strength of SHCC, cubes with dimension of 40 mm × 40 mm × 40 mm were prepared, as seen in Figure 39. Those cubes were cut from a SHCC prism with dimension of 150 mm × 40 mm × 40 mm (see Figure 40). For every batch of SHCC, three prism specimens of SHCC were prepared and cured in different environments and ages:

i. Cured for 14 days in standard curing conditions and then tested;
ii. Cured for 28 days in standard curing conditions and then tested;
iii. Cured for 14 days in standard curing conditions and then sealed for 28 days in airtight conditions at 20 (± 2) °C next to the beams. (Please note: it is the exact same treatment as laminates in the beams). After this, the specimen was ready to be tested.

Note: The expression "standard curing conditions" refers to the specific enviroment conditions in a climate room which are defined in NEN-EN 12390-2. This room has a temperature of 20 (± 2) °C and relative humidity >95%.

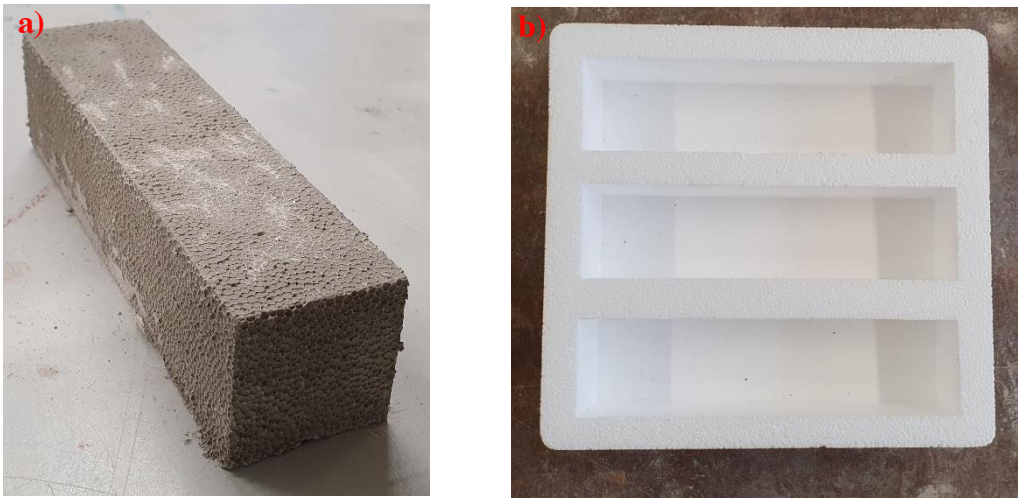

Figure 40 a) SHCC prism specimen 150 mm ×40 mm ×40 mm. b) Styrofoam mold (160 mm long) for 3 SHCC prism specimens

To determine the so-called scale factor, six standard size cubes (150 × 150 × 150 mm^3) have been prepared at different ages and under two different curing conditions, see points i) and ii) above for more details. Due to limitations in the volume of the Hobart mixer, those cubes had to be cast in separate batches than the prisms and the laminates.

To verify the tensile strength of SHCC, dog bone specimens have been prepared with dimension shown in Figure 41 and tested under the uniaxial tensile test set-up. Top and bottom edges have been glued to thick steel plates to reduce eccentric bending moments and increase the bonding area with the set-up. Specimens were loaded by prescribed deformation of 0,005mm/sec. The strain was defined as the average ratio of the changes in measurement lengths of 80 mm in two LVDTS. For every batch of SHCC, four dog bone specimens were prepared and cured at different conditions:

i. Two specimens were cured for 28 days in standard curing conditions and then tested;
ii. Two specimens were cured for 14 days in standard curing conditions and then sealed for 28 days in airtight conditions at 20 (± 2) °C next to the beams. (Please note: it is the exact same treatment as laminates in the beams). After this, the specimens were ready to be tested.

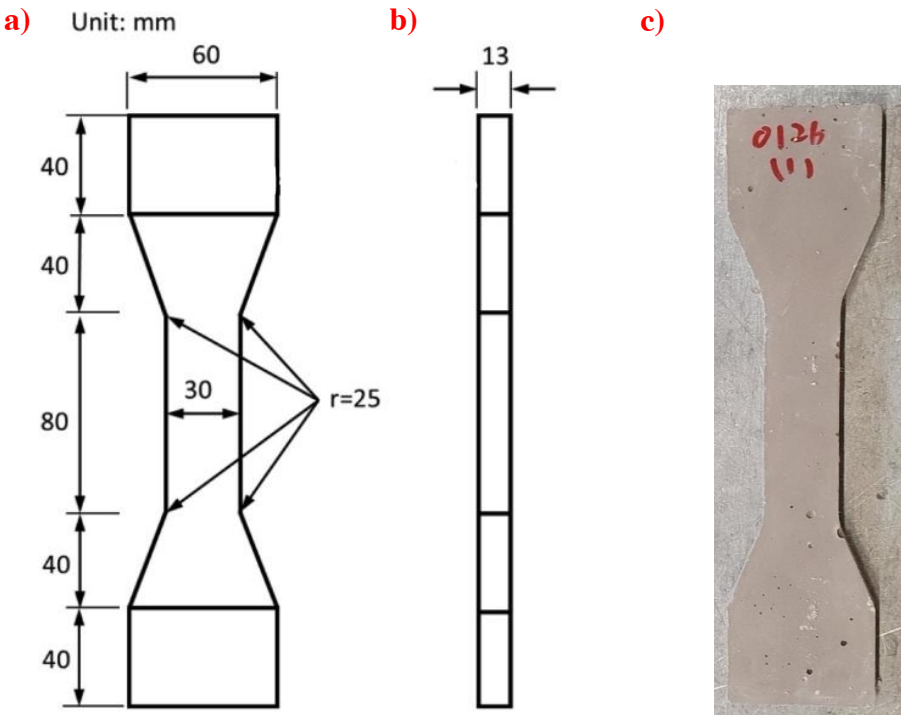

Figure 41 Details of SHCC dog bone specimens: a) front view [53]; b) side view (mm) [53]. c) typical SHCC dog bone specimen

From the literature study in section 2.2.1 and 2.2.2, an important point to attention regarding the behaviour of SHCC has been drawn. Shrinkage of SHCC is at least twice as big as shrinkage of normal concrete. This results in residual stresses at the interface between SHCC and normal concrete. Therefore, it has been decided to measure shrinkage behaviour of SHCC. For this purpose, two set of three prism specimens each (shown in Figure 42) has been prepared with different curing conditions.

Figure 42 Left: SHCC prism specimens (150 mm ×40 mm ×40 mm) for shrinkage test. Right: Setup for length measurement of a prism specimen.

4.3.3 Normal concrete cubes and prism specimens

It was decided to do also a quality check for normal concrete. For this purpose, six cube specimens with a dimension of 150 mm × 150 mm × 150 mm and three prism specimens with a dimension of 400 mm × 100 mm ×100 mm were prepared. The shapes are thus in accordance with NEN-EN 12390-1. The curing conditions for those specimens were the same. They were

sealed with foil and kept at 20 (± 2) °C for 28 days next to the beams. The cubes were subjected to the uniaxial compressive test to verify compressive strength. The prims were loaded to obtain Young's modulus of normal concrete. Those specimens were loaded in three cycles up to $f_c/3$ as specified in NEN-EN 12390-13. The speed of loading was set on 0,5 kN/sec.

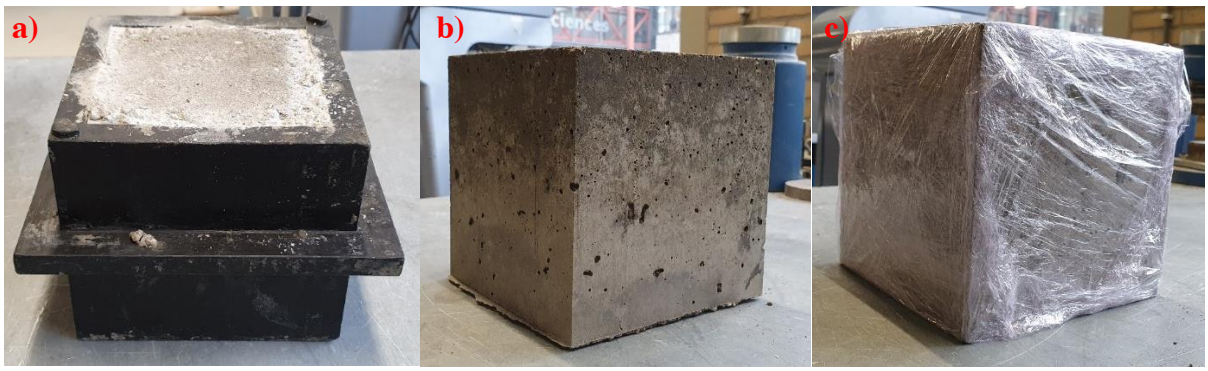

Figure 43 Normal concrete cube specimen 150 mm × 150 mm × 150 mm. a) cube in mould; b) perspective view of concrete cube; c) sealed cube specimen.

Figure 44 Normal concrete prism specimen 400 mm × 100 mm × 100 mm. a) perspective view of concrete prism; b) prism in mould; c) sealed prism specimen.

After complying the test on the concrete prism, those specimens were cut into three cubes with a dimension of 100 mm × 100 mm × 100 mm, see Figure 45. The cubes were subjected to the uniaxial compressive test to verify the compressive strength of the concrete, but foremost to check the quality of the prism specimens.

Figure 45 Normal concrete cube specimens 100 mm × 100 mm × 100 mm

4.4 Structural testing and bending setups of beams

In this section, the description of measuring setups and the three-point bending configuration that have been used during the testing of the beams are provided. First, the three-point bending configuration is presented. As mentioned in section 4.1.2, this configuration remained the same for all beams. After this, the detailed description of setups of the first series of the beams are given and subsequently in the last part, monitoring setups of the second series of the beams are reported.

4.4.1 Three-point bending configuration

Beams were loaded by a concentrated load introduced by the hydraulic piston shown in Figure 46. It has been decided to generate this load as prescribed deformation. This type of loading is often referred to as displacement control because an applied load is increased by adding small increments of displacement. In this particular test, a value of 0.01 [mm/s] was selected for the increment values. The path length refers to the displacement of the piston. The displacement control allows for measuring the deformation of beams from elastic behaviour and nonlinear up to the failure and even beyond the peak load.

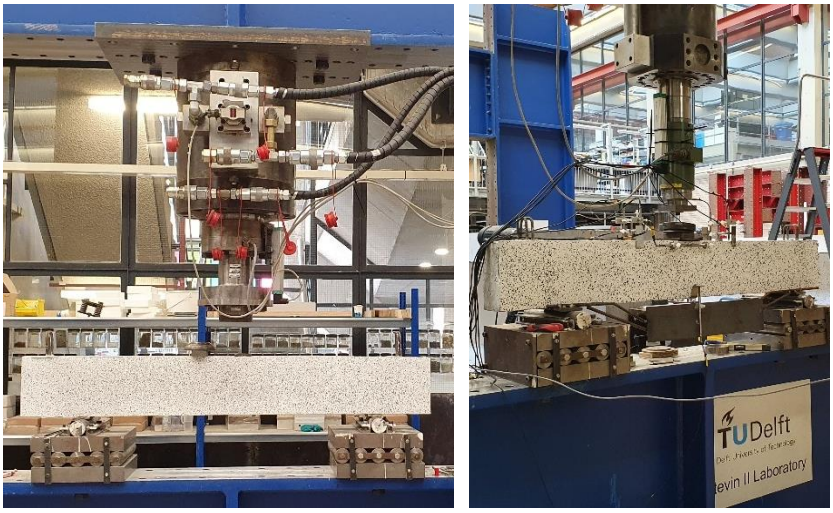

Figure 46 Right: hydraulic piston 1000 kN (first series).
Left: hydraulic piston 400 kN (second series).

The loading condition for every beam in all series was the same. It consisted of an 8 mm thick soft pad that spread the load evenly over the loading area. The purpose of those soft pad is to reduce the unevenness of the top surface of a beam. Otherwise, those irregularities would lead to stress concentrations which could have affected the experimental results. On top of this soft pad, the steel plate with a thickness of 10 mm was situated. The loading area was 100 mm × 50 mm (width × length) and was centred along the double symmetric axis.

The beams in the first series were simply supported on steel plates with a thickness of 8 mm. Those plates were glued to concrete to even the surface. The area of each support plate for the reference beam was 120 mm × 50 mm (width × length). The area of each support plate for hybrid beams was 90 mm × 50 mm (width × length). This means that hybrid beams in the first series were supported only at the normal concrete part.

The beams in the second series were simply supported as well. For this purpose steel plates with a thickness of 12 mm had been used. The area of each support plate for the reference beam and the hybrid beam 'B1' was 150 mm × 55 mm (width[1] × length). However, the other

[1] The width of those steel plates (150 mm) was larger than the width of the beams (120 mm).

hybrid beam ‘B2’ was supported by steel plates with an area of 95 mm × 50 mm (width × length) each. The hybrid beam ‘B2’ was only supported on the normal concrete part.

4.4.2 The bending setups of beams

The behaviours of beams were monitored by two independent techniques: Linear Variable Data Transformers (LVDTs), and Digital Image Correlation (DIC). The bending set-ups was based on the work of Haung et al. [49].

LVDT is a reliable and accurate technique to measure a particular distance. It converts transverse motion into an electrical signal which can be translated to displacement. The obtained data is correlated with the magnitude of load to obtain a displacement curve. The disadvantage of this method is that LVDT sensors have to be physically attached to an object of interest. The other limitation is that the LVDT sensor measures motion only in one dimension, therefore operator has to know beforehand crucial spots of interest.

DIC captures photos with specified time intervals during loading of the beams and employs tracking algorithms to accurately register changes between photos. It uses contrast of colours between grids, therefore, the speckle pattern is applied to obtain strong contrast between points. DIC is able to monitor 3D fields, however, the 2D field has been monitored in this experiment. The huge advantage of this method is non-contact feature. However, this technique is considered often less accurate for measuring displacement and strain fields compared to LVDTs. The 2D measurements becomes less accurate when out-of-plain motion occurs. DIC is suitable for capturing development and crack pattern which results in more deep understanding of failure mechanisms. It is therefore important during preparation of the speckle pattern that white ground colour should not have thick layer otherwise it may conceal small cracks. Furthermore, an image analysis software package, GOM Correlate 2019 {v 2.0.1} [54], has been used to evaluate data obtain from photos.

The reference beam in the first series

The first beam that has been tested was a reference RC beam without shear reinforcement. The one side was monitored by DIC and the other side was monitored by LVDTs, see Figure 47.

Figure 47 Two side views of the reference beam. Photo on the top: the configuration of LVDTs. Photo on the bottom: the speckle pattern for DIC.

The detailed LVDTs configuration is shown in Figure 48. In total six sensors have been installed. LVDTs with number 1, 2 and 3 has been installed in compressive zone of the beam. LVDTs with number 4 and 5 had the task to measure the outer fibres in the tension zone. The task of those LVDTs was to measure horizontal displacement. To keep the track on the vertical displacement, LVDT number 6 has been mounted.

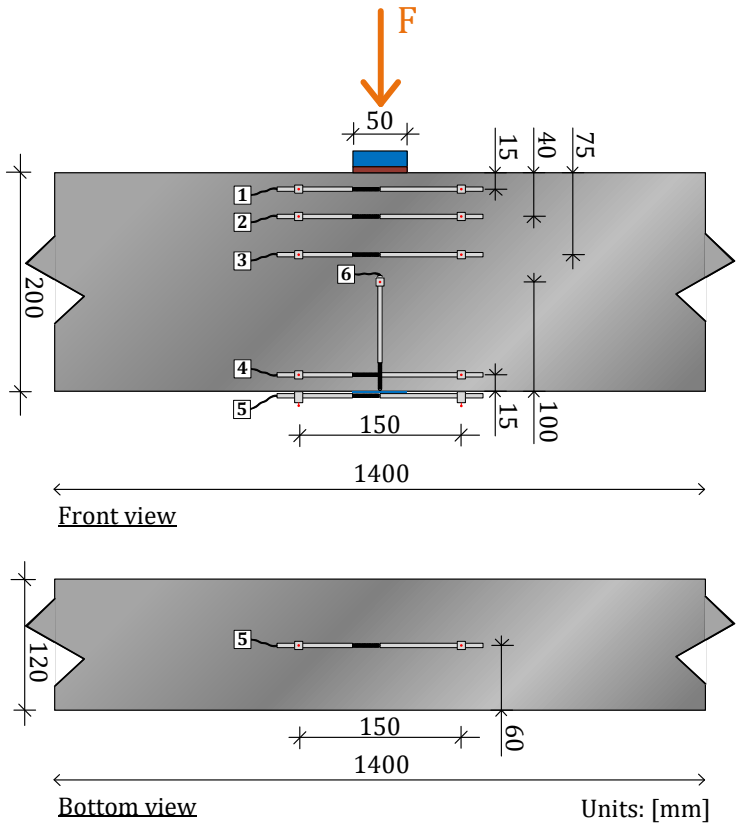

Figure 48 The drawings for the configuration of LVDTs on the reference beam without shear reinforcement.

The hybrid beam with smooth interface in the first series

The second beam that has been tested was a hybrid beam with smooth laminates without shear reinforcement. Just like reference beam, the one side was monitored by DIC and the other side was monitored by LVDTs, see Figure 49 and 50. Additionally, LVDTs were installed on the top of the beam to measure relative displacements of laminates with respect to normal concrete part.

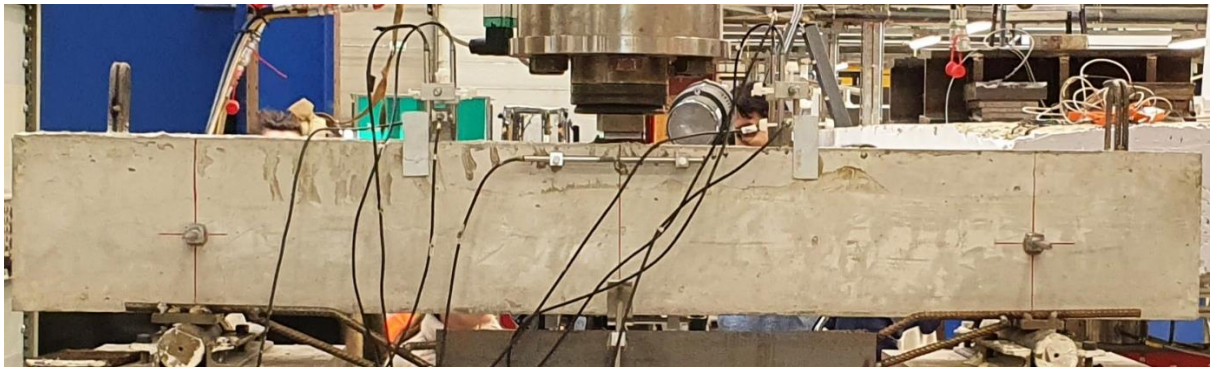

Figure 49 Side views of the beam with smooth laminates with the configuration of LVDTs.

Figure 50 Side views of the beam with smooth laminates with the speckle pattern for DIC.

The detailed LVDTs configuration is shown in Figure 51. In total nine sensors have been installed. LVDTs with numbers from 1 to 4 measure relative vertical displacement of laminates with respect to normal concrete part. LVDTs with numbers from 5 to 8 measure relative vertical displacement of laminates. LVDT number 9 measures vertical displacement of the beam.

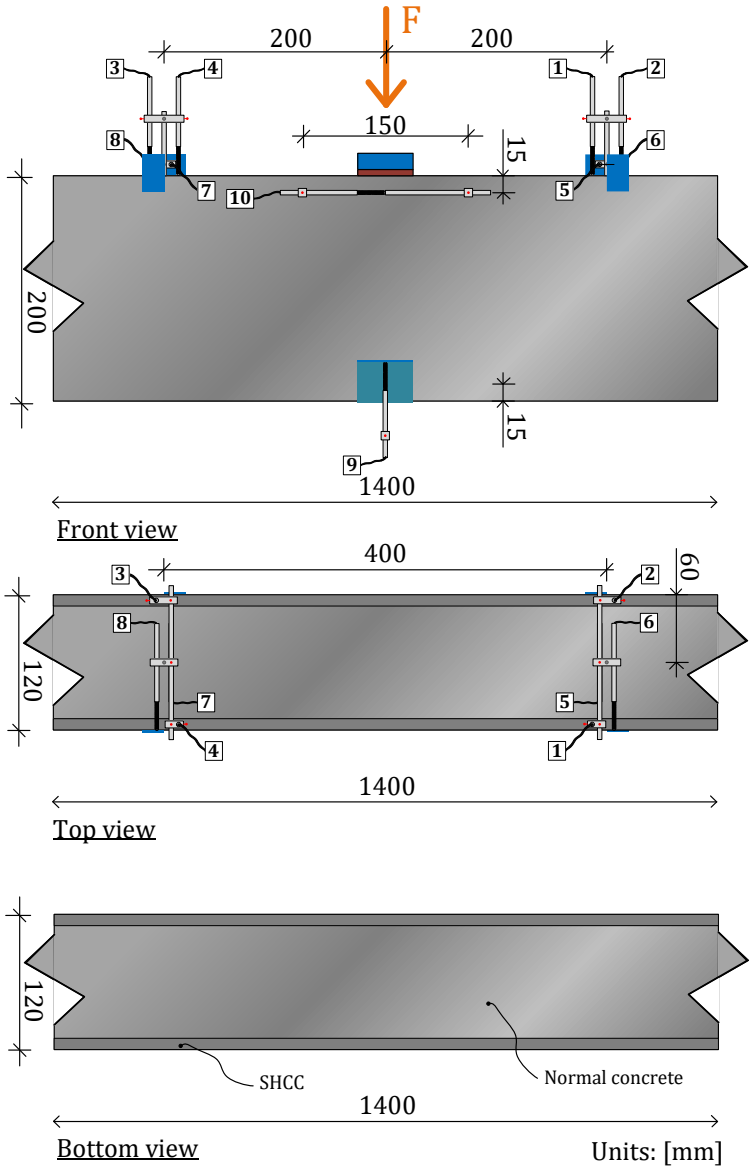

Figure 51 The drawings for the configuration of LVDTs on the beam with smooth laminates.

The hybrid beam with shear keys laminates in the first series

The third beam that has been tested was a hybrid beam with shear keys laminates without shear reinforcement. This beam was monitored by DIC from both sides (see Figure 52) because the unequal thickness of the laminates could trigger an unusual failure mechanism. As can be seen in the Figure below, two different techniques have been used to make those speckle patterns. The speckle pattern in the first picture in Figure 52 was prepared using a porous painting roller. The other speckle pattern in the second picture in Figure 52 was obtained by spraying black paint with an airbrush. Despite their different appearance, both patterns performed their work excellently. However, the latter pattern showed less noise in the measurements, therefore, is advisable to apply the pattern using an airbrush. Just like in the beam with smooth laminates, LVDTs were installed on the top of the beam to measure relative displacements of laminates with respect to the normal concrete core.

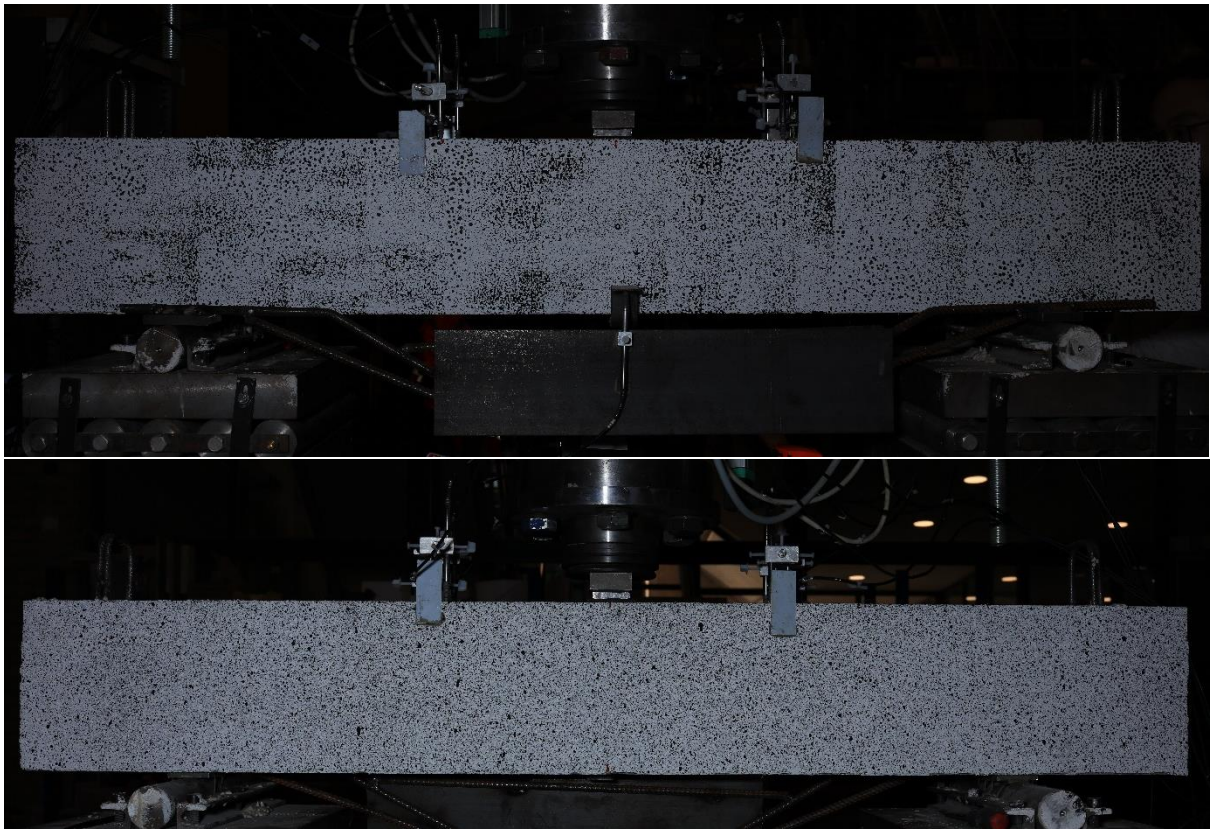

Figure 52 Two side views of the beam with laminates shear keys without shear reinforcement. Photo on the top: the speckle pattern on laminate K2 for DIC. Photo on the bottom: the speckle pattern on laminate K1 for DIC

The detailed LVDTs configuration is shown in Figure 53. In total nine sensors have been installed. LVDTs with numbers from 1 to 4 measure relative vertical displacement of laminates with respect to normal concrete part. LVDTs with numbers from 5 to 8 measure relative vertical displacement of laminates. LVDT number 9 measures vertical displacement of the beam. At the bottom of the beam no LVDT has been installed.

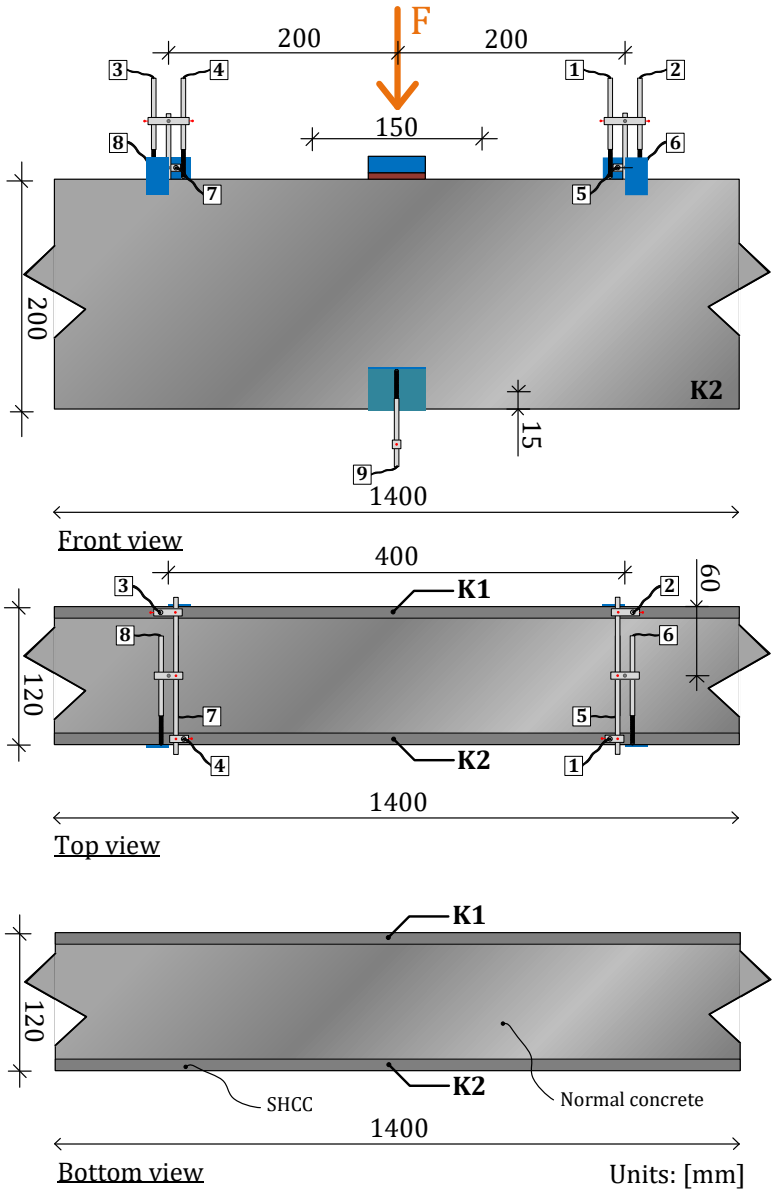

Figure 53 The drawings for the configuration of LVDTs on the beam with shear keys laminates.

The reference beam in the second series

The fourth beam that have been tested was the reference beam with shear reinforcement. Both side was monitored by DIC and additionally, the one side was monitored by LVDTs, see Figure 54 and 55.

Figure 54 The speckle pattern on the reference beam with shear reinforcement for DIC.

Figure 55 The speckle pattern with LVDTs on the reference beam with shear reinforcement for DIC.

The detailed LVDTs configuration for this beam is shown in Figure 56. Only three LVDTs had been placed on this beam. To measure vertical displacements, LVDT with number 1 was installed. LVDT with number 2 was responsible to measure deformation at a distance of 15 mm from the top fibre. The last LVDT with number 3 measured the bottom fibre's deformation.

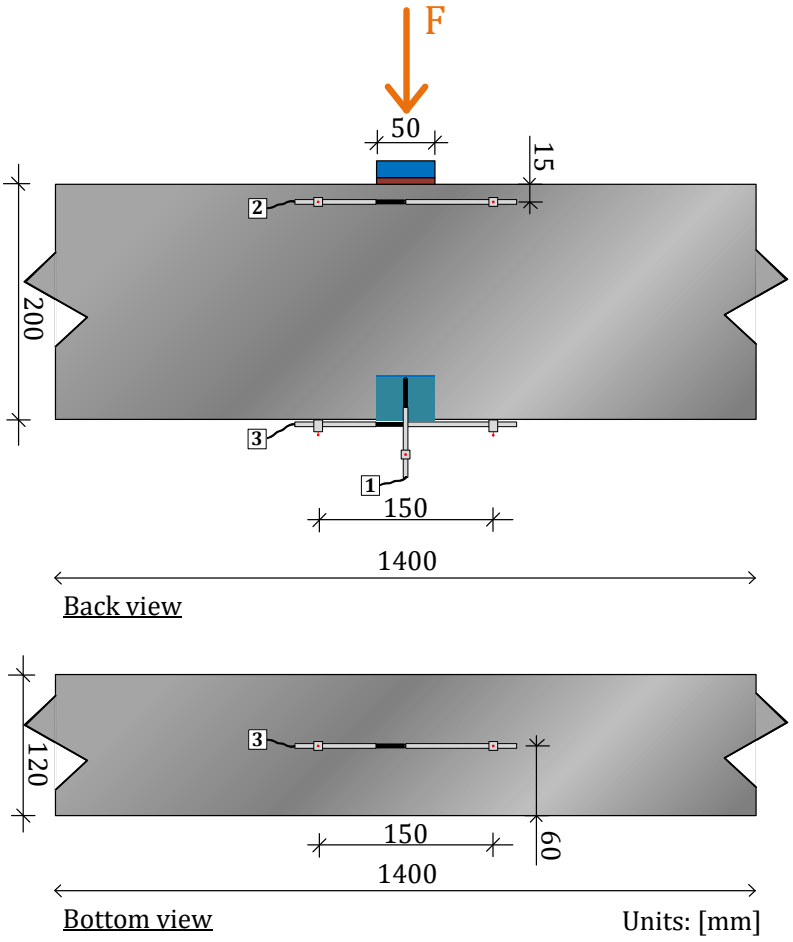

Figure 56 The drawings for the configuration of LVDTs on the reference beam with shear reinforcement.

The hybrid beam [B1] with shear reinforcement in the second series

The five beam that has been tested was a hybrid beam with shear keys laminates strengthen by shear reinforcement in the second series. From now on, this beam will denoted as the hybrid beam B1. Both side was monitored by DIC and additionally, the one side was monitored by LVDTs, see Figure 57.

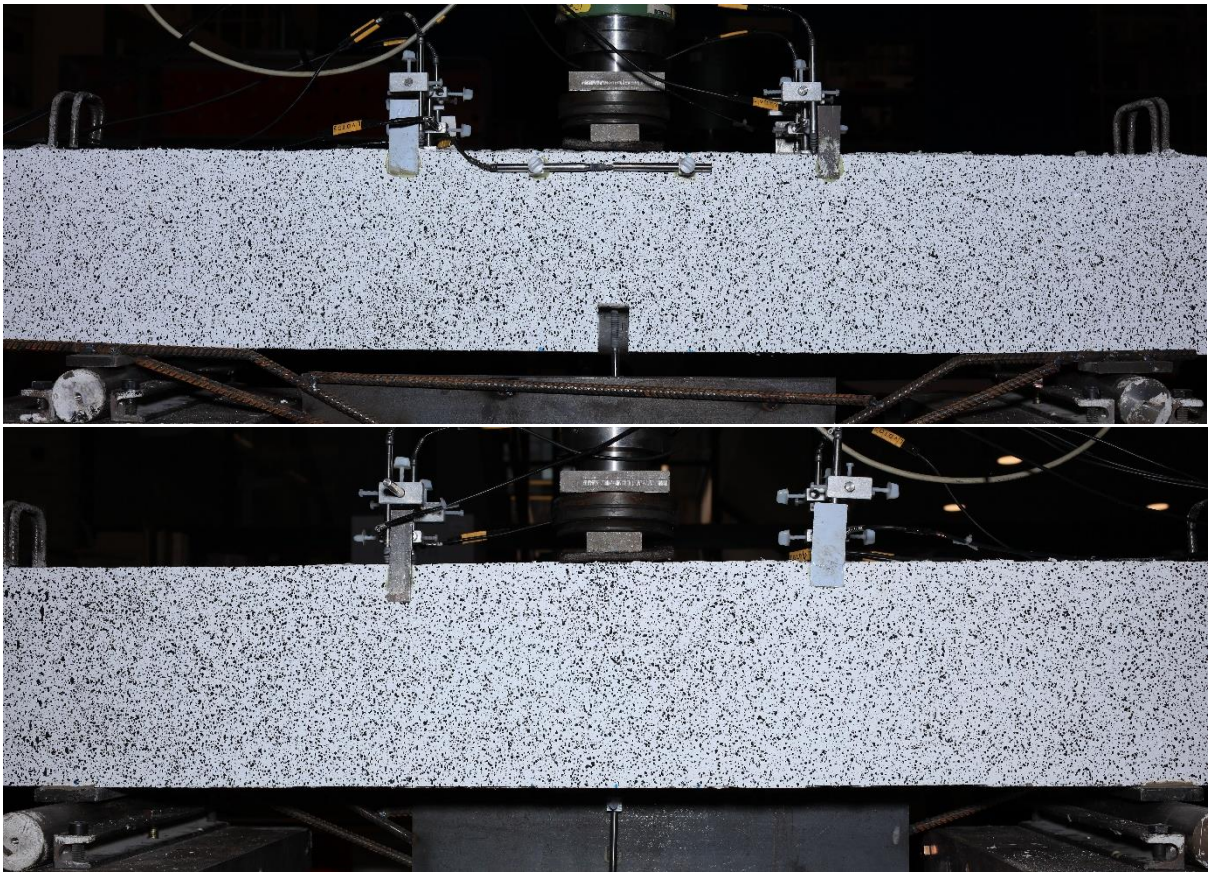

Figure 57 Two side views of the hybrid beam B1

The detailed LVDTs configuration is shown in Figure 58. In total ten sensors have been installed. The duty of LVDT with number 1 is to measure the vertical deformation of the beam. LVDT with number 2 measures deformation at a distance of 15 mm from the top fibre. LVDTs with numbers from 3 to 6 measure relative vertical displacement of laminates with respect to normal concrete part. LVDTs with numbers from 7 to 10 measure relative vertical displacement of laminates.

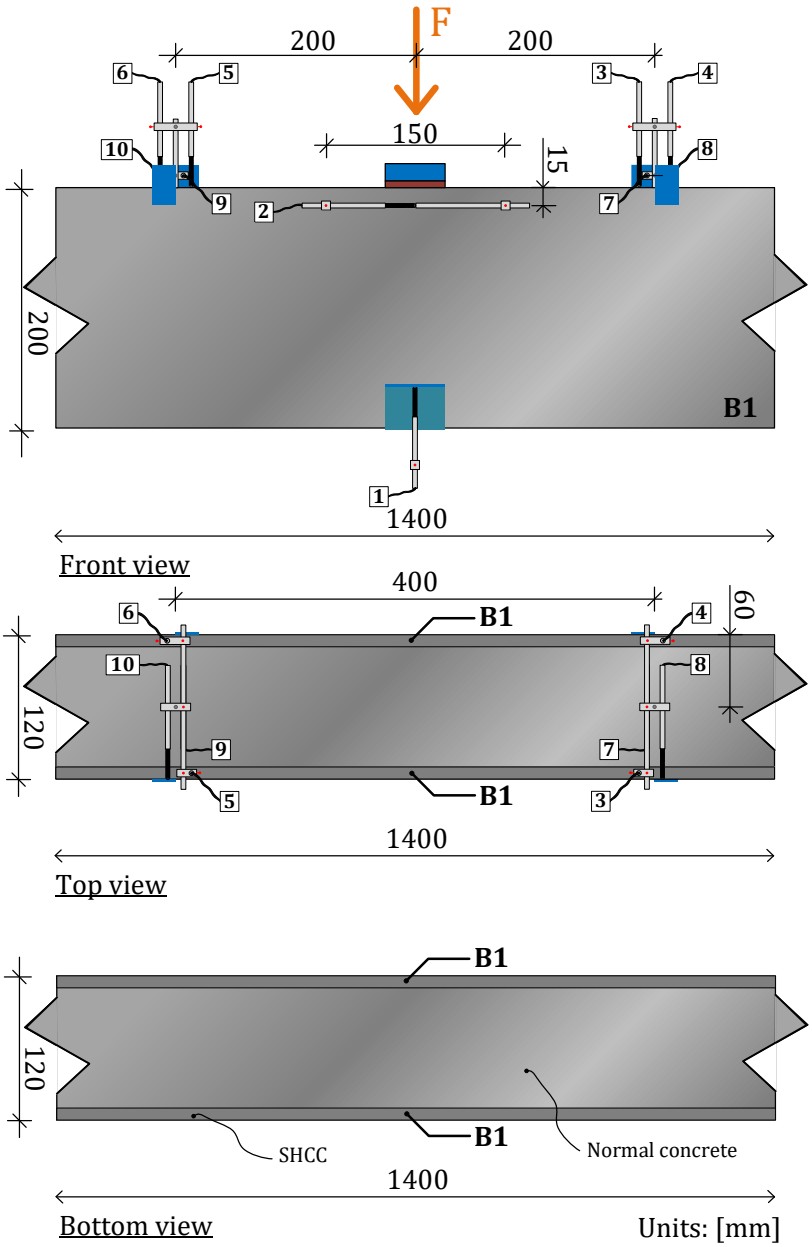

Figure 58 The drawings for the configuration of LVDTs on the hybrid beam B1

The hybrid beam [B2] with shear reinforcement in the second series

The five beam that has been tested was a hybrid beam with shear keys laminates strengthened by shear reinforcement in the second series. This beam will denoted as the hybrid beam B2.

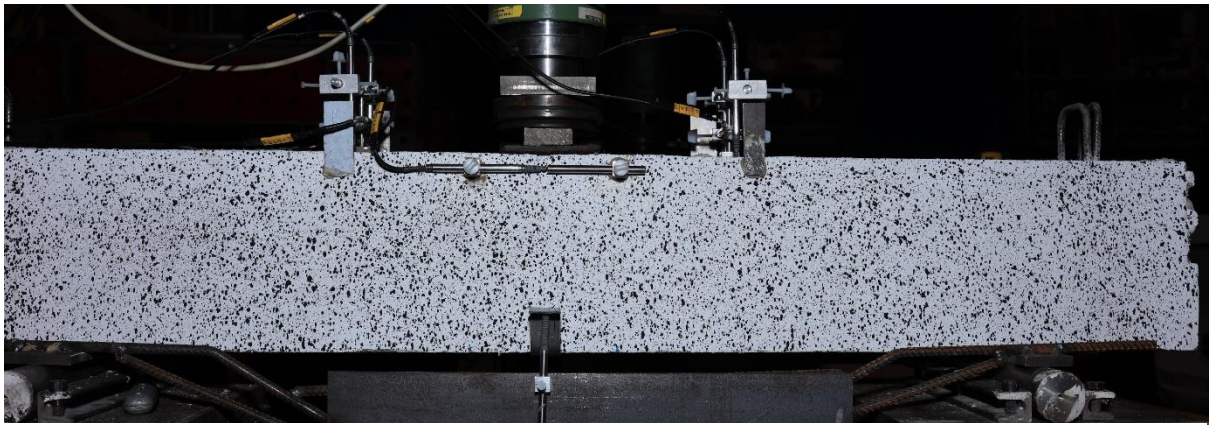

Figure 59 The speckle pattern for DIC + the configuration of LVDTs on the hybrid beam B2.

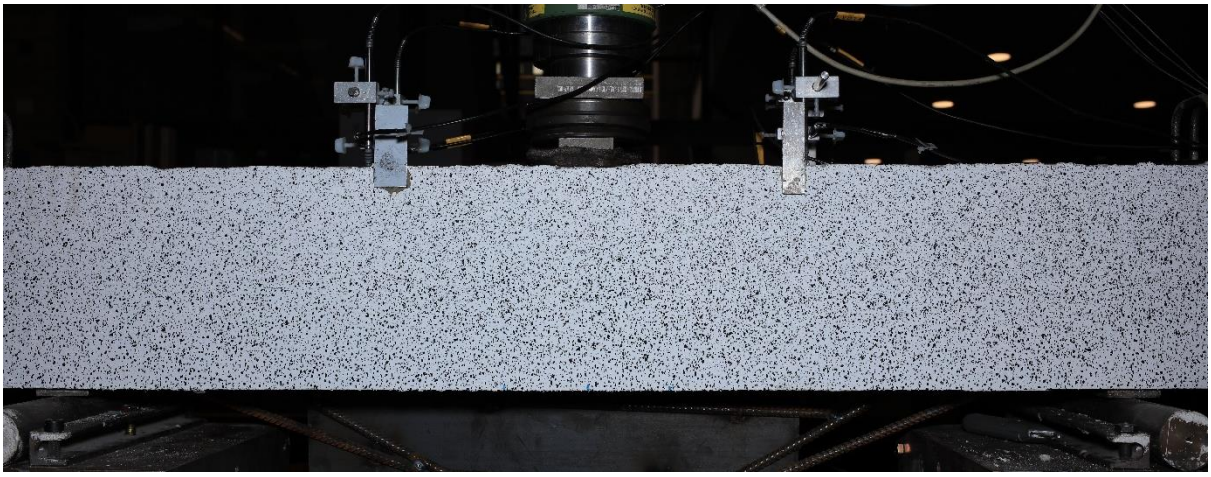

Figure 60 The other side of the hybrid beam B2. The speckle pattern for DIC and the configuration of LVDTs is visible.

Both side was monitored by DIC and additionally, the one side was monitored by LVDTs, see Figure 59 and 60. The detailed LVDTs configuration is shown in Figure 61. This configuration is exactly the same as for the hybrid B1. The bottom paragraph on the page 54 gives more detailed description of the configuration.

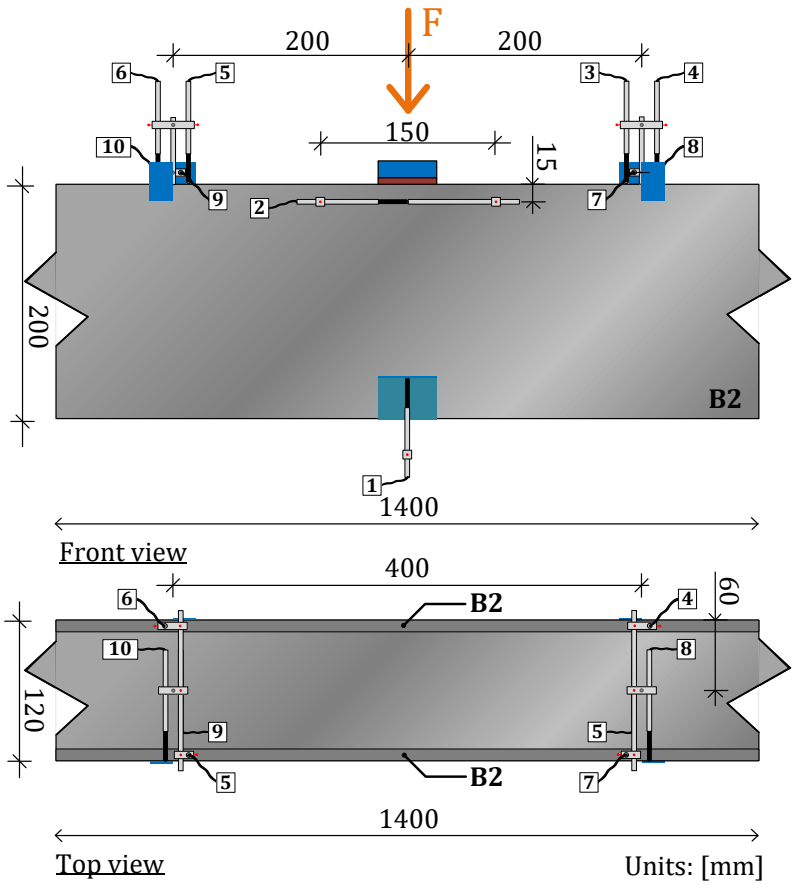

Figure 61 The drawings for the configuration of LVDTs on the hybrid beam B2

5

Experimental results

"What we know is a drop, what we don't know is an ocean."

Isaac Newton

The three-point bending test was conducted on four hybrid SHCC-concrete beams and two reference RC beams. In this chapter, the recorded behaviours of those beams will be shown and analysed. The results of the quality control of concrete and SHCC have been reported as well. Finally, all results are critically examined and discussed.

In this chapter, the results of all experiments mentioned in the previous chapter are presented. In the first section, the mechanical properties of normal concrete and SHCC are given. In the second section, the structural responses of all (hybrid) beams are given. Their capacity, deflection, failure modes and energy dissipation are discussed here as well.

5.1 Material test results

This section is subdivided into two parts: mechanical performance of normal concrete, mechanical performance of SHCC.

5.1.1 Mechanical performance of normal concrete

The results of the uniaxial compressive test on six standard cubes (150 × 150 × 150 mm^3) are shown in Table 7. The results of secant modulus of elasticity in compression on four prisms (400 × 100 × 100 mm^3) is shown in Table 9. Section 4.3.3 provides more detailed information about those specimens. The specimens' notation is defined as follows: the first part indicates the type of material; the second part refers to the individual name {C: standard cube, mc: medium cube, P: prism}; the third part indicates the age of a specimen in days.

Table 7 The results of compressive test on normal concrete cubes (150 × 150 × 150 mm^3)

Series nr.	Specimen ID	Compressive strength [MPa]	Average compressive strength [MPa]	Standard deviation [MPa]
First (without TR)	NC_C1_28	30,00	29,07	± 1,08
	NC_C2_28	27,43		
	NC_C3_28	29,79		
	NC_C4_28	28,60		
	NC_C5_28	30,45		
	NC_C6_28	28,14		
Second (with TR)	NC_C7_35	28,92	31,73	± 1,89
	NC_C8_35	34,20		
	NC_C9_35	34,05		
	NC_C10_35	30,44		
	NC_C11_35	31,68		
	NC_C12_35	31,09		

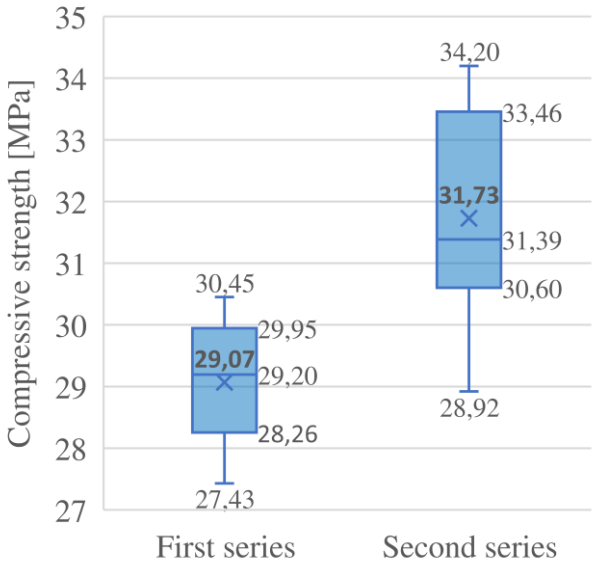

Specimens from the second series showed a slightly higher average compressive strength and a slightly larger standard deviation of compressive strength compared to the results of the first series, as displayed in Figure 62. Despite that, the strength of concrete from both series has reached its anticipated strength class of C20/25 according to "identity criteria" found in Tabel B.1 of NEN-EN 206 + NEN 8005:2017 document, see Table 8.

Figure 62 Variation in two sets of compressive strength on NC cubes (150 × 150 × 150 mm^3).

Table 8 Identity criteria for the compressive strength according to NEN-EN 206.

Series nr.	Specimen ID	Criterium 1: $f_{cm} \geq f_{ck} + 2$ [MPa]	Criterium 2: $f_{ci} \geq f_{ck} - 4$ [MPa]	Strength Class
First (without TR)	NC_C1_28	29,07 ≥ 27	30,00 ≥ 21,00	C20/25
	NC_C2_28		27,43 ≥ 21,00	
	NC_C3_28		29,79 ≥ 21,00	
	NC_C4_28		28,60 ≥ 21,00	
	NC_C5_28		30,45 ≥ 21,00	
	NC_C6_28		28,14 ≥ 21,00	
Second (with TR)	NC_C7_35	31,73 ≥ 27	28,92 ≥ 21,00	C20/25
	NC_C8_35		34,20 ≥ 21,00	
	NC_C9_35		34,05 ≥ 21,00	
	NC_C10_35		30,44 ≥ 21,00	
	NC_C11_35		31,68 ≥ 21,00	
	NC_C12_35		31,09 ≥ 21,00	

Table 9 provides only one result from the second series. The other two prisms were rejected due to poor compaction of concrete during casting, see Appendix C.1 for the explanation. To show quality of the remaining concrete prism, the results of the uniaxial compressive test on three cubes (100 × 100 × 100 mm^3) cut from this prism are reported in Table 10.

Table 9 The results of elastic modulus of normal concrete prisms (400 × 100 × 100 mm^3)

Series nr.	Specimen ID	Young's modulus [MPa]	Average Young's modulus [MPa]	Standard deviation [MPa]
First (without TR)	NC_P1_28	32638	33031	± 552
	NC_P2_28	32644		
	NC_P3_28	33813		
Second (with TR)	NC_P4_35	34486	×	×

Table 10 The results of compressive test on normal concrete medium cubes (100 × 100 × 100 mm^3) after 35 days of sealing.

Series nr.	Specimen ID	Compressive strength [MPa]	Average compressive strength [MPa]	Standard deviation [MPa]
Second (with TR)	NC_mc1_35	34,87	32,57	± 1,97
	NC_mc2_35	30,04		
	NC_mc3_35	32,82		

Due to the influence of the scale factor on the compressive strength of normal concrete, the results of smaller cubes are higher than the results of standard cubes. According to NEN 8005+C1:2017 Table G, the correction factor due to this phenomenon equals 0,91 for a cube with 100 × 100 × 100 mm^3 dimensions. Hence, the corrected average compressive strength equals 29,64 MPa which is more or less in line with Table 7. For this reason, this prism has been labelled as a good quality specimen.

5.1.2 Mechanical performance of strain hardening cementitious composite

The primary results of the uniaxial compressive test on SHCC cubes (40 × 40 × 40 mm^3) are presented in Table 11. However, the complete list of those results can be found in Table D-3 (see Appendix D). Further, the results of the uniaxial tensile test on standard dog bone specimens are reported in Figure 64 and Table 14 and 15. Finally, the results of shrinkage on SHCC prisms (150 × 40 × 40 mm^3) are provided in Figure 67. Section 4.3.2 provides more detailed information about curing conditions and testing procedures of all those specimens. To distinguished specimens from each other, the specimens' types are formulated as follows: the first part indicates a laminate(s) or a hybrid beam or a purpose {Sm: smooth laminates, K1: shear key laminate of the first batch, K2: shear key laminate of the second batch, B1: hybrid beam B1, B2: hybrid beam B2, ST: shrinkage test, SF: scale factor}; the second part refers to the individual name {C: standard cube, c: small cube, d: dog bone specimen, p: prism specimen}; the third part indicates the age of a specimen in days {days in the climate room + days in sealing}. As already documented in previous chapter, the K1 laminate is slightly thicker in certain spot than the K2 laminate. Some dog bone specimens had to be recreated (indicated with symbol 'R') because original specimens had an initial curvature caused by a faulty mould.

Table 11 The primary results of compressive test on SHCC cubes (40 ×40 ×40 mm^3)

Series nr.	Specimen ID	Compressive strength [MPa]	Average compressive strength [MPa]	Standard deviation [MPa]
First (without TR)	Sm_c1_14+28	70,491	68,957	± 2,437
	Sm_c2_14+28	65,518		
	Sm_c3_14+28	70,863		
	K1_c1_14+28	65,302	66,269	± 2,827
	K1_c2_14+28	63,393		
	K1_c3_14+28	70,111		
	K2_c1_14+28	61,777	64,118	± 2,082
	K2_c2_14+28	63,741		
	K2_c3_14+28	66,836		
Second (with TR)	B1_c1_21+35	72,107	69,764	± 4,737
	B1_c2_21+35	74,028		
	B1_c3_21+35	63,158		
	B2_c1_21+35	77,143	75,376	± 1,972
	B2_c2_21+35	76,361		
	B2_c3_21+35	72,623		

Looking at the table above, it can be concluded that the target compressive strength of 60 MPa has been reached. Despite five separated batches, the mean values and standard deviations remained in the acceptable limits, see Figure 63. Table 12 shows the primary results of quality control groups for shrinkage specimens. Those results are proof that the target compressive strength for shrinkage specimens has been indeed reached. However, the complete list of those results can be found in Table D-4 (see Appendix D). It is worth noticing that the average compressive strength of SHCC is 2,1 – 2,3 factor[1] greater than that of normal concrete.

[1] Based on the compressive strength results on cubes (150 × 150 × 150 mm^3) [Table 7 vs Table 13]

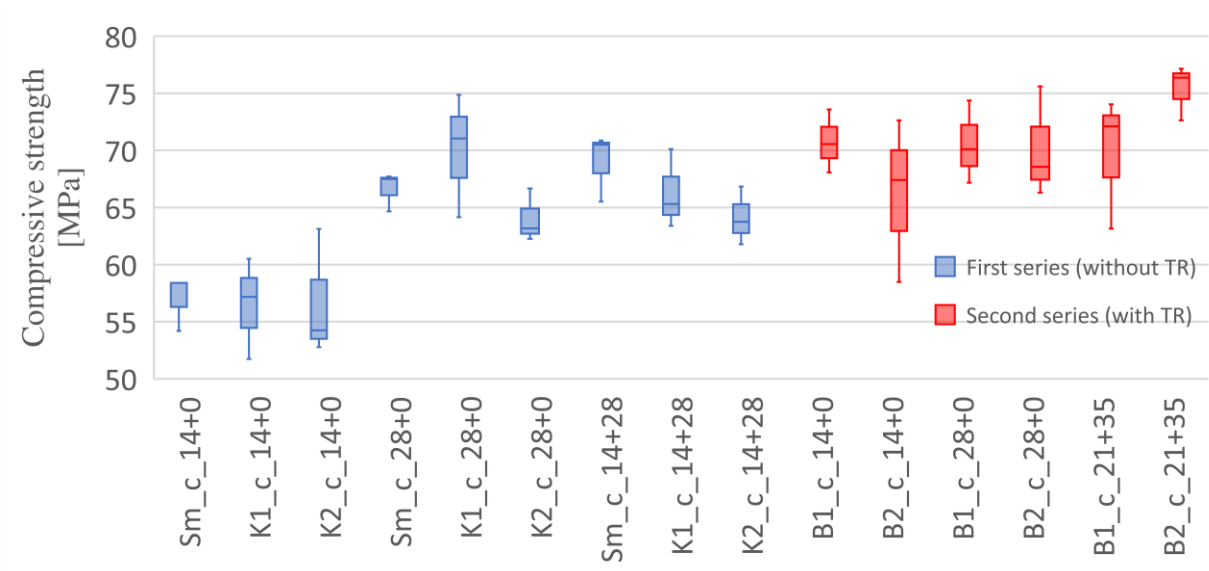

Figure 63 SHCC compressive strength in different curing conditions, see Table D-3.

Table 12 The primary results of compressive test on SHCC cubes (40 × 40 × 40 mm³)

Series nr.	Specimen ID	Compressive strength [MPa]	Average compressive strength [MPa]	Standard deviation [MPa]
Not applicable	ST_c1_14+28	77,265	72,795	± 3,361
	ST_c2_14+28	71,959		
	ST_c3_14+28	69,161		

Concrete compressive strength decreases as sample size increases, this phenomena is called 'the size effect'. As seen in Table 13, the size effect factor for this specific SHCC mix is estimated to be around 0,97. It is rather small and therefore the compressive strength of small SHCC cubes can be directly be compared with compressive strength of standard NC cubes. The complete list of those results can be found in Table D-5 (see Appendix D).

According to the experiment of He [50] (inventor of the mix composition), Young's modulus of this particular SHCC equals 16,5 (± 1,4) GPa.

Table 13 The primary results of compressive test on SHCC cubes (150 × 150 × 150 mm³)

Series nr. // Beam	Specimen ID	Compressive strength [MPa]	Average compressive strength [MPa]	Standard deviation [MPa]
Second // B1	SF_C1_21+35	64,21	68,14	± 3,05
	SF_C2_21+35	68,56		
	SF_C3_21+35	71,64		

Two different curing conditions had no significant effect on the tensile properties of SHCC. The anticipated mechanical properties of this particular SHCC have been reached. Compared to the first series, the results of the second series are more uniform due to eliminating an initial curvature of the dog bone specimens by using the steel mould.

Not all dog specimens at age of 56 days were successfully tested. Three of four specimens failed outside the range of LVDTs. The failure was due to too extensive oiling of the mould prior to casting which damaged microcracking bridging between cement past and fibres. It can be concluded that the mechanical properties of SHCC were not an issue here.

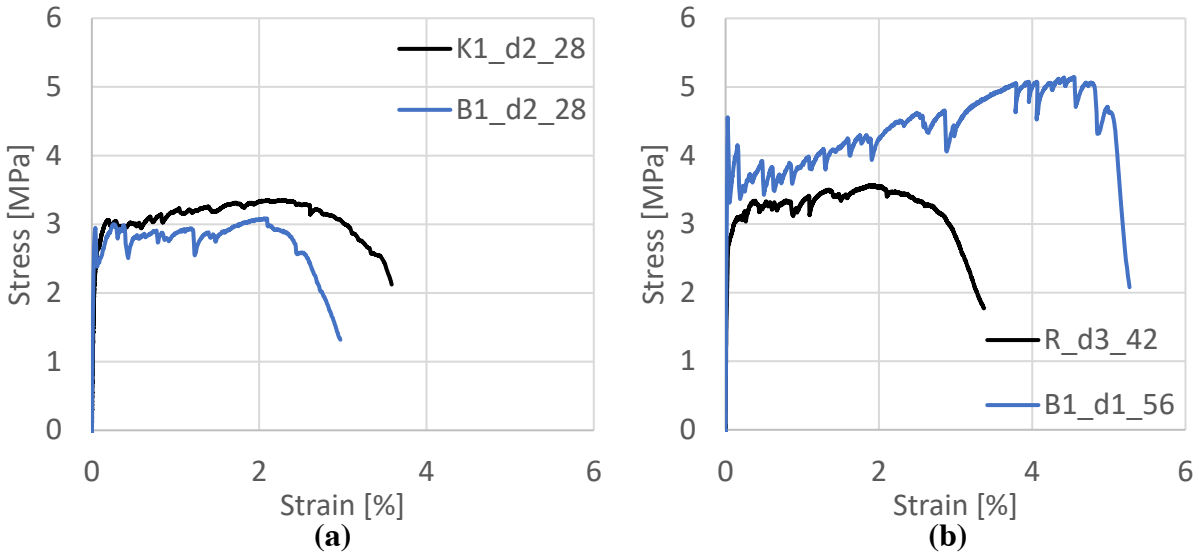

Figure 64 Representative tensile stress-strain curves of SHCC after (a) 28 days standard curing and (b) 14 days standard curing + 28 days of sealing (42 days total) or 21 days standard curing + 35 days of sealing (56 days total).

Table 14 Uniaxial tensile test results on SHCC samples after 28 days standard curing.

Series nr.	Specimen ID	Ultimate tensile strength [MPa]	Tensile strain at 90% strength [%]	Average ultimate tensile strength [MPa]	Average tensile strain at 90% strength [%]
First (without TR)	Sm_d1_28	3,92	3,67	3,61 (± 0,32)	2,81 (± 0,87)
	Sm_d2_28	3,29	1,94		
	K1_d1_28	3,25	1,42	3,30 (± 0,05)	2,22 (± 0,80)
	K1_d2_28	3,35	3,02		
	K2_d1_28	3,98	3,02	3,89 (± 0,09)	2,35 (± 0,68)
	K2_d2_28	3,80	1,67		
Second (with TR)	B1_d1_28	2,71	1,62	2,90 (± 0,19)	2,01 (± 0,39)
	B1_d2_28	3,09	2,39		
	B2_d1_28	3,25	2,07	3,60 (± 0,35)	1,93 (± 0,15)
	B2_d2_28	3,95	1,78		

Table 15 Uniaxial tensile test results on SHCC samples short after beam tests.

Series nr.	Specimen ID	Ultimate tensile strength [MPa]	Tensile strain at 90% strength [%]	Average ultimate tensile strength [MPa]	Average tensile strain at 90% strength [%]
Not applicable	R_d1_42	3,31	1,99	3,52 (± 0,16)	2,27 (± 0,33)
	R_d2_42	3,69	2,08		
	R_d3_42	3,57	2,74		
Second (with TR)	B1_d1_56	5,14	4,84	×	×
	B2_d1_56[a)]	4,42*	×		

[a)] The sample failed outside the LVDT range, hence the ultimate tensile strength may be higher.

The tensile stress-strain curve can be divided into three phases, see Figure 65 a). The first phase is called the initial elastic stretch where the material behaves linearly. The slope of this line equals the initial Young's modulus of the material. At the sign of the first crack, the second phase is officially started. This phase is called the strain-hardening stage. Opposite to normal concrete, SHCC does not grow cracks locally but forms multiple parallel cracks during an increase in loading, as seen in Figure 65 b). In tensile stress-strain curves of SHCC, small drops and increases of stress can be noted due to the formation of those parallel cracks. The last stage is the phase of the final fracture. The strength of microcracking bridging between cement past and fibres is exited and the material fails. Figure 66 shows the typical crack pattern of SHCC.

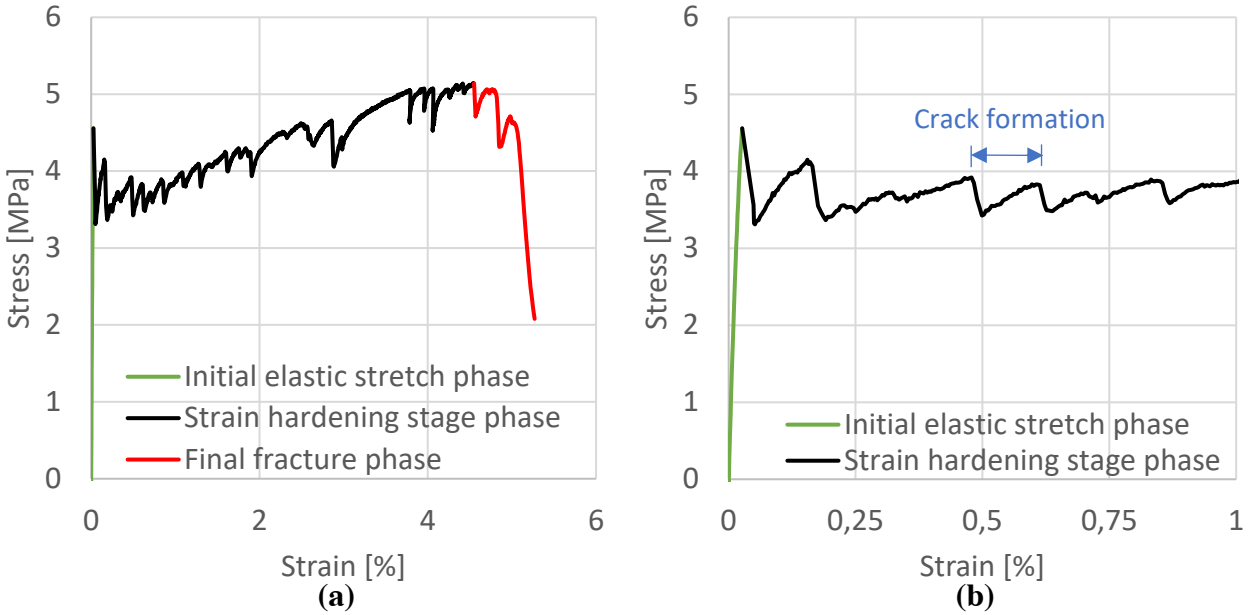

Figure 65 (a) The typical tensile stress-strain curves of SHCC {specimen: B1_d1_56} divided into three phases. (b) Close-up on the typical initial elastic stretch.

Figure 66 The crack pattern of SHCC. Specimen: B1_d1_56.

The literature study conducted in Chapter 2 has highlighted possible problems caused by different rates and magnitudes of shrinkage between normal concrete and SHCC. Since CEM III/B is used as the binder for this specific SHCC mix, the shrinkage of SHCC is expected to be significant since the presence of slag in this type of cement is known for causing more shrinkage than without it. Figure 67 shows the shrinkage strain of SHCC for different ages and

two different curing conditions. Detailed information on the corresponding data points can be found in Tables D-1 and D-2 (see Appendix D). It is observed that curing conditions had a significant impact on the shrinkage strain. Specimens with longer curing time showed an almost twofold the reduction of shrinkage. However, the shrinkage of this SHCC is still factor three larger than the values of other SHCCs found in the literature study.

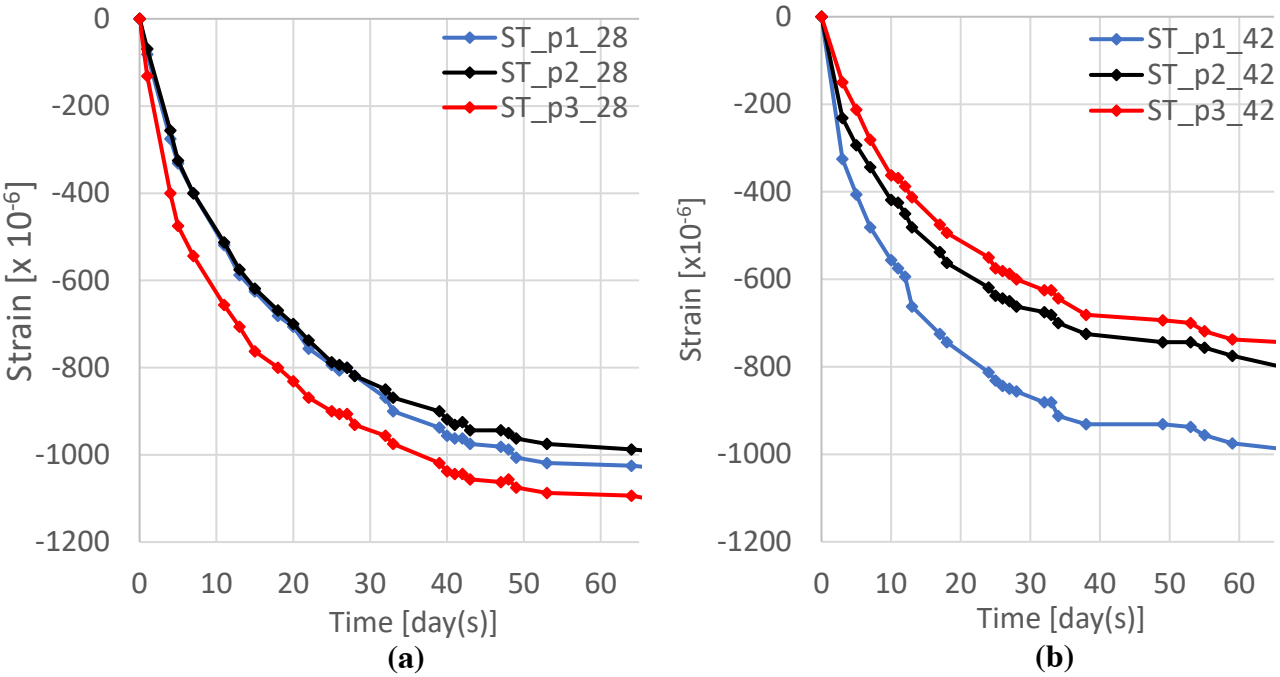

Figure 67 Shrinkage history of SHCC in the standard environment after (a) 28 days standard curing and (b) 14 days standard curing + 28 days of sealing.

5.2 Structural test results of (hybrid) beams

As already mentioned in the previous chapter, three beams have been tested in every series. In total six beams have been tested: two reference beams with and without transverse reinforcement, and four hybrid beams with and without transverse reinforcement. The section is divided into six parts. First, the load-deflection responses of all beams are reported and discussed. In the next part, the load-strain relationships are presented and explained. In the third subsection, the cracking developments and failure modes of the beams are shown. In the fourth part, the interface displacements between SHCC laminates and normal concrete are reported and discussed. In the fifth subsection, the stiffness degradation of the beams is discussed. In the sixth part, energy dissipation is elaborated. And in the last part, growth rates of main diagonal cracks are reported.

5.2.1 Load deflection response

To evaluate the shear capacity of hybrid beams without transverse reinforcement, two hybrid beams and one RC beam were tested. The latter one is the reference beam. As mentioned before, testing of all beams were under displacement control. Figure 68 shows the load midspan deflection relationships of those beams. The data obtained from LVDTs for vertical deflection and DIC match almost perfectly with each other, see Appendix E. The most crucial results of the first series are summarised in Table 16.

The ultimate vertical force (F_{max}) acting on the reference beam was 53,5 kN. According to the analytical calculation in section 3.1 based on the Eurocode 2 approach, the expected failure should happen at 55,3 kN which is more or less the same value that has been found in the experiments. The difference could be explained by the stochastic nature of mechanical properties of materials, and neglecting the self-weight of the beam in the calculations. The midspan deflection at the peak load was 1,46 mm. After peak load, the reference beam still showed ductility due reinforcement dowel effect until the vertical midspan deflection arrives at 3,13 mm.

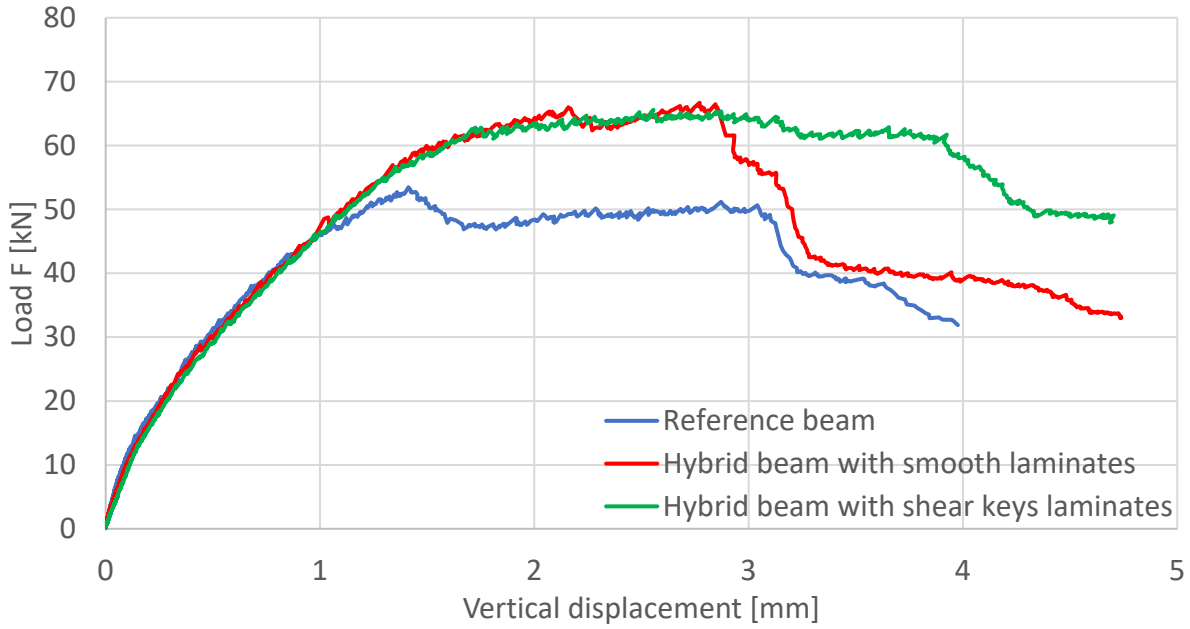

Figure 68 Load F versus vertical deflection of the (hybrid) beams without transverse reinforcement at midspan.

The ultimate vertical forces (F_{max}) acting on the hybrid beam with smooth laminates and on the hybrid beam with shear keys laminates were 66,7 kN and 65,6 kN respectively. The capacities of those hybrid beams were 13,2 kN and 12,1 kN higher than the reference beam without shear reinforcement respectively. Putting into perspective, the capacity has increased by 24,7% for the hybrid beam with smooth laminates and by 22,6% for the hybrid beam with shear keys laminates. The midspan deflection at the peak load was 2,77 mm for the hybrid beam with smooth laminates and 2,56 mm for the hybrid beam with shear keys laminates. Both hybrid beams show plateaus before the failure, see Figure 68 once more time. Such behaviours showed a bit more warning before the sudden failure of those hybrid beams compared to the reference beam without shear reinforcement.

Table 16 The experimental results on (hybrid) beams without transverse reinforcement

Series nr.	Specimen without transverse reinforcement	Ultimate capacity [kN]	Δ in ultimate capacity compared to reference group [kN]	Δ in ultimate capacity compared to reference group [%]	Vertical displacement at peak load [mm]
	Reference beam {120 × 200 mm²}	53,5	-	-	1,46
First (without TR)	Hybrid beam with smooth laminates {120 × 200 mm²}	66,7	+ 13,2	+ 24,7	2,77
	Hybrid beam with shear keys laminates {120 × 200 mm²}	65,6	+ 12,1	+ 22,6	2,56

To evaluate the shear capacity of hybrid beams with transverse reinforcement, two hybrid beams and one RC beam were tested. The latter one is the reference beam. Also this time, testing was under displacement control. Figure 69 shows the load midspan deflection relationships of those beams. The data obtained from LVDTs for vertical deflection and DIC do not match entirely, see Appendix E. Due to the noise in the pictures, data from DIC have slightly offset to the right, but it is still in the acceptable range to be trusted for the analysis. The most crucial results of the beams with TR in the second series are summarised in Table 17.

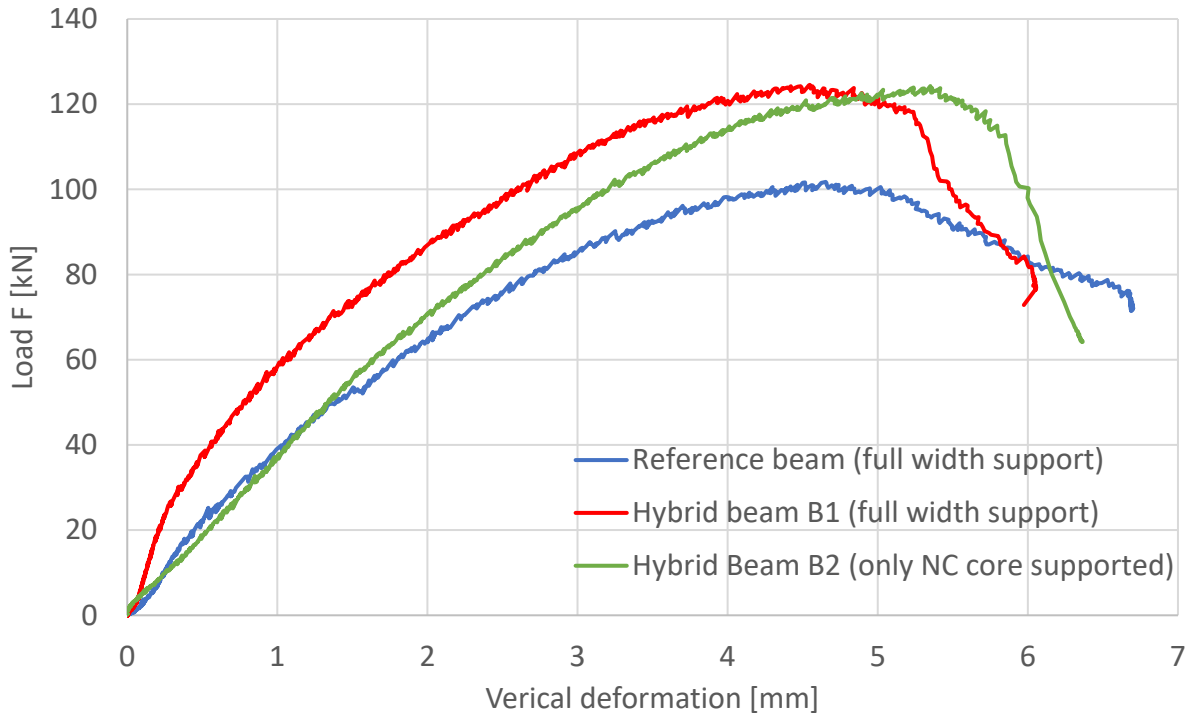

Figure 69 Load F versus vertical deflection of the (hybrid) beams with transverse reinforcement at midspan.

Table 17 The experimental results on (hybrid) beams with transverse reinforcement

Series nr.	Specimen with transverse reinforcement	Ultimate capacity [kN]	Δ in ultimate capacity compared to reference group [kN]	Δ in ultimate capacity compared to reference group [%]	Vertical displacement at peak load [mm]
Second (with TR)	Reference beam {120 × 200 mm²}	101,8	-	-	4,65
	Hybrid beam B1 {120 × 200 mm²}	124,5	+ 22,7	+ 22,3	4,54
	Hybrid beam B2 {120 × 200 mm²}	124,2	+ 22,4	+ 22,0	5,35

The ultimate vertical force (F_{max}) acting on the reference beam was 101,8 kN. According to the calculation in section 3.2 based on the Eurocode approach, the expected failure should happen at 83,8 kN which is 18,0 kN less than the value that has been found in the experiments. The difference could be explained by the conservative shear model used for slightly shear-reinforced beams by Eurocode 2, as has been proved by Cladera et al. [55]. The model of EC2 does not consider a concrete contribution. A more in-depth analysis has been made in section 6.1.2 on this subject. The vertical deflection at midspan at the peak load before forces dropped considerably equals 4,65 mm. This beam showed less sudden and brittle failure than the reference beam in the first series. This can be attributed to the presence of shear reinforcement which in combination with concrete formed the truss-carrying mechanism.

The ultimate vertical forces (F_{max}) acting on the hybrid beams B1 and B2 were 124,5 kN and 124,2 kN respectively. This means that the capacities of those hybrid beams were 22,7 kN and 22,4 kN higher than the reference beam with shear reinforcement respectively. Putting into perspective, the capacity has increased by 22,3% for the hybrid beam B1 and by 22,0% for the hybrid beam B2. The vertical deflection at midspan at the peak load equalled 4,54 mm for the hybrid beam B1, and 5,35 mm for the hybrid beam B2. The hybrid beam B1 had roughly the same magnitude for the midspan deflection at the peak load as the reference beam with shear reinforcement. The hybrid beam B2 deflected 15% more at the peak load than its reference beam hence this deflection has increased by 0,70 mm.

In Appendix E, Figure E-7 shows experimental results of all beam specimens together in one graph.

5.2.2 Load strain response

The analysis of the load-strain relationships refers to the values measured by LVDTs and DIC along the various depths of a beam specimen at its mid-span. Figure 70 covers the concrete strains of the beams in the first series, and Figure 71 presents the concrete strains of the beams in the second series. In Appendix E, Figures E-8 and E-9 show the magnitude of load versus concrete strains of fibres at various heights for the first and the second series respectively.

In general, the specimen with transverse reinforcement (the second series) showed larger strain values than the specimen without it (the first series). Moreover, the reference beams showed smaller strain values than their corresponding hybrid beams since the hybrid beams carried larger loads.

All tested hybrid beams have surpassed the yielding strain (2,0‰) of their longitudinal reinforcement at their failures. The normal strains in the longitudinal bars remained in the hardening phase and did not reach the fracture point of B500 steel. At failure, the tensile strain values measured on the bottom of the beams without shear reinforcement were 2,0‰, 2,5‰ and 2,4‰ for the reference beam and the hybrid beam with smooth laminates and the hybrid beam with shear keys laminates, respectively, while for the beams with shear reinforcement, the tensile strain were 2,7‰ (the reference beam), 3,5‰ (the hybrid beam B1) and 2,9‰ (the hybrid beam B2). Since the reference beams carried lower ultimate force than their corresponding hybrid beams, the tensile strain of the reference beams at the bottom should be lower than the corresponding hybrid beams. And indeed, this can be observed.

According to the data, all tested beams did not reach the ultimate concrete compressive strain of 3,5‰ which EN 1992-1-1 assumes for ≤ C50/60. In the case of SHCC, the ultimate compressive strain is estimated to be around 0,38% according to Yu et al. [56]. At failure, the compressive strain values measured on 15 mm from the top of the beams without shear reinforcement were 0,9‰, 1,4‰ and 1,4‰ for the reference beam and the hybrid beam with smooth laminates and the hybrid beam with shear keys laminates, respectively, while for the beams with shear reinforcement, the compressive strains were 2,1‰ (the reference beam), 2,8‰ (the hybrid beam B1) and 1,9‰ (the hybrid beam B2). However, true concrete compressive strains of hybrid beams could not be measured since the laminates obstruct access to normal concrete cores. Any slip in the interface between a normal concrete core and an SHCC laminate affects measured values. Therefore, it can be concluded that the reference beam did not reach the ultimate concrete compressive strain of 3,5‰ and definitely not the ultimate SHCC compressive strain of 0,38%. And as for those hybrid beams, the situation is unclear. More about it in the next two subsections.

According to the mechanical principles of three-point bending, a strain development in a rectangular cross-section at midspan should have been straight line. Looking at Figure 70 and 71, the strain developments are not straight at all. It should not be forgotten that the straight strain lines are only occurring in the mechanical fiber model. In this model, the cross section is modeled as a collection of initially straight fibers which are parallel to the beam neutral axis. This model does not account for heterogonies properties of concrete or SHCC, like for example Young's modulus. In reality, not every mechanical fibre (thus not physical fibre) would be equal stiff in a material. Furthermore, measurement errors are not taken into account.

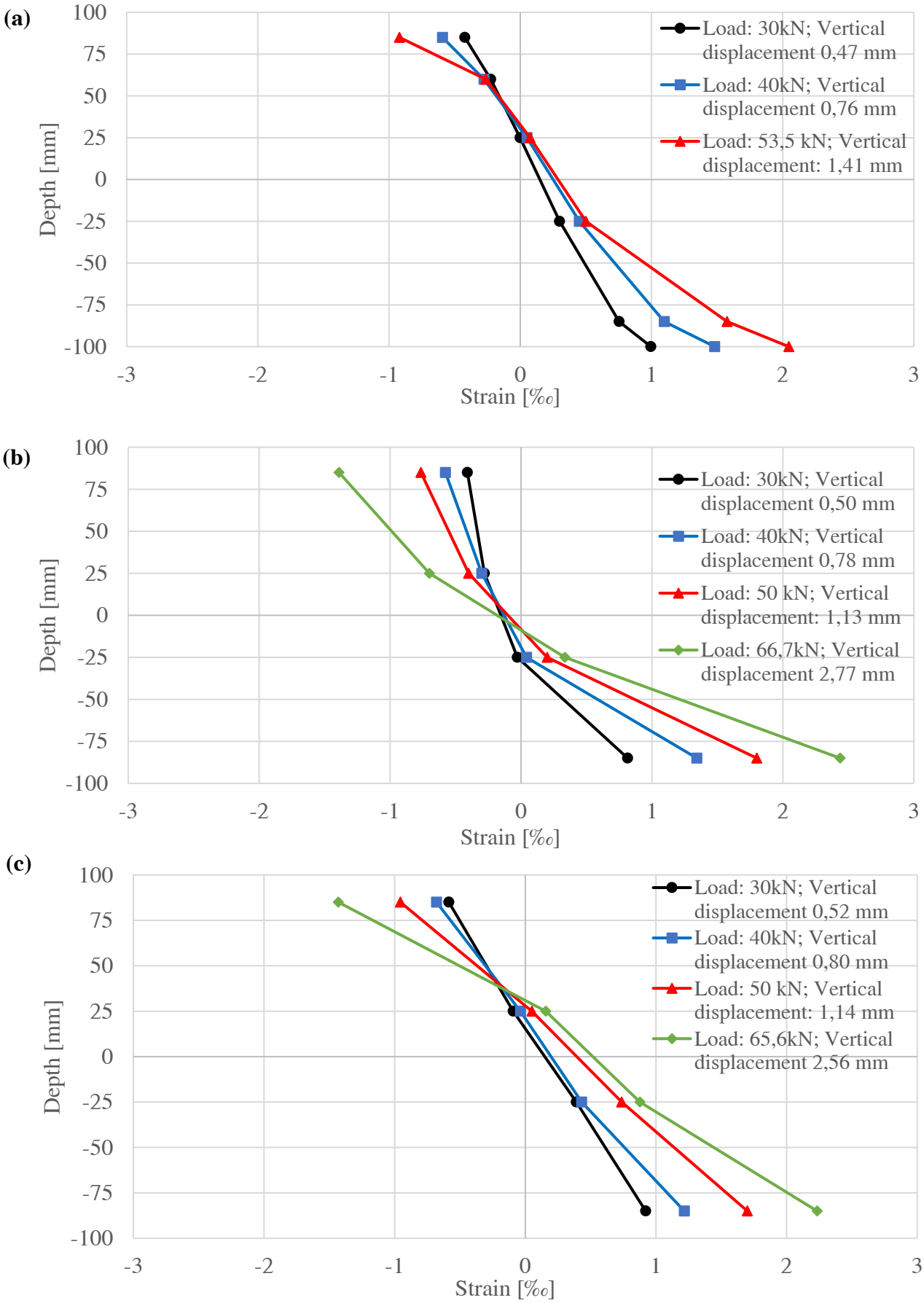

Figure 70 Horizontal strains of fibres at various depths. Beams are without transverse reinforcement: (a) Reference beam; (b) Hybrid beam with smooth laminates; (c) Hybrid beam with shear keys laminates.

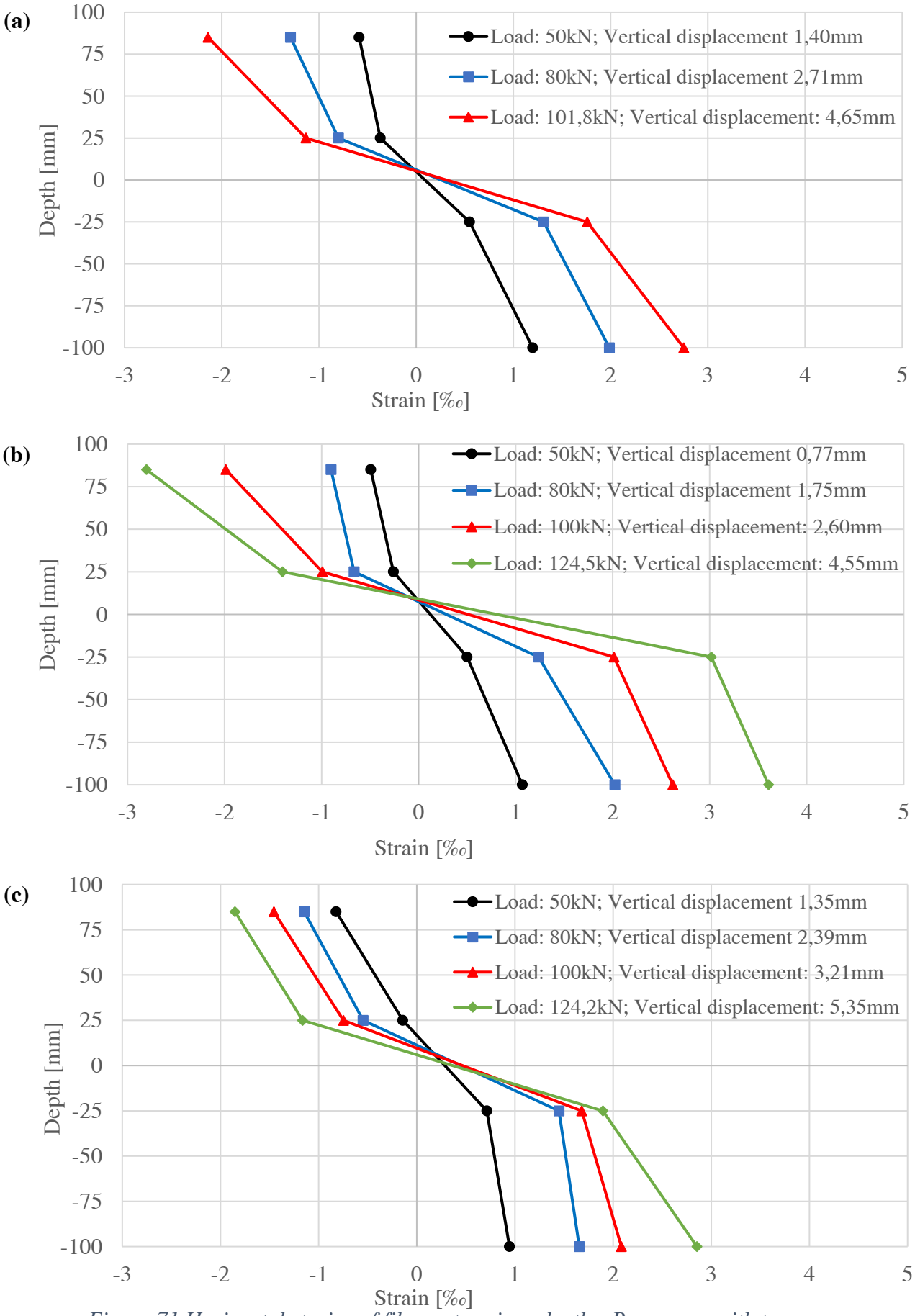

Figure 71 Horizontal strains of fibres at various depths. Beams are with transverse reinforcement: (a) Reference beam; (b) Hybrid beam B1; (c) Hybrid beam B2.

5.2.3 Cracking development and failure modes

5.2.3.1 Reference beam without transverse reinforcement

Figure 72 illustrates the formation of the crack pattern in the reference beam without shear reinforcement. The first flexural crack appeared at the bottom of the mid-span of the beam at the load level of 14,5 kN. Upon increasing the load, other several flexural cracks have developed at the bottom as well but further from the proximity of the mid-span. The full pattern of those flexural cracks has developed at the load level of 43,2 kN (80,7% of the maximum applied load), see Figure 72 a). Adding a higher load has resulted in the inclination of those cracks towards the loading spot, as seen in Figure 72 b). Just after the peak force, see Figure 72 c), the dominant diagonal crack started to widen and expand from the neutral axis towards the compression zone, as seen in Figure 72 d). The shear angle of the main crack equalled 34,6°. Since the ultimate concrete compressive strain has not been exited (see section 5.2.2) at the peak load of 66,7 kN, the main crack can be categorized as diagonal tension failure which is typical for beams with $\eta_a \approx 3{,}0$. A more detailed description of this type of failure can be found in section 2.1.1

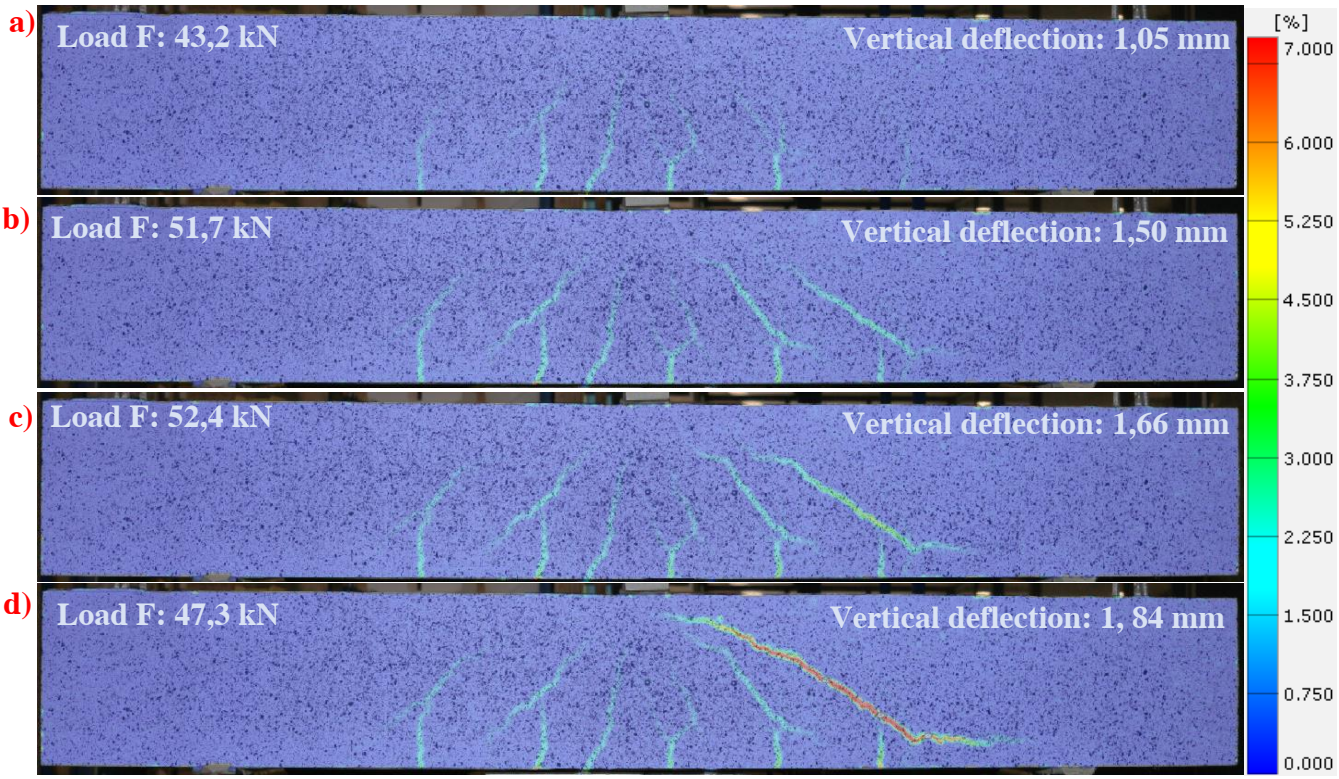

Figure 72 Crack pattern evolution in reference beam without shear reinforcement: major principle strain fields at various loading stages. a) full flexural crack pattern. b) inclination of cracks. c) maximal load. d) post development of failure crack beyond peak load capacity.

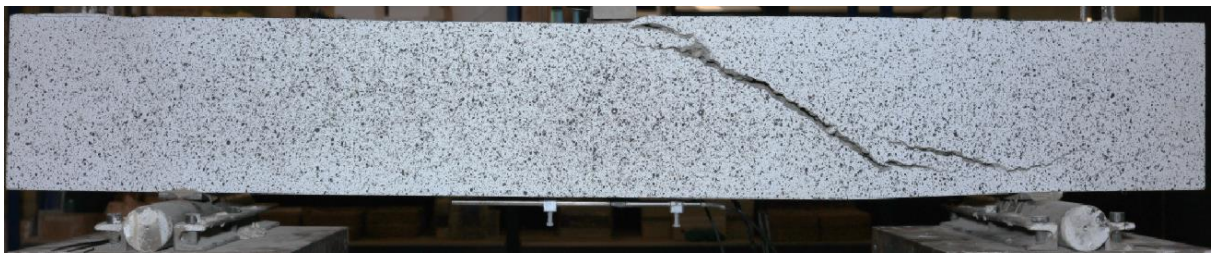

Figure 73 Final crack pattern of reference beam without transverse reinforcement

5.2.3.2 Hybrid beam with smooth laminates without transverse reinforcement

The failure mechanism of this hybrid beam with smooth laminates without shear reinforcement is quite fascinating. Figure 74 presents the evolution of the crack pattern at the progressive loading rate. The first flexural crack appeared at the bottom of the mid-span of the beam at the load level of 17,8 kN. When load F reached 52,2 kN (80,0% of the maximum applied load), the flexural crack pattern was completed. After load F had increased further, the cracks started to incline toward the application of load. Furthermore, new diagonal cracks appear at the neutral axis of the beam. At this point, it seems like the right diagonal crack would be the main crack failure. Suddenly, the left diagonal crack started to grow and expand in its width as the load increased. Hence, this beam experienced diagonal tension failure at the peak load of 65,9 kN. The shear angle of the main crack equalled 29,7°. After the peak load, the SHCC laminate on front side have started to delaminated completely from the NC core and fall of in the last phase.

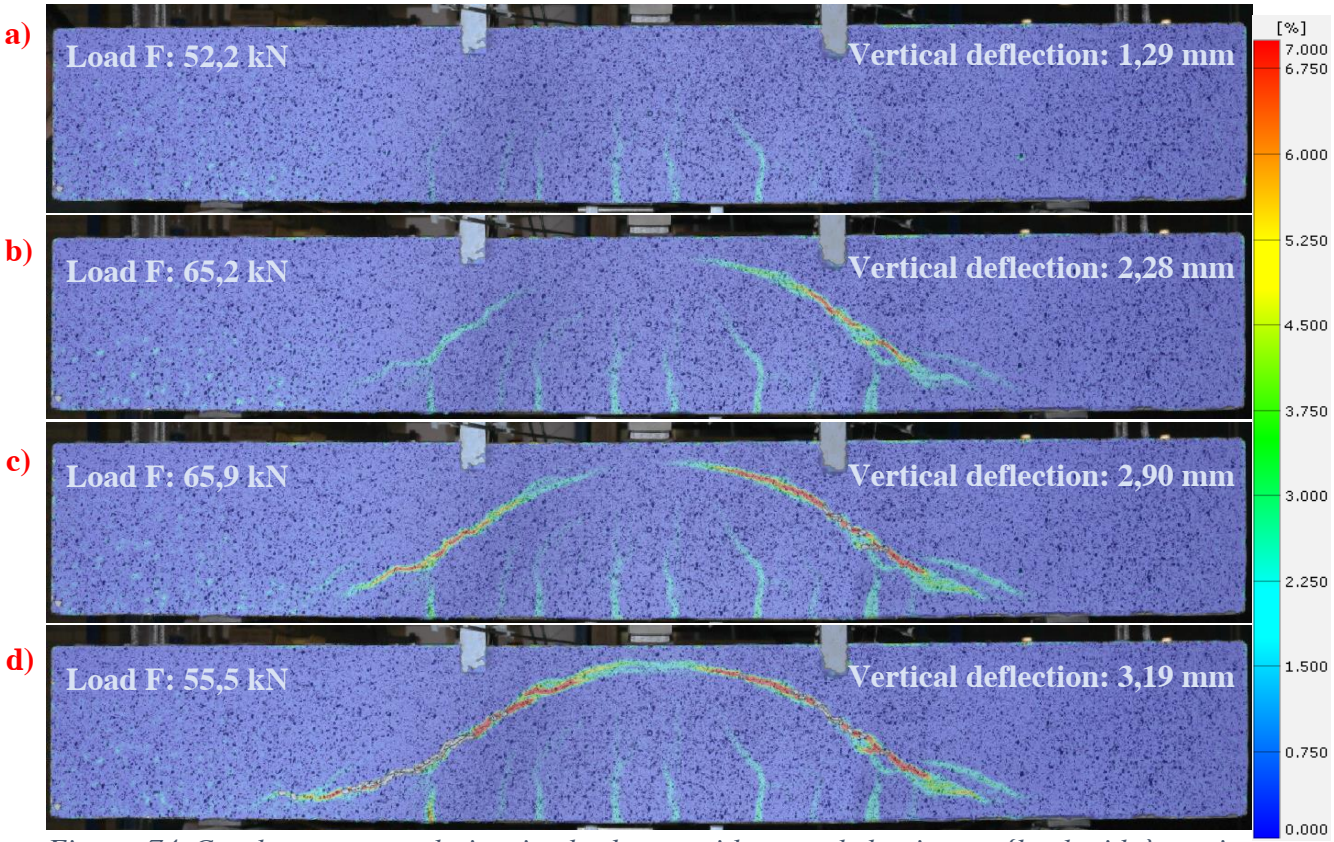

Figure 74 Crack pattern evolution in the beam with smooth laminates {back side}: major principle strain fields at various loading stages. a) full flexural crack pattern. b) inclination of cracks. c) maximal load. d) post development of failure cracks beyond maximal load capacity.

Figure 75 Final crack pattern of the beam with smooth laminates {back side}

5.2.3.3 Hybrid beam with shear keys laminates without transverse reinforcement

The failure mechanism of the hybrid beam with shear keys laminates without shear reinforcement is interesting as well. Figure 76 and 79 show the formation of the crack pattern on the K1 and the K2 side respectively. The first flexural crack appeared at the bottom of the mid-span of the beam at the load level of 20,8 kN (the K1 side). The load level at which the first flexural crack at the K2 side is unknown since LVDT09 blocked the camera view. When the load of 45,4 kN (70% of the maximum applied load) has been reached, the flexural cracks have stabilised. After increasing the load further, those cracks started to incline towards the loading area. Looking at Figure 76 c), it seems like the left diagonal crack would be the main crack. However, with an increase in the load, the right side has localised the main diagonal crack, as seen in Figure 76 d). The total through-thickness of laminates was the smallest on this side, see Figure 35, so the main crack appeared there. The concrete core of the beam has cracked at the same location as the laminates did, as seen in Figure 78. At the peak load of 64,2 kN, the hybrid beam experienced diagonal concrete tension failure with a shear angle of 24,3° for the K1 side and 37,5° for the K2 side. The difference in the shear angle between those sides is considerable. Most likely it has to do with different thicknesses of laminates.

It is interesting to notice that the hybrid beams without shear reinforcement developed diagonal cracks on the left and right spans almost simultaneously. But in the end, only one crack has localized and became the main crack. Looking at the reference beam, there was only one diagonal crack in the development.

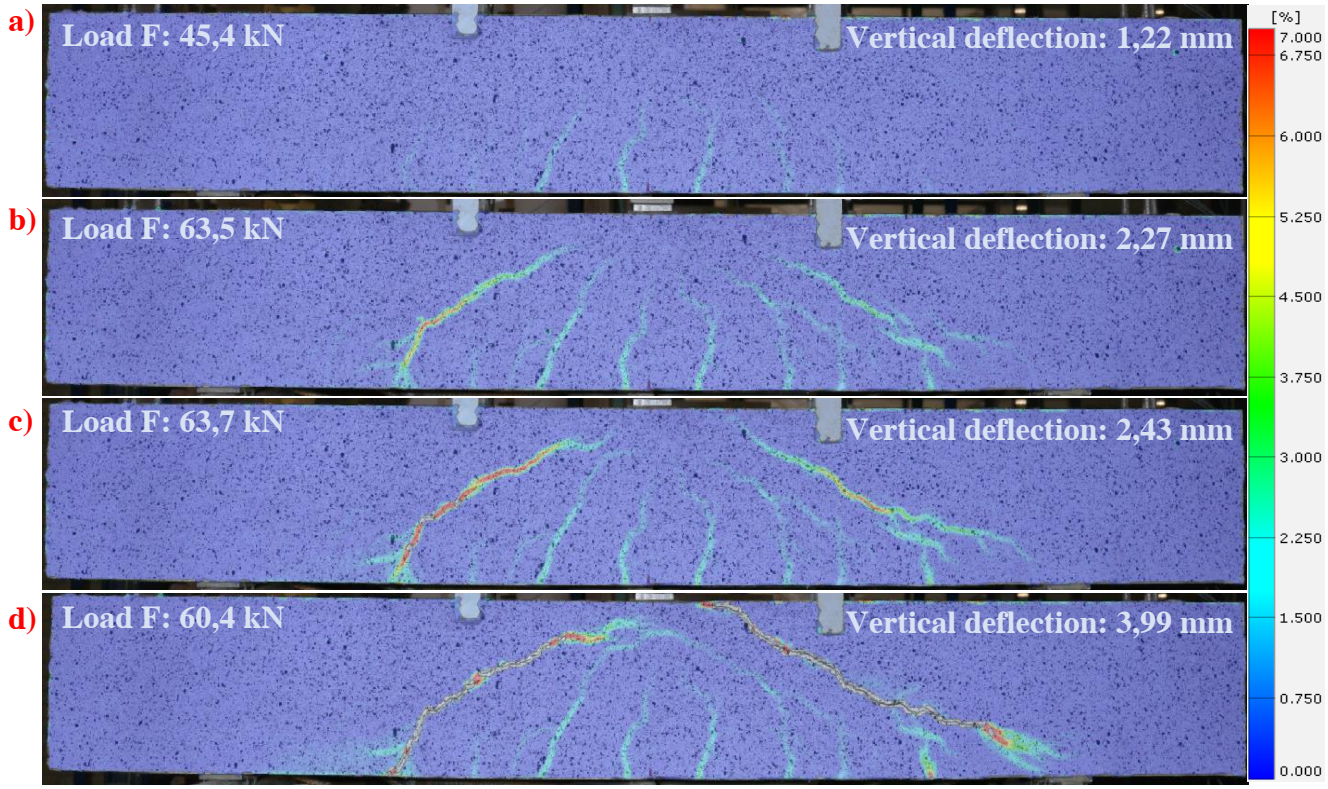

Figure 76 Crack pattern evolution in the beam with shear keys laminates: major principle strain fields at various loading stages. a) full flexural crack pattern. b) inclination of cracks. c) shear crack propagation (the peak load). d) failure pattern at the ultimate deflection. {K1 side view}

Figure 77 Final crack pattern of beam with shear keys laminates (a) K1 and (b) K2 side view.

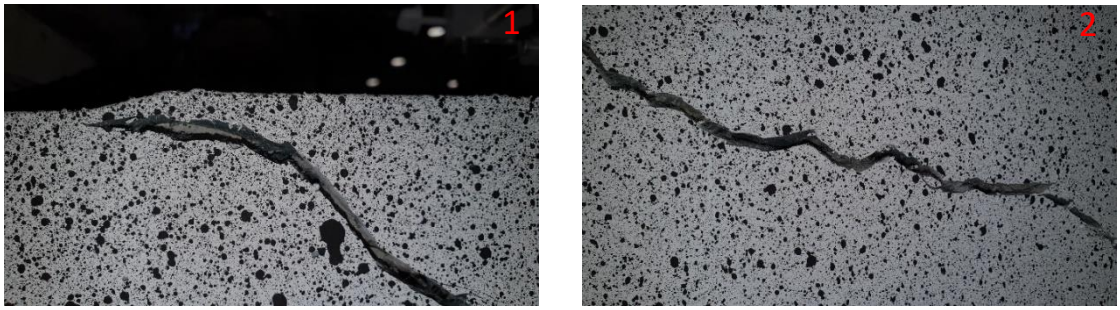

Figure 78Close-up on the details indicated in Figure above. Detail 1: crack penetrates through SHCC K1 laminate and normal concrete. Detail 2: upper part of K1 laminate slip.

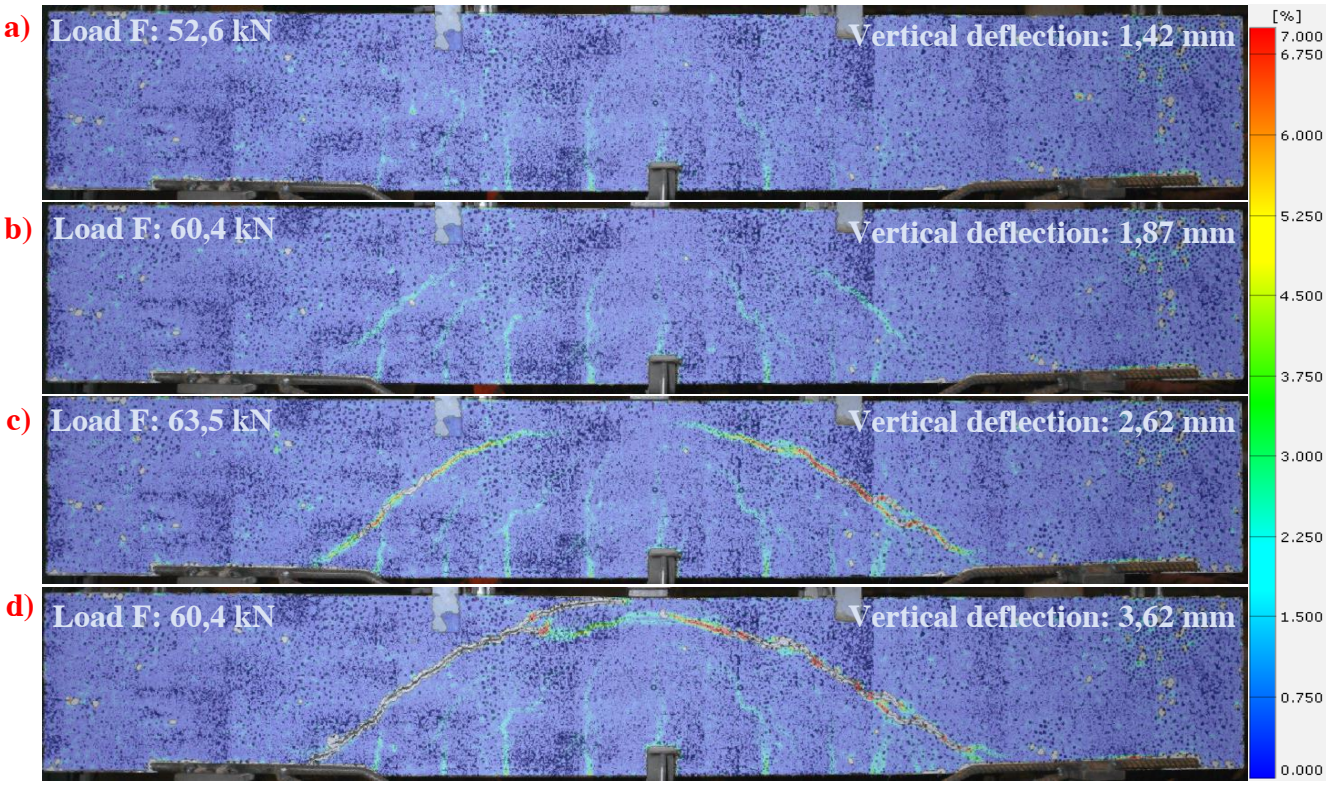

Figure 79 Crack pattern evolution in the beam with shear keys laminates: major principle strain fields at various loading stages. a) full flexural crack pattern. b) inclination of cracks. c) shear crack propagation (the peak load). d) failure pattern at the ultimate deflection. {K2 side view}

5.2.3.4 Reference beam with transverse reinforcement

Figure 80 and 82 illustrate the formation of the crack pattern in the reference beam with shear reinforcement. The first flexural crack appeared at the bottom of the mid-span of the beam at the load level of 19,7 kN. The full pattern of those flexural cracks has developed at the load level of 51,9 kN (50,9% of the maximum applied load), as seen in Figure 80 and 82 a). After applying more load, the cracks start to incline. Cracks that were situated further from the midspan inclined more. Most inclined cracks experience the largest shear stresses and therefore started to widen around the neutral axis of the beam. The crack started to propagate to the location of the load application with shear angles of 36,4° (the font view) and 38,7° (the back view). The main crack only went through one stirrup which was located close to the applied load. However, the crack started at the rigid point between the longitudinal bars and the other stirrup located which was located close to the support. The beam failed in shear without crushing concrete in the compressive zone near support at the peak load of 101,8 kN.

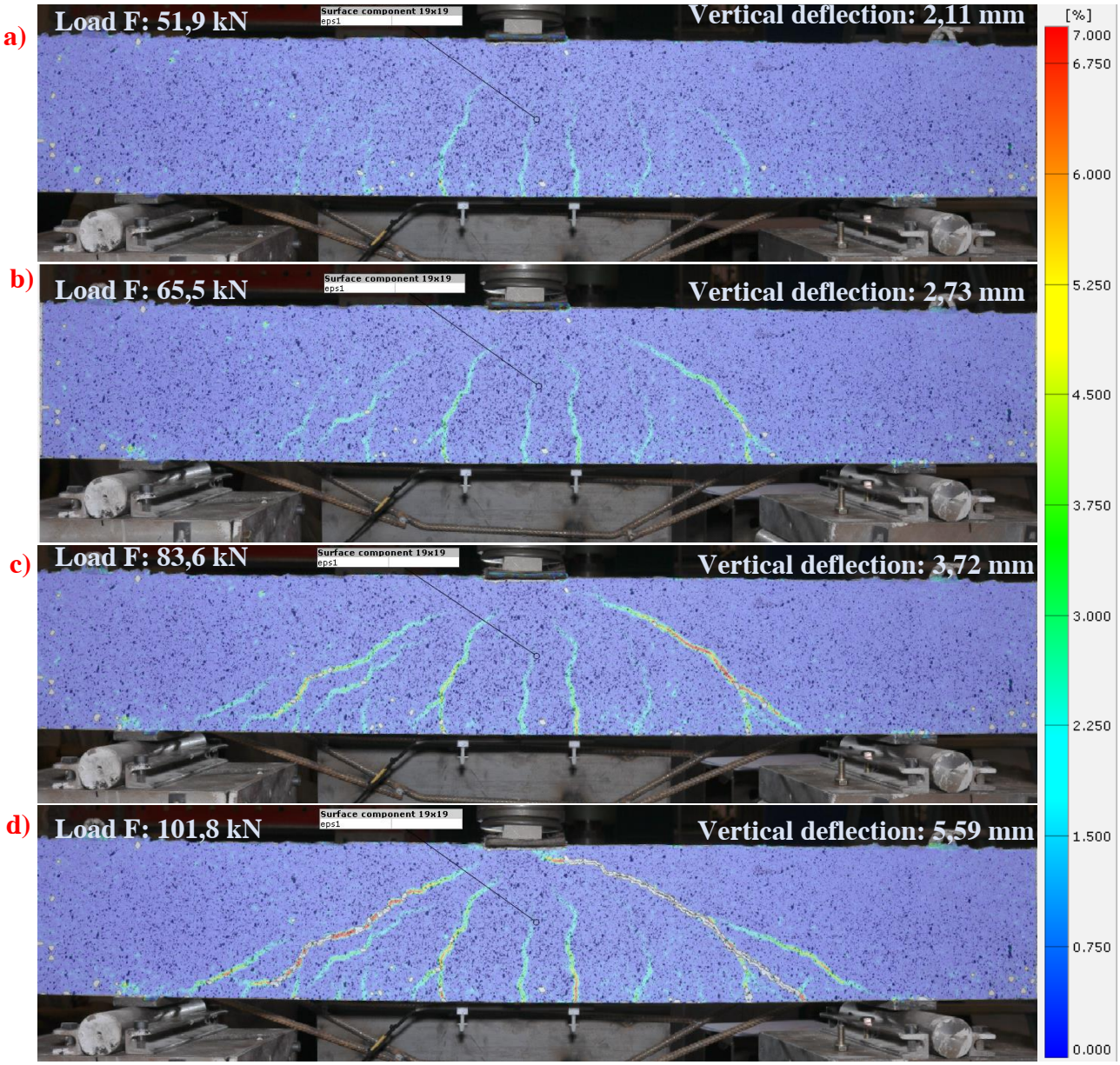

Figure 80 Crack pattern evolution in reference beam with shear reinforcement: major principle strain fields at various loading stages [front view]. a) full flexural crack pattern. b) inclination of cracks. c) formation of failure crack. d) the maximal load.

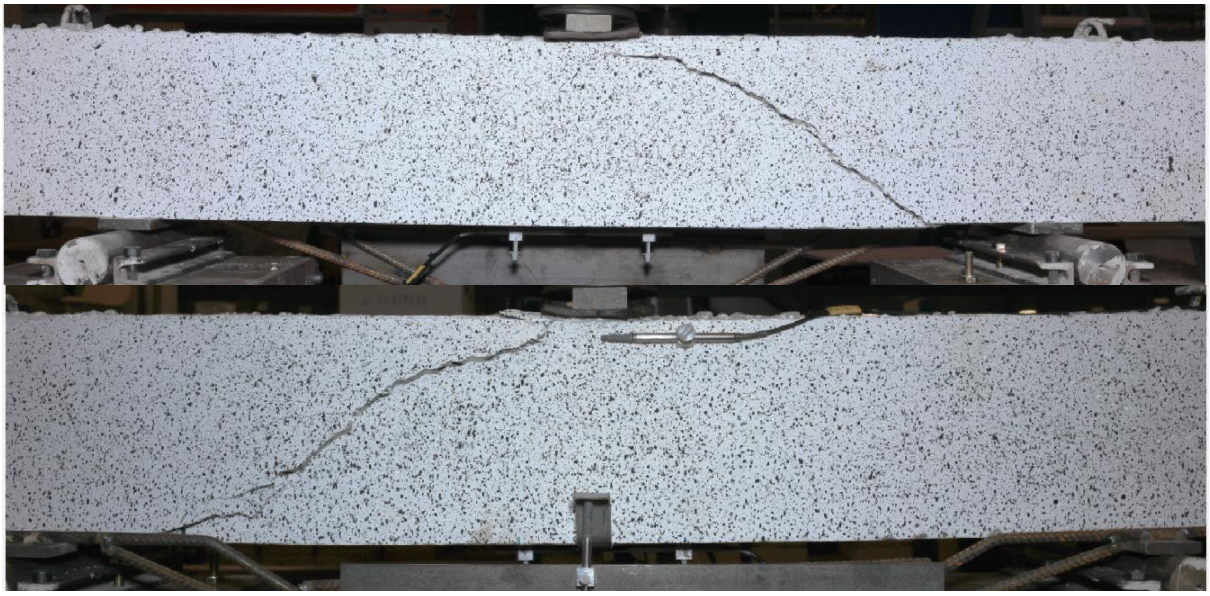

Figure 81 The final crack pattern of refence beam with shear reinforcement. Top picture: the front view. Bottom picture: the back view.

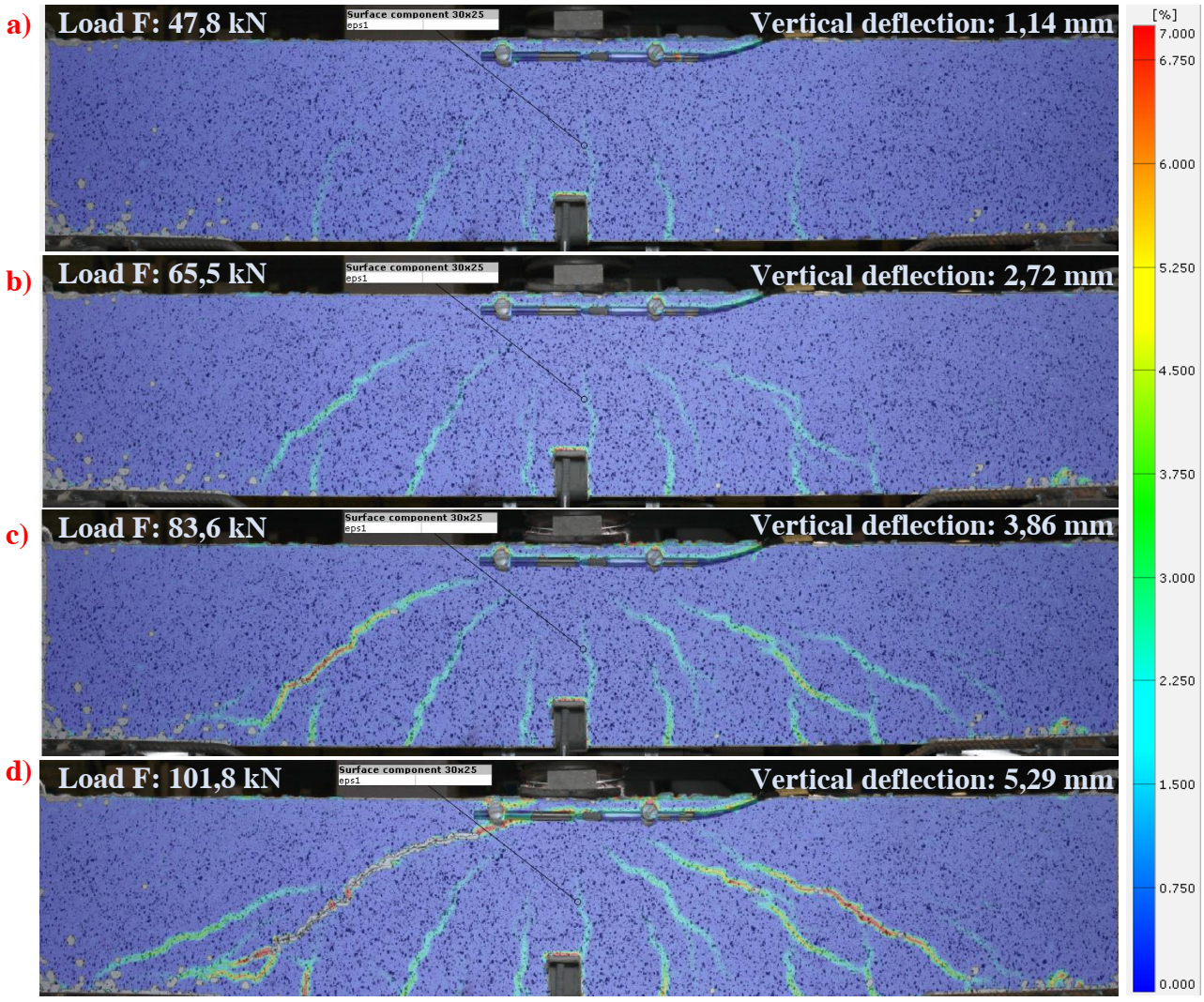

Figure 82 Crack pattern evolution in reference beam with shear reinforcement: major principle strain fields at various loading stages [back view]. a) full flexural crack pattern. b) inclination of cracks. c) formation of failure crack. d) the maximal load.

5.2.3.5 Hybrid beam B1 with transverse reinforcement

Figure 83 and 85 present the evolution of the crack pattern at the progressive loading rate. The first flexural crack appeared at the bottom of the mid-span of the beam at the load level of 26,5 kN. At the load of 64,8 kN (52,3% of the peak load), the full flexural crack pattern has developed, see Figure 83 and 85 a). Upon application of higher load, cracks started to incline and grow towards the loading area with shear angles of 35,9° (the font view) and 32,6° (the back view), as seen in Figure 83 and 85 b). After reaching the loading plate, the cracks experienced widening at the neutral axis of the beam, see Figure 83 and 85 c). The main crack only crossed one stirrup which was located close to the mid-span, as seen in Figure 83 and 85 d). Altogether, this hybrid beam experienced shear failure at the peak load of 124,5 kN.

Similarly to the hybrid beams without shear reinforcement, the (hybrid) beams with shear reinforcement did develop diagonal cracks on the left and right spans almost simultaneously. In contrast, this hybrid beam with stirrups showed the dispersed cracking of SHCC laminates, similar to those during the testing of dog bone specimens. The RC beam with shear reinforcement did not show this kind of dispersed cracking behaviour.

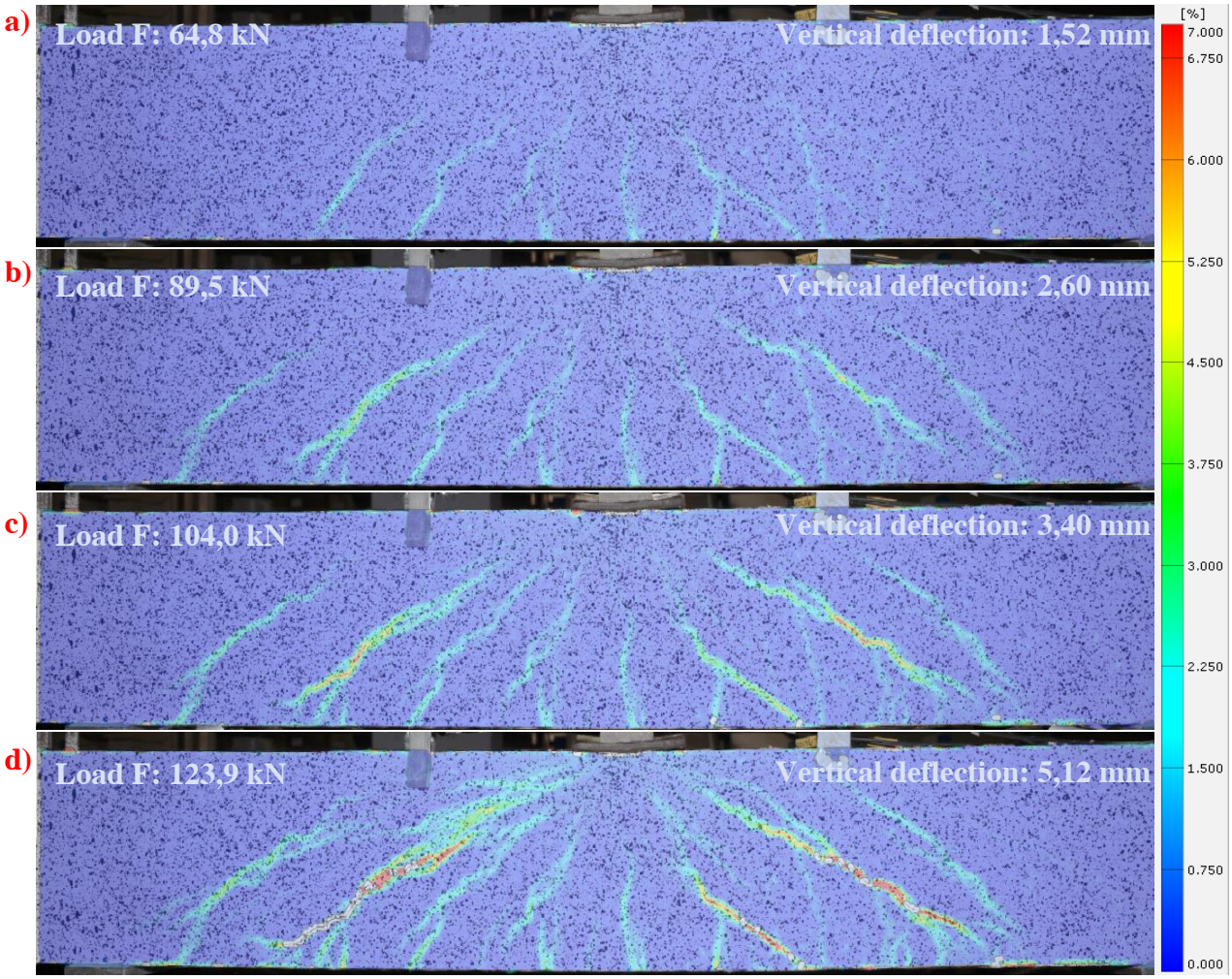

Figure 83 Crack pattern evolution in the hybrid beam B1 with shear reinforcement: major principle strain fields at various loading stages [back view]. a) full flexural crack pattern. b) inclination of cracks. c) formation of failure crack. d) the maximal load.

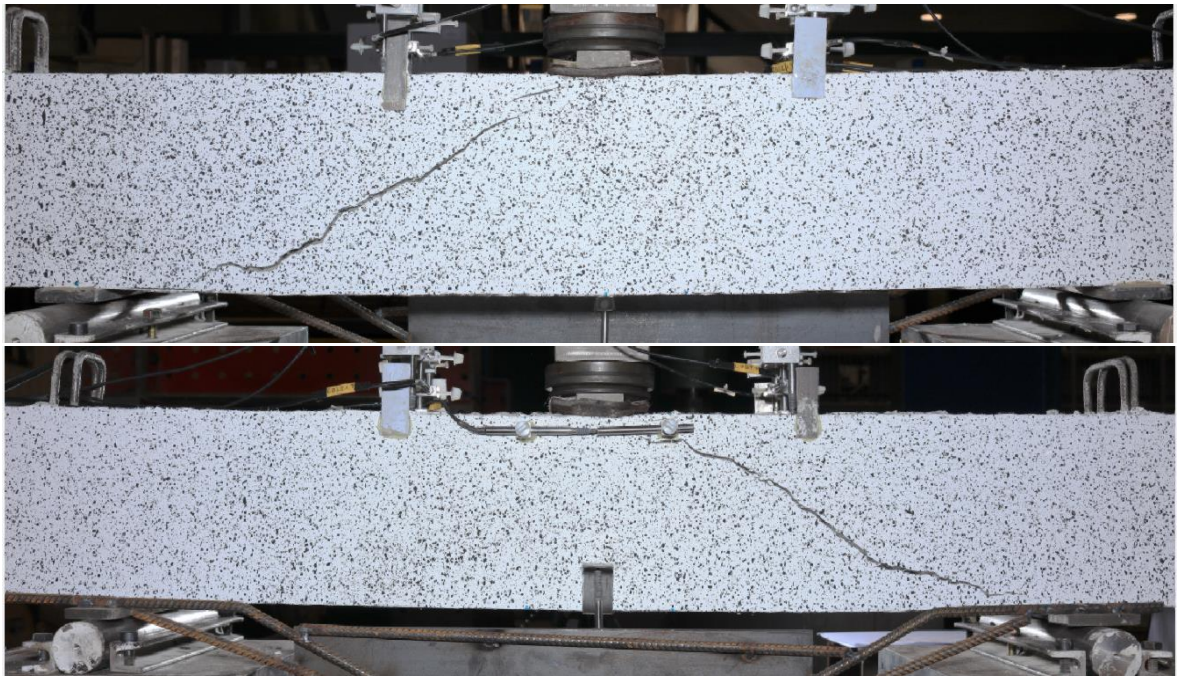

Figure 84 The final crack pattern of the hybrid beam B1 with shear reinforcement Top picture: the back view. Bottom picture: the front view.

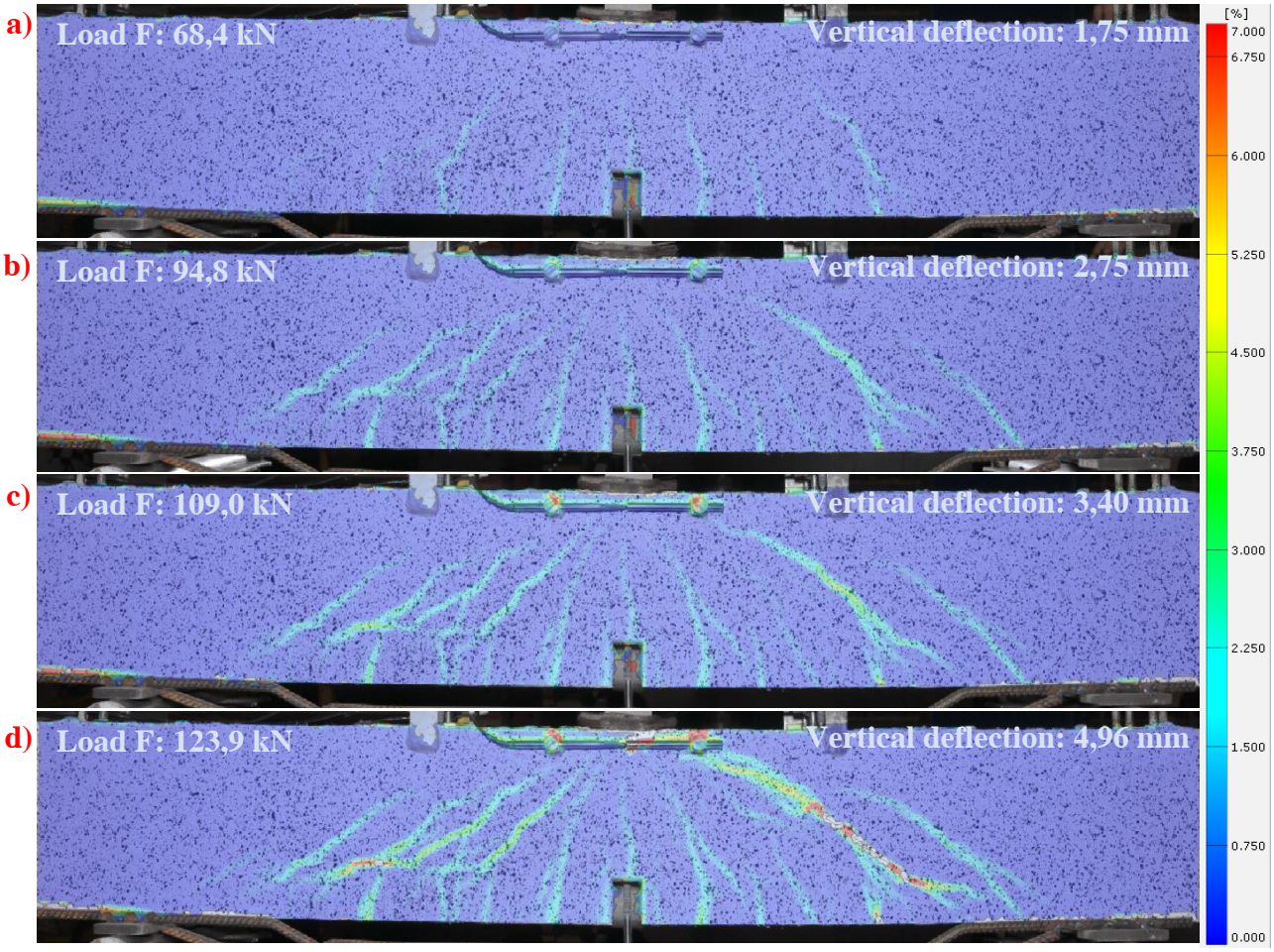

Figure 85 Crack pattern evolution in the hybrid beam B1 with shear reinforcement: major principle strain fields at various loading stages [front view]. a) full flexural crack pattern. b) inclination of cracks. c) formation of failure crack. d) the maximal load.

5.2.3.6 Hybrid beam B2 with transverse reinforcement

Since unexpected large noise in DIC of the back view, the data from this DIC could not be used in this analysis. Fortunately, the data of DIC in the front view have good correlation with LVDTs' data, so the analysis will be based only on those measurements. Figure 86 shows the formation of the crack pattern at different loading stages. The first flexural crack occurred at the load level of 26,2 kN. After reaching the load level of 48,6 kN (39,1% of the peak load), the full flexural crack pattern stabilised, see Figure 86 a). Soon after, those cracks start to incline towards the application of the load, as seen in Figure 86 b). At the same time, new diagonal cracks appear at the neutral axis of the beam. Those cracks grow under the angle of 29,3° towards the loading plate, but also towards the supporting plate. The main crack crossed one stirrup which was located close to the mid-span. The origin of the crack was at the rigid point between the longitudinal bars and the other stirrup located which was located close to the support. Altogether, this hybrid beam experienced shear failure at the peak load of 124,2 kN.

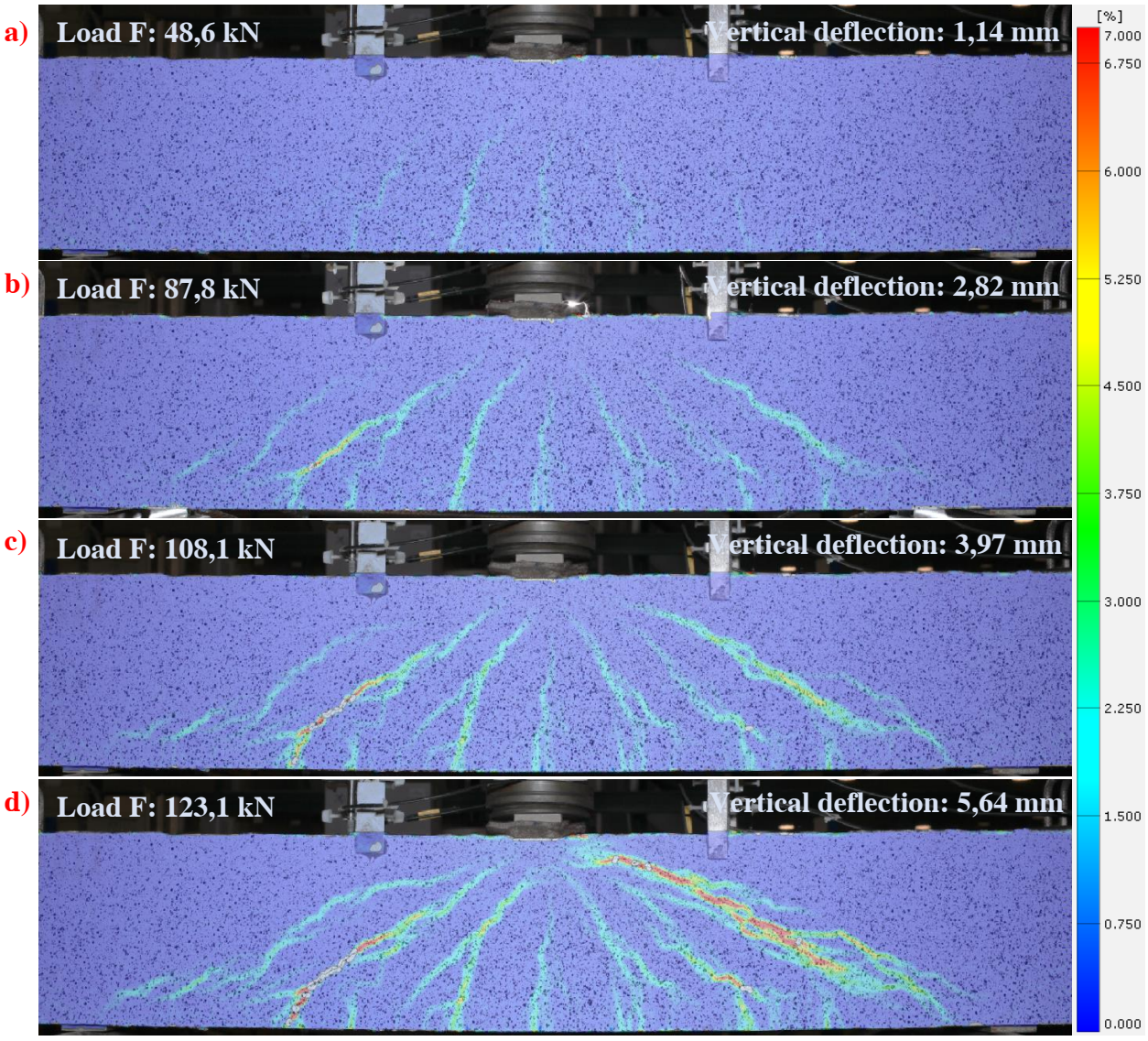

Figure 86 Crack pattern evolution in the hybrid beam B2 with shear reinforcement: major principle strain fields at various loading stages [front view]. a) full flexural crack pattern. b) inclination of cracks. c) formation of failure crack. d) the maximal load.

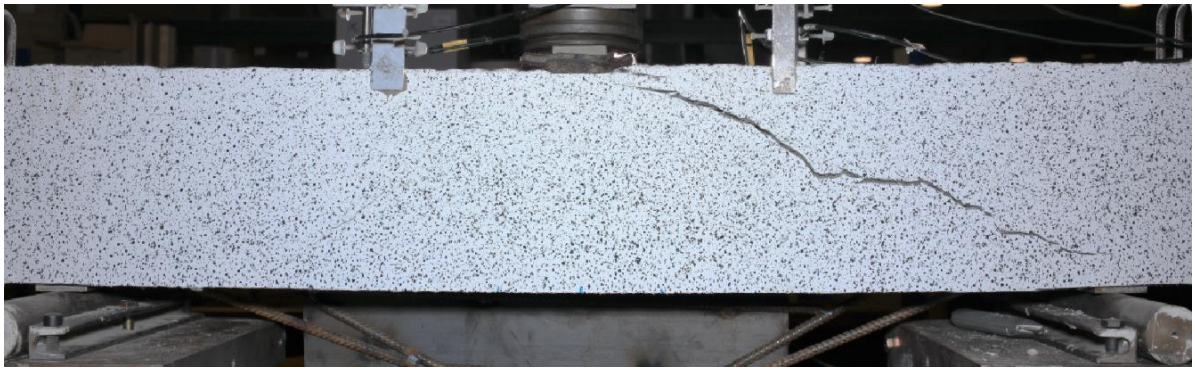

Figure 87 The final crack pattern of hybrid beam B2 with shear reinforcement [front view].

This hybrid beam have developed diagonal cracks on the left and right spans, like the reference beam did. But, those cracks were more dispersed, similar to the hybrid beam B1.

5.2.3.7 Overview of cracking development and failure modes

Table 18 summarizes the test results, namely peak load, deflection at peak load, failure mode and shear angle of main failure crack.

Table 18 Results in terms of peak load, deflection at peak load, failure mode and shear angle

Series nr.	Specimen type	Peak Load [kN]	Deflection at peak load [mm]	Failure mode	Shear angle [a] [°]
First (without TR)	Reference beam {120 × 200 mm²}	53,5	1,46	Diagonal tension failure	34,6
	Hybrid beam with smooth laminates {120 × 200 mm²}	66,7	2,77	Diagonal tension failure	29,7
	Hybrid beam with shear keys laminates {120 × 200 mm²}	65,6	2,56	Diagonal tension failure	24,3 (K1) 37,5 (K2)
Second (with TR)	Reference beam {120 × 200 mm²}	101,8	4,65	Shear	36,4 (front) 38,7 (back)
	Hybrid beam B1 {120 × 200 mm²}	124,5	4,54	Shear	35,9° (font) 32,6° (back)
	Hybrid beam B2 {120 × 200 mm²}	124,2	5,35	Shear	29,3° (front)

[b] The words in parentheses refer to the specific sides of the beams

5.2.4 Interface displacement

All hybrid beams in this experiment were visually inspected for signs of any delamination after demoulding and two days later shortly before testing. During demoulding of the beams, no partial nor full delamination of SHCC laminates from normal concrete cores has been spotted. However, prior to the testing of the hybrid beam with smooth laminates, partial delamination has been clearly visible, as seen in Figure 88. The reason for those bonding failures in this hybrid beam was the differential shrinkage between SHCC laminates and the NC core. The other hybrid beams did not show any sign of delamination prior to their testing.

Figure 88 Partial delamination of laminates prior to testing. The bottom laminate (in this picture) is the laminate which delaminated completely during the test.

Figure 89 shows the largest slip and opening measurements of SHCC laminates in the first series relative to normal concrete cores. The detailed measurements are provided in Appendix E, see Figures from E-12 to E-19. As shown in the graphs below, the maximum values for the smooth interface are much higher than the rough interface. The 'rough interface' refers to the interface between a shear key laminate and a normal concrete core. According to the requirement specified in fib Bulletin 43 [57], an ultimate slip of smooth interface should not exceed 2 mm and an ultimate width of the opening should not exceed 0,1 mm. When displacement exceeds one of the criteria, lateral separation should be assumed. Since those criteria have been violated during the testing of the hybrid beam with smooth SHCC laminates, see Figure 89, delamination is acknowledged. It can be argued that it has happed after the peak load. The visual proof is shown in Figure 90. The delamination of this smooth laminate was spotted with the naked eye at approximately 2,6 mm deflection of the beam.

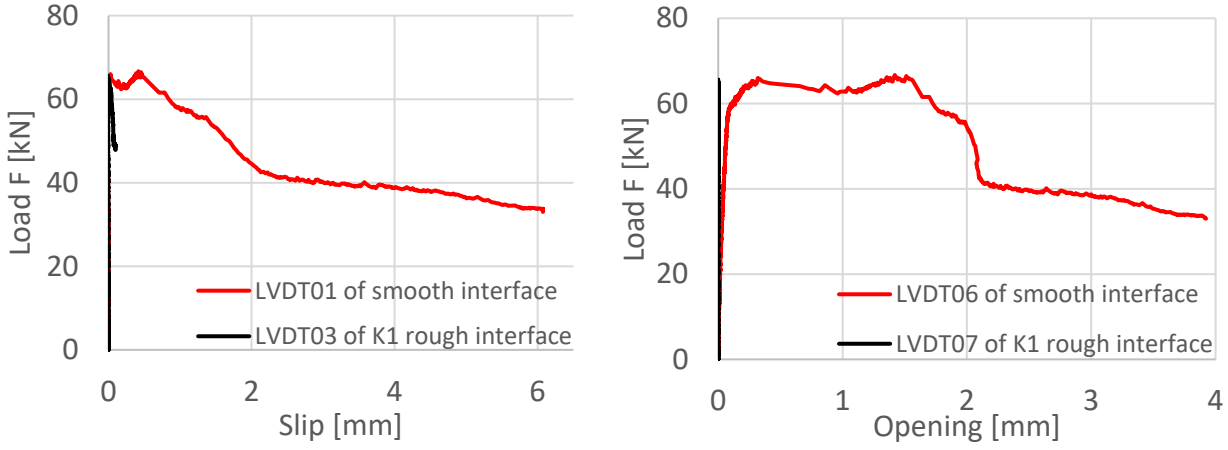

(a) Slip – Vertical displacement **(b) Opening – Horizontal displacement**

Figure 89 Largest interface displacement (slip and opening) measured for hybrid beams without transverse reinforcement.

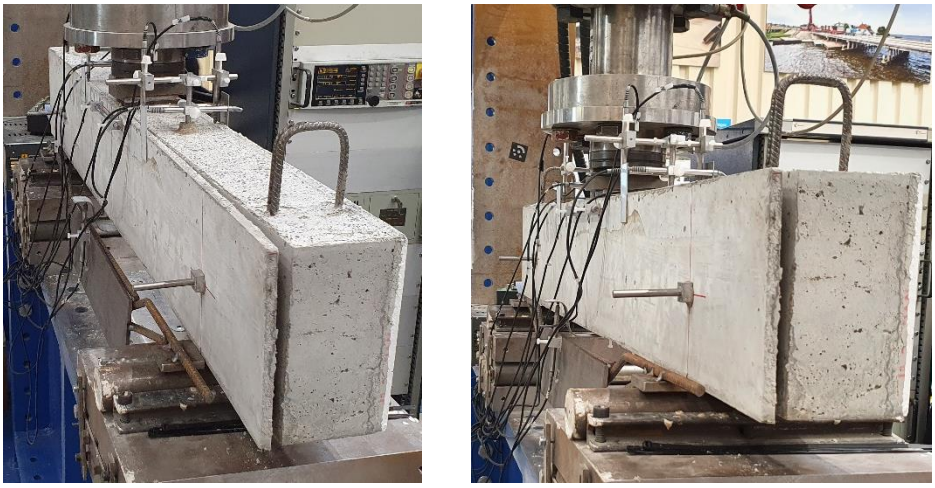

Figure 90 Delamination of the laminate on the front side. Pictures were taken after the test.

The rough interface of K1 laminate has displace less relative to the normal concrete core than K2 laminate did. The interface slip did not exceed 0,1 mm nor the interface opening did not exceed 0,051 mm. According to the requirement specified in fib Bulletin 43 [57], an ultimate slip of rough interface should not exceed 2,5 mm and an ultimate width of the opening should not exceed 1,1 mm. The values are thus lower than those criteria, therefore SHCC laminates with shear keys did not delaminate from this hybrid beam without shear reinforcement.

Figure 91 illustrates the largest slip and opening measurements of SHCC laminates with shear keys relative to normal concrete cores in the second series. The rough interfaces in hybrid beam B1 did not exceed 0,27 mm slip nor 0,80 mm opening. Those values are still lower than the requirement specified in fib Bulletin 43 [57], so the laminates in hybrid beam B1 have not separated during the testing of the beam. In hybrid beam B2, the largest slip and opening measurements are unknown because the holder responsible for holding LVDT05, LVDT06, LVDT09 and LVDT10 have tilted during the testing due to cracking in the NC core, as seen in

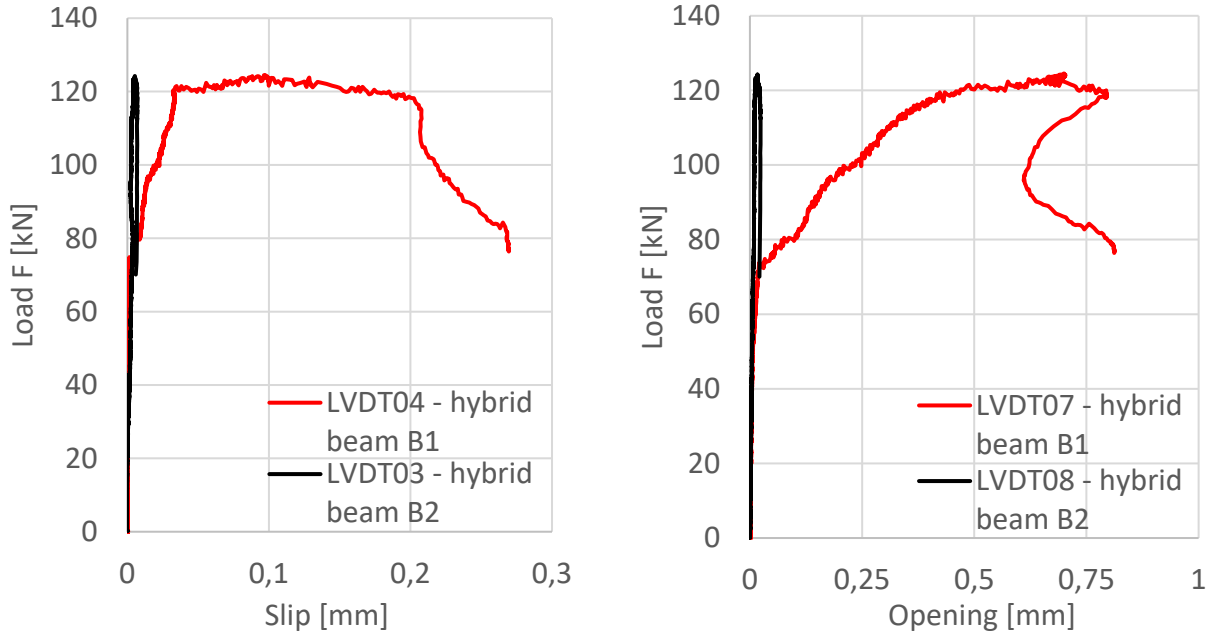

(a) Slip – Vertical displacement **(b) Opening – Horizontal displacement**

Figure 91 Largest interface displacement (slip and opening) measured for hybrid beams with transverse reinforcement.

Figure 92. This crack originated from the load application and has been growing towards the holders during the loading. This caused errors in the measurements in the governing slip and opening. The measurements were higher than in reality, but even including those errors the criteria of fib Bulletin 43 [57] have not been exceeded. Therefore it is safe to say that laminates of hybrid beam B2 have not delaminated. The detailed measurements for hybrid beams B1 and B2 are provided in Appendix F, see Figures from E-18 to E-21.

Figure 92 The close-up on final cracks of the hybrid beam B2 with shear reinforcement. Top picture: the top view of the load application. Bottom picture: the side view near load application.

5.2.5 Stiffness degradation

The initial stiffnesses of the beams are summarized in Table 19. Of course, there are many definitions of the initial stiffness of RC beams in the literature. They all do agree that is about the initial slope of the linear zone of a load-displacement curve. However, it is still debated at which percentage of the maximum load ends this linear zone. In general, it is somewhere between 10% and 40% of the maximum load. In this study, it is calculated as 20% of the maximum capacity of a beam. The stiffness of a simply supported beam with a point load at midspan was determined by forget-me-nots, see Figure 93. The equation for the initial Young's modulus of the system is as follows:

$E_{ini} = \frac{1}{48} \cdot \frac{F \cdot L^3}{I} \cdot \frac{1}{w}$ where: F = 20% of the maximum load (N); L = span of simply supported beam (mm); I = second moment of area (mm^4); w = deflection of the beam at 20% of the maximum load.

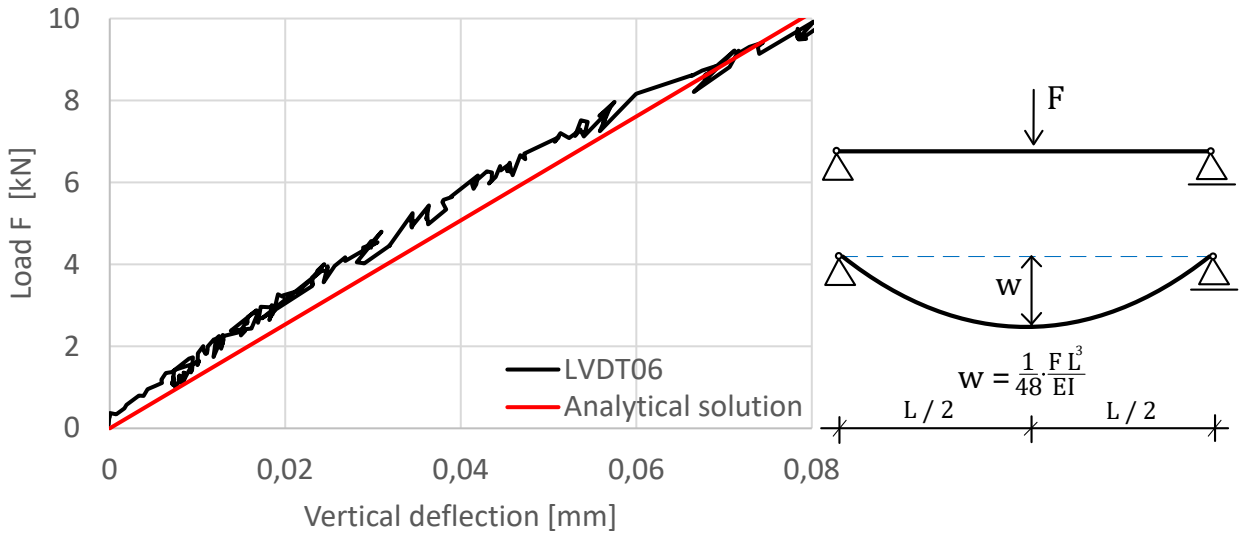

Figure 93 On the right: Close-up of Figure 94 with analytical solution plotted. Load F versus vertical deformation of the reference beam without transverse reinforcement. On the left: forget-me-nots of a simply supported beam.

Table 19 Initial stiffness and Young's modulus of beams

Series nr.	Specimen type	20% of peak load [kN]	Deflection at 20% of peak load [mm]	Initial stiffness [kN/mm]	Initial Young's modulus [MPa]
First (without TR)	Reference beam {120 × 200 mm²}	10,7	0,087	122,476	31895
	Hybrid beam with smooth laminates {120 × 200 mm²}	13,3	0,145	92,043	23670
	Hybrid beam with shear keys laminates {120 × 200 mm²}	13,1	0,156	84,260	21943
Second (with TR)	Reference beam {120 × 200 mm²}	20,4	0,451	45,174	11764
	Hybrid beam B1 {120 × 200 mm²}	24,9	0,266	93,736	24410
	Hybrid beam B2 {120 × 200 mm²}	24,8	0,546	45,481	11844

The initial stiffness of the RC beam without shear reinforcement was 24,8% higher than that of the hybrid beam with smooth laminates without shear reinforcement, and was 31,2% higher than that of the hybrid beam with shear keys laminates without shear reinforcement. The initial Young's modulus of this reference beam was approximately the same magnitude as Young's modulus of normal concrete prisms, as seen in Table 9.

The initial stiffness of the reference beam with transverse reinforcement was 63,1% lower than the reference beam without transverse reinforcement. It is odd since Young's modulus of the normal concrete prism in the second series was similar in quality to that of the first series. It seems like the reference beam with shear reinforcement was not properly densified on the vibrating table during casting, see Appendix C.2. The surfaces of the beam looked good during visual inspection. The same can be said about hybrid beam B2 since its initial stiffness was 62,9% lower than that of the reference beam with transverse reinforcement. The hybrid beam B2, however, showed expected initial stiffness which was only 23,5% lower than that of the reference beam with shear reinforcement. Figure 95 illustrates the initial vertical deflections of every beam. At higher loads, cracks in concrete and SHCC cause stiffness deterioration.

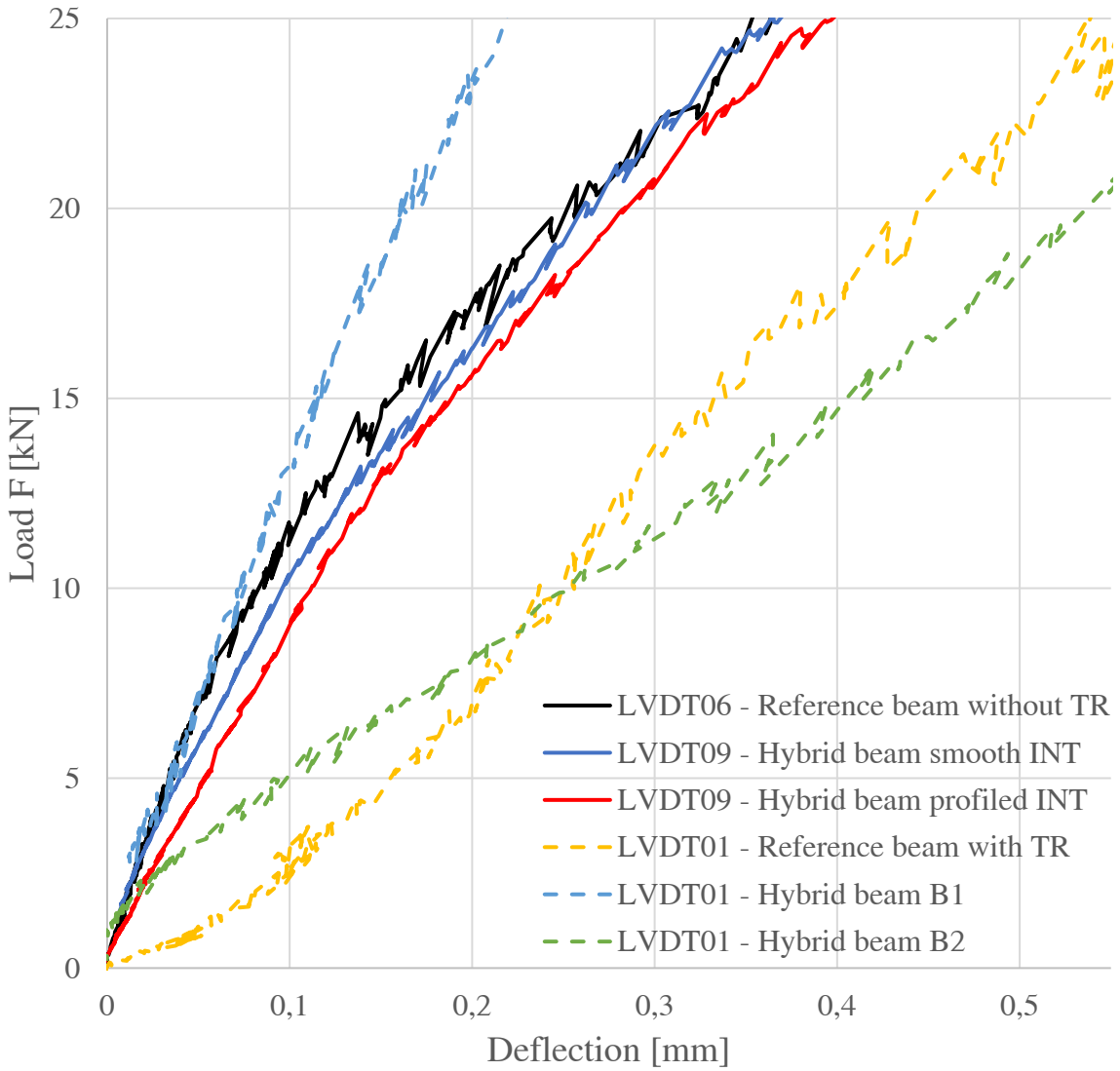

Figure 95 Load F versus vertical midspan deflection of the beams. The solid line shows beams without transverse reinforcement (TR). The dashed line represents beams with TR. The "INT" abbreviation stands for the word: interface.

5.2.6 Energy dissipation capacity

Whether loading a simple beam or a complex structure, the area under their load-deflection curves (A) equals the work (W) generated by the force (F). If a system does not return to its original state, it means that energy has dissipated from the system. The essential feature of (concrete) structures is their ability to absorb energy before their collapse. The energy dissipation capacity of a beam can therefore be defined as the area under its load deflection curve until its maximum load is reached.

The energy dissipation capacity of the beams are summarized in Figure 96. From the results is clear that the hybrid beams dissipate more energy than their conventional counter parts. The hybrid beam with smooth laminates without shear reinforcement and the hybrid beam with shear keys laminates without shear reinforcement have absorbed 173% (86,05 kNmm) and 318% (158,21 kNmm) more energy, respectively, than the reference beam without shear reinforcement. The difference in energy dissipation between those two hybrid beam can be explained due to weaker bond of the smooth SHCC laminate with the NC core compared to the SHCC laminate with shear keys.

Furthermore, the RC beam with transverse reinforcement has dissipated 514% (256,27 kNmm) more energy than the RC beam without transverse reinforcement. The hybrid beams B1 and B2 have absorbed 27% (82,89 kNmm) and 39% (118,2 kNmm) more energy, respectively, than their reference beam.

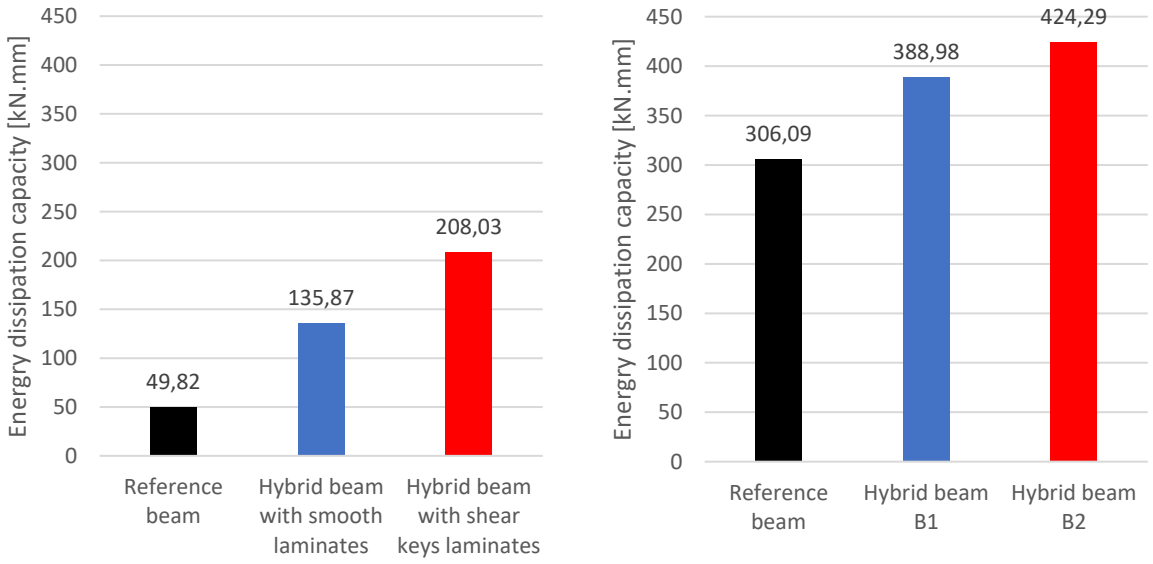

Figure 96 Energy dissipation capacities of the beams (a) without transverse reinforcement and (b) with transverse reinforcement

5.2.7 Growth rate of main diagonal cracks

Analysis of the growth rate of the main diagonal cracks was carried out using DIC. The growth rate of a crack can be obtained by taking the difference in major principle strain between two load stages. The major principle strain rates of the reference beam without shear reinforcement are shown in Figure 97. This figure attempts to provide an overview of the growth rate of the main diagonal crack just before the failure in the reference beam. As can be seen, the rate of the main crack only increases in its width as the load approach its peak. Figure 99 and 100 show the major strain rates of the hybrid beams without shear reinforcement. In contrast to the reference beam, the major stain rates in the hybrid beams fluctuated. This occurs at lower F load than any peak load of hybrid beam without transverse reinforcement. But at the same time, F load at fluctuation is higher by roughly 19% than the peak load of the reference beam without stirrups. The cause of why it happens will be explored and discussed in the follow-up chapter.

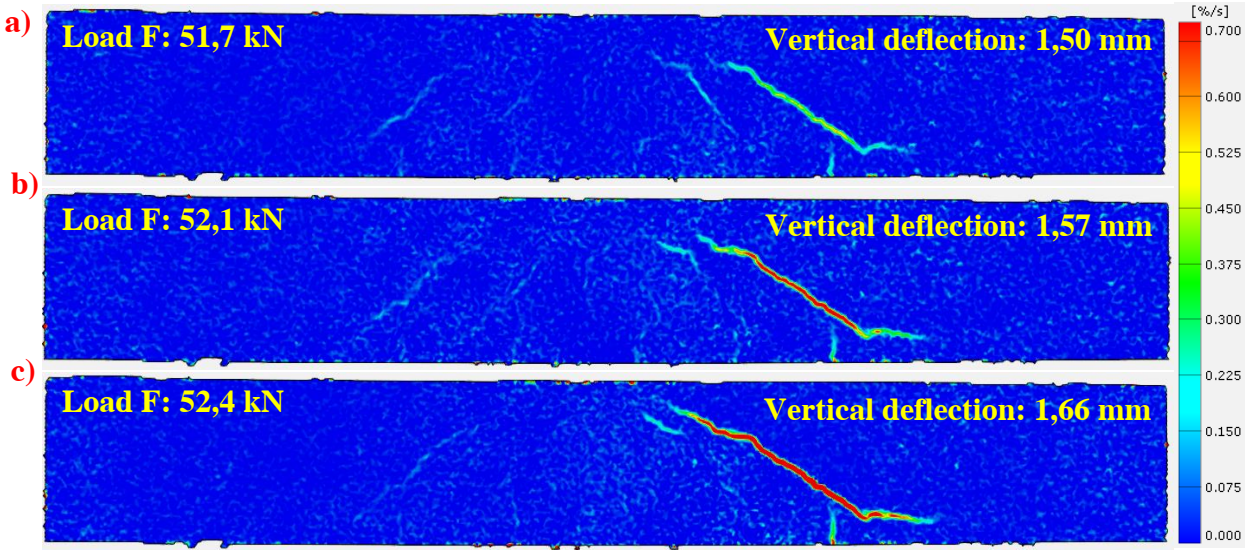

Figure 97 Major principle strain rate evolution in reference beam without shear reinforcement at various loading stages: a) & b) just before the peak load; c) the maximal load.

Furthermore, the hybrid beams with shear reinforcement did not show this kind of behaviour. The main diagonal crack of those beams had no sudden jumps during their growth. The situation with transversal reinforcement was therefore better because there was still some ductility available by stirrups and as consequence, the cracks at the surface did not open rapidly. Additionally, the SHCC had sufficient time to disperse the major strain, see Figure 98. Hence, the diagonal cracks were less localized.

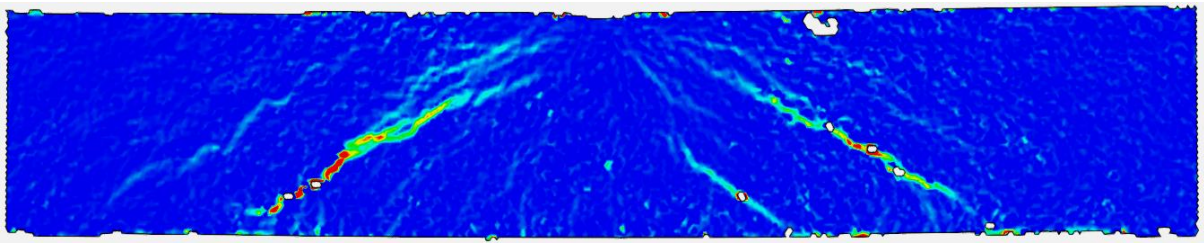

Figure 98 Typical major principle strain rate evolution in hybrid beam with shear reinforcement. Same scale as in the previous figure.

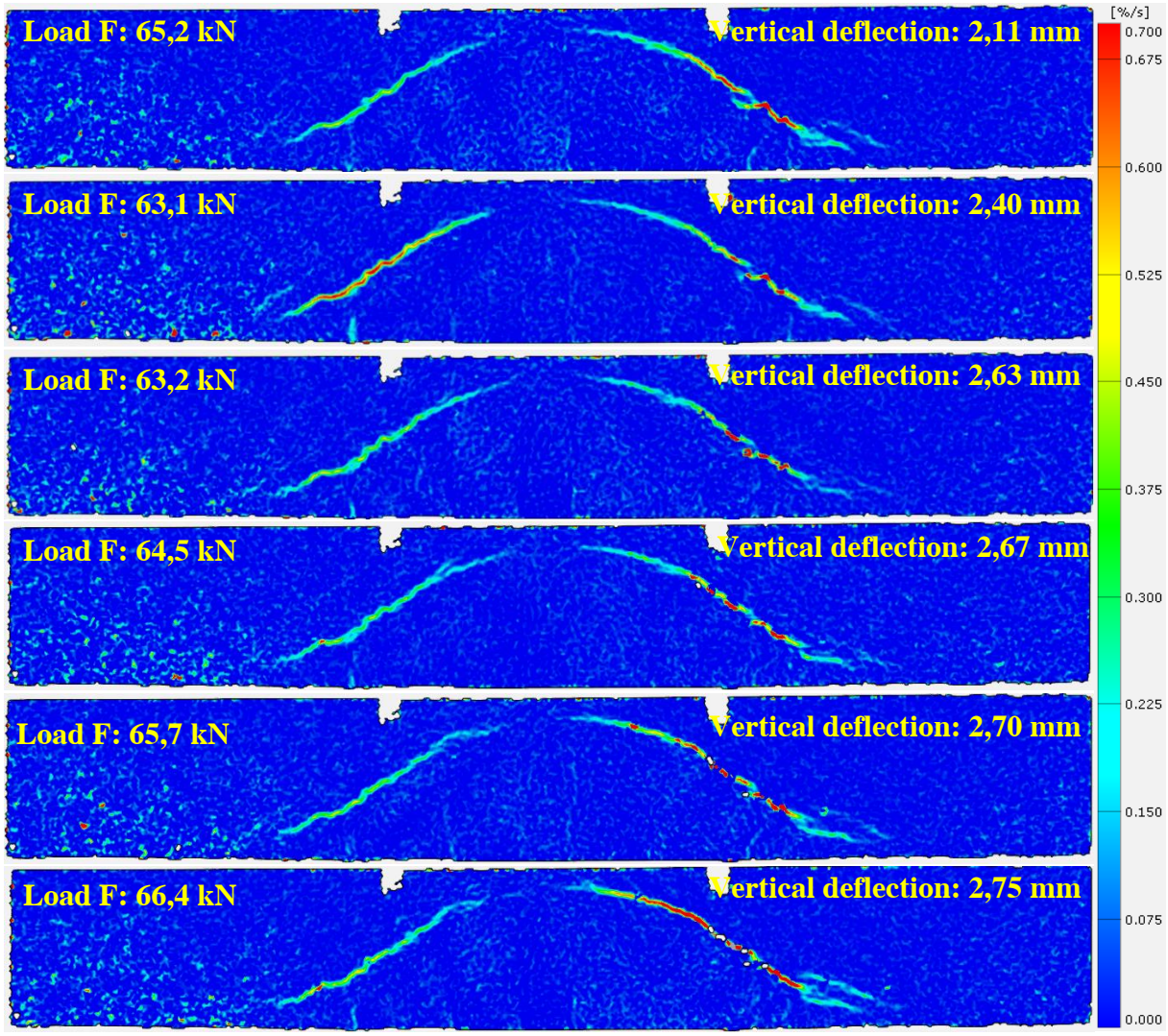

Figure 99 Major principle strain rate evolution in hybrid beam without shear reinforcement with smooth laminates at various loading stages.

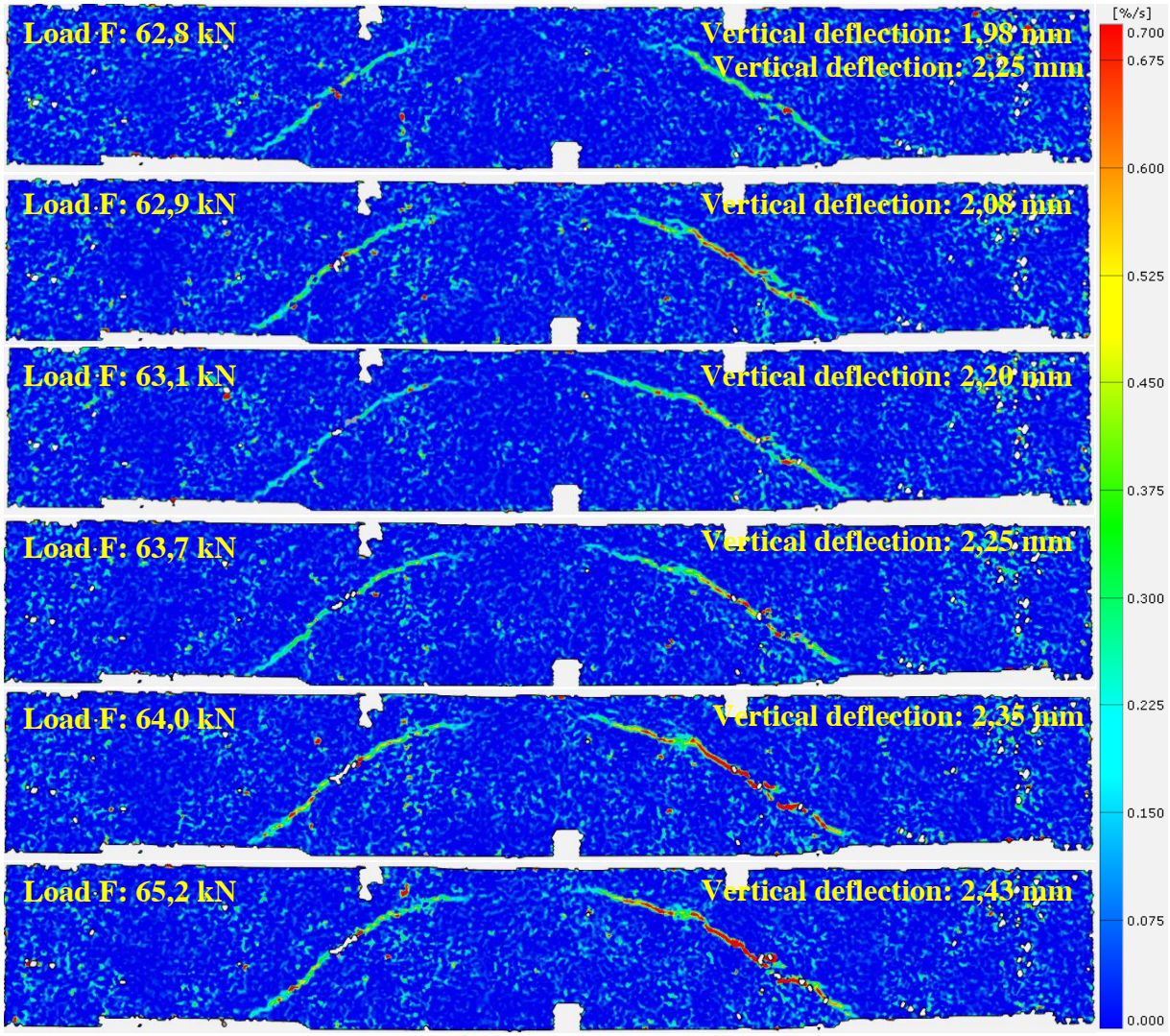

Figure 100 Major principle strain rate evolution in hybrid beam without shear reinforcement with shear keys laminates at various loading stages. {K2 side view}

6

Analysing results in-depth & Discussion

"The heart of mathematics consists of concrete examples and concrete problems"

Paul Richard Halmos

In this chapter, the equations are listed for the prediction of the ultimate shear strength capacities of the hybrid beams. During the designing of RC beams, the model for calculating the resistance of RC beams was based on the Eurocode 2 approach. But this approach is insufficient in the case of hybrid beams since EC2 does account for the contribution of SHCC laminates to the shear capacity of a beam. For this reason, the Eurocode 2 approach has been modified based on proposed models in current literature in such a way that it does. All limitations of modified approaches are listed. Furthermore, all results are critically examined and discussed at the end of this chapter.

The first section shows the calculation of the theoretical shear capacities of the (hybrid) beams with and without shear reinforcement from this experiment. In the second section, the theoretical shear capacities of (hybrid) beams, which have been found in the literature, are calculated. The last section discusses all results found in the experiments and the literature in order to explain some trends. In the paragraph below, the main parameters are listed which have been used for the design of those beams.

6.1 Theoretical shear capacity of (hybrid) beams – analytical methods

These sections focus on the analytical methods that could predict the shear capacities of the hybrid beams with and without shear reinforcement. The first subsection focus on the first case and the latter case is shown in the last subsection. In the second subsection, more detailed calculations have been performed on the shear capacity of the RC beam with shear reinforcement since the Eurocode 2 approach could not predict the capacity of this beam correctly. In the paragraph below, the main parameters are listed which have been used for the design of those beams.

Material properties and mechanical properties for beams in this experiment

The self-weight of beams is neglected. The beams were loaded by the concentrated load 'F' at mid-span. The beams are simply supported. The theoretical capacities are based on mean values:

Geometric parameters:

$Span$	$L = 1$	$[m]$
$Cover$	$c = 25$	$[mm]$
$Height$	$h = 200$	$[mm]$
$Width$	$b = 120$	$[mm]$
$Second\ moment\ of\ area$	$I = \frac{1}{12} \cdot b \cdot h^3 = 8 \cdot 10^7$	$[mm^4]$

Reinforcement parameters:

$Average\ yield\ strength$	$f_{ym} = 560$	$[MPa]$
$Young's\ modulus$	$E_s = 200$	$[GPa]$
$Diameter\ of\ longitudinal\ reinforcement$	$\emptyset_{16}^{L} = 16$	$[mm]$
$Numbers\ of\ longitudinal\ rebars$	$n = 2$	$[-]$
$Area\ of\ longitudinal\ reinforcement$	$A_{sl} = n \cdot \frac{\pi \cdot \emptyset_{16}^{L\ 2}}{4} = 402{,}12$	$[mm^2]$
$Effective\ height$	$d = h - c - \frac{\emptyset_{16}^{L}}{2} = 167$	$[mm]$
$Longitudinal\ reinforcement\ ratio$	$\rho_{sl} = \frac{A_{sl}}{b \cdot d} \cdot 100\% = 2{,}01$	$[\%]$

Concrete parameters:

Properties of C20/25 according to NEN-EN 1992-1-1:2011 Table 3.1:

$Characterstic\ compressive\ strength$	$f_{ck} = 20$	$[MPa]$
$Mean\ compressive\ strength$	$f_{cm} = 28$	$[MPa]$
$Mean\ Young's\ modulus$	$E_{cm} = 30$	$[GPa]$

6.1.1 Theoretical shear capacity of hybrid beams without transverse reinforcement (first series)

The Eurocode 2 approach slightly overestimated the shear capacity of the RC beam without stirrups by 1,8 kN, see section 5.2.1. In this case, the model of EC2 was accurate enough so with some modification it may be possible to determine the shear capacity of the hybrid beams without shear reinforcement.

The contribution to the shear capacity of a hybrid beam with SHCC laminates on both sides without shear reinforcement consists of the shear capacity of reinforced normal concrete without shear reinforcement ($V_{Rm,c}$) and the shear capacity of SHCC laminates (V_{SHCC}), so the expression looks as follows:

$$V_{Rm,hybrid} = V_{Rm,c} + V_{SHCC} \qquad \textit{(Eq. 6.1)}$$

Eurocode 2

The first contribution due to NC in the above equation is based on the model provided in NEN-EN 1992-1-1:2011 §6.2.2. Substituting Eqs. 3.2 and 3.3 into the following expression leads to:

$$V_{Rm,c} = max\{v_{Rd,min}; v_{Rm,c}\} \cdot b_c \cdot d = 1{,}379 \cdot 100 \cdot 167 = 23{,}03\ \text{kN} \qquad \textit{(Eq. 6.2)}$$

,where: b_c is the width of normal concrete core.

Note that the value of ρ_{sl} does not change since the width of the core plus the total thickness of SHCC laminates equals b.

The second contribution due to SHCC in Eq. 6.1 can be calculated by the simplified model, which is proposed by Baghi [58], or by the truss model which is proposed by Wang et al. [44].

Simplified model by Baghi [58]

The proposed model for the shear resistance of an SHCC plate by Baghi [58] is based on the idea of the maximum shear stress in a rectangular non-cracked cross-section. The model assumes the perfect bonding between an SHCC laminate and a normal concrete core. The full height utilization of an SHCC laminate is assumed as well. In the case of a hybrid beam with laminates on both sides, the contribution of those SHCC laminates to the shear capacity can be expressed as follows:

$$V_{SHCC} = 2 \cdot \left(\frac{1}{3} \cdot t_{SHCC} \cdot h_{SHCC} \cdot f_{t,SHCC}\right) \qquad \textit{(Eq. 6.3)}$$

where t_{SHCC} is the total thickness of SHCC laminates, h_{SHCC} is the height of SHCC laminates, $f_{t,SHCC}$ is the ultimate tensile strength of SHCC.

Looking at the hybrid beams with shear keys laminates, Eq. 6.3 is valid since the SHCC laminate(s) did not detach from the NC core at the peak load. Furthermore, the equation can be slightly modified to account for imprecation in the total through-thickness of SHCC laminates:

$$V_{SHCC} = 2 \cdot \left(\frac{1}{3} \cdot h_{SHCC} \cdot \left(t_{SHCC,K1} \cdot f_{t,SHCC,K1} + t_{SHCC,K2} \cdot f_{t,SHCC,K2} \right) \right)$$
$$= 2 \cdot \left(\frac{1}{3} \cdot 200 \cdot (9 \cdot 3{,}52 + 5 \cdot 3{,}52) \right) = 6{,}57\ kN \qquad \textit{(Eq. 6.4)}$$

where t_{SHCC} was splatted in the governing through-thickness of K1 laminate ($t_{SHCC,K1}$) and the governing through-thickness of K2 laminate ($t_{SHCC,K2}$), K1 and K2 laminates had their induvial ultimate tensile strength.

Substituting Eqs. 6.2 and 6.4 into Eq. 6.1:

$$V_{Rm,hybrid} = V_{Rm,c} + V_{SHCC} = 23{,}03 + 6{,}57 = 29{,}6\ kN \qquad \textit{(Eq. 6.5)}$$

Thus, the shear capacity of the hybrid beam with shear keys laminates without shear reinforcement equals:

$$F_V = V_{Rm,hybrid} \cdot 2 = 29{,}6 \cdot 2 = 59{,}2\ \text{kN} \qquad \textit{(Eq. 6.6)}$$

According to experimental data, this hybrid beam failed at 66,7 kN, see Table 16, which is 7,5 kN higher than the above theoretical prediction.

Truss model by Wang et al. [44]

In order to estimate the shear capacity of an RC beam with stirrups, engineers may draw a virtual truss inside the beam. It is a trick that helps them to simplify the problem. The forces in this model are carried by the virtual members which are subdivided in the compression and the tension members. In the case of the compression members (struts and chord), the concrete properties are assigned to those members. For the tension members, the properties of reinforcement are selected. In latter case, there are two sets of the properties for reinforcement: longitudinal and transversal. The properties of longitudinal and transversal reinforcement are located in the tension chord and tension webs, respectively. In conventional RC beams, the latter properties are defined by stirrups. Since SHCC has excellent tensile properties compared to normal concrete, the properties of SHCC can be assigned to the tension webs, see Figure 101.

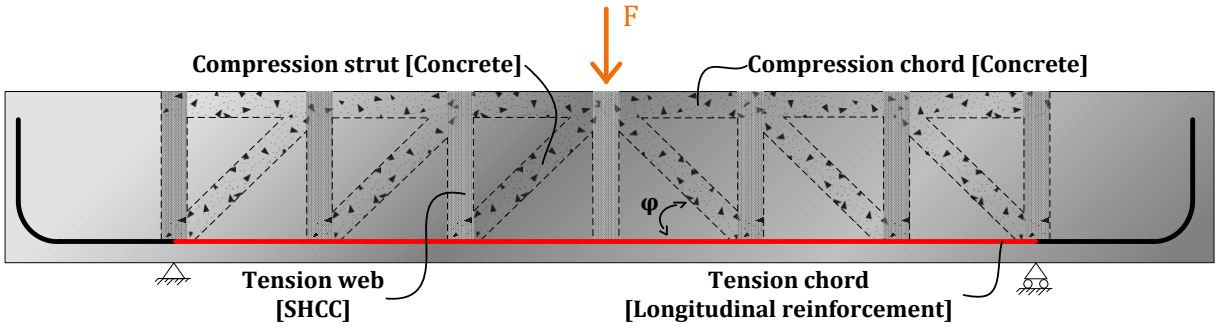

Figure 101 Example of a truss model in a hybrid beam without transverse reinforcement

Wang et al. [44] argue that the complex stress patterns in a hybrid beam could be solved by the strut and tie model, see Figure 102. This model is only valid for beams with the span ratio greater than or equal to 2,5. The contribution of SHCC laminates to the shear capacity in a hybrid beam can be expressed as follows:

$$V_{SHCC} = \eta \cdot \beta \cdot f_{t,SHCC} \cdot \frac{h_{SHCC}}{cos\varphi} \cdot t_{SHCC} \cdot cos\varphi \qquad \textit{(Eq. 6.7)}$$

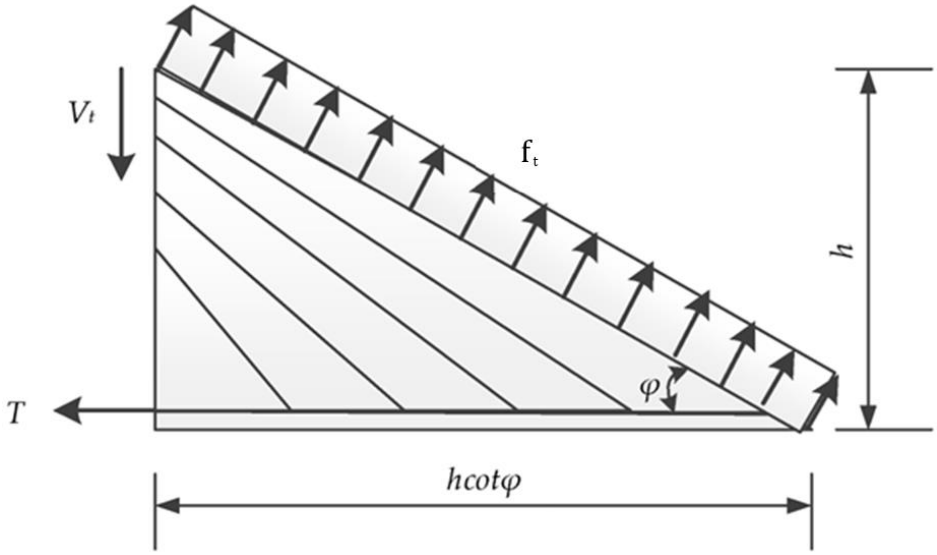

Figure 102 SHCC body for Truss Model [44]

To take into account the debonding of SHCC laminates from a NC core, the Reduction Coefficient (η) is introduced. The suggested values by Wang et al. [44] for smooth laminates with the thickness of 20 mm and 40 mm are 0,6 and 0,4 respectively. Since laminates with shear keys are at low risk of debonding, η is set to 1,0. To correct for the change[1] of the tensile reinforcement ratios in the beam, the Influence Coefficient of Reinforcement Ratio (β) is used. The proposed expression for β by Wang et al. [44] is:

$$\beta = -23{,}04 \cdot \frac{\rho_{sl}}{100} + 1{,}00 \qquad \textit{(Eq. 6.8)}$$

So for all hybrid beams in this study, Influence Coefficient of Reinforcement Ratio is:

$$\beta = -23{,}04 \cdot \frac{2{,}01}{100} + 1{,}00 = 0{,}537 \qquad \textit{(Eq. 6.9)}$$

In the case of the hybrid beam with shear keys laminates without shear reinforcement, the contribution of SHCC laminates to the shear capacity according to Eq. 6.7 equals:

$$V_{SHCC} = 1{,}0 \cdot 0{,}537 \cdot 3{,}52 \cdot 200 \cdot 14 = 5{,}29\ kN \qquad \textit{(Eq. 6.10)}$$

Substituting Eqs. 6.2 and 6.10 into Eq. 6.1:

$$V_{Rm,hybrid} = V_{Rm,c} + V_{SHCC} = 23{,}03 + 5{,}29 = 28{,}3\ kN \qquad \textit{(Eq. 6.11)}$$

[1] The strain in longitudinal bars influence the shear capacity of a beam, see section 6.2.1.

Thus, the shear capacity of the hybrid beam with shear keys laminates without shear reinforcement equals:

$$F_V = V_{Rm,hybrid} \cdot 2 = 28{,}3 \cdot 2 = 56{,}6 \text{ kN} \qquad \textit{(Eq. 6.12)}$$

As mentioned before, this hybrid beam failed at 66,7 kN with a vertical deflection of 2,56 mm, see Table 16, which is 10,1 kN more than the above value. But according to experimental results, the contribution of the SHCC laminates was 12,1 kN which is more or less in accordance with Eq. 6.10 ($F_{SHCC} = 5{,}29 \cdot 2 = 10{,}6$ kN). It seems like the NC core failed at the higher load than in the case of the reference beam even though the NC part in the reference beam was 20 mm wider. Looking at Figure 100, it was observed that the main diagonal crack has gained a significant increase in growth for a very short period before reverting to a slower pace of growth. This happened at around 62,9 kN with a midspan vertical deflection of 2,08 mm. After this event, the hybrid beam could still sustain the increasing load. It seems like during this very short moment major redistribution of internal forces took place since SHCC experience considerable increase in the strain which later return to the pre-event value. Most probably, part of the NC core could not resist more load at this point and had to transfer part of the load to the SHCC webs. Under rapid increase of new internal force, the SHCC had no time to properly spread this. As consequence, the crack has localised in the SHCC web and did not form multiple parallel cracks like the SHCC does during the uniform stretching rate of dog bone specimen, see Figure 66.

From the experiment on the hybrid beam with smooth laminates without shear reinforcement, the contribution of the shear capacity of SHCC laminates equalled 13,2 kN ($V_{SHCC} = \frac{13{,}2}{2} = 6{,}6\ kN$), see Table 16. Eq. 6.7 can be rewritten to find the Reduction Coefficient of smooth laminates with a thickness of 10 mm in the following way:

$$\eta = \frac{V_{SHCC}}{\beta \cdot f_{t,SHCC} \cdot h_{SHCC} \cdot t_{SHCC}} = \frac{6{,}6 \cdot 10^3}{0{,}537 \cdot 3{,}52 \cdot 200 \cdot 20} = 0{,}87 \qquad \textit{(Eq. 6.13)}$$

Thus according to this model, the utilization of two smooth laminates with a thickness of 10 mm was only 87% in this hybrid beam. It seems like the SHCC did not activate completely for some reason. To investigate this specific mechanical behaviour, let us have a brief look at lower and upper bounds.

In order to find lower bound limit, the superior tensile properties of SHCC have to be disregard for a moment and instead assume their values equals to that of NC. Since the cross-section consist of the SHCC and the NC part, the expression for shear capacity of NEN-EN 1992-1-1:2011 §6.2.2 can be modified in the following way:

$$V_{Rm,hybrid,lower} = 0{,}18 \cdot k \cdot \rho_{sl}^{\frac{1}{3}} \cdot \left(f_{cm}^{\frac{1}{3}} \cdot A_c^{eff} + f_{c,SHCC}^{\frac{1}{3}} \cdot A_{SHCC}^{eff} \right) \qquad \textit{(Eq. 6.14)}$$

where: $A_c^{eff} = b_c \cdot \mathrm{d}$ and $A_{SHCC}^{eff} = t_{SHCC} \cdot \mathrm{d}$

The lower bound limit after substituting Eq. 3.1 into Eq. 6.14 equals:

$$V_{Rm,hybrid,lower} = 0{,}18 \cdot 2 \cdot 2{,}01^{\frac{1}{3}} \cdot \left(28^{\frac{1}{3}} \cdot 100 \cdot 167 + 69^{\frac{1}{3}} \cdot 20 \cdot 167 \right) = 29{,}3\ kN \qquad \textit{(Eq. 6.15)}$$

$$F_{V,lower} = V_{Rm,hybrid,lower} \cdot 2 = 29{,}3 \cdot 2 = 58{,}6\ kN \qquad \textit{(Eq. 6.16)}$$

The upper bound limit, however, takes into the account the superior tensile properties of SHCC to their full extended. Using combined approach of EC2 and the Truss model by Wang et al. [44] with the Reduction Coefficient equal to 1 results in:

$$V_{SHCC} = 1{,}0 \cdot 0{,}537 \cdot 5{,}14 \cdot 200 \cdot 20 = 11{,}04\ kN \qquad \textit{(Eq. 6.17)}$$

The upper bound limit after substituting Eqs. 6.2 into Eq. 6.14 equals:

$$V_{Rm,hybrid,upper} = V_{Rm,c} + V_{SHCC} = 23{,}03 + 11{,}04\ = 34{,}1\ kN \qquad \textit{(Eq. 6.18)}$$

$$F_{V,lower} = V_{Rm,hybrid,upper} \cdot 2 = 30{,}6 \cdot 2 = 68{,}2\ kN \qquad \textit{(Eq. 6.19)}$$

According to experimental data, the hybrid beam with smooth laminates failed at 65,6 kN with a vertical deflection of 2,77 mm, see Table 16. This ultimate force value is between the lower and upper bound limits. As shown in Eq. 6.17, the upper theoretical contribution of SHCC laminates equals ($F_{SHCC} = 11{,}04 \cdot 2 =$) 22,08 kN which is almost double the value found in the experiment (13,2 kN).

Nevertheless, the part of the NC core may have failed sooner at around 65,2 kN with a vertical deflection of 2,40 mm than the SHCC laminates. The evidence for this statement can be seen in Figure 99. Like in the case of the hybrid beam with shear keys, the unusual brittle behaviour of the SHCC on the surface was observed as well. The growth of the main diagonal crack accelerates for a very short period before reverting to slower growth rate. As explained before, this observation indicates for redistribution of internal forces. It seems like Young's modulus of SHCC, which is lower than that of NC, did not allow for sufficient activation of the SHCC in an earlier stage of loading. Consequently, the NC core had to resist a significant portion of shear force which had to be (partly) transferred to the SHCC webs. Since NC is a brittle material, there must have been a sudden redistribution of internal forces which is more violent than the case of a gradual redistribution of forces. Further analysis is provided in section 6.2 where the results are compared with the results of experimental benchmarks from the literature.

6.1.2 Theoretical shear capacity of RC beam with (minimum) transverse reinforcement (second series)

The reference beam with stirrups sustained a higher load than the model of Eurocode 2 has originally predicted. As already mentioned in section 5.2.1, this beam failed at 101,8 kN but the target shear capacity equals 83,8 kN according to the design calculations prescribed by the EC2 approach, see section 3.2. The difference between those two values is therefore 18,0 kN which is 16,9% higher than the predicted shear capacity of the Eurocode 2 model.

The model of EC2 is easily applicable however due to its simplicity it overlooks some crucial factors according to Cladera et al. [55] which make it conservative for lightly shear-reinforced beams (like this reference beam in this experiment). In the case of slightly shear reinforcement, the concrete contribution to shear capacity becomes evident since it is an important factor when the stirrups contribution is low.

Cladera and Marí have recognized this issue and have proposed a model [59] where the shear contribution of concrete is taken into account but also adding an extra term which takes the influence of the shear friction due to the transverse reinforcement into account. They called their model '*General Shear Design Method (GSDM)*'. According to this model, the shear

capacity (V_{Rm}) of a beam with shear reinforcement is the summation of the shear capacities of concrete ($V_{Rm,c}$) and transverse reinforcement ($V_{Rm,s}$).

$$V_{Rm} = V_{Rm,c} + V_{Rm,s} \qquad \textit{(Eq. 6.20)}$$

Furthermore, there is no beam in the world which is loaded with pure shear (no bending moment). The shear resistance of a cross-section is thus the strength under shear force and bending moment. Therefore, the proposed model of Cladera et al. [59] requires input of shear and moment values at the location of interest. Figure 103 shows the governing section (the location of interest) in the case of the reference beam with stirrups.

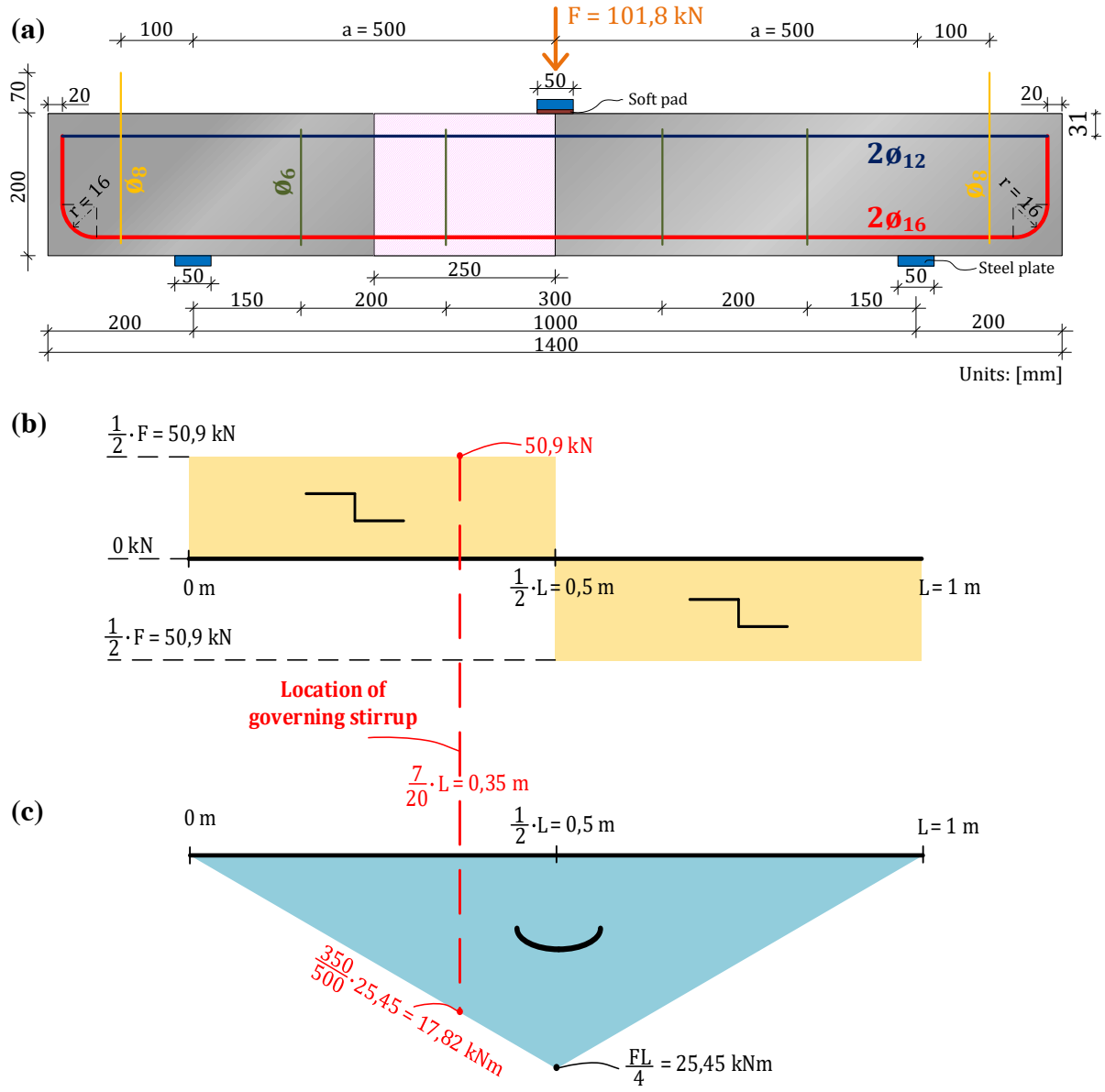

Figure 103 (a) Side view of the design of the RC beam with shear reinforcement. The highlighted area indicates the governing stirrup. (b) Shear and (c) moment diagram of a simply supported beam loaded by concentrated load at the midspan.

So, for beams with stirrups and $f_{cm} \leq 100\ MPa$, the shear strength consists of those two components according to Cladera et al. [59]:

$$V_{Rm,s} = \frac{A_{sw}}{s} \cdot z \cdot f_{ym} \cdot \cot(\theta) \qquad \textit{(Eq. 6.21)}$$

$$V_{Rm,c} = \left[0{,}17 \cdot \xi \cdot \sqrt{\rho_{sl}} \cdot {f_{cm}}^{0,2} \cdot \tau^{1/3}\right] \cdot \mathrm{b} \cdot \mathrm{d} \qquad \textit{(Eq. 6.22)}$$

The values of the constant 0,17 and the powers which are used in Eq. 6.22 has been calibrated by more than 100 empirical results. The percentage of longitudinal reinforcement (ρ_{sl}) that contributes to the shear strength is not limited to 2,0% like in EC2.

The equation for the size effect factor proposed by Cladera et al. [59] is as follows:

$$\xi = 1 + \sqrt{\frac{200}{s_x}} \leq 2{,}75 \qquad \textit{(Eq. 6.23)}$$

where, s_x is minimum of z or the vertical distance between longitudinal distributed reinforcement. In this case, s_x equals 132,25 mm. Note that z has been already calculated in Eq. 3.8.

$$\xi = 1 + \sqrt{\frac{200}{132{,}25}} = 2{,}23 \leq 2{,}75 \qquad \textit{(Eq. 6.24)}$$

The shear stress in the beam can by found in the following way:

$$\tau = \frac{V}{b \cdot z} = \frac{50{,}9 \cdot 10^3}{120 \cdot 132{,}25} = 3{,}21 \leq 3\ MPa \qquad \textit{(Eq. 6.25)}$$

$$\frac{\tau}{f_{cm}} = \frac{3}{28} = 0{,}11 \geq 0{,}05 \qquad \textit{(Eq. 6.26)}$$

Substituting Eqs. 6.24 and 6.25 into Eq. 6.22, the contribution of concrete in the reference beam with transverse reinforcement is:

$$V_{Rm,c} = \left[0{,}17 \cdot 2{,}23 \cdot \sqrt{2{,}01} \cdot 28^{0,2} \cdot 3^{1/3}\right] \cdot 120 \cdot 167 = 30{,}3\ kN \qquad \textit{(Eq. 6.27)}$$

In contrast to the Eurocode 2 approach, the angle of the inclined struts (θ) has to be calculated in the model by Cladera et al. [59], and it is calculated by the following expression:

$$\theta = 20 + 15 \cdot \varepsilon_{x,st} + 45 \cdot \frac{\tau}{f_{cm}} \qquad \textit{(Eq. 6.28)}$$

where, $\varepsilon_{x,st}$ is the longitudinal strain in the stirrup with unit 1/1000 and is determined by following equation:

$$\varepsilon_{x,st} = 0{,}5 \cdot \frac{\frac{M_E}{z} + V_E}{E_s \cdot A_{sl}} \cdot 1000 = 0{,}5 \cdot \frac{\frac{17{,}82 \cdot 10^6}{132{,}25} + 50{,}9 \cdot 10^3}{200 \cdot 10^3 \cdot 402{,}12} \cdot 1000 = 1{,}15 \leq \qquad \textit{(Eq. 6.29)}$$

Substituting Eqs. 6.25 and 6.29 into Eq. 6.28:

$$\theta = 20 + 15 \cdot 1 + 45 \cdot \frac{3}{28} = 39{,}8° \leq 45° \qquad \textit{(Eq. 6.30)}$$

The angle from Eq. 6.30 is much higher than it has been assumed during the design of this reference beam (21,8°), see Eq. 3.16. In reality, the experimental angle of the critical inclined diagonal crack was 34,6°, as seen in Table 18, which is much closer to the above solution than the initial chosen one.

The contribution of stirrups in the reference beam with transverse reinforcement is obtained by substituting Eqs. 3.15 and 6.30 into Eq. 6.21:

$$V_{Rm,s} = \frac{56{,}55}{250} \cdot 132{,}25 \cdot 560 \cdot \cot(39{,}8°) = 20{,}1\ kN \qquad \textit{(Eq. 6.31)}$$

Substituting Eqs. 6.27 and 6.31 into Eq. 6.26:

$$V_{Rm} = 30{,}3 + 20{,}1 = 50{,}4\ kN \qquad \textit{(Eq. 6.32)}$$

The maximal shear capacity ($V_{Rm,max}$) has been already calculated in Eq. 3.17 and it is lower than the solution of Eq. 6.32, therefore the risk of crushing of concrete strut is unlikely. Hence, the shear capacity of the reference beam with transverse reinforcement according to the model by Cladera et al. [59] equals:

$$F = 2 \cdot V_{Rm} = 2 \cdot 50{,}4 = 100{,}8\ kN \qquad \textit{(Eq. 6.33)}$$

The value from Eq. 6.33 is only 1 kN smaller than the experimental value. As has been demonstrated above, the shear contribution of concrete in this particular case was 39,9% which by the Eurocode 2 approach this term is neglected. But, this assumption of EC2 makes considerable underestimation of shear capacity for the beam with low shear-reinforced beams.

6.1.3 Theoretical shear capacities of hybrid beams B1 and B2 with (minimum) transverse reinforcement (second series)

The main contributors to the shear capacity of a hybrid beam with SHCC laminates on both sides with shear reinforcement consist of the shear capacity of transverse reinforcement ($V_{Rm,s}$) and the shear capacity of SHCC laminates (V_{SHCC}). As explained in the previous section 6.1.2, the contribution of NC to the shear capacity ($V_{Rm,c}$) is significant for lightly shear-reinforced beams, according to [59]. Since the Eurocode 2 approach was not capable to predict the shear capacity accurately, the contribution as a result of NC and shear reinforcement will be based on the model by Cladera et al. [59]. All things considered, the expression looks as follows:

$$V_{Rm,hybrid} = V_{Rm,c} + V_{Rm,s} + V_{SHCC} \qquad \textit{(Eq. 6.34)}$$

Since the shear reinforcement of the reference beam and hybrid beams B1 and B2 were the same, the contribution of $V_{Rm,s}$ in the above equation remains the same as in the solution of Eq. 6.31. However, the contribution of $V_{Rm,c}$ changes since the NC cores is 20 mm less wider than width of the reference beam. As consequence, the shear stress in the beam equals:

$$\tau = \frac{V}{b \cdot z} = \frac{50{,}9 \cdot 10^3}{100 \cdot 132{,}25} = 3{,}84 \leq 3\ MPa \qquad \textit{(Eq. 6.35)}$$

Please note that calculated value of τ did not change even though the hybrid beams are less wide since the value is limited to 3 MPa.

After substituting Eqs. 6.24 and 6.35 into Eq. 6.22, the shear capacity of the NC cores equals:

$$V_{Rm,c} = \left[0{,}17 \cdot 2{,}23 \cdot \sqrt{2{,}01} \cdot 28^{0{,}2} \cdot 3^{1/3}\right] \cdot 100 \cdot 167 = \ 25{,}2\ kN \qquad \textit{(Eq. 6.36)}$$

Simplified model by Baghi [58]

As mentioned in section 6.1.1, the contribution of SHCC laminates in the webs of a hybrid beam can be estimated by the simplified model proposed by Baghi [58]. It is a very basic model which does not account for anything apart from tensile strength of SHCC and geometry of laminates.

Solving Eq. 6.3 leads to:

in the case of the hybrid beam B1:

$$V_{SHCC,B1} = 2 \cdot \left(\frac{1}{3} \cdot 20 \cdot 200 \cdot 5{,}14\right) = 13{,}7\ kN \qquad \textit{(Eq. 6.37)}$$

in the case of the hybrid beam B2:

$$V_{SHCC,B2} = 2 \cdot \left(\frac{1}{3} \cdot 20 \cdot 200 \cdot 4{,}42\right) = 11{,}8\ kN \qquad \textit{(Eq. 6.38)}$$

Truss model by Wang et al. [44]

The other method to estimate contribution of shear capacity due to SHCC laminates is Truss model by Wang et al. [44]. As mentioned in section 6.1.1, the model takes additionally into account the deboning of SHCC laminates from a NC core and the interaction between SHCC and longitudinal reinforcement.

Substituting Eq. 6.9 into Eq. 6.3 leads to:

in the case of the hybrid beam B1:

$$V_{SHCC,B1} = 1{,}0 \cdot 0{,}537 \cdot 5{,}14 \cdot 200 \cdot 20 = 11{,}0\ kN \qquad \textit{(Eq. 6.39)}$$

in the case of the hybrid beam B2:

$$V_{SHCC,B2} = 1{,}0 \cdot 0{,}537 \cdot 4{,}42 \cdot 200 \cdot 20 = 9{,}5\ kN \qquad \textit{(Eq. 6.40)}$$

As the last step, all contributions were summed up. The solutions of Eq. 6.34 for the hybrid beams with shear reinforcement are provided in Table 20. Looking at the results, the truss model by Wang et al. [44] was much closer to experimental values of the shear capacity contributions of the SHCC laminates than the simplified model by Baghi [58]. But in the end, the combination of the General Shear Design Method (GSDM) by Cladera et al. [59] with the simplified model came closer to experimental values of the total shear capacities than the

combination of the GSDM with the truss model. The underestimation of the shear capacity of the NC cores by GSDM is the issue even though is much more precise than the EC2 approach.

Table 20 Experimental and theoretical shear capacities of hybrid beams with transverse reinforcement.

	Experimental results		**Theoretical shear capacities**			
Specimen type	**Peak load [kN]**	**Δ in ultimate capacity compared to reference group [kN]**	**GSDM + Simplified model [kN]**	**V_{SHCC} acc. to Simplified model [kN]**	**GSDM + Truss model [kN]**	**V_{SHCC} acc. to Truss model [kN]**
Hybrid beam B1	124,5	+ 22,7	118,0	+ 27,4	112,6	+ 22,0
Hybrid beam B2	124,2	+ 22,4	114,2	+ 23,6	109,6	+ 19,0

Looking at Figure 83, 85, 86 or even 98, it can be observed that the dispersed cracking of SHCC is similar to those during the testing of dog bone specimens, see Figure 66. Moreover, the growth of the main diagonal cracks in hybrid beams with shear reinforcement did not flocculate much. In addition, the theoretical shear capacities according to the truss model by Wang et al. [44] match the experimental shear capacity contributions of SHCC laminates. All evidence points to the fact that the SHCC laminates were fully activated in contrast to the hybrid beams without shear reinforcement. Most likely, the stirrups cushioned the sudden redistribution of the internal forces due to their large Young's modulus which pulled the significant part of the force flow toward themselves. Hence, the transfer of the internal force towards the SHCC webs was more gradual than in the case of hybrid beams without shear reinforcement. As a consequence of the smaller gradient of the additional force, the SHCC laminates in the webs experienced a smaller sudden jump in the strain since the transverse reinforcement absorbed a significant portion of the internal forces from the NC core after it has fractured. Hence, the SHCC developed its typical crack pattern in a later stage which is a sign of full activation of the tensile properties.

6.2 Theoretical shear capacity of (hybrid) beams – results comparison with experimental benchmarks

This section provides results comparisons between this study and previous experiments which are related to this topic. The goal is to achieve a better understanding of the shear capacity of a hybrid beam. In total two experimental benchmarks were thoroughly examined to find correlations.

6.2.1 Results comparison with experimental investigation by Zhang et al. (2015)

Figure 104 shows the load midspan deflection relationships of beams from the first series and additionally, the (hybrid) beams of Zhang et al. from their experiment [43]. All those beams were not provided with shear reinforcement. The most crucial results of the first series as well as the results of Zhang et al. [43] are summarised in Table 21. A detailed overview of material properties and geometry parameters is given in Table 22.

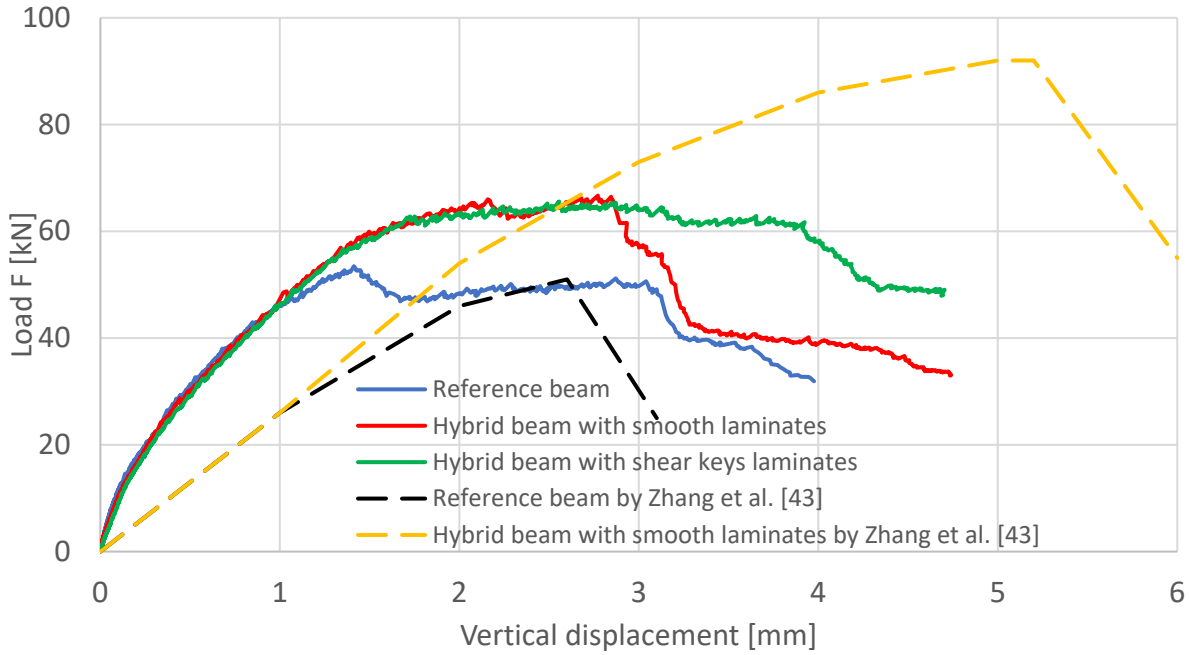

Figure 104 Load F versus vertical deflection of the (hybrid) beams without transverse reinforcement at midspan.

In general, the results of Zhang et al. [43] differ from this thesis's results. Firstly, their RC beam has almost the same shear capacity as the reference beam of the first series, although concrete in those beams belongs to the same concrete class moreover, their beam has a smaller width, which is counter-intuitive. Secondly, the hybrid beams improved shear capacity by 41% according to their results. It is approximately three times larger than the value found in the experiment of this thesis.

In order to understand why the reference beam of Zhang et al. [43] has achieved comparable shear capacity with a smaller cross-section as the reference beam in the first series, let us first see if the Eurocode 2 approach is capable to predict the capacity. But keep in mind that the total area of longitudinal reinforcement and the second moment of area were 60,9% and 16,9% smaller, respectively, compared to the reference beam in the first series, as seen in Table 22. Furthermore, the shear span parameters (η_a) were equalled in both studies.

Table 21 The comparison of between experimental results on (hybrid) beams without transverse reinforcement

Ref.	Specimen without transverse reinforcement	Ultimate capacity [kN]	Δ in ultimate capacity compared to reference group [kN]	Δ in ultimate capacity compared to reference group [%]	Vertical displacement at peak load [mm]
This study (1st series)	Reference beam {120 × 200 mm²}	53,5	-	-	1,46
	Hybrid beam with smooth laminates {120 × 200 mm²}	66,7	+ 13,2	+ 24,7	2,90
	Hybrid beam with shear keys laminates {120 × 200 mm²}	65,6	+ 12,1	+ 22,6	3,95
Zhang et al. [43]	Reference beam {100 × 200 mm²}	51	-	-	2,75
	Hybrid beam with smooth laminates {120 × 200 mm²}	92	+ 41	+ 80	5,50

Table 22 Comparison of beams without transverse reinforcement: a detailed overview of material properties and geometric parameters

		In the study of Zhang et al. [43]	*This study (1st series)*	| Difference |	
Material properties	**Average compressive strength of concrete [MPa]**	27	29,07 (± 1,08)	2,07 (± 1,08)	7,1% (± 3,7%)
	Young's modulus of concrete [MPa]	23500	33031 (± 552)	9531 (± 552)	28,9% (± 1,7%)
	Average compressive strength of SHCC [MPa]	91	66,448 (± 2,449)	24,552 (± 2,449)	36,9% (± 3,7%)
	Average tensile strength of SHCC [MPa]	6,2	3,52 (± 0,16)	2,68 (± 0,16)	76,1% (± 4,5)
	Average tensile strain at 90% strength [%]	1,6	2,27 (± 0,33)	0,67 (± 0,33)	29,5% (± 14,5%)
	Young's modulus of SHCC [MPa]	29000	16500[a)]	12500	75,8%

	Characteristic yield strength of steel [MPa]	345[b)]	500	155	31,0%
Geometric parameters	**The second moment of area [×10⁴ mm⁴] of RC beams**	6666,7	8000	1333,3	16,7%
	The second moment of area [×10⁴ mm⁴] of hybrid beams	8000	8000	0	0%
	Total area of longitudinal reinforcement [mm²]	157,08	402,12	245,04	60,9%

a) This value comes from the experiment [50] of He (inventor of the mix composition).
b) It is most probably a type error in the paragraph of [43] "2.1.2. Reinforcements and concrete". It should be 1050 MPa, see the below analysis for the explanation.

Theoretical shear capacity of RC beam without transverse reinforcement from experimental investigation [43] by Zhang et al. (2015)

The total area of longitudinal reinforcement:

$$A_{sl} = n \cdot \frac{\pi \cdot \emptyset_{10}^{L\ 2}}{4} = 2 \cdot \frac{\pi \cdot 10^2}{4} = 157{,}08\ mm^2 \qquad \textit{(Eq. 6.41)}$$

The longitudinal reinforcement ratio of the reference beam of Zhang et al. [43] equals:

$$\rho_{sl,REF} = \frac{A_{sl}}{b_c \cdot d} \cdot 100\% = \frac{157{,}08}{100 \cdot 165} \cdot 100\% = 0{,}95\% \qquad \textit{(Eq. 6.42)}$$

According to NEN-EN 1992-1-1:2011 §6.2.2:

$$k = \min\left\{1 + \sqrt{\frac{200}{d}}; 2{,}0\right\} = \min\left\{1 + \sqrt{\frac{200}{165}}; 2{,}0\right\} = 2{,}0 \qquad \textit{(Eq. 6.43)}$$

$$v_{Rm,min} = 0{,}035 \cdot k^{\frac{3}{2}} \cdot \sqrt{f_{cm}} + k_1 \cdot \sigma_{cp} = 0{,}035 \cdot 2^{\frac{3}{2}} \cdot \sqrt{27} + 0{,}15 \cdot 0 = 0{,}514 \frac{N}{\text{mm}^2} \qquad \textit{(Eq. 6.44)}$$

$$v_{Rm,c} = 0{,}18 \cdot k \cdot \left(\rho_{sl,REF} \cdot f_{cm}\right)^{\frac{1}{3}} = 0{,}18 \cdot 2 \cdot (0{,}95 \cdot 27)^{\frac{1}{3}} = 1{,}062 \frac{N}{\text{mm}^2} \qquad \textit{(Eq. 6.45)}$$

$$V_{Rm,c} = max\{v_{Rd,min}; v_{Rm,c}\} \cdot b_c \cdot d = 1{,}062 \cdot 100 \cdot 165 = 17{,}5\ \text{kN} \qquad \textit{(Eq. 6.46)}$$

Thus, the shear capacity of the beam equals:

$$F_V = V_{Rm,c} \cdot 2 = 17{,}5 \cdot 2 = 35{,}0\ \text{kN} \qquad \textit{(Eq. 6.47)}$$

The Eurocode 2 approach underestimated the shear capacity in this case when compared to the experimental results of Zhang et al. [43]. Their reference beam had the shear capacity of approximately 51 kN which is 16 kN (45,7%) more than the calculated capacity with EC2.

Since there is still a large disagreement on the governing mechanism of shear failure of RC beams without shear reinforcement in the scientific community, the Eurocode 2 approach is based only on totally empirical results without bulletproof theory on shear failure mechanism.

For this reason, EC2 prediction is very poor at estimating shear capacity for various longitudinal reinforcement ratios according to Collins et al. [60]. In practice, this ratio is more diversified than the original database on which Eurocode 2 model is based on. They argue that in the practical scenario the η_a/ρ_{sl} parameter is quite homogeneous unlike in the laboratory configurations. This happens due to the fundamental difference during the designing of the beam. In practice, engineers designing their beams more often for the flexural failure rather than for the shear failure since they like to avoid brittle and sudden failures due to safety reasons. But in the laboratory, scientists want to ensure a shear failure before a flexural failure if they want to investigate the former one or vice versa. In this kind of configuration, the shear span parameter (η_a) and longitudinal reinforcement ratio (ρ_{sl}) are not correlated and thus creating unrealistically scenarios where often ρ_{sl} is selected ridiculous high just to prevent the flexural failure for the sake of shear failure. To illustrate this problem, Collins et al. [60] have plotted graph where the predictions of three important codes EC2, CSA and ACI are plotted together with experiments representing the practical situations but then without shear reinforcement. Additionally, the results of this study and Zhang et al. [43] has been added as well, see Figure 105.

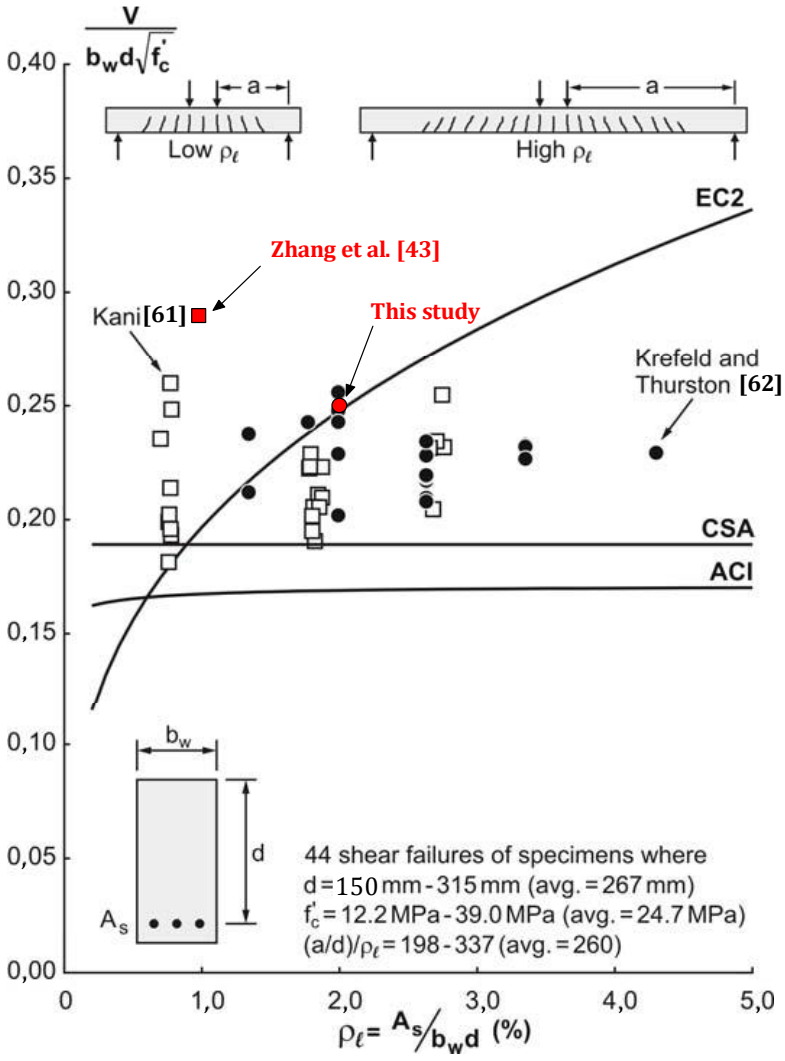

Figure 105 Effect of changing ρ_{sl} while keeping steel stress σ_{sl} constant [60]

From the empirical evidence, it is clear that the impact of changing ρ_{sl} has huge consequence on the shear prediction of EC2. According to Collins et al. [60], from those 44 experiments, the average test to predicted ratio is 0,93 with a COV 17,3%. But there are case like the reference beam of Zhang et al. [43] where the model is too conservative with the ratio of 1,46. In other cases where the ratio is 0,69 according to Collins et al. [60]. But to be more precise, it is not the effect of the amount of the longitudinal reinforcement in the cross-section, but rather the normal strain in those bars that influence the shear capacity, see Figure 106, since it affects the angle of the inclined struts (θ) and the width of the cracks.

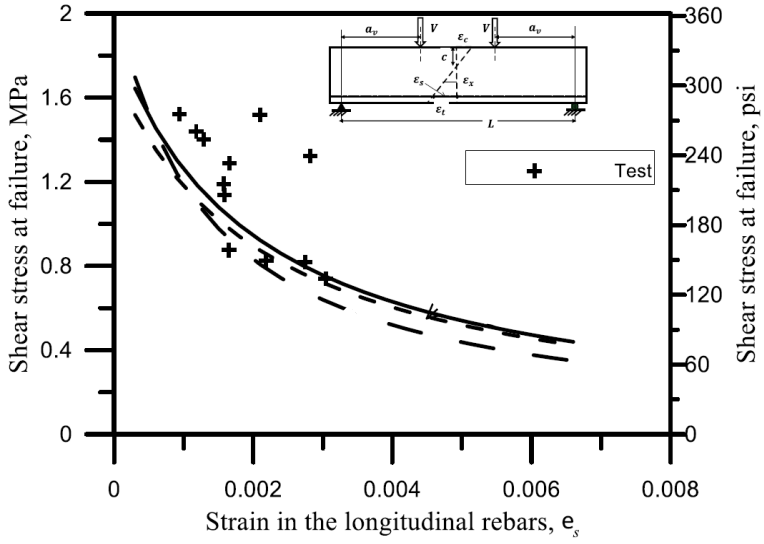

Figure 106 Shear stress at failure versus normal strain in longitudinal reinforcement [63]

Shuraim [63] has studied a database with the results of 232 beams collected from ten different sources. He tried to cover a wide range of parameters (f_c, ρ_{sl}, e_x, η_a, d) that may influence the shear capacity of an RC beam. According to his assessment of trends, the reference beam of Zhang et al. [43] should have a lower shear capacity than the reference beam from the first series, because:

- If the internal arm d decreases then the shear strength of a concrete beam decreases. In this specific case, their beam had d equal to 165 mm which was 2 mm smaller than the reference beam from this study.
- If ρ_{sl} decreases then the shear strength of a concrete beam decreases. In this specific case, their reference beam had a 52,7% smaller ratio than the reference beam from this study.
- High f_{cm} is associated with higher shear strength and especially for beams with low ρ_{sl}. However, the difference in concrete compressive strength was only 7,1% in this case. Moreover, the concrete had lower strength than the reference beam from this study.
- If the normal strain (e_s) in flexural reinforcement decreases then the shear strength of a concrete beam increases. The reference beam of Zhang et al. had certainly a higher strain value than the reference beam from this study because their beam had lower A_s.

As can be seen from the above bullet points, the results of their reference beam differs significantly from other observations.
Looking at the flexural capacity of Zhang's reference beam:

$$M_{Rm} = N_s \cdot \mathrm{z} = 157{,}08 \cdot 345 \cdot 165 \cdot 0{,}9 = 8{,}05\ kNm \qquad \textit{(Eq. 6.48)}$$

And the moment at failure:

$$M_E = \frac{F_E \cdot L}{4} = \frac{51 \cdot 1}{4} = 12{,}75\ kNm \qquad \textit{(Eq. 6.49)}$$

As it can be seen from the above calculations, the moment at failure was 12,75 kNm however the theoretical flexural capacity is only 8,05 kNm. This means that the reinforcement should yield at 63% of the peak load already, but it did not. The reported yield strength of reinforcement by Zhang et al. [43] is most probably incorrect. It is speculated that the properties of reinforcement bars with a diameter 10 mm and 25 mm have been swapped by accident, see the subparagraph "2.1.2. Reinforcements and concrete" in [43]. The steel with yield strength of 1050 MPa and Young's modulus 200 GPa could have been used for bars with 10 mm diameter since its properties allow it to carry this specific load. Furthermore, $2\varnothing_{10}$ with yield strength of 1050 MPa are capable of carrying the peak loads of their hybrid beams. Therefore, for further analysis of their results, the properties of this type of steel will be used instead of the reported one.

Theoretical shear capacity of hybrid beam without transverse reinforcement from experimental investigation [43] by Zhang et al. (2015)

Apart from the difference in the results between the reference beams without shear reinforcement of this study and Zhang et al. [43], there is considerable inequality in the shear capacities between the hybrid beams of those two studies. The hybrid beam of Zhang et al. [43] was capable of outperforming the shear capacity of its reference beam by 41 kN, see Table 21, which is almost three times better than the values of 13,2 kN found in this study. To understand why the enhancement of shear capacity in the case of Zhang et al. [43] was much greater, let us highlight the characteristics of those cases.

In general, the mechanical properties of SHCC used in [43] were superior to these of the master thesis experiment, see Table 22. The average tensile strength and Young's modulus of Zhang's SHCC were 2,68 MPa (76,1%) and 12,5 GPa (75,8%) higher than the SHCC used in this study, but also the average compressive strength was 24,6 MPa (28,9%) stronger. In contrast, the average compressive strength of concrete in both cases was almost equal, but Young's modulus of concrete of Zhang et al. [43] was 9,5 GPa (28,9%) smaller than that of hybrid beams in the first series. Hence, the load midspan deflection of Zhang's hybrid beam was less strip due to its lower initial stiffness compared to the results of the hybrid beams in the first series, as shown in Figure 104. In theory, it does not affect the carrying capacity of a simply supported beam since this system is kinematically and statically determined. There is also a significant difference of 60,9% in the longitudinal reinforcement ratios which may potentially impact the shear capacity of a hybrid beam like it does in RC beams, as explained on the previous page. Therefore, it is highly doubly that the simplified model by Baghi [58] is capable of predicting the shear capacity contribution of SHCC since it does no take the longitudinal reinforcement in the account. To verify this statement, Eq. 6.3 is substitute with the parameters of Zhang's hybrid beam:

$$V_{SHCC} = 2 \cdot \left(\frac{1}{3} \cdot 20 \cdot 200 \cdot 6{,}2\right) = 16{,}5\ kN \qquad \textit{(Eq. 6.50)}$$

Converting to the force as a result of SHCC laminates:

$$F_{SHCC} = 2 \cdot V_{SHCC} = 2 \cdot 16{,}5 = 33\ \text{kN} \qquad \textit{(Eq. 6.51)}$$

As it can be seen, the difference between the above solution and the experimental value is 8 kN (19,5%) which is a lot compared to the difference of 1,0 kN (8,3%) found in this study, see section 6.1.1. The other method to estimate contribution of shear capacity due to SHCC laminates is Truss model by Wang et al. [44]. In contrast to the previous model, Wang et al. have included the influence of longitudinal reinforcement ratio in their model. They did this by introducing the Influence Coefficient of Reinforcement Ratio (β) into their equation.

The longitudinal reinforcement ratio of the hybrid beam of Zhang et al. [43] equals:

$$\rho_{sl,Hybrid} = \frac{A_{sl}}{b_c \cdot d} \cdot 100\% = \frac{157{,}08}{120 \cdot 165} \cdot 100\% = 0{,}79\% \qquad \textit{(Eq. 6.52)}$$

So substituting Eq. 6.52 into Eq. 6.8 allows for obtaining β:

$$\beta = -23{,}04 \cdot \frac{0{,}79}{100} + 1{,}00 = 0{,}817 \qquad \textit{(Eq. 6.53)}$$

In the case of Zhang's hybrid beam, the contribution of SHCC laminates to the shear capacity according to Eq. 6.7 equals:

$$V_{SHCC} = 1{,}0 \cdot 0{,}817 \cdot 6{,}2 \cdot 200 \cdot 20 = 20{,}3\ kN \qquad \textit{(Eq. 6.54)}$$

Converting to the force as a result of SHCC laminates:

$$F_{SHCC} = 2 \cdot V_{SHCC} = 2 \cdot 20{,}3 = 40{,}6\ \text{kN} \qquad \textit{(Eq. 6.55)}$$

Thus, the difference between the above solution and the experimental value is only 0,4 kN (1,0%) which is considerably more accurate than the simplified model by Baghi [58]. Furthermore, there is a significant difference in the theoretical shear capacities due to SHCC laminates between Zhang et al. [43] and this study. The value of Eq. 6.54 (20,3 kN) is almost four times larger than that of the hybrid beam with shear keys (5,3 kN), see Eq. 6.10. When compared those two cases, three inputs were different: tensile strength of SHCC (6,2 MPa vs 3,52 MPa), a total thickness of SHCC laminates (20 mm vs 14 mm), and ρ_{sl} (0,79% vs 2,01%). The first two inputs are responsible for a 67,4% increase in the theoretical capacity (see Figure 107) and are straightforward to understand: higher tensile strength in combination with higher total area leads to higher carrying force. However, the last input, the longitudinal reinforcement ratio, requires more effort to be understood since it is not directly connected with shear resistance. As proven by Collins et al. [60] and Shuraim [63], the normal strain in longitudinal reinforcement does affect the shear capacity of an RC beam. To verify this, the necessary analysis and calculation will be performed in the upcoming paragraphs.

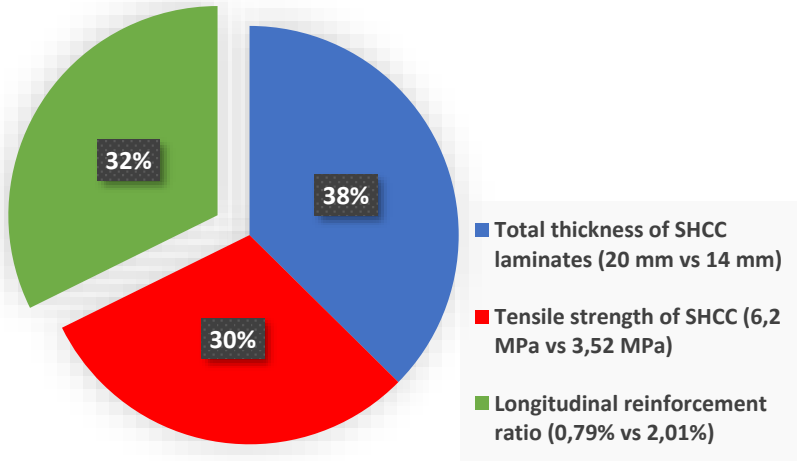

Figure 107 The difference in theoretical capacity between Zhang et al. [43] and the results of this study results from:

To make normal strain comparison fair, the load of 50 kN has been selected as the reference point since it is very close to the peak loads of the reference beams of Zhang et al. [43] and this study (first series). It should be noted that the mechanical behaviour at this load level is not under the ultimate limit state, but rather under non-limit state (NLS), as a result, not all assumption valid in ULS will automatically hold for NLS. The stress distributions and deformation under ULS and NLS are not equal, see Figure 108. The obvious implication is the location of the neutral axis that depends on the stress level and cracking stage in a concrete beam.

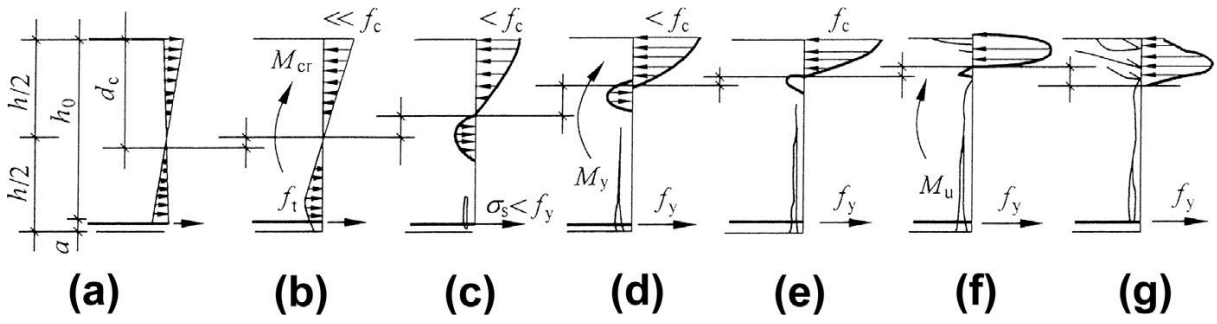

Figure 108 Developments of sectional stress and crack of beam: (a) before cracking, (b) just cracking, (c) after cracking, (d) yielding of reinforcement, (e) after yield, (f) ultimate state, (g) descending branch [64].

Often, the neutral axis is located slightly the below middle line before the cracking of concrete since the most of longitudinal reinforcement is located in the lower part of the cross-section, see Figure 108 a). After the concrete has cracked, the concrete part contributes less and less to tensile stresses than before, but the stresses in the compression zone are still too small than the compressive strength of concrete, so stresses are linear distributed at this point. The only way to find a new equilibrium is to shift the neutral axis upwards. Suddenly, the tension force in the cross-section has to be carried mainly by reinforcement and the neutral axis has to move up again, see Figure 108 c). The stress distribution in concrete becomes non-linear. After reaching the yielding of reinforcement, the tensile force is constant if the hardening of steel is disregarded. So the only way to increase the bending moment is to increase the internal arm "z" by moving the neutral axis again, see Figure 108 d). While the compression stress in concrete is slowly reaching f_c, the neutral axis moves further upwards, see Figure 108 e).

The codes such as Eurocode 2 primarily focus on the ultimate and serviceability limit states of a cross-section, see Figure 108 f). To simplify calculation, Eurocode 2 allows to use the simplified stress-strain relationships like rectangular stress distribution where two concrete compressive equivalent coefficients are given: α_1 (EC2 notation: η) and β_1 (EC2 notation: β). The factor α_1 is needed to determine the effective strength and β_1 to find the position of the combined compressive force. However, those coefficients are only allowed to be use in a limit state and EC2 does not provide coefficients necessary for a non-limit state.

In the paper [65], Han et al. were capable to numerically simulate the nonlinear stress distribution in the concrete compression zone under non-limit state. Moreover, they developed practical equations which allow to find necessary α_1 and β_1 for a non-limit state. Their method assumed that the plane in the cross-section remained plane after deformation — and the concrete part in tension has fully cracked.

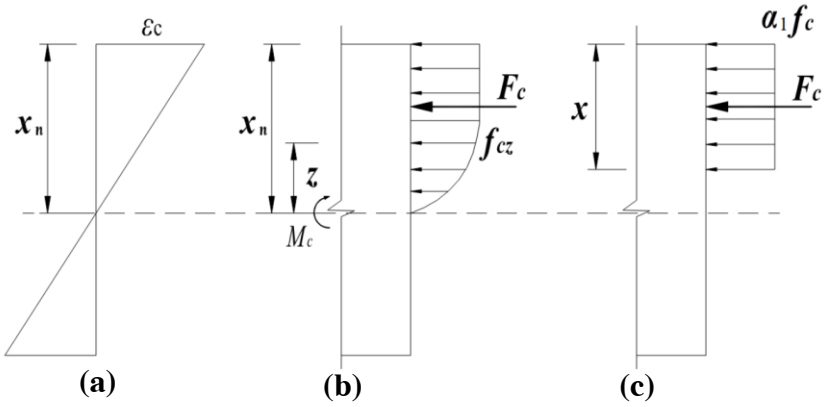

Figure 109 (a) Strain, (b) stress and (c) equivalent rectangular stress distribution. [65]

The equation for the concrete compressive equivalent coefficients under a non-limit state by Han et al. [65] are as follows:

$$\alpha_1 \cdot \beta_1 = \xi_1 + \xi_2 \cdot \frac{\varepsilon_c}{\varepsilon_{cu}} \qquad \textit{(Eq. 6.56)}$$

$$\beta_1 = \eta_1 + \eta_2 \cdot \frac{\varepsilon_c}{\varepsilon_{cu}} \qquad \textit{(Eq. 6.57)}$$

$$\alpha_1 = \zeta_1 + \zeta_2 \cdot \frac{\varepsilon_c}{\varepsilon_{cu}} \qquad \textit{(Eq. 6.58)}$$

Table 23 Parameters of concrete compressive equivalent coefficients for ≤ C50 [65]

Concrete strain level $\frac{\varepsilon_c}{\varepsilon_{cu}}$		ξ_1	ξ_2	η_1	η_2	ζ_1	ζ_2
I	≤ 0,3	0,015	1,382	0,665	0,117	0	0
II	≤ 0,6	0,190	0,799	0,650	0,167	0,320	0,1
II	≤ 1,0	0,475	0,325	0,630	0,200	0,795	0,540

Figure 110 shows the strain and stress distribution in the non-limiting state under the bending moment M. As consequence, the equilibriums of internal forces and moments according to [65] are:

$$\sum Forces = 0 \rightarrow \alpha_1 \cdot \beta_1 \cdot f_c \cdot b_c \cdot x_n + f_{cs} \cdot A_{cs} = f_s \cdot A_s \qquad \textit{(Eq. 6.59)}$$

$$\sum Moments = 0 \rightarrow M = f_s \cdot A_s \cdot \left(d - \frac{\beta_1 \cdot x_n}{2}\right) + f_{sc} \cdot A_{sc} \cdot \left(\frac{\beta_1 \cdot x_n}{2} - a_0\right) \qquad \textit{(Eq. 6.60)}$$

Where: $x_n = \frac{\varepsilon_c}{\varepsilon_c + \varepsilon_s} \cdot \mathrm{d}$ and $\varepsilon_{sc} = \frac{d - a_0}{d} \cdot \varepsilon_c - \frac{a_0}{d} \cdot \varepsilon_s$;

under the assumption that reinforcement does not yield, so: $f_s = E_s \cdot \varepsilon_s \leq f_y$

and $f_{sc} = E_{sc} \cdot \varepsilon_{sc} \leq f_y$

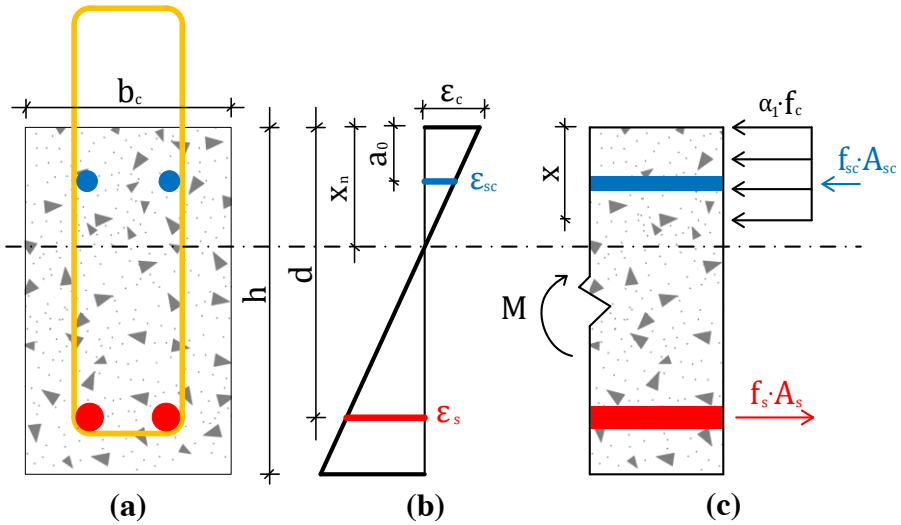

Figure 110 (a) Schematization of cross-sections. (b) Strain and (c) equivalent rectangular stress distribution in non-limit state.

The only unknowns in Eqs. 6.59 and 6.60 are ε_s and ε_c, so having two unknowns and two equations problem can be solved. Han et al. did a great job solving this exact problem in their paper [65] but even for cases when the reinforcement at the top and/or bottom yield. Unfortunately, it is not valid for a hybrid beam with SHCC web layers since those laminates contribute to the internal equilibrium of forces.

To make it valid for a hybrid beam case, the model of Han et al. [65] has been modified by adding extra terms for the SHCC contribution. Since hybrid beams of Zhang et al. [43] and this study did not developed a bonding failure during their shear failures, the modified model is assuming perfect bonding between a NC core and SHCC laminates. Furthermore, the plane in the cross-section remained plane, see Figure 111b).

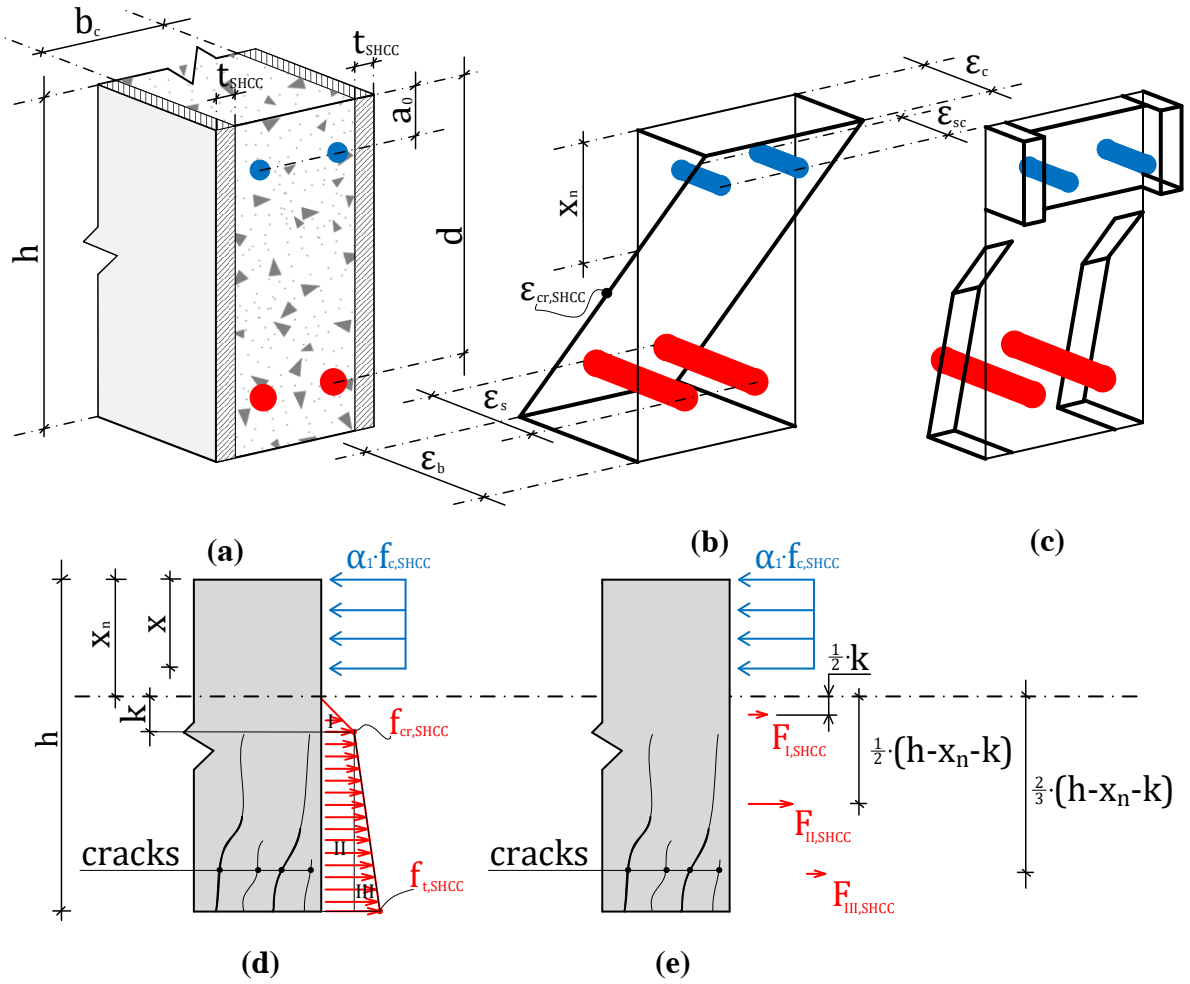

Figure 111 (a) Schematization of cross-sections. (b) Strain and (c) equivalent stress distribution in non-limit state. (d) Equivalent stress and (e) force distribution in SHCC laminate in non-limit state.

Figure 111 shows the strain and stress distribution in the non-limiting state under the bending moment M. Since the compression area of SHCC laminates is much smaller than the area of normal concrete in the compression zone x_n, the same concrete compressive equivalent coefficients (α_1 and β_1) will be used for equivalent rectangular compressive stress distribution of SHCC in the compression zone. It is a slightly conservative assumption for low strain levels in the compression zone, but it makes calculation much easier. Furthermore, SHCC will behave elastically in the uncracked height k. In the cracked region, however, SHCC will show its strain hardening properties until reaching its ultimate strain ($\varepsilon_{tu,SHCC}$). The tensile stress distribution has been split in three regions: I. elastic region; II. ideal elastoplastic region; III. strain hardening region, as seen in Figure 111 d) and e).

So, the equilibriums of internal forces and moments in a hybrid beam are defined as follows:

$$\sum Forces = 0 \rightarrow \alpha_1 \cdot \beta_1 \cdot \left(f_c \cdot b_c + f_{c,SHCC} \cdot b_{SHCC}\right) \cdot x_n + f_{cs} \cdot A_{cs} = f_s \cdot A_s + F_{I,SHCC} + F_{II,SHCC} + F_{III,SHCC} \quad \textit{(Eq. 6.61)}$$

$$\sum Moments = 0 \rightarrow$$

$$M = f_s \cdot A_s \cdot \left(d - \frac{\beta_1 \cdot x_n}{2}\right) + f_{sc} \cdot A_{sc} \cdot \left(\frac{\beta_1 \cdot x_n}{2} - a_0\right) + + F_{I,SHCC} \cdot \left(k + \frac{3 \cdot \beta_1 \cdot x_n}{2}\right) + F_{II,SHCC} \cdot \frac{(d + k + (1 - \beta_1) \cdot x_n)}{2} + + F_{III,SHCC} \cdot \left(\frac{d}{3} + \frac{2 \cdot (k + x_n)}{3} - \frac{\beta_1 \cdot x_n}{2}\right) \quad \textit{(Eq. 6.62)}$$

Where: $F_{I,SHCC} = \frac{1}{2} \cdot E_{SHCC} \cdot \varepsilon_{cr,SHCC} \cdot k \cdot b_{SHCC}$;

$F_{II,SHCC} = f_{y,SHCC} \cdot (h - x_n - k) \cdot b_{SHCC}$;

$F_{III,SHCC} = \frac{1}{2} \cdot E_{sh,SHCC} \cdot \left(\varepsilon_b - \varepsilon_{cr,SHCC}\right) \cdot (h - x_n - k) \cdot b_{SHCC}$;

$x_n = \frac{\varepsilon_c}{\varepsilon_c + \varepsilon_s} \cdot$ d and $\varepsilon_{sc} = \frac{d - a_0}{d} \cdot \varepsilon_c - \frac{a_0}{d} \cdot \varepsilon_s$;

under the assumption that reinforcement does not yield, so: $f_s = E_s \cdot \varepsilon_s \leq f_y$ and $f_{sc} = E_{sc} \cdot \varepsilon_{sc} \leq f_y$, but also assuming that $\varepsilon_b \leq \varepsilon_{tu,SHCC}$

Here as well, the only unknowns are ε_s and ε_c in Eqs. 6.61 and 6.62, so the problem in the case of a hybrid beam can be solved.

Calculation and analysis of stain in flexural reinforcement

In essence, Eqs. 6.59 and 6.60 will be used to find the strain in flexural reinforcement in the reference beams, and Eqs. 6.61 and 6.62 will be used to find the strain in flexural reinforcement in the hybrid beams. As mentioned before, the load of 50 kN has been selected as the reference point, so the moment at this load equals:

$$M = \frac{F \cdot L}{4} = \frac{50 \cdot 1}{4} = 12{,}50\ kNm \quad \textit{(Eq. 6.63)}$$

All required inputs are summarised on the next page. Table 24 provides the necessary geometric parameters for both studies. Figure 112 a) gives the schematization of steel and SHCC tensile properties. Please note that models assume no yielding of the rebars. According to experimental data, see section 5.2.2, the yielding of longitudinal reinforcement did not occur at this load level. In the case of the beams of Zhang et al., strains were not measured. Figure 112 b) shows how the tensile properties of the SHCC of Zhang et al. have been estimated.

The set of equations has been solved by a script written in Maple 2020.2 (Build ID 1502365). Maple is a programming language which uses symbolic and numeric computing environment. The whole script is shown in Appendix F.

Table 24 Geometric input

Ref.	Specimen	h [mm]	d [mm]	b_c [mm]	b_{SHCC} [mm]	a_0 [mm]	A_s [mm²]	A_{sc} [mm²]
This study (1st series)	Reference beam	200	167	120	×	31	402,12	226,19
	Hybrid beam			100	20			
Zhang et al. [43]	Reference beam		165		×	×	157,08	×
	Hybrid beam				20			

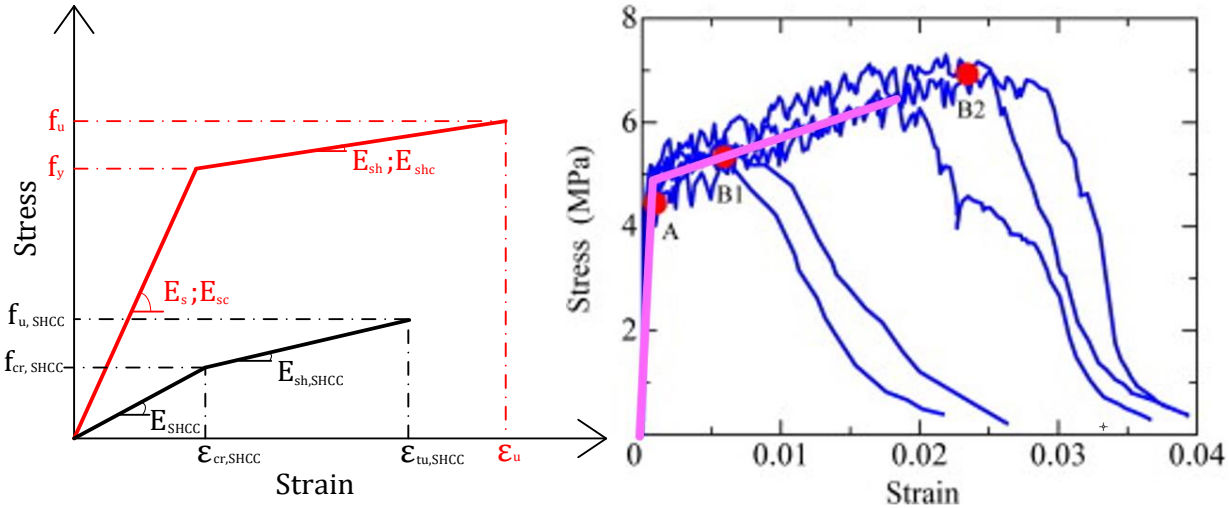

Figure 112 (a) Idealised stress-strain diagrams for reinforcing steel for tension and compression (red line) and idealised stress-strain diagrams for SHCC in tension (black line). (b) stress-strain curves of SHCC from [43] with plotted idealised stress-strain diagram.

Table 25 Material input

	Steel			Concrete		SHCC				
Ref.	E_s (E_{sc}) [GPa]	f_y [MPa]	ε_u [%]	f_c [MPa]	ε_{cu} [‰]	E_{SHCC} [GPa]	$f_{cr,SHCC}$ [MPa]	$f_{tu,SHCC}$ [MPa]	$\varepsilon_{cr,SHCC}$ [‰]	$\varepsilon_{tu,SHCC}$ [%]
This study (1st series)	200	560	5,0	29,07	3,5	16,5	3	3,52	0,25	2,27
Zhang et al. [43]		1050		27		29,0	4,35	6,2	0,15	2,0

Solving equations leads to interesting discoveries, see Table 26. The strain in flexural reinforcement in the beams of Zhang et al. [43] is 2,4 – 2,5 higher than that of the beams from this study. Moreover, there is a huge difference in strain in the longitudinal reinforcement between the control and experimental group of Zhang et al. [43]. To be exact, the difference in absolute value is 0,0352%. In contrast, the difference in absolute value is only 0,0072% in this study. The calculated ε_s approximates the experimental values[1], see Figure 70 (-67 mm).

Table 26 Solution of reference beams and hybrid beams under non-limit state

Ref.	Specimen	ε_s [%]	ε_c [‰]	f_s [MPa]	x_n [mm]	$\sum F_{SHCC}$ [kN]
This study (1st series)	Reference beam	0,1091	0,726	218,3	66,71	×
	Hybrid beam	0,1019	0,647	203,8	64,87	7,67
Zhang et al. [43]	Reference beam	0,2772	1,552	554,3	59,24	×
	Hybrid beam	0,2420	0,984	483,9	47,69	13,34

But why does it matter? As explained by Collins et al. [60] and Shuraim [63], the reduction of strain in flexural reinforcement has a positive effect on the shear capacity of a beam. Figure 106 shows the exponential relationship between strain in longitudinal reinforcement and normative shear stress at failure. Consequently, the reduction of the higher strain, as in Zhang's case, is less effective than the reduction of the lower strain, as in the case of this study. However, the difference in strain between control and experimental specimen was so high in Zhang's case that it led to a noticeable enhancement of the shear capacity of a beam: the failure stress at failure should have increased by roughly 10%, according to Figure 106.

Looking at Mohr's circle for steel, reducing the strain in the x-direction (normal) will improve the limit of strain in the y-direction (shear). It may be related to the higher dowel action of longitudinal reinforcement since it works in the y-direction. Eventually, it would result in higher shear capacity.

But why did the SHCC webs laminates in the hybrid beam of Zhang et al. [43] reduce more strain in the flexural reinforcement than in the hybrid beams from the first series? To answer this question, we have to look again at Table 22. Zhang's SHCC had higher tensile strength and Young's modulus which resulted in sooner activation of their laminates but also contributed more, see the last column of Table 26. Since the area of longitudinal bars of their hybrid beam was 60,9% smaller, it resulted in higher stress reduction. And since Youngs's modulus of steel did not change, the constitutive equation of stress-strain relationships tells us that the strain has to be reduced by the same amount.

In conclusion, the difference in the results between Zhang et al. [43] and this study are caused by two important factors. The primary factor, the tensile properties of Zhang's SHCC were better that the tensile properties of SHCC of this study. Not only tensile strength was higher, but also Young's modulus which helped to activate SHCC sooner in the case of Zhang's hybrid beams. The secondary factor is the effect of higher strain in the longitudinal reinforcement of Zhang's hybrid beam due to the lower longitudinal reinforcement ratio than in this study. As explained in the study [60] by Collins et al., the shear capacity is correlated with the amount of strain in longitudinal reinforcement along its axes.

[1] The normal strain of longitudinal reinforcement was not measured directly.

6.2.2 Results comparison with experimental investigation by Wei et al. (2020)

Figure 17 (on page 23) shows the load midspan deflection relationships of (hybrid) beams of Wei et al. from their experiment [45]. All beams, which will be discussed in this section, were provided with shear reinforcement. The most crucial results of Wei et al. [45] alongside the results of the second series are summarised in Table 27. A detailed overview of material properties and geometry parameters is given in Table 28.

Table 27 Comparison of between experimental results on (hybrid) beams with transverse reinforcement

Ref.	Specimen with transverse reinforcement	Ultimate capacity [kN]	Δ in ultimate capacity compared to reference group [kN]	Δ in ultimate capacity compared to reference group [%]	Vertical displacement at peak load [mm]
This study (2nd series)	Reference beam {120 × 200 mm²}	101,8	-	-	4,65
	Hybrid beam B1 {120 × 200 mm²}	124,5	+ 22,7	+ 22,3	4,54
	Hybrid beam B2 {120 × 200 mm²}	124,2	+ 22,4	+ 22,0	5,35
Wei et al. [45]	Reference beams {180 × 350 mm²}	330,4	-	-	4,3
	Hybrid beams with smooth laminates {200 × 350 mm²}	392,6	+ 62,2	+ 18,8	4,5

It is obvious to say, that the results of Wei et al. differ substantially from the results of this experiment due to the size effect. Furthermore. the shear span parameter (η_a) of their beams is noticeably smaller $(2{,}5 < 3)$ which has implications on the shear capacity and failure mechanism, but more about it later. Their cross-section is more heavily reinforced in the longitudinal direction (+510,4%) and slightly more in the transverse direction (+20,0%) than the beams in the second series. The type of steel used for longitudinal direction was the same, but weaker steel have been used for the stirrups. Additionally, the effective depth of their beams is 70,1% higher. On the material level, their concrete has a 13,5% higher compressive strength, but a 24,6% smaller Young's modulus. Their Young's modulus is much lower than the value provided by EC2. There is no additional information provided about NC by the authors of this paper. Most of those factors mentioned above, except for the size effect, weaker steel for the stirrups and Young's modulus of concrete, work in favour of the shear capacity. For clarity, Young's modulus of concrete has hardly any effect on the shear capacity of the reference beams.

The results of hybrid beams between those studies differ due to better properties of SHCC in the case of Wei et al. Their SHCC had 94,6% higher tensile strength and 112,1% larger Young's modulus. But their tensile strain at 90% strength was 38,0% lower.

Table 28 Comparison of beams with transverse reinforcement: a detailed overview of material properties and geometric parameters

		Wei et al. [45]	*This study (2nd series)*	| Difference |	
Material properties	**Average compressive strength of concrete [MPa]**	36[a)]	31,73 (± 1,89)	4,27 (± 1,89)	13,5% (± 6,0%)
	Young's modulus of concrete [MPa]	26000	34486	8486	24,6%
	Average compressive strength of SHCC [MPa]	120	72,570 (± 3,355)	47,43 (±3,355)	65,4% (± 4,6%)
	Average tensile strength of SHCC [MPa]	10 (± 1,2)	5,14	4,86 (± 1,2)	94,6% (± 23,3%)
	Average tensile strain at 90% strength [%]	3	4,84	1,84	38,0%
	Young's modulus of SHCC [MPa]	35000	16500[b)]	18500	112,1%
	Mean yield strength of long. steel [MPa]	585	560	25	4,5%
	Mean yield strength of stirrup steel [MPa]	335	560	225	40,2%
	Mean tensile strength of stirrup steel [MPa]	530	605	75	12,4%
Geometric parameters	**Effective depth [mm]**	284	167	117	70,1%
	The second moment of area [$\times 10^4$ mm^4] of RC beams	64312,5	8000	56312,5	703,9%
	The second moment of area [$\times 10^4$ mm^4] of hybrid beams	71458,3	8000	63458,3	793,2%
	Total area of longitudinal reinforcement in tension zone [mm^2]	2454,37	402,12	2052,25	510,4%
	The cross-section area of single stirrup [mm^2]	56,55	56,55	0	0%
	Spacing between stirrups [mm]	200	250	50	20,0%

a) The specimen type: cube. The specimen size:100 × 100 × 100 mm^3.
b) This value comes from the experiment [50] of MSc Shan He (inventor of the mix composition).

Theoretical shear capacity of RC beams without transverse reinforcement from experimental investigation [45] by Wei et al. (2020)

In order to determine the theoretical shear capacity of the reference beams (group B) from Wei's experiment, the approach of GSDM by Cladera et al. [59] has been used. This method has been explained in detail in section 6.1.2.

The longitudinal reinforcement ratio of the reference beams (group B) of Wei et al. [45] equals:

$$\rho_{sl,Refernce} = \frac{A_{sl}}{b_c \cdot d} \cdot 100\% = \frac{2454{,}37}{180 \cdot 284} \cdot 100\% = 4{,}81\% \qquad \textit{(Eq. 6.64)}$$

The load on the reference beam in the governing section

$$V_E = \frac{330{,}4}{2} = 165{,}2\ kN;\ M_E = \frac{330{,}4 \cdot 0{,}71}{4} = 58{,}646\ kNm$$

The size effect factor is obtained by solving Eq. 6.23:

$$\xi = 1 + \sqrt{\frac{200}{0{,}9 \cdot 284}} = 1{,}88 \leq 2{,}75 \qquad \textit{(Eq. 6.65)}$$

The shear stress in the beam can by found in the following way:

$$\tau = \frac{V}{b \cdot z} = \frac{165{,}2 \cdot 10^3}{180 \cdot 0{,}9 \cdot 284} = 3{,}59 \leq 3\ MPa \qquad \textit{(Eq. 6.66)}$$

$$\frac{\tau}{f_{cm}} = \frac{3}{36} = 0{,}083 \geq 0{,}05 \qquad \textit{(Eq. 6.67)}$$

Substituting Eqs. 6.64, 6.65 and 6.66 into Eq. 6.22, the contribution of concrete in the reference beam with transverse reinforcement is:

$$V_{Rm,c} = \left[0{,}17 \cdot 1{,}88 \cdot \sqrt{4{,}81} \cdot 36^{0{,}2} \cdot 3^{1/3}\right] \cdot 180 \cdot 0{,}9 \cdot 284 = 95{,}2\ kN \qquad \textit{(Eq. 6.68)}$$

The longitudinal strain in the stirrup according to Eq. 6.29:

$$\varepsilon_{x,st} = 0{,}5 \cdot \frac{\frac{58{,}646 \cdot 10^6}{0{,}9 \cdot 284} + 165{,}2 \cdot 10^3}{200 \cdot 10^3 \cdot 1472{,}62} \cdot 1000 = 1{,}34 \leq 1 \qquad \textit{(Eq. 6.69)}$$

The angle of the inclined struts can be calculated using Eq. 6.28:

$$\theta = 20 + 15 \cdot 1 + 45 \cdot \frac{3}{36} = 38{,}8° \leq 45° \qquad \textit{(Eq. 6.70)}$$

The contribution of stirrups in the reference beam with transverse reinforcement is obtained by substituting Eq. 6.70 into Eq. 6.21:

$$V_{Rm,s} = \frac{56{,}55}{200} \cdot 0{,}9 \cdot 284 \cdot 335 \cdot \cot(38{,}8°) = 30{,}1\ kN \qquad \textit{(Eq. 6.71)}$$

Substituting Eqs. 6.68 and 6.71 into Eq. 6.26:

$$V_{Rm} = 95{,}2 + 30{,}1 = 125{,}3\ kN \qquad \textit{(Eq. 6.72)}$$

Hence, the theoretical shear capacity of the reference beam with transverse reinforcement according to the model by Cladera et al. [59] equals:

$$F = 2 \cdot V_{Rm} = 2 \cdot 125{,}3 = 250{,}6\ kN \qquad \textit{(Eq. 6.73)}$$

The value of Eq. 6.73 is 79,8 kN (24,2%) lower than the experimental value (330,4 kN). In Wei's reference beams, an unusual type of reinforced steel has been used for stirrups. The mean yielding and tensile strength of this steel were 335 MPa and 530 MPa, respectively. The tensile-to-yielding strength ratio equalled 1,58. Arguably, it would be more realistic to use tensile strength steel properties in Eq. 6.71 for such type of steel. In contrast, reinforcing steel B500 the tensile-to-yielding strength ratio is at least 1,08. For such steel, it is logical to use yielding strength since the ratio is small.

Theoretical shear capacity of hybrid beam without transverse reinforcement from experimental investigation [45] by Wei et al. (2020)

Since their beam has been heavily flexural reinforced, it has been proposed to use an effective longitudinal reinforcement ratio. The effective area of longitudinal reinforcement is defined as the area of the tensile reinforcement minus the area of the compression reinforcement:

$$A_{sl,eff} = A_{sl} - A_{slc} = 2454{,}37\ - 981{,}75 = 1472{,}62\ mm^2 \qquad \textit{(Eq. 6.74)}$$

Thus the effective longitudinal reinforcement ratio of Wei's hybrid beams equals:

$$\rho_{sl,Hybrid,eff} = \frac{A_{sl,eff}}{b_c \cdot d} \cdot 100\% = \frac{1472{,}62}{200 \cdot 284} \cdot 100\% = 2{,}59\% \qquad \textit{(Eq. 6.75)}$$

Substituting Eq. 6.75 into Eq. 6.8 allows for obtaining β:

$$\beta = -23{,}04 \cdot \frac{2{,}59}{100} + 1{,}00 = 0{,}403 \qquad \textit{(Eq. 6.76)}$$

In the case of Wei's hybrid beams, the contribution of SHCC laminates to the shear capacity according to Eq. 6.7 equals:

$$V_{SHCC} = 1{,}0 \cdot 0{,}403 \cdot 10 \cdot 350 \cdot 20 = 28{,}2\ kN \qquad \textit{(Eq. 6.77)}$$

Converting to the force as a result of SHCC laminates:

$$F_{SHCC} = 2 \cdot V_{SHCC} = 2 \cdot 28{,}2 = 56{,}4\ \text{kN} \qquad \textit{(Eq. 6.78)}$$

The solution of Eq. 6.78 does not match the experimental value (62,2 kN). There are two reason for this. First, the truss model by Wang et al. [44] was calibrated for beams with shear span parameter equal 3. As explained in their paper [44], the arch mechanism becomes an important factor for beams with η_a under 2,5. The arch mechanism has been covered in the literature study, see section 2.1.1. Second reason are the mechanical properties of Wei's SHCC.

To be more precise: the standard deviation of tensile strength of the SHCC is approximately 1,2 MPa. When this parameter is included then the lower and upper bound limits becomes:

$$V_{SHCC} = 1{,}0 \cdot 0{,}403 \cdot \{10 \pm 1{,}2\} \cdot 350 \cdot 20 = [24{,}8\,;\,31{,}6]\ kN \qquad \textit{(Eq. 6.79)}$$

Converting to the force as a result of SHCC laminates:

$$F_{SHCC} = 2 \cdot V_{SHCC} = 2 \cdot [24{,}8\,;\,31{,}6]\ = [49{,}6\,;\,63{,}2]\ \text{kN} \qquad \textit{(Eq. 6.80)}$$

So the experimental value does fall in this range. From those calculation can be concluded that SHCC laminates were fully utilised. Even though, authors have reported a partial debonding in the midspan at the ultimate load, but “the system was able to maintain integrity” quoted from their paper [45]. So, bonding strength between the NC cores and the SHCC laminates was sufficient in this particular case.

6.3 Discussion

The outcomes of this research have provided insight into the shear behaviours of hybrid beams with and without transverse reinforcement. In general, the hybrid beams have obtained higher shear capacity than the control group. This statement has been confirmed by the literature [10, 43, 44, 45] on this specific subject. Therefore, all evidence suggests that the hypothesis of this research is correct. The question that remains is to what extent can the shear capacity be enhanced by having SHCC web layers attached to the reinforced concrete beam when compared to the control reinforced concrete beam.

According to experimental data from this study, the hybrid beams without shear reinforcement increased their shear capacity by 13,2 kN and 12,1 kN compared to their reference beam. The hybrid beam with the smooth interface between its NC core and the SHCC laminates did perform slightly better than the hybrid beam with the profiled interface. It must be noted that the thickness of shear keys laminates was 30% thinner in one specific location. Indeed, this has reduced the shear capacity of the hybrid beam to some extent. In contrast, the hybrid beams with shear reinforcement achieved much better outcomes by enhancing the shear capacity by 22,7 kN and 22,4 kN in comparison with their reference beam. The hybrid beam which was supported at its full width produced slightly higher resistance against shear loading than the hybrid beam which was only supported at its NC core. It is therefore evident that supporting a hybrid beam with shear reinforcement at its NC core does not necessarily results in a significant lose of the shear capacity. However, it might not be true for hybrid beams with thicker SHCC web laminates since the reduction of supporting width will much greater, but this is beyond the scope of this research.

The evolution of crack patterns during the loading was substantially different between the RC beam without transverse reinforcement to the beams that were shear reinforced by SHCC web laminates and/or stirrups. The beams which were shear reinforced showed the development of diagonal cracks on the left and right spans almost simultaneously. Just before the peak load, only one diagonal crack in each beam has localised which led to the failure of the particular beam. Whereas the RC beam without stirrups showed the development of only one diagonal crack during its testing. There is a remarkable difference between the hybrid beams with and without transverse reinforcement. The hybrid beams with lightly shear reinforcement showed dispersed cracking of their SHCC laminates in contrast to the hybrid beams without stirrups. In the latter, the crack in SHCC webs has for the most part localised. Besides, all hybrid beams had smaller experimental angles of the critical inclined diagonal crack smaller than that of the RC beam without transverse reinforcement.

From design calculation using Eurocode 2 approach, the RC beam without stirrups was very close to reaching its target capacity of 55,3 kN. According to experimental data, this beam sustained a peak load of 53,5 kN. The same cannot be said about the RC beam with stirrups which failed at 101,8 kN. But according to the EC2 approach, this beam should reach only 83,8 kN. So where did this extra shear capacity come from? According to

Cladera et al. [55], the model of EC2 overlooks some crucial factors which could explain this observation. In the case of the lightly shear-reinforced beams (like this reference beam in this experiment), the primary overlooked factor is the normal concrete contribution to shear capacity. For this reason, they have proposed their own model GSDM [59] which takes this contribution into account together with other factors. According to GSDM, the theoretical shear capacity equals 100,8 kN which is more or less the same value that has been found during the experiment. Although calculations with the Eurocode 2 approach are generally faster and easier than with the GSDM approach, the computation time using the GSDM is not that bad for

the accuracy that it offers. According to GSDM, the reference beam with stirrups should fail at 100,8 kN.

In addition to the shear capacity contribution of an NC core and transverse reinforcement, a hybrid beam has obviously SHCC web laminates which must be considered during estimating shear capacity. Two models have been found in the literature that takes the shear contribution of SHCC laminates in the webs. The simplified model by Baghi [58] is based on the idea of the maximum shear stress in a rectangular non-cracked cross-section. It is a very basic model which takes only the geometrical and tensile strength of SHCC into account. And there is the deterministic model by Wang et al. [44] which uses a truss analogy. They have added deterministic reduction factors to compensate for the delamination of SHCC laminates from an NC core but also the effect of the longitudinal reinforcement. In the case of hybrid beams with shear reinforcement, it has been established that the truss model is more accurate in its prediction than the simplified model. However, both models failed to predict accurately the shear contribution of SHCC laminates in the first series. According to the truss model by Wang et al. [44], theoretical F_{SHCC} is almost double the experimental value. Most presumably, the SHCC laminates were not fully activated. The deep analysis showed that hybrid beams without stirrups experience accelerated growth of their main diagonal cracks for a very short period before reverting to slower growth rates. This observation indicates for quick redistribution of internal forces. It seems like Young's modulus of SHCC, which is lower than that of NC, did not allow for sufficient activation of the SHCC in an earlier stage of loading. Consequently, the NC core had to resist a significant portion of shear force which had to be (partly) transferred to the SHCC webs. Since NC is a brittle material, there must have been a sudden redistribution of internal forces which is more violent than the case of a gradual redistribution of forces.

In contrast to hybrid beams without transverse reinforcement, the SHCC laminates were activated in the hybrid beam with shear reinforcement as mentioned earlier. The empirical evidence of no peak flocculation in the growth of the main diagonal cracks in hybrid beams with shear reinforcement gives a strong signal that those cracks had more ductility. Most likely, the stirrups cushioned the sudden redistribution of the internal forces due to their large Young's modulus which pulled the significant part of the force flow toward themselves. Hence, the transfer of the internal force towards the SHCC webs was more gradual than in the case of hybrid beams without shear reinforcement. As a consequence of the smaller gradient of the additional force, the SHCC laminates in the webs experienced a smaller sudden jump in the strain since the transverse reinforcement absorbed a significant portion of the internal forces from the NC core after it has fractured. Hence, the SHCC developed its typical crack pattern in a later stage which is a sign of full activation of the tensile properties.

From the comparison of the results between Zhang et al. [43] and this study, it became obvious that the experimental results were distinctly different from each other. In their case, the SHCC laminates (smooth interface) in the hybrid beams without stirrups have contributed three times more shear capacity than the SHCC laminates from this study in the first series even though the beams were equal size. The same cannot be said about their reference beam which was 20 mm less wide than the rest of the beams. Despite the fact that their reference beam was smaller in its width, the whole difference cannot be ascribed to this fact. From analytical calculations based on EC2, their reference beam should only sustain 35,0 kN but in reality, the peak load reached 51 kN. It is almost the same capacity as that of the reference beam from the first series. After consulting the literature on a wide range of parameters (f_c, ρ_{sl}, e_x, η_a, d) that may influence the shear capacity, it became obvious that their beams brakes all trends. Therefore, the results should be classified as an outlier since it does not follow the trends of the

hundreds of other results. However, two particular parameters were standing out in their beam, namely the area of the longitudinal reinforcement in the tension zone, and Young's modulus of SHCC. The area was significantly smaller and Young's modulus had almost the double value than the (hybrid) beams from this study.

Using the truss model by Wang et al. [44], the theoretical F_{SHCC} of Zhang's hybrid beam is almost identical to the experimental value. It is probable that their SHCC was almost fully activated since Young's modulus of their SHCC was 75,8% higher. In general, the properties of their SHCC were higher than the properties of the SHCC from this study. Even though they were higher, those properties do not fully explain such a large contribution to shear capacity due to SHCC. It seems like it had to do something with low area of the flexural reinforcement (A_{sl}). In their case, the Influence Coefficient of Reinforcement Ratio (β) was extremely high due to A_{sl} parameter. After analysing strain in the longitudinal reinforcement under a non-limit state (NLS), it became evident that Zhang's hybrid beam reduced significantly more strain compared to its control group than the hybrid beams in the first series compared to the control group in the first series. As explained by M. Collins et al. [60] and B. Shuraim [63], the reduction of strain in flexural reinforcement has a positive effect on the shear capacity of a beam. Lower strain helps in generating higher dowel action of longitudinal reinforcement since steel is further away from yielding.

So in the case of hybrid beams without transverse reinforcement, it is highly important to make sure that Young's modulus of SHCC is higher than that of NC. Otherwise, the SHCC laminates of a hybrid beam without TR will not be fully utilised as experimentally proven in this study. In contrast, the hybrid beams with (minimum) transverse reinforcement and with Young's modulus of SHCC about half smaller than that of NC did not show this limitation. Furthermore, the tensile strength of SHCC is positively correlated with the contribution of the shear capacity in the hybrid beams with or without TR. Therefore, this property should be as high as possible after the criteria of Young's moduli is satisfied.

From the comparison of the results between Wei et al. [45] and this study, it has been established that the shear span parameter (η_a) may play a key role in deciding the type of failure mechanism. Wei's beams had a larger cross-section but they had smaller η_a than the beams used in this study. The shear span parameter was 2,5, which is 0,5 smaller compared to this study, but it may be sufficient for their SHCC laminates to develop the arch mechanism. The arch mechanism is known for enhancing shear capacity. However, this effect is not taken into account in the truss model by Wang et al. [44], as consequence the theoretical value was underestimated. This truss model is only accurate for the beams with η_a equal to 3 since it was calibrated for.

However not all evidence point to the arch mechanism that caused this inaccuracy. There is also a standard deviation of the tensile strength of SHCC. After calculating the lower and upper bound limits, the experimental values fall in this range. Most probably, it is the interaction of both effects on the contribution due to SHCC laminates to shear capacity.

In essence, the simplified model by Baghi [58] can be used for preliminary calculations since it straight forward to use. However, during USL analysis, the truss model by Wang et al. [44] should be used in the design calculations since it takes the risk of delamination of SHCC laminates but also takes into account the effect of reinforcement ratios. This truss model seems to be easy to implement in EC2 since already includes the strut and tie modelling for concrete. But before the implication of this model in the practices, better calibration of β and η factors are required. For these reason, more experimental data are still needed to obtained satisfactory accuracy using this approach.

There is some point of attention regarding the interface between SHCC and NC. During preparation for the experiment, the hybrid beam with smooth laminates showed partial delamination of all laminates near the side edges of the beam. This happened two days after the beam has been taken out of the mould. The smooth bonding system between the SHCC laminates and the NC core was not strong enough to withstand differential drying shrinkage between the SHCC and the NC over this short period of time. Even though it had not influenced the peak load, it should definitely be addressed before a practical application. For clarity, the hybrid beams with the profiled interface between the NC cores and the SHCC laminates did not have this issue.

Analysis of the initial stiffness of the beams with transverse reinforcement showed problems with the quality of NC. It seems like the concrete was not properly densified on the vibrating table during the second casting. It is odd since Young's modulus of the normal concrete prism in the second series was similar in quality to that of the first series. Also from visual inspection, the beams looked fine. Most importantly, this issue did not affect the ultimate capacities of the beams, but the effects of the difference in support boundary conditions of hybrid beams with shear reinforcement regarding the deflection behaviours could not be extracted from such data.

7

Conclusions & Recommendations

"The roots of education are bitter, but the fruit is sweet."

Ἀριστοτέλης *Aristotélēs* (Aristotle)

This chapter concludes the effects of the Strain-Hardening Cementitious Composite laminates on the shear behaviour of hybrid SHCC-concrete beams. Inspired by previous successful research on the topic, new experimental benchmarks on RC beams with shear strengthening using SHCC laminates have been established. This research distinguishes itself from other studies by the fact that normal concrete was cast between older SHCC laminates, consequently, forming the old-new interface concrete SHCC connections. Furthermore, two different types of SHCC-concrete interface have been used in hybrid beams, namely smooth and profiled ones. Its main focus is on the shear capacity of such a hybrid SHCC-concrete system. But other aspects of this complex phenomenon will be touched on.

7.1 Conclusions

This master's thesis research aimed to establish knowledge regarding the strengthening of reinforced concrete beams using 10 mm Strain-Hardening Cementitious Composite laminates under shear loading. The main research question, however, focuses on the extent of increased shear capacity due to SHCC web layers attached to the sides of an RC beam. To answer this question, the shear capacities of four hybrid beams were tested in a three-point bending set-up against the shear capacities of two pristine counterparts. The shear span parameter of all beams equalled 3.

From those tests, it has been established that hybrid beams are more efficient in carrying the shear load than conventional RC beams. The hybrid beams without shear reinforcement enhanced the ultimate shear capacity by 22,6% (12,1 kN) and 24,7% (13,2 kN). The hybrid beam with smooth laminates reached a higher load capacity than the hybrid beam with shear keys laminates. This was caused by an unintended deviation of 30% from the total through-thicknesses of shear keys laminates in the critical location of this particular beam. The hybrid beams with transverse reinforcement enhanced the shear capacity by 22,3% (22,7 kN) and 22,0% (22,4 kN). The hybrid beam B1 with shear reinforcement, which was supported at its full length, has reached a slightly higher load capacity than the hybrid beam B2 with shear reinforcement which was only supported at its normal concrete core. The difference in boundary conditions of hybrid beams did not affect the carrying capacity of shear load.

Answering the first sub-question: there is still a lack of knowledge regarding the interface concrete connection between old SHCC and new NC available in current literature. However, it was established that the factors that have a positive effect on the strength of an interface between new-SHCC/old-concrete are: SHCC compressive strength, normal concrete compressive strength curing age of the specimen, curing environment (temperature and relative humidity), interface roughness, fibres types, (if applied) additional binding agent strength, surface roughness, interlocking mechanism, type of cement and differential shrinkage.

The smooth bonding system between the SHCC laminates and the NC core was not strong enough to withstand differential drying shrinkage between the SHCC and the NC over a short period of time. The hybrid beam with smooth laminates showed partial delamination of all laminates near the side edges of the beam after two days after demoulding. The beams with SHCC web laminates, which were provided with shear keys, did not show this kind of behaviour. But most importantly, no hybrid beam in this experiment has failed due to debonding failure. So, answering the second sub-question based on the results of the shrinkage tests: it is observed that curing conditions had a significant impact on the shrinkage strain of SHCC. Specimens with a longer curing time (14 days in the curing room and then sealed for 28 days) showed almost twice the reduction of shrinkage than the specimens with a shorter curing time (28 days in the curing room). Since the SHCC laminates were threat the same as the first specimen, this curing condition has helped reduced almost twice the stress due to differential drying shrinkage between a NC core and a SHCC laminate. Hence, more capacity of an interface was reserved for transferring the actual load.

In contrast to the smooth interfaces, the interfaces between the SHCC laminates with shear keys and the NC core did not show any sign of delamination before and during load testing. Based on this evidence, it has been concluded that this bonding system is stronger than the smooth one.

Furthermore, the hybrid beams without shear reinforcement have improved the vertical displacement at their peak load compared to that of their reference beam. The midspan deflection at the peak load was 98,6% higher for the hybrid beam with smooth laminates and

170,5% higher for the hybrid beam with shear keys laminates compared to that of their counterpart. The brittle failure modes were not fully prevented in this case: those hybrid beams did not collapse immediately but more gradually. The hybrid beam B2 has improved the vertical displacement at its peak load by 15,1% compared to that of its reference beam. In contrast, the hybrid beam B1 did not improve the vertical displacement before failure.

After performing the analytical analysis, it has been established that the hybrid beams without transverse reinforcement did not fully activate their SHCC laminates. After consulting with the literature, it has been found that some hybrid beams without shear reinforcement were capable of utilising their SHCC webs. It seems like hybrid beams with a higher Young's modulus of SHCC than NC could activate their SHCC laminates more efficiently. So answering the third sub-question, the hybrid beams with a minimum amount of shear reinforcement did not have the issue of activating their SHCC webs compared to the hybrid without any transverse reinforcement.

The shear loading capacity of a hybrid beam with the shear span parameter of 3 or greater can be predicted with good accuracy by combining General Shear Design Method (GSDM) approach (developed by Cladera et al. [59]) for the RC part with the truss model by Wang et al. [44] for the contribution due to SHCC laminates. This method slightly underestimates the shear capacity of a hybrid beam. The simplified model for the contribution of an SHCC part by Baghi [58] should however be used only for preliminary calculations since the model is less accurate in general.

The results of this research demonstrate the effectiveness and practical feasibility of RC beams strengthened by 10 mm SHCC laminates under shear loading. It must be noted that effectiveness of SHCC found in this study were smaller compared to the other results from the literature. But still, such an innovative system also allows for building slender members, but also increases the quality and safety of concrete structures since SHCC laminates would be manufactured at prefab factories and not cast-in-situ.

7.2 Recommendations

The use of SHCC laminates in the beams without transverse reinforcement showed less promising results than anticipated. Therefore further research and optimizations are needed before this innovative idea can be executed in practice. The major issue of a hybrid beam without stirrups is guaranteeing of full activation of SHCC properties. It is therefore recommended to use cementitious materials with higher Young’s modulus for this purpose.

The secondary issue of hybrid beam is its bonding strength at the interface between SHCC laminates and a normal concrete core. It is not recommended to use smooth SHCC laminates due to a lack of confidence in long-term endurance against differential drying shrinkage between the SHCC and a NC core. The experiments showed that the difference in rate and magnitude of shrinkage between those two materials is significant. Hence, a smooth SHCC laminate might partially delaminate or even delaminate complete from the concrete core in long run. It is therefore advised to perform experiment(s) that would prove or disprove the hypothesis that by adding shear keys on an SHCC laminate the consequence of differential drying shrinkage between SHCC and normal concrete are mitigated.

From the tests on the hybrid beams, the hybrid beam with shear keys in the interface outperforms the beam with smooth laminates since this profiled interface did not show any partial delamination prior to testing. However, there is still no experimental investigation performed on how strong both interfaces are. It is therefore highly advisable to perform research on the strength of interface for new-concrete-old-SHCC connections since most previous

studies regarding this topic concentrated on the bonding properties of an interface between new SHCC to old NC.

From an execution point of view, the shear keys on a laminate are slightly inconvenient. Because in practice transverse reinforcement has to be provided, a sufficient geometrical clearance is required to place the stirrups. Shear keys reduce this clearance by their height and therefore, they might block the space allocated for the stirrups. This issue has to be taken into account during the design of the beam. It is advisable to make guidelines regarding this issue for other engineers.

A great topic for research would be hybrid connections since concrete members have to be somehow connected to the rest of the structure. The concrete connections are known for their tight allocations of reinforcement. The superior mechanical properties of SHCC might help with that issue. SHCC elements placed at the strategic location could reduce the amount of reinforcement or make the connection slender. Such a system would probably have a great positive influence on sustainability due to the small crack pattern and ductility of SHCC. Mastering this technology could open doors for a new prefabrication system made out of SHCC.

References

[1] Gagg, C. R. (2014). *Cement and concrete as an engineering material: An historic appraisal and case study analysis*. Engineering Failure Analysis. Volume 40 pp. 114-140. DOI: https://doi.org/10.1016/j.engfailanal.2014.02.004

[2] Marsh, A. T., Velenturf, A. P., & Bernal, S. A. (2022). *Circular Economy strategies for concrete: implementation and integration*. Journal of Cleaner Production, 362, 132486. DOI: https://doi.org/10.1016/j.jclepro.2022.132486

[3] Liu, Y., Pang, B., Wang, Y., Shi, C., Zhang, B., Guo, X., Zhou, S., & Wang, J. (2022). *Life-cycle maintenance strategy of bridges considering reliability, environment, cost and failure probability CO2 emission reduction: A bridge study with climate scenarios*. Journal of Cleaner Production, 379, 134740. DOI: https://doi.org/10.1016/j.jclepro.2022.134740

[4] Luković, M., (2016). *Influence of interface and Strain Hardening Cementitious Composite (SHCC) properties on the performance of concrete repairs*. ISBN 978-94-6186-590-8

[5] Luković, M., Hordijk, D.A., Huang, Z. & Schlangen, E. (2019). *Strain hardening cementitious composite (SHCC) for crack width control in reinforced concrete beams. Heron, 64 (1/2), 189-206*

[6] Schlangen, E., Šavija, B., Figueiredo, S. C., de Mendoça Filho, F. F., & Luković, M. (2017). Mechanical Properties of Ductile Cementitious Composites Incorporating Microencapsulated Phase Change Materials. *Strain-Hardening Cement-Based Composites*, 115–122. DOI: https://doi.org/10.1007/978-94-024-1194-2_13

[7] Li, V. C. (2019). *Sustainability of Engineered Cementitious Composites (ECC) Infrastructure. In: Engineered Cementitious Composites (ECC)*. Springer, Berlin, Heidelberg. DOI: https://doi.org/10.1007/978-3-662-58438-5_8

[8] Huang, Z. (2017) *Flexural behaviour of reinforced concrete beams with a layer of SHCC in the tension zone*, MSc thesis

[9] Singh, S. (2019) *Influence of Interface and Type of Strain Hardening Cementitious Composite (SHCC) on Crack Control in SHCC-Concrete Hybrid Beams*, MSc thesis

[10] Arif, A. (2020) *Numerical Study of Shear Strengthening of Reinforced Concrete Beams using Strain-Hardening Cementitious Composites*, MSc thesis

[11] Yang, Y., (2014). *Shear Behaviour of Reinforced Concrete Members without Shear Reinforcement.* ISBN 978-94-6169-516-1

[12] Ghaffar, A., Javed, A., Ur Rehman, H., Ahmed, K. & Ilyas, M. (2010). *Development of Shear Capacity Equations for Rectangular Reinforced Concrete Beams.* Pak. J. Engg. & Appl. Sci. Vol. 6.

[13] Andermatt, M. F. & Lubell, A. S. (2013). *Behavior of Concrete Deep Beams Reinforced with Internal Fiber-Reinforced Polymer—Experimental Study.*

[14] Abad, B. F., Lantsoght, E. & Yang, Y. (2019). *Shear capacity of steel fibre reinforced concrete beams.* In Proceedings of the FIB Symposium, Krakow, Poland, pp 27–29.

[15] Bogdándy, B. (2021). *The shear resistance of a member without shear reinforcement according to Eurocode 2; the error of the calculated value and the mechanical explanation of the problem.* DOI: https://doi.org/10.1556/1848.2021.00236

[16] Zhao, J. & Song, T. (2011). *Fiber-Reinforced Rapid Repair Material for Concrete Pavement.* Advanced Materials Research 168, 870. DOI: https://doi.org/10.4028/www.scientific.net/AMR.168-170.870

[17] Wang, P., Jiao, M., Hu, C., Tian, L., Zhao, T., Lei, D. & Hua, F. (2020). *Research on Bonding and Shrinkage Properties of SHCC-Repaired Concrete Beams.* DOI: https://doi.org/10.3390/ma13071757

[18] Mustafa, S., Singh, S., Hordijk, D., Schlangen, E. & Luković, M. (2022). *Experimental and numerical investigation on the role of interface for crack-width control of hybrid SHCC concrete beams.* DOI: https://doi.org/10.1016/j.engstruct.2021.113378

[19] Qian, S., Zhou, J. De Rooij, M. R., Schlangen, E. Ye, G. & Van Breugel, K. (2009). *Self-healing behavior of strain hardening cementitious composites incorporating local waste materials.* DOI: https://doi.org/10.1016/j.cemconcomp.2009.03.003

[20] Lepech, M. D. & Li, V. C. (2009). *Water permeability of engineered cementitious composites.* DOI: https://doi.org/10.1016/j.cemconcomp.2009.07.002

[21] The Yarn Guru India Inc. (2021). *PVA Fibre for Concrete, For Construction*. Retrieved January 10, 2022 from: https://www.indiamart.com/proddetail/pva-fibre-for-concrete-19546384673.html

[22] Ahammed, S. (2020). *High Modulus Polyethylene (HMPE)*. Retrieved January 10, 2022 from: https://www.slideshare.net/SAMIUN0501/high-modulus-polyethylene-hmpe

[23] Lin, W. & Yoda, T. (2017). *Chapter Seven - Steel Bridges*. Bridge Engineering, pp 111-136. https://doi.org/10.1016/B978-0-12-804432-2.00007-4

[24] Illston, J. M. & Domone, P. (Eds.). (2001). *Construction Materials — Their nature and behaviour*. Third Edition. Page: 413. ISBN 0-419-26860 (pbk)

[25] Du, E., Dong, S. & Sun, J. (2018). *Concrete Bonding Properties of Polyvinyl-Alcohol Fibre in Fabricated Structures*. Chemical Engineering Transactions, 66, 1057-1062. DOI: https://doi.org/10.3303/CET1866177

[26] Kiron, M. I. (2016). *High Performance Polyethylene Fibers – An Overview*. Retrieved January 3, 2022 from: https://textilelearner.net/high-performance-polyethylene-fibers-an-overview/

[27] Vlasblom, M. (2018). 18 - *The manufacture, properties, and applications of high-strength, high-modulus polyethylene fibers*. Handbook of Properties of Textile and Technical Fibres (Second Edition), 66, 699-755. DOI: https://doi.org/10.1016/B978-0-08-101272-7.00018-3

[28] Li VC. (2019). Engineered Cementitious Composites (ECC) Bendable Concrete for Sustainable and Resilient Infrastructure. Michigan, USA: Springer. Retrieved on

December 10, 2021 from: https://www.indiamart.com/proddetail/pva-fibre-for-concrete-19546384673.html

[29] Tadepalli, P. R., Mo, Y. L. & Hsu, T. T. C. (2015). *Mechanical properties of steel fibre concrete*. Magazine of Concrete Research, pp. 462-474. DOI: https://doi.org/10.1680/macr.12.00077

[30] Abdallah, S., Fan, M. & Rees, D.W.A. (2018). *Bonding Mechanisms and Strength of Steel Fiber–Reinforced Cementitious Composites: Overview*. DOI: https://doi.org/10.1061/(ASCE)MT.1943-5533.0002154

[31] Marcos-Meson, V., Fischer, G., Edvardsen, C., Skovhus, T. L. & Michel, A. (2019). *Durability of Steel Fibre Reinforced Concrete (SFRC) exposed to acid attack – A literature review*. DOI: https://doi.org/10.1016/j.conbuildmat.2018.12.051

[32] Van Zijl, G.P.A.G., & Slowik, V. (Eds.) (2017). *A Framework for Durability Design with Strain-Hardening Cement-Based Composites (SHCC),* pp 68 - 69. ISBN 978-94-024-1013-6. DOI: https://doi.org/10.1007/978-94-024-1013-6.

[33] Zhu, H., Zhang, D., Wang, Y., Wang, T. & Li, V. C. (2021). *Development of self-stressing Engineered Cementitious Composites (ECC)*. DOI: https://doi.org/10.1016/j.cemconcomp.2021.103936

[34] Tarr, S. (2012, September 6). *A Concrete Mixture Shrinkage Potential — Achieving better slabs by understanding a mix's shrinkage potential.* Retrieved on January 10, 2022 from: https://www.concreteconstruction.net/how-to/materials/concrete-mixture-shrinkage-potential_o

[35] Li, M. & Li, V.C. (2011). *Behavior of ECC/concrete layer repair system under drying shrinkage conditions*. Publication at: www.researchgate.net/publication/228617167

[36] Yang, E.H., Yang, Y. & Li, V.C. (2007). *Use of high volumes of fly ash to improve ECC mechanical properties and material greenness*. ACI Materials Journal, 104 (6), pp. 303-311

[37] Karagüler, M. E. & Yatağan, M. S. (2018). *Effect of aggregate size on the restrained shrinkage of the concrete and mortar*. MOJ Civil Eng. 2018;4(1):15–21. DOI: https://doi.org/10.15406/mojce.2018.04.00092

[38] Tian, J., Wu, X., Zheng, Y., Hu, S., Du, Y., Wang, W., Sun, C. & Zhang, L. (2019). *Investigation of interface shear properties and mechanical model between ECC and concrete*. DOI: https://doi.org/10.1016/j.conbuildmat.2019.06.188

[39] Gao, S., Zhao, X., Jinli, Q., Guo, Y. & Hu, G. (2019). *Study on the bonding properties of Engineered Cementitious Composites (ECC) and existing concrete exposed to high temperature*. DOI: https://doi.org/10.1016/j.conbuildmat.2018.11.136

[40] Wang, B., Xu, S. & Liu, F. (2016). *Evaluation of tensile bonding strength between UHTCC repair materials and concrete substrate*. DOI: https://doi.org/10.1016/j.conbuildmat.2016.02.149

[41] Şahmaran, M., Yücel, H. E., Yildirim, G. & Al-Emam, M. (2014). *Investigation of the Bond between Concrete Substrate and ECC Overlays*. DOI: https://doi.org/10.1061/(ASCE)MT.1943-5533.0000805

[42] Mo, M. & Li, V. (2016). *The influence of surface preparation on the behaviour of ECC/concrete layer repair system under drying shrinkage conditions*. Publication at: https://www.researchgate.net/publication/268424297

[43] Zhang, Y., Bai, S., Zhang, Q., Xie, H. & Zhang, X. (2015). *Failure behavior of strain hardening cementitious composites for shear strengthening RC member*. Construction and Building Materials, Volume 78, Pages 470-473 DOI: https://doi.org/10.1016/j.conbuildmat.2015.01.037

[44] Wang, G., Yang, C., Pan, Y. Zhu, F., Jin, K., Li, K. & Nanni, A. (2019). *Shear behaviors of RC beams externally strengthened with engineered cementitious composite layers*. Materials, 12(13):2163. DOI: https://doi.org/10.3390/ma12132163

[45] Wei, J., Chen, Y., Wu, C. & Leung, C. K. Y. (2020). *Shear strengthening of reinforced concrete beams with high strength strain hardening cementitious composites (HS-SHCC)*. Mater Struct, 53 (4). DOI: https://doi.org/10.21012/FC10.233281

[46] Wu, X., Kang, T. H.-K., Lin, Y. & Hwang, H.-J. (2018). *Shear strength of reinforced concrete beams with precast High-Performance Fiber-Reinforced Cementitious Composite permanent form*. Compos Struct, 200, pp. 829-838. DOI: https://doi.org/10.1016/j.compstruct.2018.06.007

[47] Shang, X., Yu, J., Li, L. & Lu, Z. (2020). *Shear strengthening of fire damaged RC beams with stirrup reinforced engineered cementitious composites*. Eng Struct, 210, Article 110263 DOI: https://doi.org/10.1016/j.engstruct.2020.110263

[48] Li, R., Deng, M., Chen, H. & Zhang, Y. (2022). *Shear strengthening of RC shear-deficient beams with highly ductile fiber-reinforced concrete*. DOI: https://doi.org/10.1016/j.istruc.2022.08.013

[49] Huang, Y. & Luković, M. (2022). *Effect of freeze-thaw cycles on shear resistance of reinforced concrete beams strengthened with UHPFRC.* In M. di Prisco, A. Meda, & G. L. Balazs (Eds.), Proceedings of the 14th fib PhD Symposium in Civil Engineering, pp. 557-564. fib. The International Federation for Structural Concrete. Publication at: https://www.researchgate.net/publication/363517592_Effect_of_freeze-thaw_cycles_on_shear_resistance_of_reinforced_concrete_beams_strengthened_with_UHPFRC

[50] He, S., Zhang, S., Luković, M. & Schlangen, E. (2022). *Effects of bacteria-embedded polylactic acid (PLA) capsules on fracture properties of strain hardening cementitious composite (SHCC)*. DOI: https://doi.org/10.1016/j.engfracmech.2022.108480

[51] European committee for standardization. (2011). *NEN-EN 197-1. Cement - Part 1: Composition, specifications and conformity criteria for common cements*.

[52] Blagojević, A. (2016). *The Influence of Cracks on the Durability and Service Life of Reinforced Concrete Structures in relation to Chloride-Induced Corrosions*. Ridderprint – the Netherlands. ISBN: 978-94-6299-275-7

[53] Zhang, S., Li, V. C. & Ye, G. (2020). *Micromechanics-guided development of a slag/fly ash-based strain-hardening geopolymer composite*. Cement and Concrete Composites, FVolume 109, 103510. DOI: https://doi.org/10.1016/j.cemconcomp.2020.103510

[54] GOM Correlate software [Computer software]. 2022. Retrieved from: www.gom.com

[55] Cladera, A. & Marí, A. R. (2007). *Shear strength in the new Eurocode 2. A step forward?*. DOI: https://doi.org/10.1680/stco.2007.8.2.57 Publication at: https://www.researchgate.net/publication/245409598

[56] Yu, J., Chen, Y. & Leung, C. K. Y. (2019). *Mechanical performance of Strain-Hardening Cementitious Composites (SHCC) with hybrid polyvinyl alcohol and steel fibers*. DOI: https://doi.org/10.1016/j.compstruct.2019.111198

[57] Béton, F Du. (2008). *Structural Connections for Precast Concrete Buildings: Guide to Good Practice*. International Federation for Structural Concrete (fib). ISBN 978-2-88394-083-3

[58] Baghi, H. (2015). *Shear Strengthening of Reinforced Concrete Beams with SHCC-FRP Panels*, PhD thesis

[59] Cladera, A. & Marí, A. R. (2004). *Shear design procedure for reinforced normal and high-strength concrete beams using artificial neural networks. Part II: beams with stirrups*. Engineering Structures 26 927–936. DOI: https://doi.org/10.1016/j.engstruct.2004.02.011

[60] Collins, M. P., Bentz. E. C., Sherwood. E. G. & Liping, X. (2007). *An adequate theory for the shear strength of reinforced concrete structures*. DOI: https://doi.org/10.1680/macr.2008.60.9.635 Publication at: https://www.researchgate.net/publication/237411162

[61] Kani, M.W., Huggins, M.W. & Wittkopp, R.R., Kani. (1979). *Shear in Reinforced Concrete*. Department of Civil Engineering, University of Toronto, Toronto, 225 pp.

[62] Krefeld, W.J. & Thurston, C.W. (1966). *Studies of the Shear and Diagonal Tension Strength of Simply-Supported Reinforced Concrete Beams*. ACI Journal, Vol. 63, No. 4, pp. 451-476.

[63] Shuraim, A. B. (2013). *A novel approach for evaluating the concrete shear strength in reinforced concrete beams*. DOI: https://doi.org/10.1590/S1679-78252014000100006

[64] Guo, Z. (2014). *Chapter 11 - Strength of Member Under Compression and Bending*. Principles of Reinforced Concrete, Pages 269-304. ISBN–13: 978-0-12-800859-1. DOI: http://dx.doi.org/10.1016/B978-0-12-800859-1.00011-6

[65] Han, J., Guo. C. & Zhang, H. (2020). *Analysis and calculation of normal section of reinforced concrete beam under non-limit state*. E3S Web of Conferences 143, 01049 DOI: https://doi.org/10.1051/e3sconf/202014301049

Appendix A. Procedure for standardized mixing of SHCC

SHCC mixtures were prepared in a Hobart mixer. This mixer is in accordance with EN 196-1.

1st step)	Dry mixing of cement and limestone powder for 5 minutes
2nd step)	Slowly add 90% of water (premixed with all SP) and mix for 3 minutes
3rd step)	Add 1/3 of fibre and mix for 1 minute
4th step)	Add 1/3 of fibre and 5% of water and mix for 1 minute
5th step)	Add 1/3 of fibre and 5% of water and mix for 1 minute
6th step)	Medium speed mixing for 2 minutes
7th step)	Low speed mixing for 2 minutes
	Total mixing time: 15 minutes

Appendix B. Small scale experiments on shear keys

B.1 Fibres bridging between shear key and laminate board

This appendix is devoted to the subject of the dimensioning of a shear key using the trial and error method. From the previous experiments, it has been observed that the fibres of SHCC have an issue filling slots while cast vertically. If the slot is too small then only cement paste of SHCC filled such slot. The central question that will be answered in this section is as follows:

What is the smallest size of shear keys on the thin SHCC laminate that give a good monolithic connection with the rest of the laminate?

A good monolithic connection of SHCC between a shear key and a laminate is defined as the present of fibres and cement paste at the interface of the extraction. Since no answer could be found in the current literature, it has been decided to cast small scale laminates with different size and shapes profiles on it.

Figure B-1 Closs up of profiled laminate. On the left: removed shear key with dimensions 10 mm × 80 mm. On the left: removed shear key with diameter of 25 mm.

During those small-scale experiments, it has been observed that the smallest dimension of a slot's perimeter is the governing factor that predicts if the fibres will be present at the interface of an extraction, see Figure B-1. Only 50% of all slots with a minimum edge size of 10 mm had a good monolithic connection. The slots with a minimum base dimension of 25 mm showed a 100% chance for a good monolithic connection. In the end, the cylinder with a diameter of 25 mm and a height of 10 mm has been selected as the shape for shear keys on profiled laminates.

B.2 Failed chipboard mesh for shear key casting

The second part of the small-scale experiments focuses on the manufacturing techniques of profiled laminates. In this section, the failed approach of the chipboard mesh will be shortly discussed. This experiment has tried to answer the following question:

How to manufacture profiled laminates using conventional manufacturing techniques?

Figure B-2 shows chipboard mesh with a perimeter of 20 mm by 20 mm. At that time, this shape of a shear key was believed to have a good interlocking mechanism due to its angularity. Figures B-3 and B-4 illustrate the state of these particular shear keys after demoulding from the chipboard mesh. Unfortunately, this idea failed because the mesh

swallowed the water from fresh SHCC and as a consequence, the mesh expanded and ruined the shear keys.

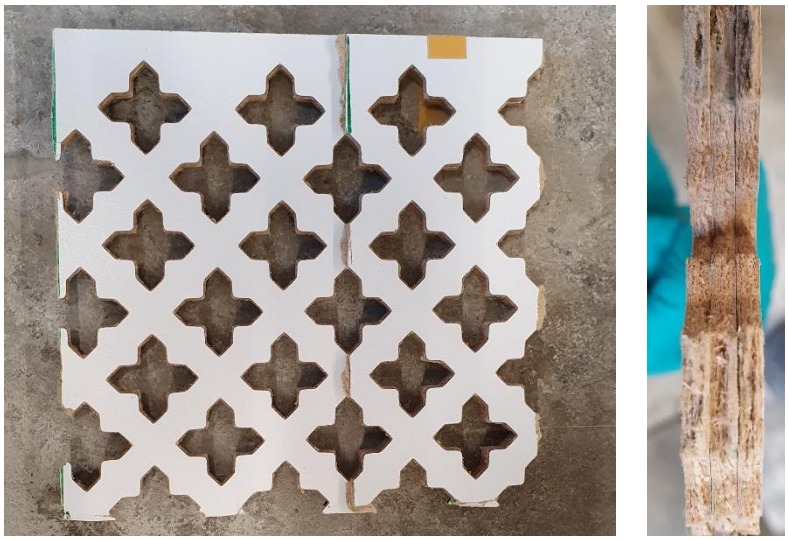

Figure B-2 Chipboard mesh

Figure B-3 Specimen during demoulding

Figure B-4 Specimen after demoulding

Appendix C. Failed specimens & samples

C.1 Normal concrete prism specimens in second series

In the second series, three prism specimens with a dimension of 400 mm × 100 mm × 100 mm have been cast for quality control of Young's modulus. Unfortunately, two specimens have been declared as failed samples due to their poor quality, see the pictures below.

Figure B-1 Three normal concrete prism specimens with a dimension of 400 × 100 × 100 mm³ [the second series].

As can be seen, the specimens in the middle and on the right side show large voids than the specimens on the right. All three specimens have been cast from the same normal concrete batch and were compacted on a vibrating table at the same time. Moulds have been filled with three steps as good engineering practices suggest. Surprisingly, the two prisms did not compact fully. This means that the position of the moulds during vibrating on the vibrating table matters.

Table C-1 The results of elastic modulus of normal concrete prisms (400 × 100 × 100 mm³)

Series nr.	Specimen ID	Young's modulus [MPa]
Second	NC_P4_35 [a)]	34486
	NC_P5_35 [b)]	31726
	NC_P6_35 [b)]	30819

a) The specimen was of good quality.
b) The specimens were of poor quality, see Figure B-1.

The deterioration of Young's modulus was limited to approx. 10% compared to the value obtained from the good quality specimen.

C.2 Possible consequence for the initial stiffness of the beams with transverse reinforcement

Comparing the results of Table 19 and C-1 (NC_P5_35 & NC_P6_35), the elastic modulus of those two NC prisms was approximately three times higher than the initial elastic modulus of the reference beam with TR and the hybrid beam B2. This may indicate that NC in those beams could be more porous than NC_P5_35 and NC_P6_35 specimens since the initial value was lower. This is related to the weaker structural integrity of NC. Even though NEN norms prescribe to use of a vibrating table and/or a concrete vibrator for densifying NC. It would be better to use a concrete vibrator (and a vibrating table) while densifying hybrid or RC beams in the future.

Appendix D. Mechanical performance of SHCC — Detailed information

Table D-1 Shrinkage history of SHCC in the standard environment after being cured for 28 days

		Unit:	[°C]	[%]	[mm]		[mm]	[mm]	[mm]	[mm]	[mm]	[mm]	[με]	[με]	[με]	[με]	[%]
Day	Date	Time	Temp	RH	Reference level	Bar length	28-1	28-2	28-3	Δ28-1	Δ28-2	Δ28-3	ST_p1_28	ST_p2_28	ST_p3_28	ave	COV
0	21/04/2022	08:35	19.4	49	-0.005		-11.034	-11.608	-10.857	11.029	11.603	10.852	0	0	0	0	0
1	22/04/2022	08:00	19.4	49	-0.005		-11.047	-11.619	-10.878	11.042	11.614	10.873	-81.2	-68.7	-131.3	93.7	29%
4	25/04/2022	07:50	19.4	48.8	-0.004		-11.077	-11.648	-10.92	11.073	11.644	10.916	-275.0	-256.3	-400.0	310.4	21%
5	26/04/2022	17:53	19.4	48.9	0.001	-14.541	-11.081	-11.654	-10.927	11.082	11.655	10.928	-331.2	-325.0	-475.0	377.1	18%
7	28/04/2022	13:30	19.4	48.9	0.002		-11.091	-11.665	-10.937	11.093	11.667	10.939	-400.0	-400.0	-543.8	447.9	15%
11	02/05/2022	11:32	19.3	49.1	0.004		-11.108	-11.681	-10.953	11.112	11.685	10.957	-518.8	-512.5	-656.3	562.5	12%
13	04/05/2022	16:26	19.4	48.9	-0.006		-11.129	-11.701	-10.971	11.123	11.695	10.965	-587.5	-575.0	-706.3	622.9	9%
15	06/05/2022	08:09	19.7	49.2	-0.004		-11.133	-11.706	-10.978	11.129	11.702	10.974	-625.0	-618.8	-762.5	668.8	10%
18	09/05/2022	08:15	19.5	47.9	-0.005	-14.554	-11.143	-11.715	-10.985	11.138	11.71	10.98	-681.3	-668.7	-800.0	716.7	8%
20	11/05/2022	08:08	19.4	52.1	0.005	-14.572	-11.137	-11.710	-10.980	11.142	11.715	10.985	-706.3	-700.0	-831.3	745.8	8%
22	13/05/2022	07:59	19.4	51.9	-0.002	-14.579	-11.152	-11.723	-10.993	11.150	11.721	10.991	-756.2	-737.5	-868.8	787.5	7%
25	16/05/2022	08:04	19.4	51.4	0.004	-14.632	-11.152	-11.725	-10.992	11.156	11.729	10.996	-793.7	-787.5	-900.0	827.1	6%
26	17/05/2022	07:59	19.4	53.4	0.004	-14.633	-11.154	-11.726	-10.993	11.158	11.73	10.997	-806.2	-793.8	-906.3	835.4	6%
27	18/05/2022	08:02	19.4	53.6	0.003	-14.633	-11.154	-11.728	-10.994	11.157	11.731	10.997	-800.0	-800.0	-906.3	835.4	6%
28	19/05/2022	08:00	19.4	53.4	0.005	-14.633	-11.155	-11.729	-10.996	11.160	11.734	11.001	-818.8	-818.8	-931.3	856.3	6%
32	23/05/2022	08:50	19.4	52.8	0.000	-14.636	-11.168	-11.739	-11.005	11.168	11.739	11.005	-868.7	-850.0	-956.3	891.7	5%
33	24/05/2022	10:03	19.4	53.3	0.001	-14.639	-11.172	-11.741	-11.007	11.173	11.742	11.008	-900.0	-868.7	-975.0	914.6	5%
39	30/05/2022	08:00	19.2	50.4	-0.003	-14.655	-11.182	-11.750	-11.018	11.179	11.747	11.015	-937.5	-900.0	-1018.8	952.1	5%
40	31/05/2022	08:20	19.4	48.4	-0.003	-14.654	-11.185	-11.753	-11.021	11.182	11.75	11.018	-956.3	-918.8	-1037.5	970.8	5%
41	01/06/2022	09:18	19.4	49.2	-0.004	-14.655	-11.187	-11.756	-11.023	11.183	11.752	11.019	-962.5	-931.3	-1043.8	979.2	5%
42	02/06/2022	08:11	19.4	50.6	-0.005	-14.655	-11.188	-11.756	-11.024	11.183	11.751	11.019	-962.5	-925.0	-1043.8	977.1	5%
43	03/06/2022	09:24	19.4	50.5	-0.004	-14.656	-11.189	-11.758	-11.025	11.185	11.754	11.021	-975.0	-943.7	-1056.3	991.7	5%
47	07/06/2022	17:44	19.3	53.2	-0.001	-14.658	-11.187	-11.755	-11.023	11.186	11.754	11.022	-981.3	-943.8	-1062.5	995.8	5%
48	08/06/2022	15:59	19.3	53.1	0.000	-14.660	-11.187	-11.755	-11.021	11.187	11.755	11.021	-987.5	-950.0	-1056.3	997.9	4%
49	09/06/2022	12:29	19.4	53.7	0.001	-14.659	-11.189	-11.756	-11.023	11.190	11.757	11.024	-1006.3	-962.5	-1075.0	1014.6	5%
53	13/06/2022	15:12	19.4	53.3	0.002	-14.690	-11.190	-11.757	-11.024	11.192	11.759	11.026	-1018.8	-975.0	-1087.5	1027.1	5%
64	24/06/2022	10:31	19.4	53.4	-0.003	-14.683	-11.196	-11.764	-11.03	11.193	11.761	11.027	-1025.0	-987.5	-1093.8	1035.4	4%
68	28/06/2022	13:33	19.4	52.7	-0.004	-14.693	-11.198	-11.766	-11.033	11.194	11.762	11.029	-1031.3	-993.8	-1106.3	1043.8	4%
70	30/06/2022	08:41	19.4	52.9	-0.001	-14.692	-11.198	-11.765	-11.032	11.197	11.764	11.031	-1050.0	-1006.3	-1118.8	1058.3	4%
74	04/07/2022	14:27	19.5	53.9	0.001	-14.690	-11.199	-11.765	-11.032	11.200	11.766	11.033	-1068.8	-1018.8	-1131.3	1072.9	4%
81	11/07/2022	09:00	19.4	53.5	-0.004	-14.693	-11.206	-11.772	-11.038	11.202	11.768	11.034	-1081.3	-1031.3	-1137.5	1083.3	4%

Table D-2 Shrinkage history of SHCC in the standard environment after being cured for 14 days and then sealed for 28 days.

		Unit:	[°C]	[%]	[mm]	[mm]	[mm]	[mm]	[mm]	[mm]	[mm]	[mm]	[με]	[με]	[με]	[με]	[%]
Day	Date	Time	Temp	RH	Reference level	Bar	14-1	14-2	14-3	Δ14-1	Δ14-2	Δ14-3	ST_p1_42	ST_p2_42	ST_p3_42	ave	COV
0	06/05/2022	08:09	19.7	49.2	-0.004		-10.924	-10.902	-11.048	10.920	10.898	11.044	0.0	0.0	0.0	0.0	0.0
3	09/05/2022	08:15	19.5	47.9	-0.005	-14.554	-10.977	-10.940	-11.073	10.972	10.935	11.068	-325.0	-231.2	-150.0	235.4	30%
5	11/05/2022	08:08	19.4	52.1	0.005	-14.572	-10.980	-10.940	-11.073	10.985	10.945	11.078	-406.3	-293.8	-212.5	304.2	26%
7	13/05/2022	07:59	19.4	51.9	-0.002	-14.579	-10.999	-10.955	-11.091	10.997	10.953	11.089	-481.3	-343.7	-281.2	368.7	23%
10	16/05/2022	08:04	19.4	51.4	0.004	-14.632	-11.005	-10.961	-11.098	11.009	10.965	11.102	-556.3	-418.8	-362.5	445.8	18%
11	17/05/2022	07:59	19.4	53.4	0.004	-14.633	-11.008	-10.962	-11.099	11.012	10.966	11.103	-575.0	-425.0	-368.7	456.2	19%
12	18/05/2022	08:02	19.4	53.6	0.003	-14.633	-11.012	-10.967	-11.103	11.015	10.970	11.106	-593.8	-450.0	-387.5	477.1	18%
13	19/05/2022	08:00	19.4	53.4	0.005	-14.633	-11.021	-10.970	-11.105	11.026	10.975	11.110	-662.5	-481.3	-412.5	518.8	20%
17	23/05/2022	08:50	19.4	52.8	0.000	-14.636	-11.036	-10.984	-11.120	11.036	10.984	11.120	-725.0	-537.5	-475.0	579.2	18%
18	24/05/2022	10:03	19.4	53.3	0.001	-14.639	-11.038	-10.987	-11.122	11.039	10.988	11.123	-743.7	-562.5	-493.7	600.0	18%
24	30/05/2022	08:00	19.2	50.4	-0.003	-14.655	-11.053	-11.000	-11.135	11.050	10.997	11.132	-812.5	-618.8	-550.0	660.4	17%
25	31/05/2022	08:20	19.4	48.4	-0.003	-14.654	-11.056	-11.003	-11.139	11.053	11.000	11.136	-831.2	-637.5	-575.0	681.2	16%
26	01/06/2022	09:18	19.4	49.2	-0.004	-14.655	-11.059	-11.005	-11.141	11.055	11.001	11.137	-843.7	-643.8	-581.3	689.6	16%
27	02/06/2022	08:11	19.4	50.6	-0.005	-14.655	-11.061	-11.007	-11.143	11.056	11.002	11.138	-850.0	-650.0	-587.5	695.8	16%
28	03/06/2022	09:24	19.4	50.5	-0.004	-14.656	-11.061	-11.008	-11.144	11.057	11.004	11.140	-856.3	-662.5	-600.0	706.3	15%
32	07/06/2022	17:44	19.3	53.2	-0.001	-14.658	-11.062	-11.007	-11.145	11.061	11.006	11.144	-881.3	-675.0	-625.0	727.1	15%
33	08/06/2022	15:59	19.3	53.1	0.000	-14.660	-11.061	-11.007	-11.144	11.061	11.007	11.144	-881.3	-681.3	-625.0	729.2	15%
34	09/06/2022	12:29	19.4	53.7	0.001	-14.659	-11.065	-11.009	-11.146	11.066	11.010	11.147	-912.5	-700.0	-643.7	752.1	15%
38	13/06/2022	15:12	19.4	53.3	0.002	-14.690	-11.067	-11.012	-11.151	11.069	11.014	11.153	-931.3	-725.0	-681.3	779.2	14%
49	24/06/2022	10:31	19.4	53.4	0.005	-14.683	-11.064	-11.012	-11.150	11.069	11.017	11.155	-931.3	-743.8	-693.8	789.6	13%
53	28/06/2022	13:33	19.4	52.7	-0.004	-14.693	-11.074	-11.021	-11.160	11.070	11.017	11.156	-937.5	-743.8	-700.0	793.8	13%
55	30/06/2022	08:41	19.4	52.9	-0.001	-14.692	-11.074	-11.020	-11.160	11.073	11.019	11.159	-956.3	-756.3	-718.8	810.4	13%
59	04/07/2022	14:27	19.5	53.9	0.001	-14.690	-11.075	-11.021	-11.161	11.076	11.022	11.162	-975.0	-775.0	-737.5	829.2	13%
66	11/07/2022	09:00	19.4	53.5	-0.004	-14.693	-11.082	-11.030	-11.167	11.078	11.026	11.163	-987.5	-800.0	-743.7	843.8	12%

Table D-3 The results of compressive test on SHCC cubes (40 × 40 × 40 mm³)

Series nr.	Specimen ID	Compressive strength [MPa]	Average compressive strength [MPa]	Standard deviation [MPa]
First	Sm_c1_14+0	54,188	56,995	± 1,985
	Sm_c2_14+0	58,396		
	Sm_c3_14+0	58,400		
	K1_c1_14+0	57,172	56,469	± 3,617
	K1_c2_14+0	51,729		
	K1_c3_14+0	60,505		
	K2_c1_14+0	63,128	56,711	± 4,579
	K2_c2_14+0	54,239		
	K2_c3_14+0	52,767		
	Sm_c1_28+0	67,720	66,625	± 1,942
	Sm_c2_28+0	67,497		
	Sm_c3_28+0	64,659		
	K1_c1_28+0	64,148	70,016	± 4,433
	K1_c2_28+0	71,039		
	K1_c3_28+0	74,862		
	K2_c1_28+0	63,166	64,03	± 1,899
	K2_c2_28+0	62,260		
	K2_c3_28+0	66,664		
	Sm_c1_14+28	70,491	68,957	± 2,437
	Sm_c2_14+28	65,518		
	Sm_c3_14+28	70,863		
	K1_c1_14+28	65,302	66,269	± 2,827
	K1_c2_14+28	63,393		
	K1_c3_14+28	70,111		
	K2_c1_14+28	61,777	64,118	± 2,082
	K2_c2_14+28	63,741		
	K2_c3_14+28	66,836		
Second	B1_c1_14+0	73,590	70,739	± 2,258
	B1_c2_14+0	70,558		
	B1_c3_14+0	68,069		
	B2_c1_14+0	58,483	66,172	± 5,840
	B2_c2_14+0	67,404		
	B2_c3_14+0	72,628		
	B1_c1_28+0	67,169	70,546	± 2,956
	B1_c2_28+0	74,369		
	B1_c3_28+0	70,100		
	B2_c1_28+0	66,296	70,153	± 3,960
	B2_c2_28+0	75,599		
	B2_c3_28+0	68,566		
	B1_c1_21+35	72,107	69,764	± 4,737
	B1_c2_21+35	74,028		
	B1_c3_21+35	63,158		
	B2_c1_21+35	77,143	75,376	± 1,972
	B2_c2_21+35	76,361		
	B2_c3_21+35	72,623		

Table D-4 The results of compressive test on SHCC cubes (40 × 40 × 40 mm³)

Series nr.	Specimen ID	Compressive strength [MPa]	Average compressive strength [MPa]	Standard deviation [MPa]
Not applicable	ST_c1_7	54,814	53,284	± 1,152
	ST_c2_7	53,003		
	ST_c3_7	52,035		
	ST_c1_14+28	77,265	72,795	± 3,361
	ST_c2_14+28	71,959		
	ST_c3_14+28	69,161		

NOTE: 'ST' stands for Shrinkage Test.

Table D-5 The results of compressive test on SHCC cubes (150 × 150 × 150 mm³)

Series nr. // beam	Specimen ID	Compressive strength [MPa]	Average compressive strength [MPa]	Standard deviation [MPa]
Second // Hybrid beam B1	SF_C1_28	69,33	68,37	± 0,70
	SF_C2_28	67,69		
	SF_C3_28	68,10		
	SF_C1_21+35	64,21	68,14	± 3,05
	SF_C2_21+35	68,56		
	SF_C3_21+35	71,64		

NOTE: 'SF' stands for Scale Factor.

Appendix E. Structural performance of (hybrid) beams — Detailed information

Beams from 1st series

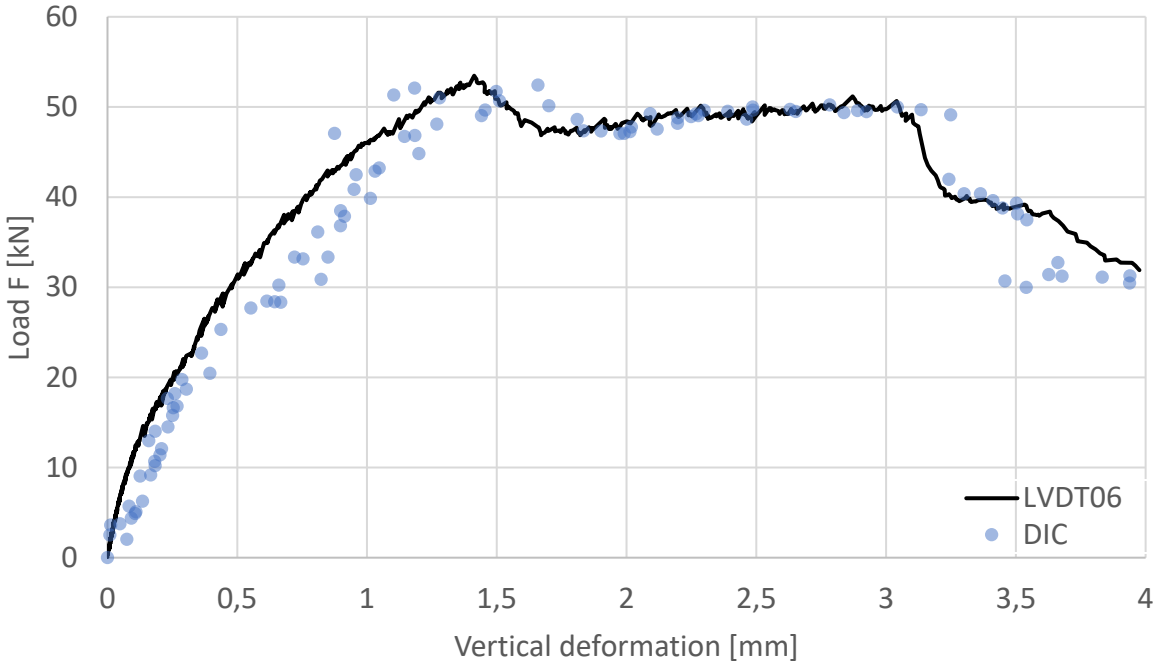

Figure E-1: Load F versus vertical deformation of the reference beam without shear reinforcement at midspan

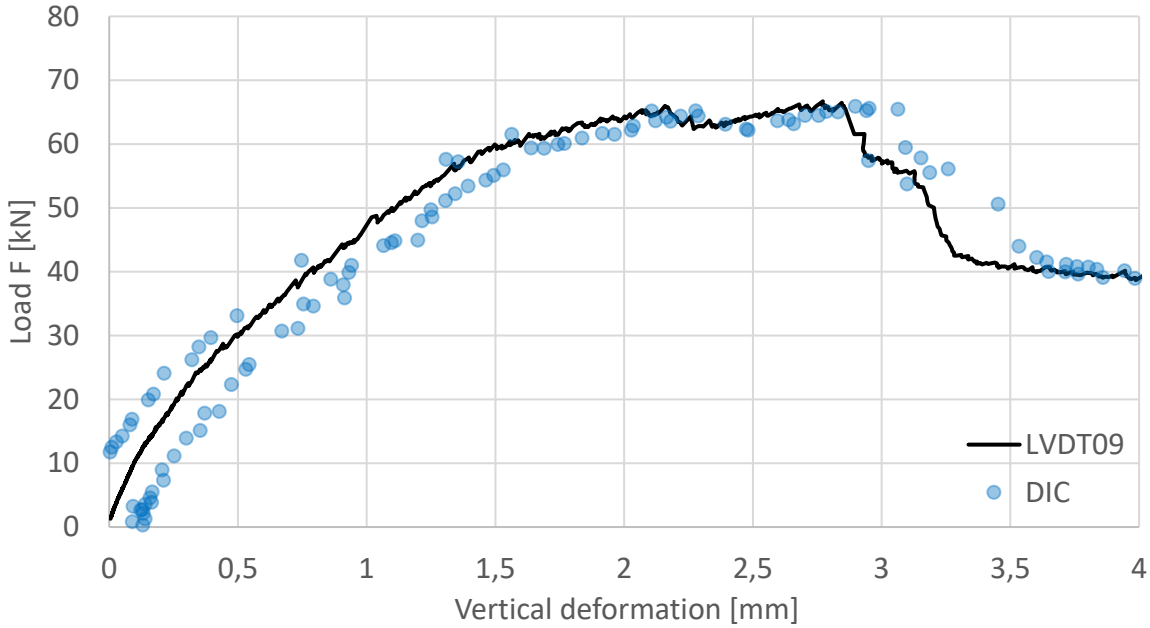

Figure E-2: Load F versus vertical deformation of the beam with smooth laminates without shear reinforcement at midspan.

Please note that DIC has problems capturing sharp changes in the graph. This issue could be fixed by increasing frequency of taking photos during testing, but then pre-processing would take more time and effort.

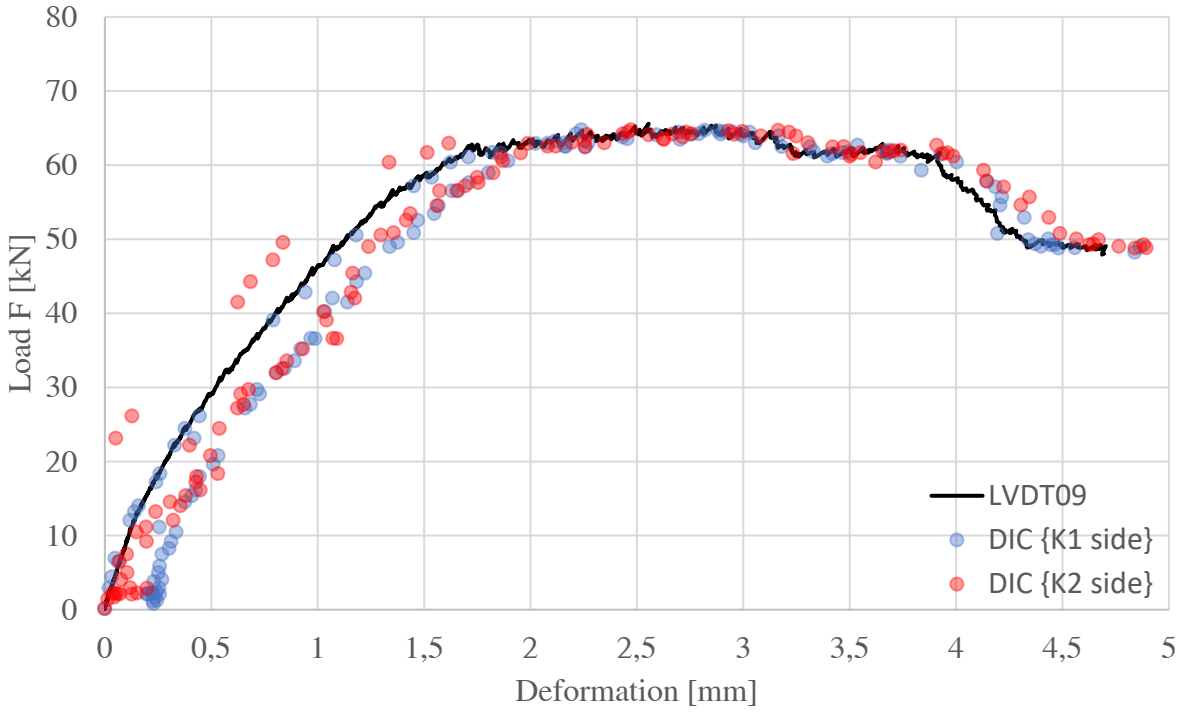

Figure E-3: Load F versus vertical deformation of the beam with shear keys laminates without shear reinforcement at midspan.

Beams from 2nd series

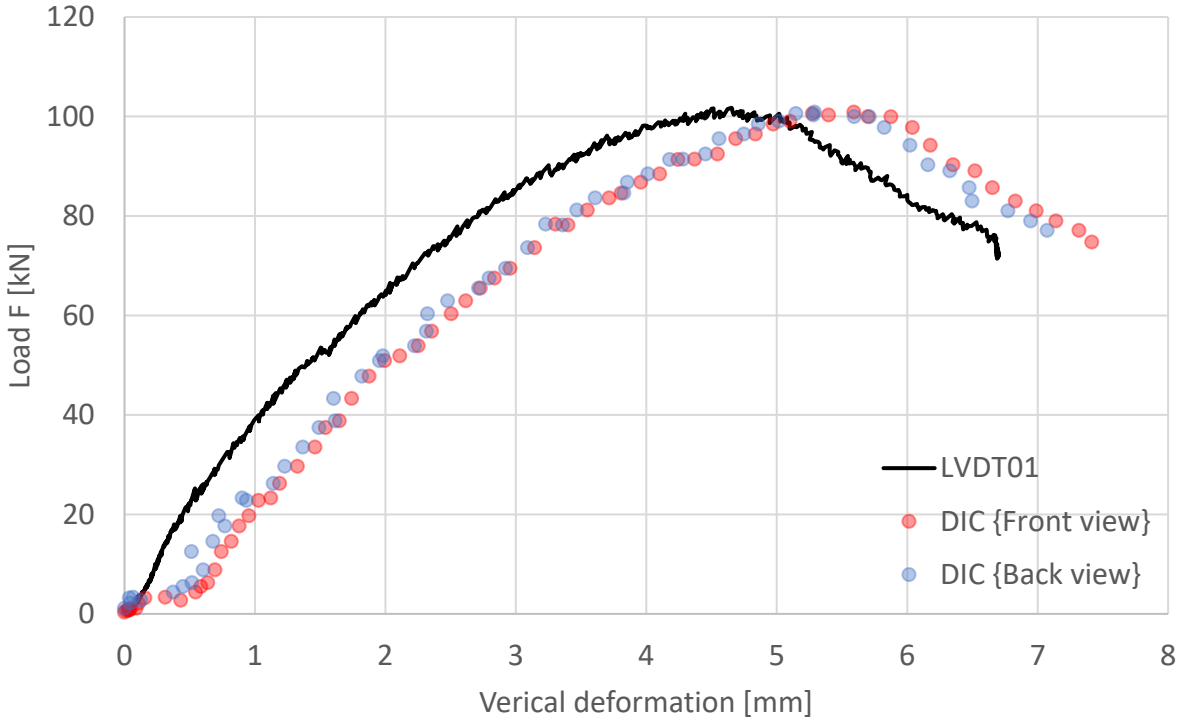

Figure E-4: Load F versus vertical deformation of the reference beam with shear reinforcement at midspan.

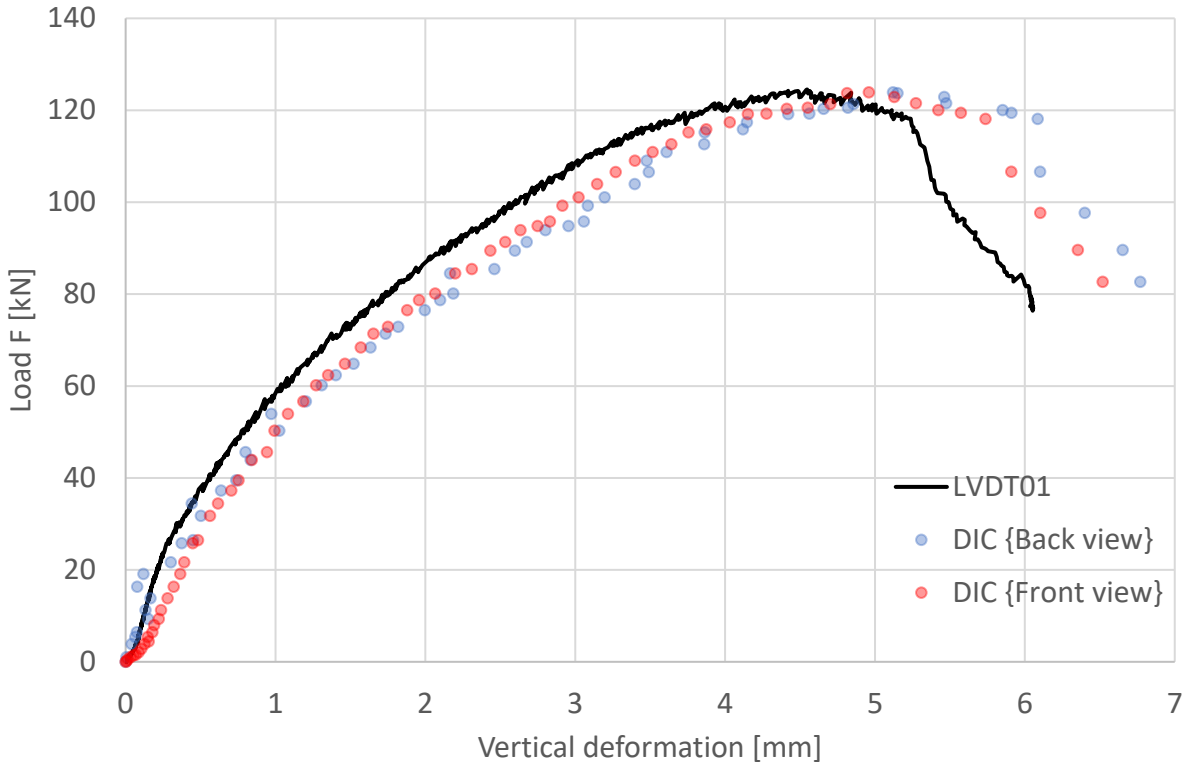

Figure E-5: Load F versus vertical deformation of the hybrid beam B1 with shear reinforcement at midspan.

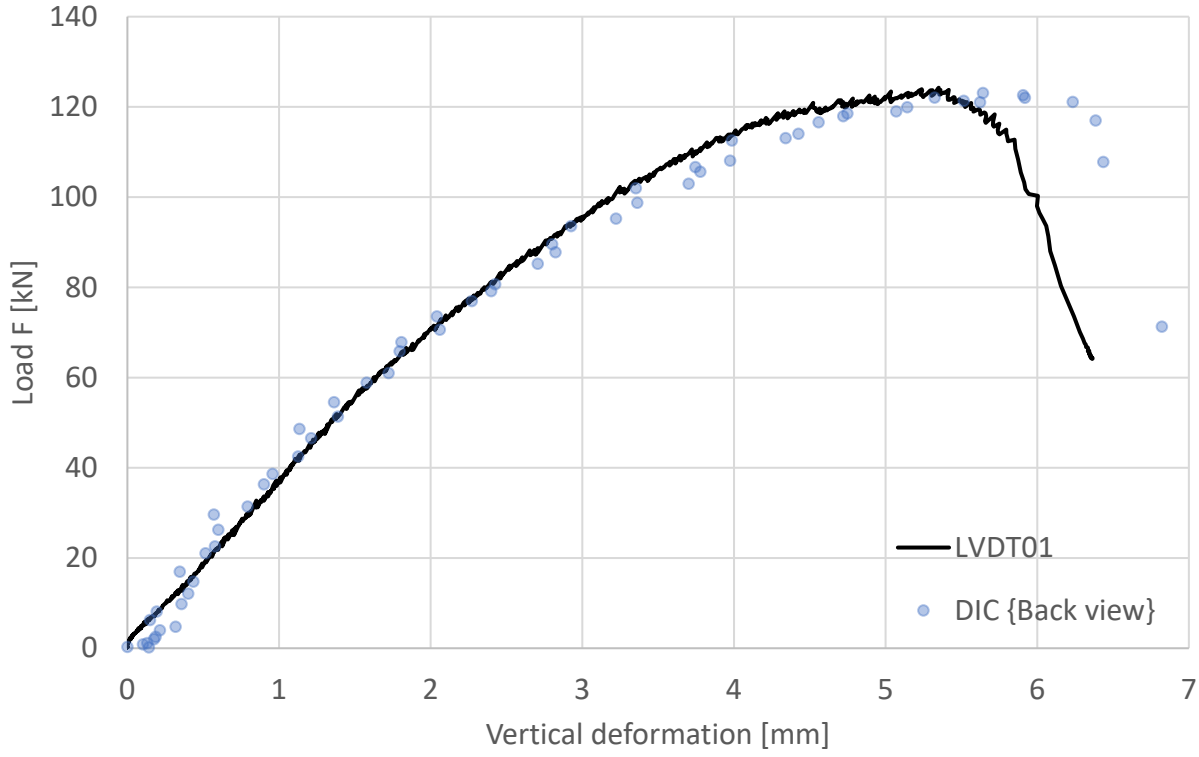

Figure E-6: Load F versus vertical deformation of the hybrid beam B2 with shear reinforcement at midspan.

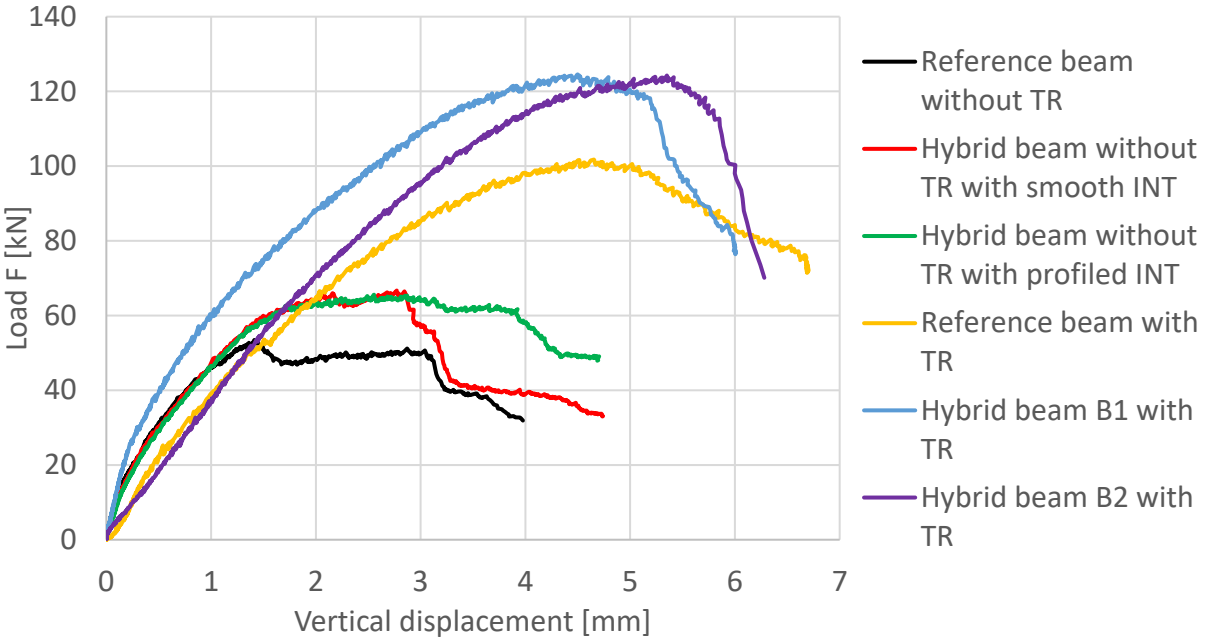

Figure E-7: Load F versus vertical deformation of all beam specimens. The "INT" abbreviation stands for the word: interface. The "TR" abbreviation stands for transverse reinforcement.

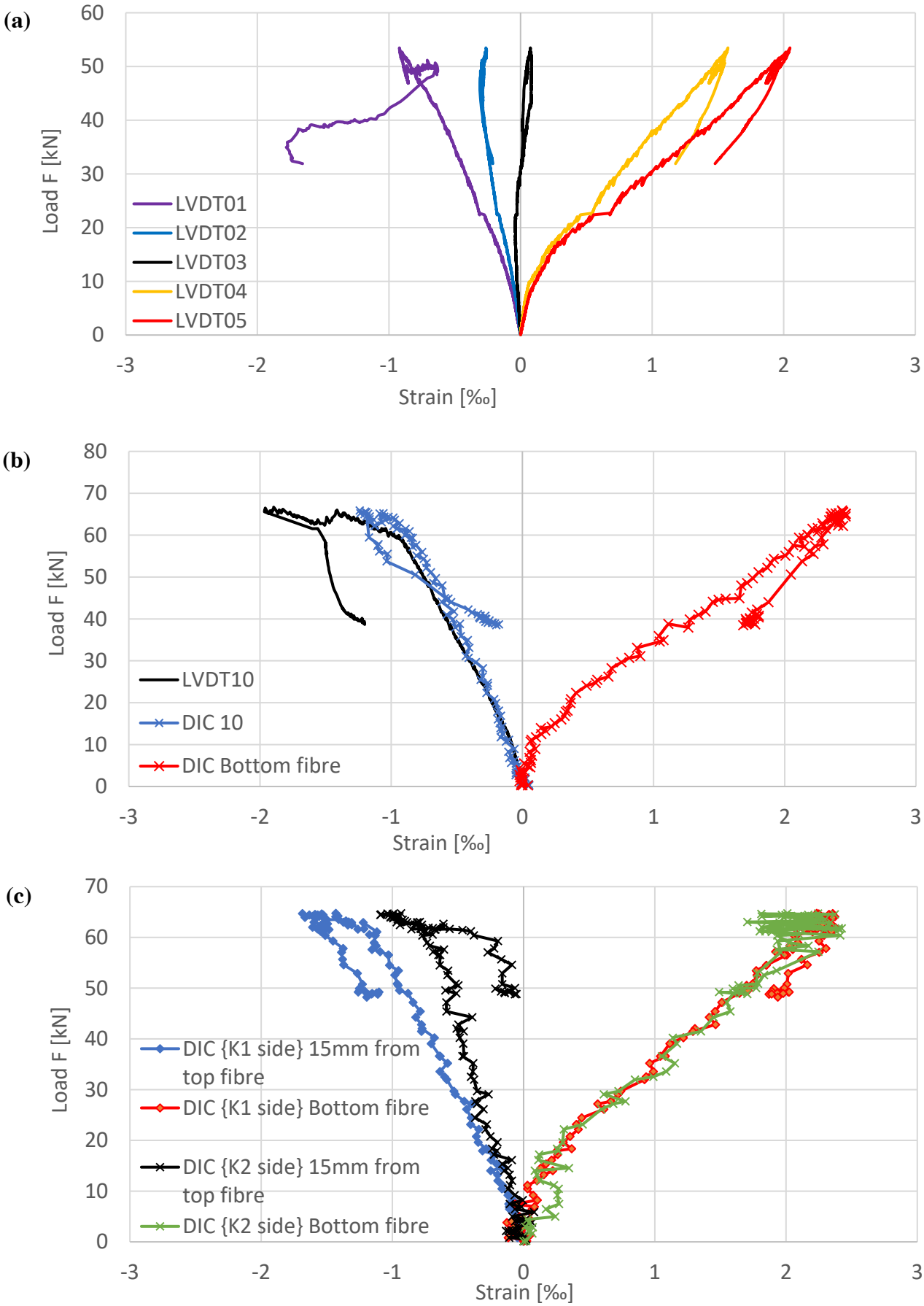

Figure E-8 Load F versus horizontal strains of fibres at various heights. Beams are without transverse reinforcement: (a) Reference beam; (b) Hybrid beam with smooth laminates;

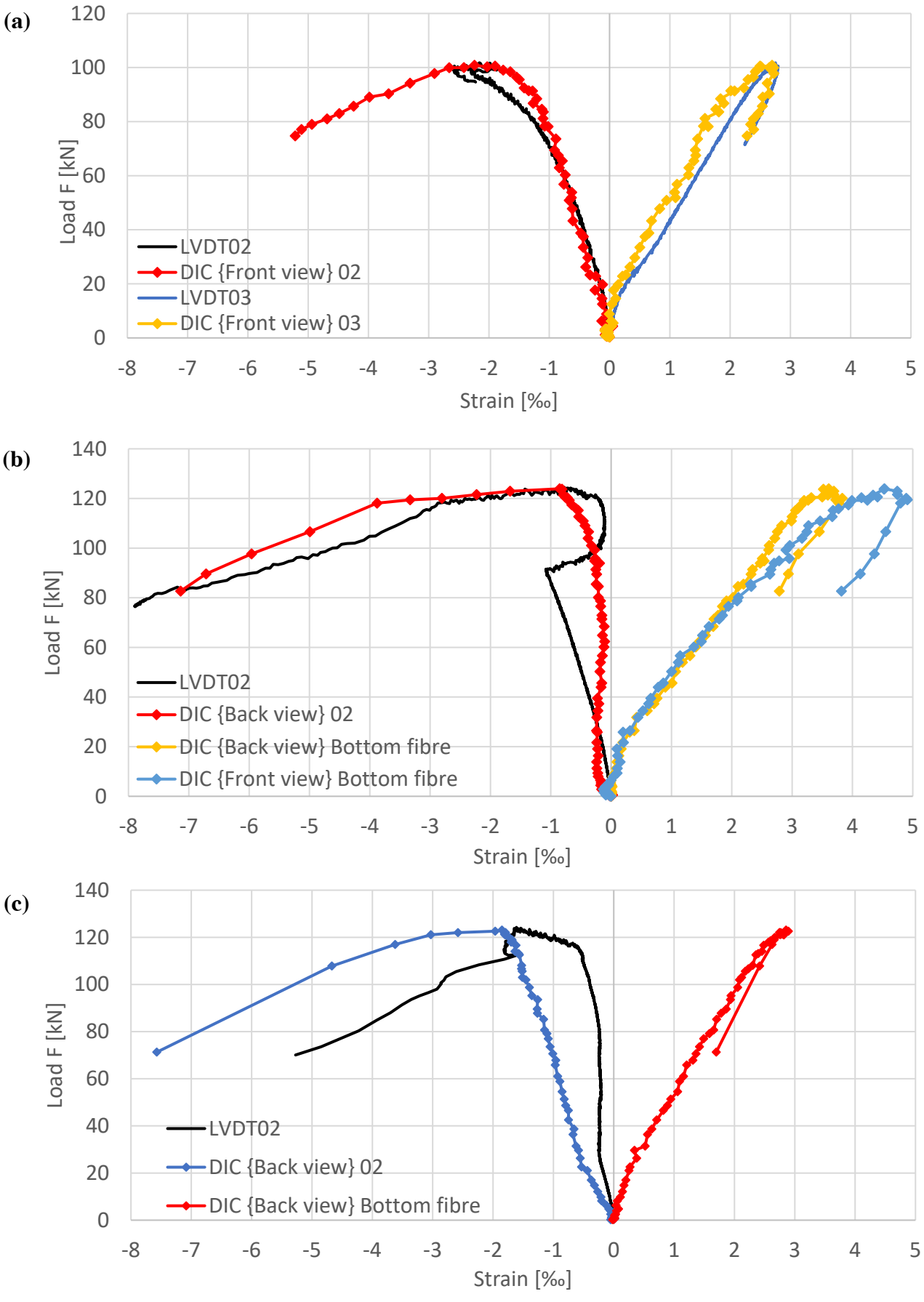

Figure E-9 Load F versus horizontal strains of fibres at various heights. Beams are with transverse reinforcement: (a) Reference beam; (b) Hybrid beam B1; (c) Hybrid beam B2.

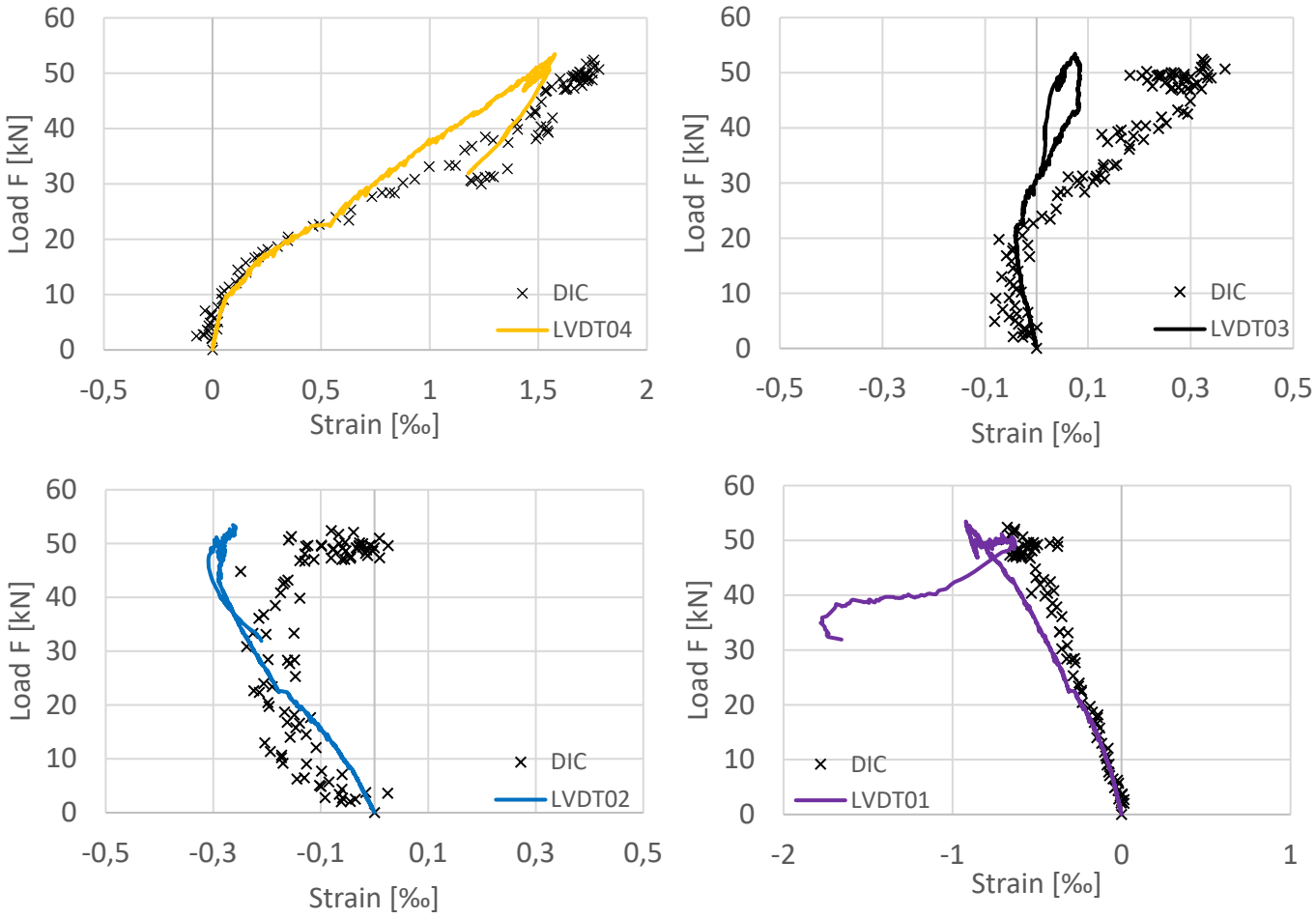

Figure E-10 Comparison of horizontal strain between DIC and LVDTs of reference beam without transverse reinforcement.

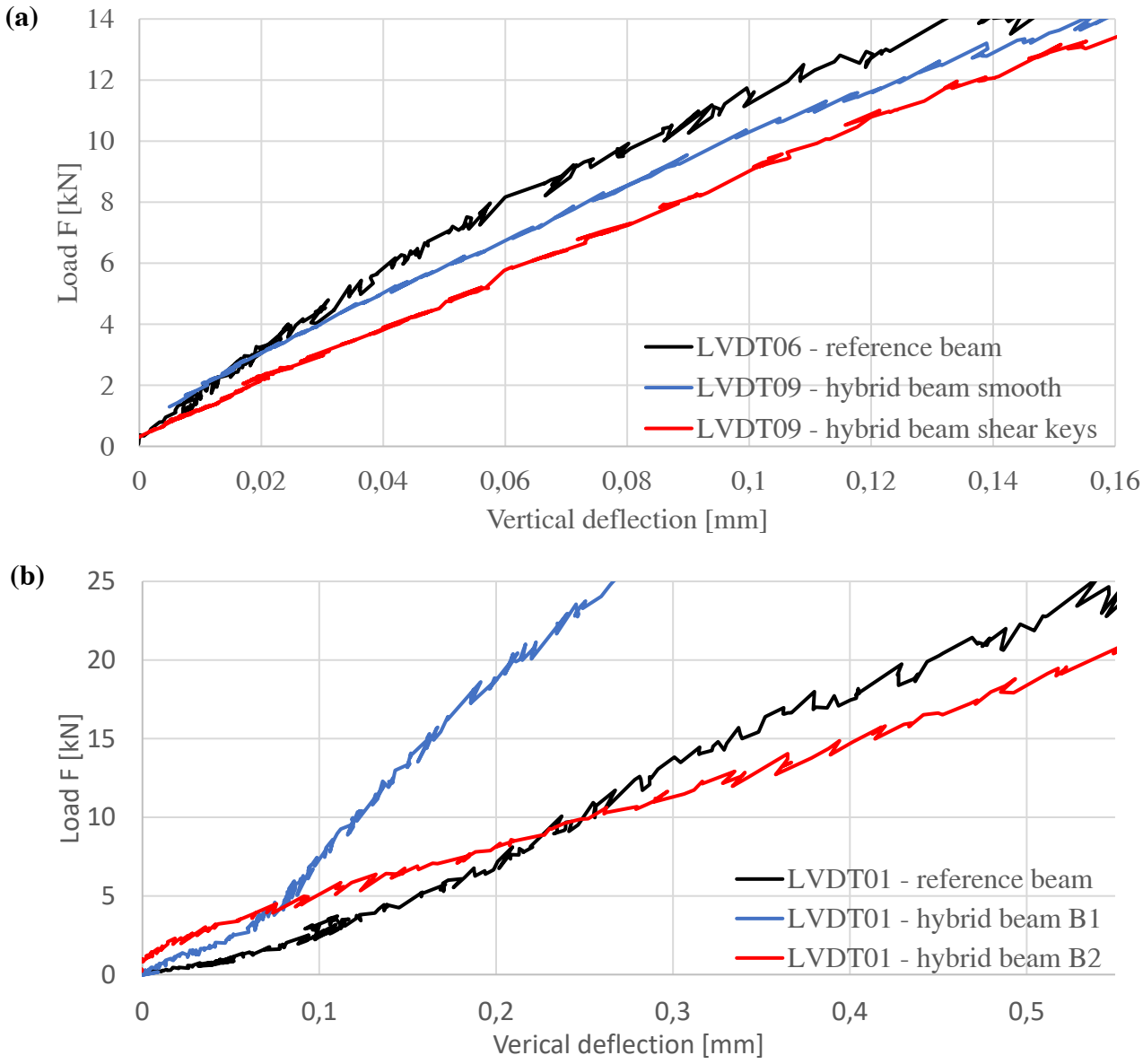

Figure E-11 Load F versus vertical deformations of beams (a) with transverse reinforcement and (b) without transverse reinforcement.

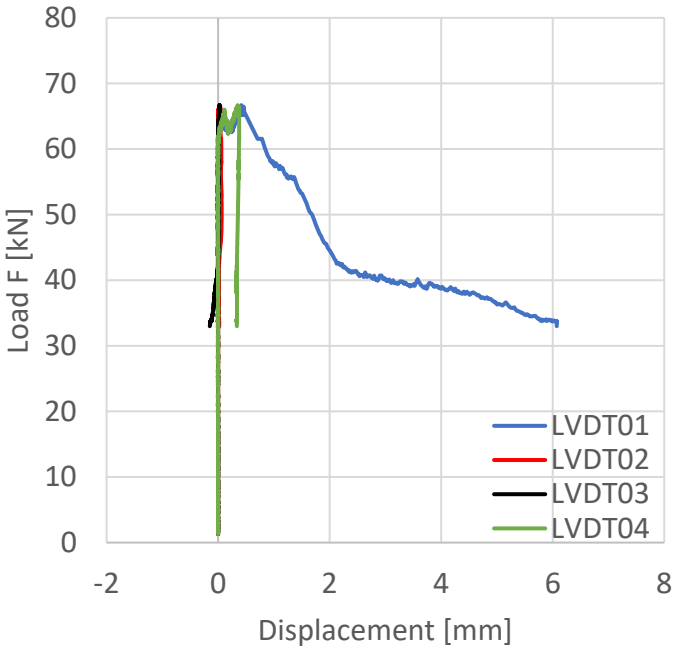

Figure E-12 Vertical displacement of laminates relative to vertical displacement of normal concrete.

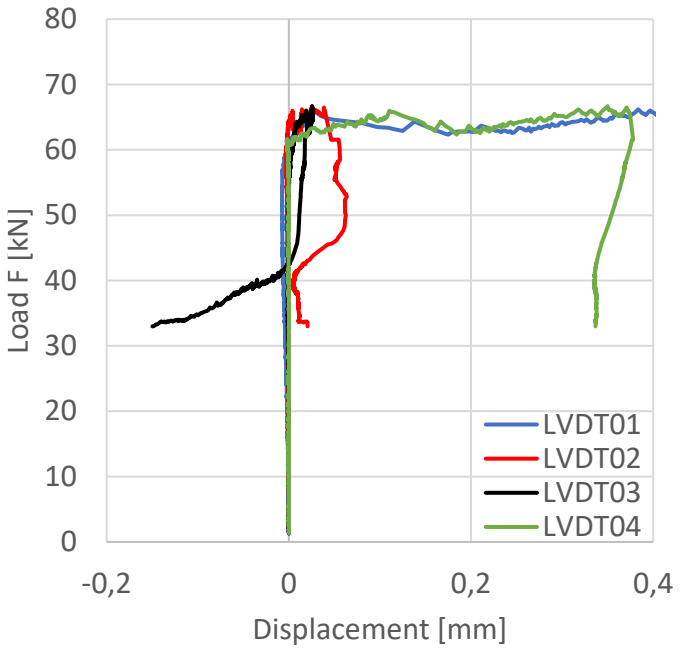

Figure E-13 Close-up: vertical displacement of laminates relative to vertical displacement of normal concrete.

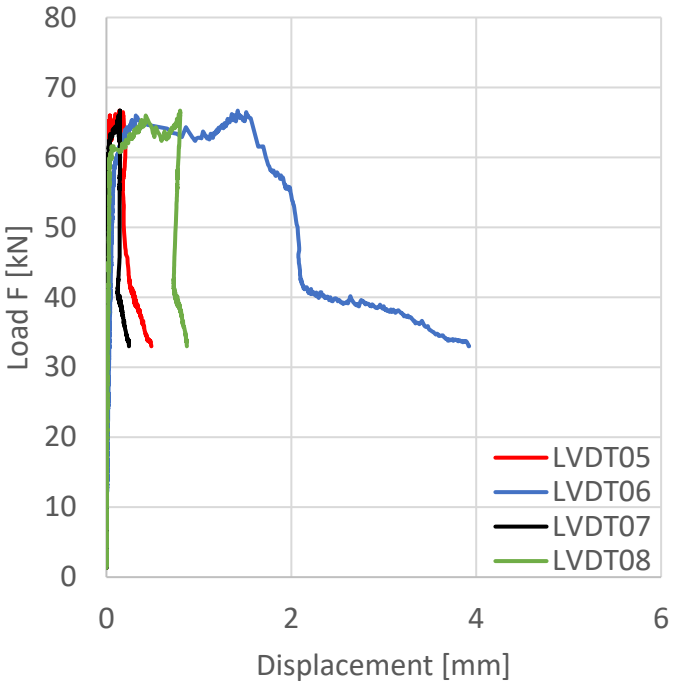

Figure E-14 Horizontal displacement of laminate relative to horizontal displacement of normal concrete.

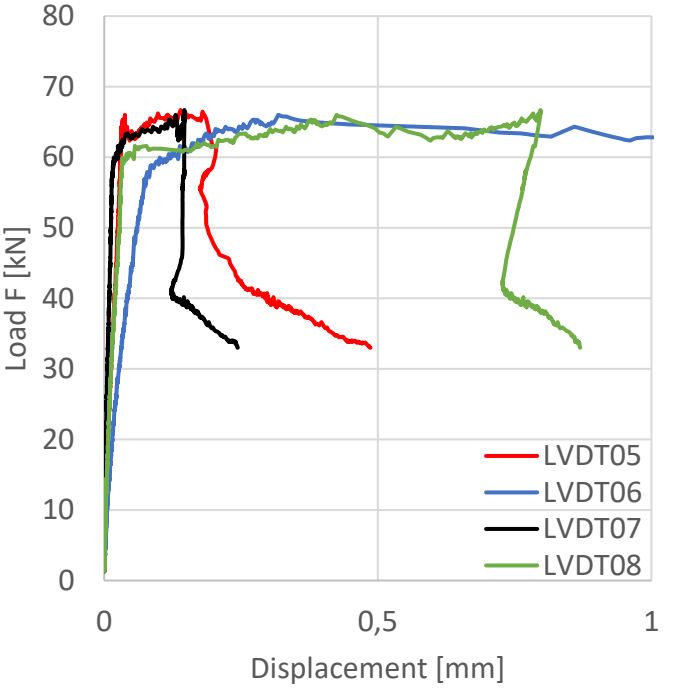

Figure E-15 Close-up: Horizontal displacement of laminate relative to horizontal displacement of normal concrete.

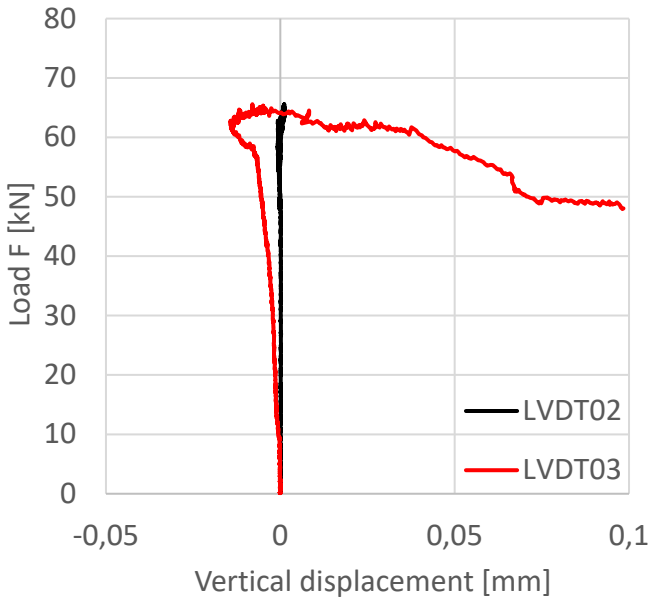

Figure E-16 Vertical displacement of K1 laminate relative to normal concrete.

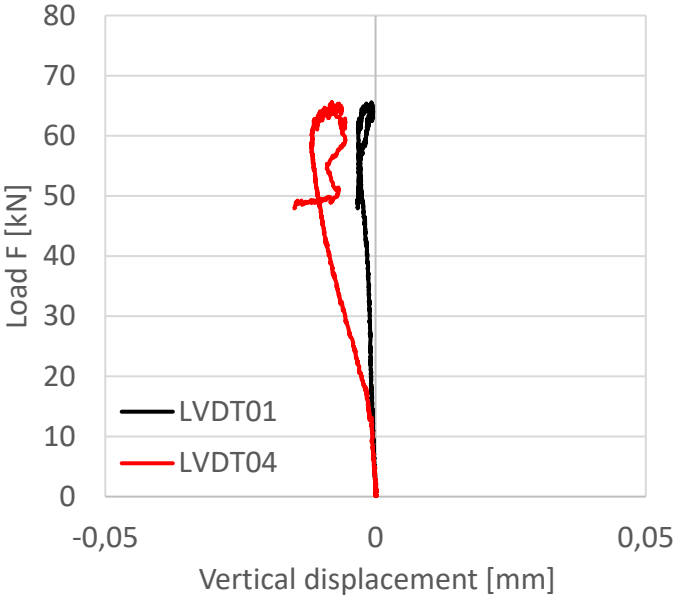

Figure E-17 Vertical displacement of K2 laminate relative to normal concrete.

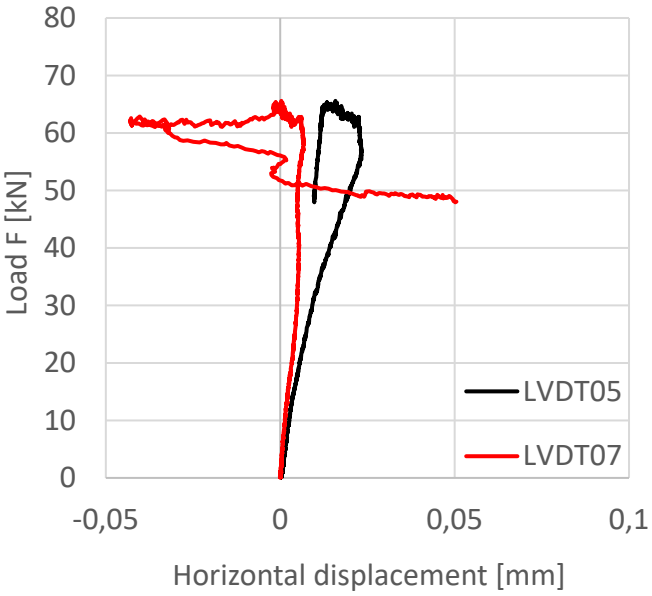

Figure E-18 Horizontal displacement of K1 laminate relative to normal concrete.

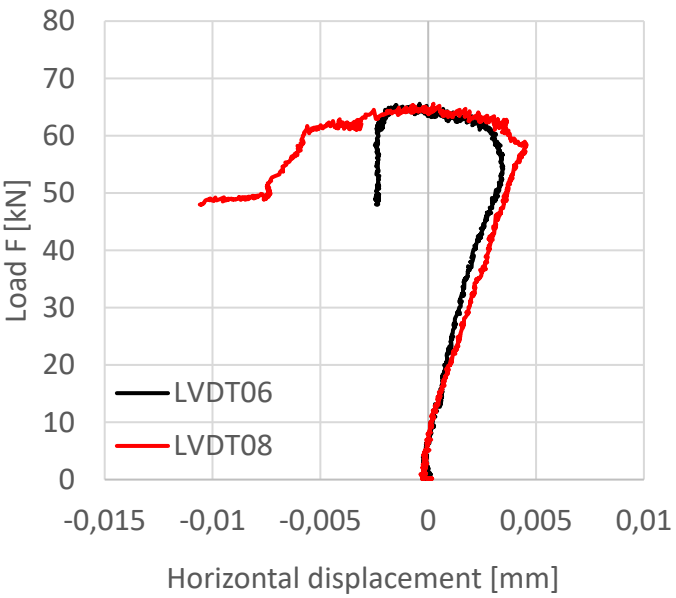

Figure E-19 Horizontal displacement of K2 laminate relative to normal concrete.

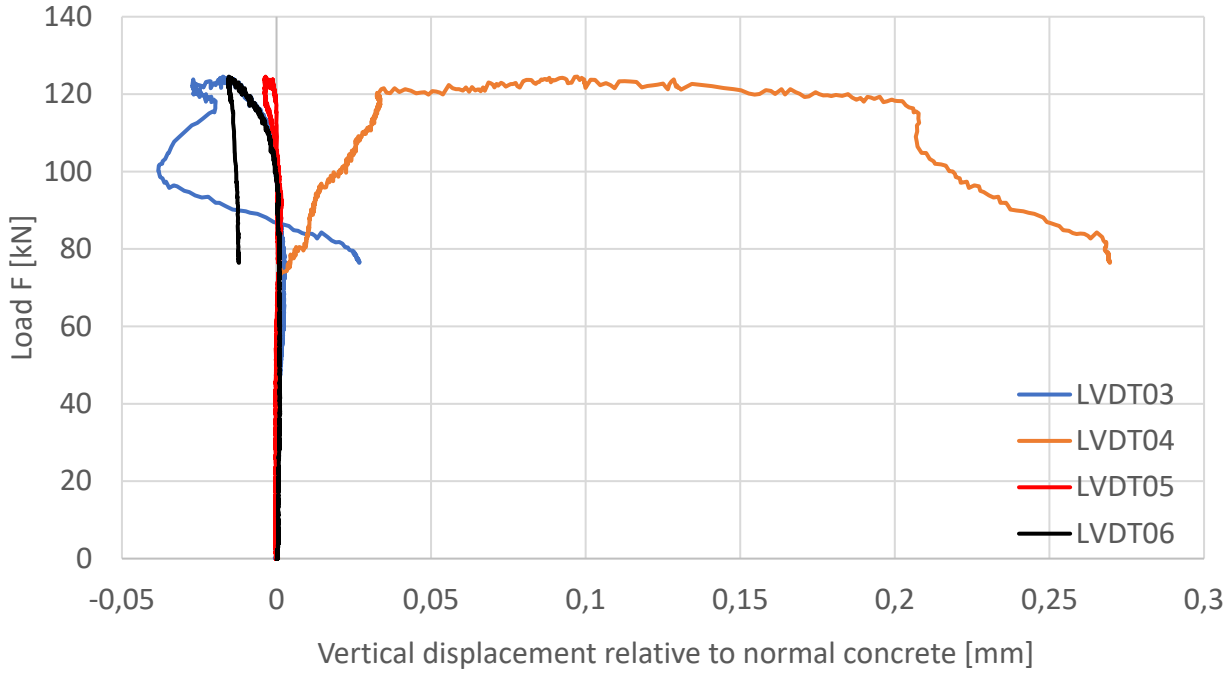

Figure E-20 Vertical displacement of laminates relative to vertical displacement of normal concrete in hybrid beam B1.

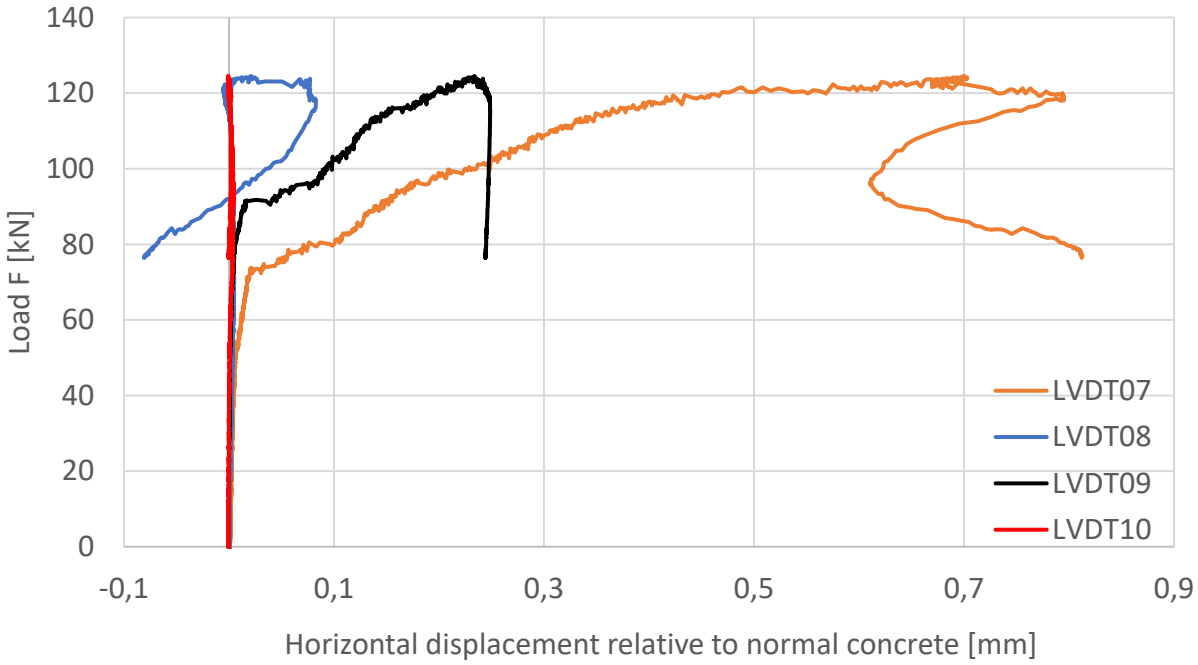

Figure E-21 Horizontal displacement of laminates relative to vertical displacement of normal concrete in hybrid beam B1.

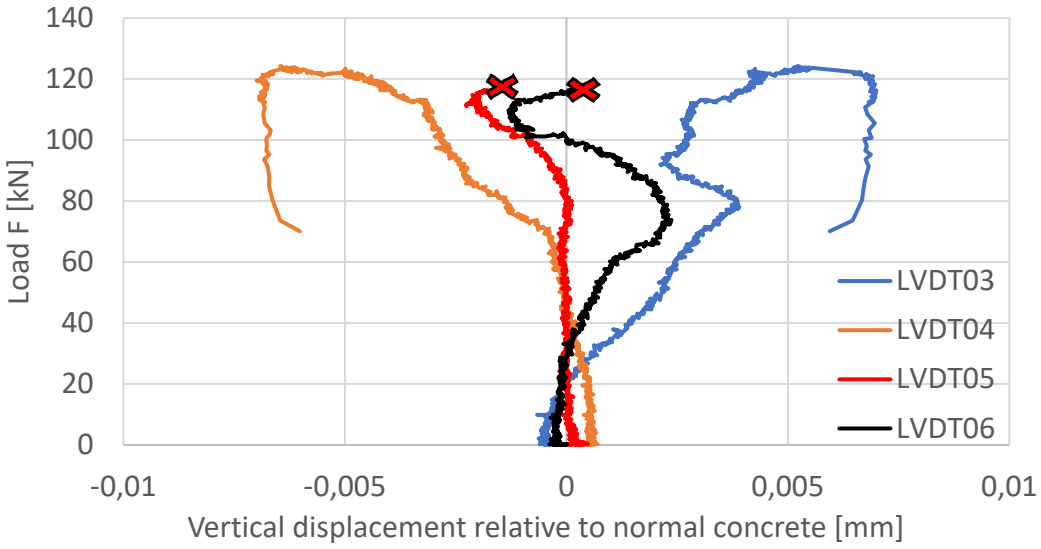

Figure E-22 Vertical displacement of laminates relative to vertical displacement of normal concrete in hybrid beam B2. The red crosses represent the moment beyond which measurement errors occurred. These faulty points have been removed.

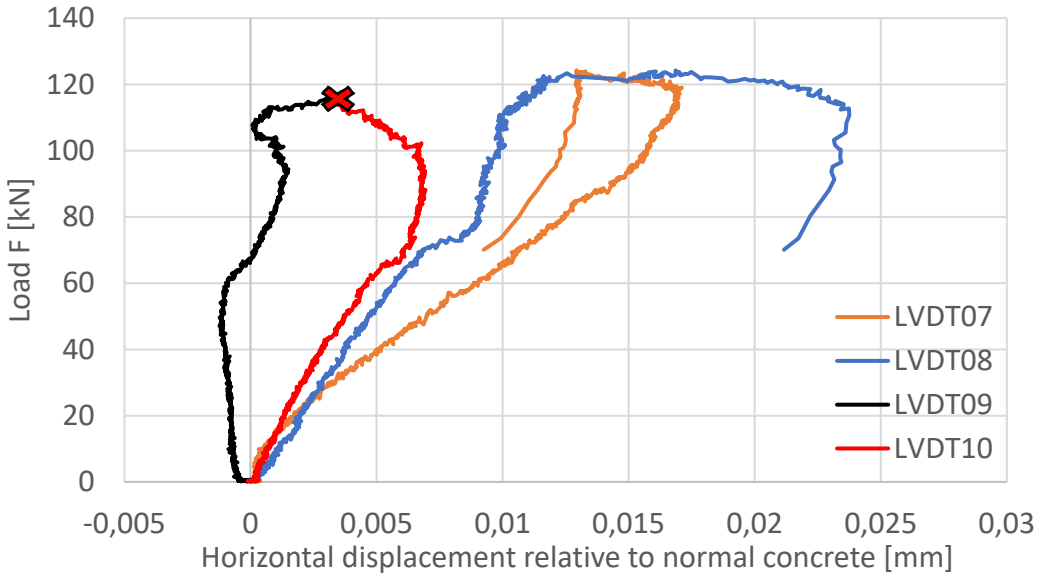

Figure E-23 Horizontal displacement of laminates relative to vertical displacement of normal concrete in hybrid beam B2. The red crosses represent the moment beyond which measurement errors occurred. These faulty points have been removed.

Appendix F. Maple script for solving non-limit state

Reference beam at 50kN (This study)

```
> restart;
> M := 12.5·10^6 : d := 167 : b := 120 : a0 := 31 : A_s := 402.12 : E_s := 200·10^3 : E_c := 33031 : f_c := 29.07 : A_sc := 226.19 :
  E_sc := 200·10^3 : epsilon_cu := 3.5/1000 :
```

The basic geometrical relationships in the cross-section:

```
> x_n := epsilon_c/(epsilon_c + epsilon_s)·d : epsilon_sc := (d − a0)/d·epsilon_c − a0/d·epsilon_s :
```

The constitutive equations:

```
> f_s := E_s·epsilon_s : f_sc := E_sc·epsilon_sc :
```

Concrete strain level I:

```
> Xi_1 := 0.015 : Xi_2 := 1.382 : eta_1 := 0.665 : eta_2 := 0.117 :
```

Model by J. Han et al. [64] :

```
> Gamma_1 := Xi_1 + Xi_2·epsilon_c/epsilon_cu : Beta_1 := eta_1 + eta_2·epsilon_c/epsilon_cu :
> eq1 := Gamma_1·f_c·b·x_n + f_sc·A_sc = f_s·A_s :
> eq2 := M = f_s·A_s·(d − Beta_1·x_n/2) + f_sc·A_sc·(Beta_1·x_n/2 − a0) :
> sol := solve({eq1, eq2}, {epsilon_c , epsilon_s}); assign(sol[1]);
```

$$sol := \{epsilon\_c = 0.0007259721735,\ epsilon\_s = 0.001091433433\},\ \{epsilon\_c = 0.1584463447,\ epsilon\_s = 0.2321958492\},\ \{epsilon\_c = -0.00003847642467,\ epsilon\_s = 0.00003935553386\},\ \{epsilon\_c = -0.0003126819449,\ epsilon\_s = 0.0006124225074\},\ \{epsilon\_c = -0.06977937006,\ epsilon\_s = 0.1430551022\} \quad (1)$$

Strain in the longitudinal reinforcement in tension zone equals:

```
> epsilon_s;
```

$$0.001091433433 \quad (2)$$

Strain in concrete at the top:

```
> epsilon_c;
```

$$0.0007259721735 \quad (3)$$

Stress in steel:

```
> f_s := E_s·epsilon_s; f_sc := E_sc·epsilon_sc;
```

$$f\_s := 218.2866866$$
$$f\_sc := 77.72189122 \quad (4)$$

Compression zone:

```
> x_n := epsilon_c/(epsilon_c + epsilon_s)·d;
```

$$x\_n := 66.70902333 \quad (5)$$

Hybrid beam at 50kN (This study)

```
> restart;
> M := 12.5·10^6 : h := 200 : d := 167 : b := 100 : a0 := 31 : A_s := 402.12 : E_s := 200·10^3 : E_c := 33031 : f_c := 29.07 : A_sc :=
  226.19 : E_sc := 200·10^3 : epsilon_cu := 3.5/1000 : b_SHCC := 20 : E_SHCC := 16500 : f_c_SHCC := 66.448 : f_y_SHCC := 3 :
  f_t_SHCC := 3.52 : epsilon_cr_SHCC := 0.025/100 : epsilon_ut_SHCC := 2.27/100 : E_h_SHCC :=
  (f_t_SHCC − f_y_SHCC)/(epsilon_ut_SHCC − epsilon_cr_SHCC) :
```

The basic geometrical relationships in the cross-section:

```
> x_n := epsilon_c/(epsilon_c + epsilon_s)·d : epsilon_sc := (d − a0)/d·epsilon_c − a0/d·epsilon_s : epsilon_b := (h − x_n)/x_n·epsilon_c : k :=
  epsilon_cr_SHCC/(epsilon_c + epsilon_s)·d :
```

The constitutive equations:

```
> f_s := E_s·epsilon_s : f_sc := E_sc·epsilon_sc :
```

Concrete strain level I:

```
> Xi_1 := 0.015 : Xi_2 := 1.382 : eta_1 := 0.665 : eta_2 := 0.117 :
```

Model:

> $Gamma\_1 := Xi\_1 + Xi\_2 \cdot \frac{epsilon\_c}{epsilon\_cu} : Beta\_1 := eta\_1 + eta\_2 \cdot \frac{epsilon\_c}{epsilon\_cu} :$

> $eq1 := Gamma\_1 \cdot f\_c \cdot b \cdot x\_n + Gamma\_1 \cdot f\_c\_SHCC \cdot b\_SHCC \cdot x\_n + f\_sc \cdot A\_sc = f\_s \cdot A\_s + \frac{1}{2} \cdot E\_SHCC \cdot epsilon\_cr\_SHCC \cdot k \cdot b\_SHCC + f\_y\_SHCC \cdot b\_SHCC \cdot (h - x\_n - k) + \frac{1}{2} \cdot E\_h\_SHCC \cdot (epsilon\_b - epsilon\_cr\_SHCC) \cdot b\_SHCC \cdot (h - x\_n - k) :$

> $eq2 := M = f\_s \cdot A\_s \cdot \left(d - \frac{Beta\_1 \cdot x\_n}{2}\right) + f\_sc \cdot A\_sc \cdot \left(\frac{Beta\_1 \cdot x\_n}{2} - a0\right) + \frac{1}{2} \cdot E\_SHCC \cdot epsilon\_cr\_SHCC \cdot k \cdot b\_SHCC \cdot \left(k + \frac{(2 - Beta\_1) \cdot x\_n}{2}\right) + f\_y\_SHCC \cdot b\_SHCC \cdot (h - x\_n - k) \cdot \frac{1}{2} \cdot (d + k + (1 - Beta\_1) \cdot x\_n) + \frac{1}{2} \cdot E\_h\_SHCC \cdot (epsilon\_b - epsilon\_cr\_SHCC) \cdot b\_SHCC \cdot (h - x\_n - k) \cdot \left(\frac{1}{3} \cdot d + \frac{2}{3} \cdot (k + x\_n) - \frac{Beta\_1 \cdot x\_n}{2}\right) :$

> $sol := solve(\{eq1, eq2\}, \{epsilon\_c, epsilon\_s\}); assign(sol[1]);$

$$sol := \{epsilon\_c = 0.0006470799910, epsilon\_s = 0.001018874553\}, \{epsilon\_c = 0.1636513955, epsilon\_s = 0.2644454825\}, \{epsilon\_c = -0.00002635483582 + 0.00005665066274\,I, epsilon\_s = -0.00001636542125 - 0.00005283517260\,I\}, \{epsilon\_c = -2.530087738\,10^{-6}, epsilon\_s = 0.00004737140906\}, \{epsilon\_c = -0.0001201461236, epsilon\_s = 0.0001902468616\}, \{epsilon\_c = -0.0002602588671, epsilon\_s = 0.0004825968378\}, \{epsilon\_c = -0.07733660988, epsilon\_s = 0.1701279429\}, \{epsilon\_c = -0.00002635483582 - 0.00005665066274\,I, epsilon\_s = -0.00001636542125 + 0.00005283517260\,I\} \quad (6)$$

Strain in the longitudinal reinforcement in tension zone equals:

> $epsilon\_s;$

$$0.001018874553 \quad (7)$$

Strain in concrete at the top:

> $epsilon\_c;$

$$0.0006470799910 \quad (8)$$

Stress in steel:

> $f\_s := E\_s \cdot epsilon\_s; f\_sc := E\_sc \cdot epsilon\_sc;$

$$f\_s := 203.7749106$$
$$f\_sc := 67.56618880 \quad (9)$$

Compression zone:

> $x\_n := \frac{epsilon\_c}{epsilon\_c + epsilon\_s} \cdot d;$

$$x\_n := 64.86513025 \quad (10)$$

The total force in SHCC:

> $\frac{1}{2} \cdot E\_SHCC \cdot epsilon\_cr\_SHCC \cdot k \cdot b\_SHCC + f\_y\_SHCC \cdot b\_SHCC \cdot (h - x\_n - k) + \frac{1}{2} \cdot E\_h\_SHCC \cdot (epsilon\_b - epsilon\_cr\_SHCC) \cdot b\_SHCC \cdot (h - x\_n - k)$

$$7666.200462 \quad (11)$$

Reference beam at 50kN (Y. Zhang et al. [43])

> $restart;$

> $M := 12.5 \cdot 10^6 : d := 165 : b := 100 : A\_s := 157.08 : E\_s := 200 \cdot 10^3 : E\_c := 23500 : f\_c := 27 : epsilon\_cu := \frac{3.5}{1000} :$

The basic geometrical relationships in the cross-section:

> $x\_n := \frac{epsilon\_c}{epsilon\_c + epsilon\_s} \cdot d :$

The constitutive equation:

> $f\_s := E\_s \cdot epsilon\_s :$

Concrete strain level II:

> $Xi\_1 := 0.190 : Xi\_2 := 0.799 : eta\_1 := 0.650 : eta\_2 := 0.167 :$

Model by J. Han et al. [64] :

> $Gamma\_1 := Xi\_1 + Xi\_2 \cdot \frac{epsilon\_c}{epsilon\_cu} : Beta\_1 := eta\_1 + eta\_2 \cdot \frac{epsilon\_c}{epsilon\_cu} :$

> $eq1 := Gamma\_1 \cdot f\_c \cdot b \cdot x\_n = f\_s \cdot A\_s :$

> $eq2 := M = f\_s \cdot A\_s \cdot \left(d - \frac{Beta\_1 \cdot x\_n}{2}\right) :$

> $sol := solve(\{eq1, eq2\}, \{epsilon\_c, epsilon\_s\}); assign(sol[1]);$

$$sol := \{epsilon\_c = 0.001552484244, epsilon\_s = 0.002771698768\}, \{epsilon\_c = 0.08388935848, epsilon\_s = 0.1154314562\}, \{epsilon\_c = -0.0009671969111 + 0.00004112351767\,I, epsilon\_s = 0.001296537640 - 0.0001230336826\,I\}, \{epsilon\_c = -0.06966908058, epsilon\_s = 0.1642123242\}, \{epsilon\_c = -0.0009671969111 - 0.00004112351767\,I, epsilon\_s = 0.001296537640 + 0.0001230336826\,I\} \quad (12)$$

Strain in the longitudinal reinforcement in tension zone equals:

> *epsilon_s*;

$$0.002771698768 \tag{13}$$

Strain in concrete at the top:

> *epsilon_c*;

$$0.001552484244 \tag{14}$$

Stress in steel:

> $f\_s := E\_s \cdot epsilon\_s$;

$$f\_s := 554.3397536 \tag{15}$$

Compression zone:

> $x\_n := \frac{epsilon\_c}{epsilon\_c + epsilon\_s} \cdot d$;

$$x\_n := 59.23891278 \tag{16}$$

Hybrid beam at 50kN (Y. Zhang et al. [43])

> *restart*;

> $M := 12.5 \cdot 10^6 : h := 200 : d := 165 : b := 100 : A\_s := 157.08 : E\_s := 200 \cdot 10^3 : E\_c := 23500 : f\_c := 27 : epsilon\_cu := \frac{3.5}{1000} :$
> $b\_SHCC := 20 : E\_SHCC := 29000 : f\_c\_SHCC := 91 : epsilon\_cr\_SHCC := \frac{0.015}{100} : epsilon\_ut\_SHCC := \frac{2}{100} : f\_y\_SHCC :=$
> $E\_SHCC \cdot epsilon\_cr\_SHCC : f\_t\_SHCC := 6.2 : E\_h\_SHCC := \frac{f\_t\_SHCC - f\_y\_SHCC}{epsilon\_ut\_SHCC - epsilon\_cr\_SHCC} :$

The basic geometrical relationships in the cross-section:

> $x\_n := \frac{epsilon\_c}{epsilon\_c + epsilon\_s} \cdot d : k := \frac{epsilon\_cr\_SHCC}{epsilon\_c + epsilon\_s} \cdot d : epsilon\_b := \frac{h - x\_n}{x\_n} \cdot epsilon\_c :$

The constitutive equation:

> $f\_s := E\_s \cdot epsilon\_s :$

Concrete strain level II:

> $Xi\_1 := 0.190 : Xi\_2 := 0.799 : eta\_1 := 0.650 : eta\_2 := 0.167 :$

Model:

> $Gamma\_1 := Xi\_1 + Xi\_2 \cdot \frac{epsilon\_c}{epsilon\_cu} : Beta\_1 := eta\_1 + eta\_2 \cdot \frac{epsilon\_c}{epsilon\_cu} :$

> $eq1 := Gamma\_1 \cdot f\_c \cdot b \cdot x\_n + Gamma\_1 \cdot f\_c\_SHCC \cdot b\_SHCC \cdot x\_n = f\_s \cdot A\_s + \frac{1}{2} \cdot E\_SHCC \cdot epsilon\_cr\_SHCC \cdot k \cdot b\_SHCC + f\_y\_SHCC$
> $\cdot b\_SHCC \cdot (h - x\_n - k) + \frac{1}{2} \cdot E\_h\_SHCC \cdot (epsilon\_b - epsilon\_cr\_SHCC) \cdot b\_SHCC \cdot (h - x\_n - k) :$

> $eq2 := M = f\_s \cdot A\_s \cdot \left(d - \frac{Beta\_1 \cdot x\_n}{2}\right) + \frac{1}{2} \cdot E\_SHCC \cdot epsilon\_cr\_SHCC \cdot k \cdot b\_SHCC \cdot \left(k + \frac{(2 - Beta\_1) \cdot x\_n}{2}\right) + f\_y\_SHCC \cdot b\_SHCC$
> $\cdot (h - x\_n - k) \cdot \frac{1}{2} \cdot (d + k + (1 - Beta\_1) \cdot x\_n) + \frac{1}{2} \cdot E\_h\_SHCC \cdot (epsilon\_b - epsilon\_cr\_SHCC) \cdot b\_SHCC \cdot (h - x\_n - k) \cdot \left(\frac{1}{3} \cdot d$
> $+ \frac{2}{3} \cdot (k + x\_n) - \frac{Beta\_1 \cdot x\_n}{2}\right) :$

> $sol := solve(\{eq1, eq2\}, \{epsilon\_c, epsilon\_s\}); assign(sol[1]);$

$$\begin{aligned} sol := {} & \{epsilon\_c = 0.0009836113640, epsilon\_s = 0.002419662007\}, \{epsilon\_c = 0.1053252806, epsilon\_s = 0.1981580609\}, \{epsilon\_c \\ & = -0.0009374815465 + 0.0001211279136\,I, epsilon\_s = 0.001072066518 - 0.0004663576989\,I\}, \{epsilon\_c = -5.745557937\,10^{-6}, \\ & epsilon\_s = 0.00001596460808\}, \{epsilon\_c = -7.789410586\,10^{-6}, epsilon\_s = 1.965671211\,10^{-7}\}, \{epsilon\_c \\ & = -0.0009919089697, epsilon\_s = 0.001233968836\}, \{epsilon\_c = -0.08974689280, epsilon\_s = 0.2563211442\}, \{epsilon\_c \\ & = -0.0009374815465 - 0.0001211279136\,I, epsilon\_s = 0.001072066518 + 0.0004663576989\,I\} \end{aligned} \tag{17}$$

Strain in the longitudinal reinforcement in tension zone equals:

> *epsilon_s*;

$$0.002419662007 \tag{18}$$

Strain in concrete at the top:

> *epsilon_c*;

$$0.0009836113640 \tag{19}$$

Stress in steel:

> $f\_s := E\_s \cdot epsilon\_s$;

$$f\_s := 483.9324014 \tag{20}$$

Compression zone:

> $x\_n := \frac{epsilon\_c}{epsilon\_c + epsilon\_s} \cdot d$;

$$x\_n := 47.68816882 \tag{21}$$

The total force in SHCC:

> $\frac{1}{2} \cdot E\_SHCC \cdot epsilon\_cr\_SHCC \cdot k \cdot b\_SHCC + f\_y\_SHCC \cdot b\_SHCC \cdot (h - x\_n - k) + \frac{1}{2} \cdot E\_h\_SHCC \cdot (epsilon\_b - epsilon\_cr\_SHCC)$
> $\cdot b\_SHCC \cdot (h - x\_n - k)$

$$13339.16557 \tag{22}$$